

**Study on Sedimentation and
Effects of Mitigating Measures at
Port of Mar del Plata, Argentina**

M.Sc. Thesis Final Report

Title

Study on Sedimentation and Effects of Mitigating Measures at Port of Mar del Plata, Argentina

State

Master of Science Thesis Final Report

Client

Fundación Bolsa de Comercio de Mar del Plata

Author

ing. J.M. (Han) Luteijn
M.Sc. graduate Coastal and River Engineering
Delft University of Technology
Faculty of Civil Engineering and Geosciences
Section Hydraulic Engineering
Student nr. 1271229
J.M.Luteijn@outlook.com

M.Sc. Thesis Committee

| | |
|-----------------------------|---|
| prof. dr. ir. M.J.F. Stive | Delft University of Technology |
| prof. dr. ir. L.C. van Rijn | Deltares & Utrecht University |
| ir. P.K. Tonnon | Deltares |
| ir. G.L.M. van der Schrieck | Delft University of Technology |
| ir. D.J.R. Walstra | Deltares & Delft University of Technology |

Date published

28 February 2013

Place published

Delft, The Netherlands

Pages

163

Keywords

Sedimentation; accretion; shoaling; shoal; sand bank; port access; navigation channel; Mar del Plata; Buenos Aires; Argentina; drifter tracking; sediment sampling; sediment analysis; depth survey; sedimentation study; NWW3; wave modelling; input reduction; reduced wave climate; evaluation of measures; sand trap; groin; hydrodynamics; initial sediment transports; Delft3D; cost estimation.

Preface

This thesis is the final report of a quantitative study on sedimentation and effect of measures in the port access of Mar del Plata, Argentina. This graduation project is carried out at research institute Deltares for the completion of the masters-program Hydraulic Engineering at the faculty of Civil Engineering and Geosciences of the Delft University of Technology. The performed research would not be achieved without the contribution of many people who I would like to thank.

First I would like to thank the members of my graduation committee: Professor Marcel Stive, Professor Leo van Rijn, Bart van der Schrieck and Dirk-Jan Walstra for their guidance and feedback on the report. Special thanks to Pieter Koen Tonnon for his daily guidance and extensive feedback.

I would also like to thank Deltares for giving me the opportunity to work on this very interesting project and for providing a place to work.

Furthermore, I would like to thank everyone who supported me by giving the information necessary to complete this thesis. Special thanks goes out to:

Alejandro Gómez, president of Foundation of the Chamber of Commerce of Mar del Plata;
Sergio Loschacoff, Maria Luisa Loidi and Geronimo Rizzo, collaborators of the Foundation of the Chamber of Commerce of Mar del Plata;

Eduardo Tomás Pezzati, president of Chamber of Commerce of Mar del Plata and president of the Regional Port Consortium;

Roberto Sciarrone and Ruben Melendez, engineers of the provincial Hydraulic Department of the Ministry of Transport and Public Services of Argentina;

José Carlos Pérez de la Sierra, engineer of National Directorate of Waterways of Argentina.

Finally, I want to thank my family, friends and especially my girlfriend Tessa for their support.

J.M. Luteijn
Delft, February 2013

Abstract

Problem definition

The city Mar del Plata has one of Argentina's largest ports and biggest seaside beach resort. After the construction of the port, a steadily growing sandbank appeared in the port entrance and considerable erosion occurred on the northern beaches. To warrant the accessibility of the port, frequent maintenance dredging is needed, but no measures have been taken to prevent/reduce shoaling of the port access. After numerous unsafe situations for vessels, large shipping companies have decided to stop berthing at Mar del Plata. Improvement of the accessibility for large ships will significantly lower the (transport) costs and results in more income and new investments in port activities and infrastructure.

Objectives

The main objective of this M.Sc. study is to identify the most promising feasible measures that improve the accessibility of the port and reduce the costs of maintenance and to quantitatively evaluate the effects and costs of these measures to support further detailed morphodynamic and design studies.

Methodology

Available literature and data is studied and reviewed to gain insight in the local system. During a field trip in the province of Buenos Aires data is collected by performing field measurements and different meetings took place with local experts and stakeholders.

To identify and quantify the physical processes influencing the accessibility of the port, a Delft3D-FLOW model of the present area around Mar del Plata is set up and validated using present and historical data. Due to the lack of (reliable) near shore wave data, the nearshore wave climate in the model is derived from offshore wave data, wind data, and bathymetric data using a Delft3D-WAVE model with a larger scale.

Various theoretical measures are evaluated. The most feasible, durable, and efficient type of measures are selected and quantitatively evaluated.

To estimate the effects of these measures, with a focus on sediment transports, each measure is simulated in the Delft3D-FLOW model. From the resulting sedimentation rates in the port entrance, the quantity of needed maintenance is estimated for each measure. To be able to compare the measures, the total costs of initial investments and future maintenance is estimated.

Conclusions

- *Maintaining the original port access, without taking additional measures* is not economic (total costs € 2.5 to € 5.4 million/year) and leads to frequent disturbance of the ship traffic. The irregular and uncertain circumstances are not attractive for companies and investors in the port and lead to higher transport costs.
- *Maintaining the original port access and construction and maintenance of a sand trap* along the southern breakwater strongly reduces the maintenance need (and the disturbance for the ship traffic) inside the access channel with 90%. The maintenance of

the sand trap can be executed on a regular base (without disturbance for other ship traffic) and the dredged material can be used to regularly nourish the eroding northern beaches. However, by applying this measure the expected reduction of total costs is 6% percent.

- *Maintaining the original port access and construction of an eastward groin* at the tip of the southern breakwater appears to be the most economical solution with 80% reduction of the total costs. The groin deflects sediment to deeper water outside the navigation area and prevents the port access from shoaling, but this can also lead to a decrease of sediment supply to the northern beaches and thereby increased beach erosion.

Contents

| | |
|--|------------|
| List of tables | x |
| List of figures | xii |
| List of photographs | xvi |
| 1 Introduction | 1 |
| 1.1 Problem definition | 1 |
| 1.2 Significance of this study | 4 |
| 1.3 Objectives | 5 |
| 1.4 Methodology | 5 |
| 1.5 Reader | 7 |
| 2 Literature review | 9 |
| 2.1 Characteristics of the coastal area | 9 |
| 2.1.1 Geomorphologic evolution | 9 |
| 2.1.2 Morphologic developments in recent centuries | 11 |
| 2.1.3 Ecology | 12 |
| 2.2 Processes influencing the accessibility of the port | 14 |
| 3 Data collection and review | 17 |
| 3.1 Wave climate | 17 |
| 3.1.1 Pressure sensor data | 17 |
| 3.1.2 Visual ship observations | 18 |
| 3.1.3 Numerical wave hindcast data | 20 |
| 3.2 Wind climate | 23 |
| 3.3 Bathymetry | 25 |
| 3.4 Tidal levels | 27 |
| 3.5 Tidal currents | 28 |
| 3.6 Sediment characteristics | 29 |
| 3.7 Longshore sediment transport | 30 |
| 3.8 Dredging and sedimentation rates | 31 |
| 3.8.1 Dredge records | 31 |
| 3.8.2 Analysis of depth survey data | 33 |
| 3.8.3 Sedimentation volumes and rates | 37 |
| 4 Potential measures to reduce sedimentation in port entrance | 39 |
| 4.1 Inventarisation of possible measures | 39 |
| 4.2 Discussion of measures | 40 |
| 4.3 Selection of most promising measures | 46 |

| | | |
|----------|--|-----------|
| 5 | Near shore wave modelling Buenos Aires | 47 |
| 5.1 | Model description | 47 |
| 5.2 | Model set-up | 47 |
| 5.3 | Model results | 50 |
| 6 | Setup hydrodynamics & sediment transports model | 51 |
| 6.1 | Model description | 51 |
| 6.2 | Modelling approach | 51 |
| 6.3 | Model set-up Delft3D-FLOW | 52 |
| 6.3.1 | Domain | 52 |
| 6.3.1.1 | Land boundary | 52 |
| 6.3.1.2 | Computational grid | 52 |
| 6.3.1.3 | Bathymetry | 53 |
| 6.3.1.4 | Thin dams and dry points | 54 |
| 6.3.2 | Time step | 54 |
| 6.3.3 | Sediment parameters | 54 |
| 6.3.4 | Initial conditions | 55 |
| 6.3.5 | Boundaries | 55 |
| 6.3.6 | Physical parameters | 55 |
| 6.3.7 | Numerical parameters | 56 |
| 6.4 | Model set-up Delft3D-WAVE | 56 |
| 6.4.1 | Computational grids | 56 |
| 6.4.2 | Boundaries and physical parameters | 57 |
| 6.4.3 | Obstacles | 61 |
| 7 | Analysis and validation of 2012 hydrodynamics & sediment transports model | 63 |
| 7.1 | Determination of effects of tide on hydrodynamics and sediment transports | 63 |
| 7.1.1 | Estimated flow directions and magnitudes around the port entrance | 63 |
| 7.1.2 | Validation of flow patterns and velocities | 63 |
| 7.1.3 | Resulting initial sediment transports around the port entrance | 66 |
| 7.2 | Determination effects waves on hydrodynamics and sediment transports | 66 |
| 7.2.1 | Effect on hydrodynamics and sediment transports | 67 |
| 7.3 | Tidal forcing and representative wind and wave climate | 69 |
| 7.3.1 | Effect of each scenario on hydrodynamics and initial sediment transport | 70 |
| 7.3.2 | Average sediment transport rates | 72 |
| 7.3.3 | Comparison with other studies to longshore transport rates | 73 |
| 7.4 | Different horizontal eddy coefficients | 73 |
| 7.4.1 | Effects on sediment transports | 73 |
| 7.4.2 | Data comparison and evaluation | 75 |

| | |
|--|------------|
| 8 Evaluation effects of measures | 77 |
| 8.1 Bathymetry with preferred navigation channel without additional measures | 77 |
| 8.1.1 Effects on sediment transports | 78 |
| 8.1.2 Data comparison and evaluation | 79 |
| 8.2 Bathymetry with preferred navigation channel and sand trap | 79 |
| 8.2.1 Effects on sediment transports | 80 |
| 8.3 Bathymetry with preferred navigation channel with eastward groin | 82 |
| 8.3.1 Effects on sediment transports | 82 |
| 8.4 Estimation costs of initial work and maintenance over 50 years | 84 |
| | |
| 9 Conclusions, discussion and recommendations | 87 |
| 9.1 Conclusions | 87 |
| 9.2 Discussion | 88 |
| 9.3 Recommendations | 89 |
| | |
| References | 91 |
| | |
| Appendices | A-1 |
| | |
| A Site visit trip Buenos Aires coast, Argentina | A-1 |
| A.1 Objectives | A-1 |
| A.2 Itinerary | A-1 |
| | |
| B Field measurements | B-1 |
| B.1 Alternative depth sounding method | B-1 |
| B.2 Sediment sampling | B-3 |
| B.3 Drifter tracking | B-6 |
| B.3.1 Methodology | B-6 |
| B.3.2 Results | B-8 |
| B.3.3 Data comparison and evaluation | B-12 |
| | |
| C Computed deep water wave climate near Mar del Plata | C-1 |
| | |
| D Computed average hour-by-hour tidal flow in port access | D-1 |
| | |
| E Computed effect waves from varying directions (without tide) | E-1 |
| | |
| F Computed hydrodynamics and sediment transports per scenario | F-1 |

List of tables

| | | |
|------------|--|----|
| Table 3.1 | Annual directional distribution of wave heights derived from Sunrise Technical Consultants (1968) (as cited by Boer, De Jonge, Brouwer, et al., 1997)..... | 17 |
| Table 3.2 | Directional distribution of wave heights derived from Algera et al. (2004)..... | 19 |
| Table 3.3 | Joint probability of occurrence of wave heights vs. wave periods derived from Algera et al. (2004) | 19 |
| Table 3.4 | Seasonal variation in distribution of mean wave directions..... | 19 |
| Table 3.5 | Directional distribution of wind speeds at Mar del Plata (38°S 37.5°W) from NWW3 model 1997-2010 | 24 |
| Table 3.6 | Equipment used for depth surveys near port of Mar del Plata..... | 25 |
| Table 3.7 | Tidal levels at Mar del Plata (in m to MSL) (SHN, 2012d) | 27 |
| Table 3.8 | Cumulative grain size distribution from sieve analysis EN 933-1 (sampling locations and methods see appendix B.2) | 29 |
| Table 3.9 | Dredging activities during the last decades..... | 32 |
| Table 3.10 | Cell properties | 34 |
| Table 3.11 | Measured and estimated sedimentation volumes and rates in different cell's (plotted in Figure 3.9)..... | 37 |
| Table 3.12 | Input parameters SED-PIT model for estimation sedimentation rates in the navigation channel | 37 |
| Table 3.13 | Sand layer thickness in the navigation channel estimated by SED-PIT model .. | 38 |
| Table 5.1 | Offshore directional distribution of wave heights at 38°S 55°W derived from NWW3 wave data | 48 |
| Table 5.2 | Model parameters used in Delft3D-WAVE | 50 |
| Table 6.1 | Overview modelling steps..... | 51 |
| Table 6.2 | Model runs using different parameters for horizontal eddy diffusivity | 56 |
| Table 6.3 | Directional distribution of wave heights (in %) derived from near shore wave model Buenos Aires at UTM21s 491126 m east, 5756185 m north on 69 m water depth | 57 |
| Table 6.4 | Relative weighted contribution to the sediment transport (W_i) | 58 |
| Table 6.5 | Numbered bins of grouped wave conditions | 58 |
| Table 6.6 | Representative scenarios of wind and wave conditions at UTM21s 491126 m east, 5756185 m north on 69 m water depth..... | 61 |
| Table 7.1 | Wave conditions and wind conditions for model runs without tide..... | 67 |
| Table 7.2 | Description of resulting conditions and phenomena around the port per wind and wave direction (visualised in appendix E) | 67 |
| Table 7.3 | Representative scenarios of wind and wave conditions at UTM21s 491126 m east, 5756185 m north on 69 m water depth..... | 69 |
| Table 7.4 | Description of typical effects on hydrodynamics and sediment transports per group of scenarios (visualised in appendix F)..... | 70 |

| | | |
|------------|---|-----|
| Table 7.5 | Contribution of wind- and wave scenarios with tide to sedimentation. (red) and erosion (blue) per littoral cell (in m ³ /day)..... | 73 |
| Table 7.6 | Model runs using different parameters for horizontal eddy diffusivity..... | 73 |
| Table 7.7 | Effect on sedimentation of different horizontal eddy coefficients. (red) or erosion (blue) rate in different cells | 74 |
| Table 8.1 | Initial sedimentation rate (in m ³ /day) per cell for different bathymetries..... | 78 |
| Table 8.2 | Specifications of modelled sand traps..... | 80 |
| Table 8.3 | Initial sedimentation rate (in m ³ /day) per cell for different sand traps..... | 81 |
| Table 8.4 | Initial sedimentation rate (in m ³ /day) per cell for different grains..... | 83 |
| Table 8.5 | Initial sedimentation rate (in m ³ /day) per cell for different measures..... | 84 |
| Table 8.6 | Initial costs per measure | 85 |
| Table 8.7 | Maintenance costs per measure over 50 years | 85 |
| Table 8.8 | Total costs per measure over 50 years..... | 85 |
| Table 9.1 | Total costs per measure over 50 years..... | 88 |
| Table 10.1 | Sediment sampling locations..... | B-4 |
| Table 10.2 | Materials used for GPS-drifter measurements..... | B-7 |
| Table 10.3 | Tide, wind, and wave data before and during drifter tracking (SHN, 2012d; WindGURU, 2012)..... | B-8 |
| Table 10.4 | Data summary drifter tracks | B-8 |
| Table 10.5 | Annual offshore wind and wave climate near Mar del Plata (part 1 of 3)..... | C-1 |
| Table 10.6 | Annual offshore wind and wave climate near Mar del Plata (part 2 of 3)..... | C-2 |
| Table 10.7 | Annual offshore wind and wave climate near Mar del Plata (part 3 of 3)..... | C-3 |
| Table 10.8 | Wind and wave conditions for model runs without tide..... | E-1 |
| Table 10.9 | Representative scenarios of wind and wave conditions | F-1 |

List of figures

| | | |
|-------------|---|----|
| Figure 1.1 | Maps of Argentina and Buenos Aires province (Universidad Nacional de Córdoba, 2007)..... | 1 |
| Figure 1.2 | Nautical chart H-251 - Port of Mar del Plata (SHN, 2010) | 2 |
| Figure 2.1 | Tectonic plate movement (Tarbuck, Lutgens, & Tasa, 2011) | 9 |
| Figure 2.2 | River systems of South America (EnchantedLearning.com, 2012) | 9 |
| Figure 2.3 | Coastal evolution north-eastern region of Buenos Aires province (Codignotto & Aguirre, 1993) | 10 |
| Figure 2.4 | Geographic map of north of Buenos Aires province (GEBSCO, 2011)..... | 11 |
| Figure 2.5 | Basic sedimentation processes in port entrance (Van Rijn, 2005) | 15 |
| Figure 3.1 | Directional distribution of wind waves (left) and swell waves (right) (The Met Office, 1994; as cited by Waterman, 1994)..... | 18 |
| Figure 3.2 | NWW3 model grid points on nautical chart (UKHO, 2006b, 2006c, 2006d, 2006e)..... | 21 |
| Figure 3.3 | Directional distribution of wave heights from NWW3 hindcast (1997-2010)..... | 22 |
| Figure 3.4 | Directional distribution of peak wave periods from NWW3 hindcast (1997-2010) | 22 |
| Figure 3.5 | Directional distribution of winds from NWW3 model 1997-2010 | 24 |
| Figure 3.6 | Cotidal chart of the Atlantic Ocean (Talley, Pickard, William J. Emery, & Swift, 2011)..... | 27 |
| Figure 3.7 | Results drifter tracking | 28 |
| Figure 3.8 | Cumulative grain size distribution obtained using EN 933-1 sieve analysis | 30 |
| Figure 3.9 | Analysed depth sounding grid points subdivided in cells (POSGAR94-6 coordinate system)..... | 34 |
| Figure 3.10 | Time series of sand layer thickness on two different locations (1999 to 2012) | 35 |
| Figure 3.11 | Example of Ordinary Least Squares curve fitting for volumetric change over time for one grid point | 36 |
| Figure 3.12 | Sand layer thickness in the navigation channel estimated by SED-PIT model | 38 |
| Figure 4.1 | Solution 1a: Sand trap at tip breakwater | 41 |
| Figure 4.2 | Solution 1b: Sand trap updrift | 41 |
| Figure 4.3 | Morphological development of channel with flow perpendicular to main axis (Van Rijn, 2005) | 41 |
| Figure 4.4 | Solution 1c: Offshore breakwater | 42 |
| Figure 4.5 | Solution 1d: (T-head) groin | 42 |
| Figure 4.6 | Solution 1e: Groin to the east | 43 |
| Figure 4.7 | Solution 1f: Move entrance | 43 |
| Figure 4.8 | Solution 2a: Extension to deep water | 44 |
| Figure 4.9 | Solution 3a: Crane pier/jetty bypass | 44 |

| | | |
|-------------|---|----|
| Figure 4.10 | Solution 3b: Jet pier bypass | 45 |
| Figure 5.1 | Nested grids for Delft3D-WAVE computation Left: 3,000x3,700 m grid, Right: 1,000x1,000 m grid..... | 49 |
| Figure 5.2 | Example a scenario of simultaneous occurring wind- (in red:) and wave conditions (in blue) | 49 |
| Figure 5.3 | Directional distribution of nearshore significant wave heights (left) and peak wave periods (right) at MSL -7 m depth contour..... | 50 |
| Figure 6.1 | Land boundary (yellow) obtained using satellite images (Google, 2012)..... | 52 |
| Figure 6.2 | Distribution of grid size resolution (square root of grid cell area) Left: Full grid, Right: Detail of grid and resolution at port entrance | 53 |
| Figure 6.3 | Wave grid..... | 56 |
| Figure 6.4 | Visual check determination T_p vs. H_s according Mangor (2007) formula | 59 |
| Figure 6.5 | Least squares curve fitting of U_{10} against H_s | 60 |
| Figure 6.6 | Example of least squares curve fitting between U_{dir} and D_m within bin nr. 16... 60 | |
| Figure 7.1 | Measured magnitudes and directions of tidal currents, using GPS-drifter tracking. Left: Drifter tracks on nautical chart (UKHO, 2006a), Right: Legend and data summary..... | 64 |
| Figure 7.2 | Model prediction of averaged tidal flow velocities (in m/s) and directions 5.5 hours before HW | 64 |
| Figure 7.3 | Model prediction of averaged tidal flow velocities (in m/s) and directions 2.5 hours before HW | 65 |
| Figure 7.4 | Model prediction of averaged tidal flow velocities (in m/s) and directions 0.5 hour before HW | 65 |
| Figure 7.5 | Mean total sediment transport over one tidal period (colours indicating magnitude in $m^3/s/m$, coordinates in 10^2 m to UTM21s) | 66 |
| Figure 7.6 | Run C: Wind and wave angle 90° w.r.t. north | 68 |
| Figure 7.7 | Run D: Wind and wave angle 135° w.r.t. north | 68 |
| Figure 7.8 | Estimated depth averaged flow velocities (left), and sediment transports (right) for scenario 1..... | 71 |
| Figure 7.9 | Estimated depth averaged flow velocities (left), and sediment transports (right) for scenario 2..... | 71 |
| Figure 7.10 | Estimated depth averaged flow velocities (left), and sediment transports (right) for scenario 3..... | 71 |
| Figure 7.11 | Estimated present net sediment transport per transect (in m^3/day) based on all scenarios (using hor. eddy diffusivity of $1 m^2/s$)..... | 72 |
| Figure 7.12 | Estimated net sediment transport in 2012 per transect (in m^3/day) based on all wind and wave scenarios with tide using different hor. eddy diffusivity coefficients In black: horizontal eddy diffusivity of $10 m^2/s$. In blue: using HLES-model | 74 |
| Figure 7.13 | Example of sediment transport for scenario 9 using different hor. eddy diffusivity coefficients Left: uniform value of $10 m^2/s$, offshore turning; Right: uniform value of $1 m^2/s$, no turning. | 75 |

| | | |
|--------------|--|------|
| Figure 8.1 | Bathymetry with preferred navigation channel according to DNVN (2011) (depths in m below MSL)..... | 77 |
| Figure 8.2 | Estimated net sediment transport per transect (in m ³ /day) just after completion of the dredging works | 78 |
| Figure 8.3 | Locations and depths of the modelled sand traps..... | 79 |
| Figure 8.4 | Estimated initial net sediment transports per transect (in m ³ /day) for different sand trap designs..... | 81 |
| Figure 8.5 | Location and lengths of the modelled groins..... | 82 |
| Figure 8.6 | Estimated initial net sediment transport per transect (in m ³ /day) for different groin designs..... | 83 |
| Figure 9.1 | Selected and simulated most promising measures to reduce sedimentation in the port entrance:..... | 87 |
| Figure 10.1 | Sediment sampling locations | B-3 |
| Figure 10.2 | Van Veen grab in opened and closed position..... | B-4 |
| Figure 10.3 | Overview drifter tracks | B-9 |
| Figure 10.4 | Drifter track A: ca. 4.5 hours before HW..... | B-9 |
| Figure 10.5 | Drifter track B: ca. 4 hours before HW..... | B-10 |
| Figure 10.6 | Drifter track C1-C3 (Green): ca. 3.5 hours before HW and Track D1-D3 (Blue): ca. 2.5 hours before HW..... | B-10 |
| Figure 10.7 | Drifter track E: ca. 1.5 hours before HW..... | B-11 |
| Figure 10.8 | Drifter track F: ca. 1 hour before HW..... | B-11 |
| Figure 10.9 | Drifter track G: ca. 45m before HW. | B-12 |
| Figure 10.10 | Computed depth averaged flow velocities (in m/s) and directions 0.5 hour after HW | D-1 |
| Figure 10.11 | Computed depth averaged flow velocities (in m/s) and directions 1.5 hours after HW | D-1 |
| Figure 10.12 | Computed depth averaged flow velocities (in m/s) and directions 2.5 hours after HW | D-2 |
| Figure 10.13 | Computed depth averaged flow velocities (in m/s) and directions 3.5 hours after HW | D-2 |
| Figure 10.14 | Computed depth averaged flow velocities (in m/s) and directions 4.5 hours after HW | D-3 |
| Figure 10.15 | Computed depth averaged flow velocities (in m/s) and directions 5.5 hours after HW | D-3 |
| Figure 10.16 | Computed depth averaged flow velocities (in m/s) and directions 5.5 hours before HW..... | D-4 |
| Figure 10.17 | Computed depth averaged flow velocities (in m/s) and directions 4.5 hours before HW..... | D-4 |
| Figure 10.18 | Computed depth averaged flow velocities (in m/s) and directions 3.5 hours before HW..... | D-5 |
| Figure 10.19 | Computed depth averaged flow velocities (in m/s) and directions 2.5 hours before HW..... | D-5 |

| | |
|---|------|
| Figure 10.20 Computed depth averaged flow velocities (in m/s) and directions 1.5 hours before HW..... | D-6 |
| Figure 10.21 Computed depth averaged flow velocities (in m/s) and directions 0.5 hour before HW..... | D-6 |
| Figure 10.22 Run A: Wind and wave angle 0° w.r.t. north | E-2 |
| Figure 10.23 Run B: Wind and wave angle 45° w.r.t. north | E-3 |
| Figure 10.24 Run C: Wind and wave angle 90° w.r.t. north | E-4 |
| Figure 10.25 Run D: Wind and wave angle 135° w.r.t. north | E-5 |
| Figure 10.26 Run E: Wind and wave angle 180° w.r.t. north | E-6 |
| Figure 10.27 Run F: Wind and wave angle 225° w.r.t. north | E-7 |
| Figure 10.28 Run G: Wind and wave angle 270° w.r.t. north..... | E-8 |
| Figure 10.29 Run H: Wind and wave angle 315° w.r.t. north..... | E-9 |
| Figure 10.30 Estimated depth averaged flow velocities (in m/s) for scenario 1..... | F-2 |
| Figure 10.31 Estimated sediment transports (in m ³ /s/m) for scenario 1 | F-3 |
| Figure 10.32 Estimated depth averaged flow velocities (in m/s) for scenario 2..... | F-4 |
| Figure 10.33 Estimated sediment transports (in m ³ /s/m) for scenario 2..... | F-5 |
| Figure 10.34 Estimated depth averaged flow velocities (in m/s) for scenario 3..... | F-6 |
| Figure 10.35 Estimated sediment transports (in m ³ /s/m) for scenario 3..... | F-7 |
| Figure 10.36 Estimated depth averaged flow velocities (in m/s) for scenario 10..... | F-8 |
| Figure 10.37 Estimated sediment transports (in m ³ /s/m) for scenario 10..... | F-9 |
| Figure 10.38 Estimated depth averaged flow velocities (in m/s) for scenario 12..... | F-10 |
| Figure 10.39 Estimated sediment transports (in m ³ /s/m) for scenario 12..... | F-11 |

List of photographs

| | | |
|-----------------|--|-----|
| Cover | Aerial photograph of port entrance Mar del Plata (Elgue, 2009) | |
| Photograph 1.1 | One of Mar del Plata's boulevards and city beaches..... | 1 |
| Photograph 1.2 | Sand extraction at southern breakwater of Mar del Plata port | 3 |
| Photograph 1.3 | Mendoza 259 C - Dredger dedicated to port of Mar del Plata | 4 |
| Photograph 2.1 | Cliffs south of Mar del Plata | 10 |
| Photograph 2.2 | Eroded beach and dunes at Mar del Tuyu..... | 12 |
| Photograph 2.3 | Execution of beach and cliff protection works south of Mar del Plata | 12 |
| Photograph 2.4 | Sea-Lions inside Mar del Plata port | 13 |
| Photograph 2.5 | Flamingos in Mar Chiquita Lagoon | 13 |
| Photograph 3.1 | Depth survey equipment used..... | 25 |
| Photograph 10.1 | Alternative depth survey set..... | B-1 |
| Photograph 10.2 | GPS-Drifters constructed and used for measurements | B-6 |

1 Introduction

1.1 Problem definition



Photograph 1.1 One of Mar del Plata's boulevards and city beaches

Mar del Plata is an Argentine city located on the coast of the Atlantic Ocean, 400 km south of Buenos Aires. With more than half a million inhabitants, it is the second largest city of Buenos Aires Province. It has one of Argentina's largest ports and the biggest seaside beach resort in Argentina with more than 2 million tourists per year.



Figure 1.1 Maps of Argentina and Buenos Aires province (Universidad Nacional de Córdoba, 2007)

The port of Mar del Plata was constructed between 1911 and 1922. It is surrounded by a southern and northern breakwater of respectively 2.7 and 1.1 km. From the head of the northern breakwater counter clockwise, the port is subdivided in a cruise terminal, naval basin, yacht basin, shipyard, cargo basin, 2 fishery basins, and an area with a floating ship dock and two dolphins for flammable materials on the southern breakwater (Figure 1.2). Overseas exports consist mainly of grain and fish. In addition, there is a considerable quantity of domestic cargo of fish and petroleum and a small quantity of imports handled (NGA, 2011).

The present situation is therefore unsafe for larger vessels and the maximum size of the vessels has been set at 120 m for the length of the vessels and 23 feet for the draft. (Boer, De Jonge, Uit het Broek, et al., 1997)

Currently at the northern breakwater, a terminal is being built for cruise ships. These ships can barely manoeuvre at low speed and because of their height and length; those ships have a relatively large leeway owing to the action of the wind.

Around 1959, a submerged pump was installed near the head of the southern breakwater to bypass sand through a pipeline to the area north of the northern breakwater. In a short time, this pump was destroyed during a storm.

To reduce sedimentation at the port entrance and for commercial sand mining, a short groin normal to the southern breakwater has been built to extract sand to from the littoral drift zone. A mobile crane (boom of 30 m) pumps the sediment to the beach from where it is removed by shovels and trucks (Photograph 1.2). The total extraction volume is estimated at 50,000 m³/year. Despite this extraction, continuously dredging is necessary to maintain the access of the port in the order of 200,000 to 300,000 m³/year, or about 700 ± 150 m³/day. (Van Rijn, 2008)



Photograph 1.2 Sand extraction at southern breakwater of Mar del Plata port

Maintenance dredging near the port entrance is expensive due to several reasons. The absence of operating Argentine dredgers in this region results in high start-up costs for dredging works due to long sailing time. In addition, the frequent rough wave conditions lead to non-workable days and therefore higher prices. Besides that, dredging near the breakwater is deceptive, needs to be executed very carefully, and therefore takes more time. In addition, during dredging in the access channel the ship traffic and the dredger(s) interfere with each other, leading to delays of both.

In 1998 the last capital dredging took place by dredging 3 million m³ solid material in the port and entrance and basins (La Capital, 2009). In 2004, 2006 and 2007 three different dredgers dredged amounts of around 150,000 m³ with a small and short lasting effect (section 3.8)

In April 2009, the National Directorate of Waterways (DNVN) purchased and repaired a trailing suction hopper dredger with a hopper capacity of 2,000 m³ (Koorevaar, Van den Akker, & Tilman, 1994) (Photograph 1.3). From August 2009, this dredger was dedicated to the port of Mar del Plata for two years with the main task to enable the access of container

vessels of 150 m trough the secondary channel. Its secondary tasks were dredging the port basins and to restore the former primary channel. At that time, the estimated amount of solid material to be dredged was (again) 3 million m³ (Ahorainfo, 2009).



Photograph 1.3 Mendoza 259 C - Dredger dedicated to port of Mar del Plata

From the start, this dredger was out of order due to various technical problems for several periods. Currently this dredger has been out of order for more than one year and there is not enough money available to repair it.

During repair periods of the dredger, the absence of dredging activities led to numerous unsafe situations for container ships that import and export (fish) products and prevented them from entering the port. Due to this, large shipping companies Hamburg Süd and Maersk have decided to stop berthing their ships at the Mar del Plata port. (Murias, 2009a, 2009b, 2009c, 2010a, 2010b, 2010c, 2012). Therefore, local companies are forced to transport their goods by trucks to the port of Buenos Aires, before they can be exported. This considerably increases the costs of transport, security, insurance and port services (La Capital, 2012).

1.2 Significance of this study

In November 2008, prof. L.C. van Rijn of Deltares (Independent knowledge institute on water soil, subsurface and infrastructure, based in The Netherlands) was invited to visit the Mar del Plata port to diagnose the problems and to advise about possible solutions. Van Rijn (2008) mentioned various methods to reduce the sedimentation processes and associated dredging. To better estimate the dredging volumes and to make an optimum design of the measures Van Rijn advised to perform a numerical model study of the currents, waves, sand transport, and sedimentation processes in the area of the harbour basin using a numerical modelling package. Subsequently the Fundación Bolsa de Comercio de Mar del Plata¹ commissioned Deltares to supervise a M.Sc. thesis study to analyse and evaluate different measures to improve the accessibility for larger vessels and limit the sedimentation in the port entrance.

This project has an importance for all stakeholders in the port of Mar del Plata. Improvement of the accessibility for larger vessels will significantly lower the (transport) costs for in- and export goods and results in more income and new investments in port activities and

¹ The **Foundation of the Chamber of Commerce of Mar del Plata** has the aim to promote and facilitate research oriented to the improvement of the social economic system with the purpose of management to the benefit of the community.

infrastructure. Measures that reduce the sedimentation rates in the navigation channel will lead to a considerable reduction of maintenance costs.

1.3 Objectives

The overall objective of this M.Sc. study is to identify the most promising safe and economic solution, which warrants the safe access of vessels with a length of 150 m, a beam of 20 m, and a maximum draft of 30 feet (9.15 m) under non-storm conditions.

Sub objectives are:

1. To restore the original main straight access channel with (leading line of 238°20' with respect to north and 100 m wide) with a new depth of 11.6 m to LAT (DNVN, 2011) and to estimate the maintenance dredging quantities involved.
2. To determine measures which reduce the cost of dredging by reducing: the quantities, frequency, disturbance, and risk of maintenance dredging.

The present study forms a follow up on the studies of Van Rijn (2008), Boer, De Jonge, Uit het Broek, et al. (1997), and the studies summarised by Lagrange (1993), with focus on a quantitative evaluation of measures to limit the sedimentation in the entrance channel by applying state-of-the-art numerical modelling. Available data is used to validate the model focusing on sediment transport. The study included a visit to Argentina for two weeks for local data collection, meetings, and discussions with stakeholders, site recognition, and to perform field measurements to obtain nearshore field data for model validation and understanding the local system. Based on initial sediment transport computations, the most promising types of solution are presented and qualitatively discussed. The results of this study can serve to support further detailed morphodynamic and design studies.

Therefore the main question for this study is: *What are the most promising feasible measures that: improve the accessibility of the port, reduce the costs of maintenance, and what are the estimated effects and costs of these measures?*

1.4 Methodology

To be able to carry out a comprehensive study on sedimentation in the port access of Mar del Plata, the following tasks are defined:

- A. Literature review
- B. Data review
- C. Data collection
- D. Generation of alternative measures
- E. Model of present situation
- F. Modelling impact of alternative measures
- G. Cost estimation

A. Literature review

A literature review has been carried out to acquire more insight in the characteristics and historic development of the coast around Mar del Plata and the physical processes and phenomena influencing it. In addition, the processes that can influence the accessibility of the port are identified.

B. Data review

A data assimilation and review is performed to gain insight in the local system and to be able to set up a hydrodynamic and sediment transport model. This is done by analysing and prioritizing the quality of available data from different stakeholders, scientific and engineering reports and papers, and internet sources. Missing data is identified and required additional field campaigns are specified.

C. Data collection

During a field trip of two weeks in the province of Buenos Aires, different meetings took place with local experts, authorities, stakeholders and the Foundation of the Chamber of Commerce of Mar del Plata. These meetings were set up to:

- Present the M.Sc. study;
- Collect up-to-date data or references to data sources;
- Collect local knowledge and experiences;
- Inventarise present and future policies;
- Discuss about the different possibilities.

To collect unavailable needed field data, different field measurements are performed:

- Bathymetric survey to obtain near shore depth soundings;
- Collection and analysis of beach and bottom sediment samples to determine the sediment characteristics;
- Drifter tracking to estimate the magnitude and direction of tidal currents near the port entrance over time.

Another objective of the field trip was site recognition by taking photographs and notes of present state and relevant features that can be of importance for this study.

D. Generation of alternative measures

Theoretical solutions are discussed and selected for further study, taking into account the opinions of experts and stakeholders.

E. Model of present situation

The yearly-averaged nearshore wave climate is derived from offshore wave data, wind data, and bathymetric data using a Delft3D-WAVE model.

A local hydrodynamics and sediment transport model is set up using Delft3D-FLOW, which is validated using the available present and historical data. The local physical processes influencing the accessibility of the port are identified and quantified from this model.

F. Modelling impact of alternative measures

Each different measure is separately tested in the hydrodynamics and sediment transport model with the bathymetry of the preferred navigation channel. From these model results, the initial sediment transports for each measure are calculated and the frequency and quantification of needed maintenance is estimated using historic frequent depth surveys.

G. Cost estimation

To compare the cost aspects of different solutions, the total costs of execution and needed future maintenance activities is roughly estimated using standard prices.

1.5 Reader

This report describes the approach and results of the subsequent research steps and is concluded by a discussion of the most promising solution and further recommendations.

Chapter 1. Introduction. In this introductory chapter, the problem definition, objectives, and methodology of this study are described.

Chapter 2. Literature review describes the evolution of the coast around Mar del Plata, ecologic values in this coastal area and the physical processes and phenomena influencing the accessibility of the port.

Chapter 3. Data collection and review. A data assimilation and review is carried out to analyse the quality of available data from different sources to be able to set up a numerical model. This chapter gives an overview of the available data. Missing data is identified and additional field measurements and calculations are reported.

Chapter 4. Potential measures to reduce sedimentation in port entrance. This section discusses all potential measurements and is concluded by a selection of the best alternatives for further study.

Chapter 5. Near shore wave modelling Buenos Aires: Depicts the set-up and results of a numerical wave model to compute the nearshore wave climates.

Chapter 6. Setup hydrodynamics & sediment transports model: Illustrates the set-up of a numerical model to identify and quantify the physical processes influencing the accessibility of the port of Mar del Plata.

Chapter 7. Analysis and validation of 2012 hydrodynamics & sediment transports model. In this chapter, the effect of tidal flows, effects of waves from different directions and sediment transport in the 2012 situation estimated by the numerical model are analysed and compared to field data.

Chapter 8. Evaluation effects of measures expounds the resulting sedimentation rates in the port entrance for each measure compared to the sedimentation rates after dredging without additional measures. Subsequently, the total costs of construction per measure and the resulting need for maintenance dredging is estimated and compared.

Chapter 9. Conclusions, discussion and recommendations: This report is concluded by a discussion of the most promising solutions and general recommendations and recommendation for further research.

2 Literature review

2.1 Characteristics of the coastal area

2.1.1 Geomorphologic evolution

The east coast of South America is categorised as “trailing edge coast”, because it is situated at the trailing edge of a continent with a collision coast (Figure 2.1). This coast is actively modified by the depositional products and erosional effects from an extensive area of high interior mountains. From all trailing edge coasts, this so-called Amero-trailing edge coast has the lowest lying coastal landforms and the widest continental shelves (> 50 km) (Inman & Nordstrom, 1971).

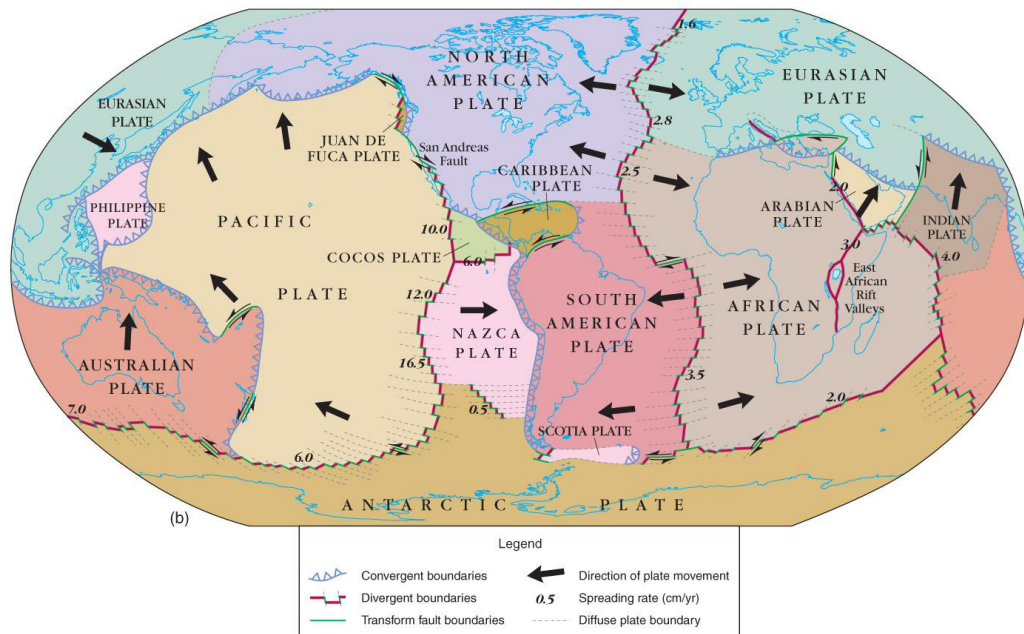


Figure 2.1 Tectonic plate movement (Tarbuck, Lutgens, & Tasa, 2011)

For 150 million years, the large river systems of South America (Figure 2.2) have been depositing sediment near their mouths. This resulted in broad, low relief coastal plains on the landward side and, on the seaward side shallow gently sloping continental shelves. Large mid-ocean waves lose energy as they progress across the shelf. (d Angremond & Pluim-Van der Velden, 2001).

The coastal area which is studied, is situated between Mar Chiquita, 33 km northeast, and Miramar, 38 km southwest of Mar del Plata. Charts of this area are shown in appendix 10.



Figure 2.2 River systems of South America (EnchantedLearning.com, 2012)

During the last Pleistocene transgression, seawaters covered the north-eastern region of Buenos Aires province reaching about 10 m above present mean sea level (Figure 2.3A).

After a regression (fall in sea level) another transgression took place and established barrier islands in the northern region about 6890 y B.P. In the southern region the now-eroded point (Figure 2.3B) was beginning to be eroded by waves. This gave rise to asymptotic ridges located south-westward into Mar Chiquita lagoon and a hooked-spit deposit to the northeast (Punta Rasa).

After a minor regression to 1.5 m above MSL (Figure 2.3C), spit building continued in the southern as well as in the northern regions.

Finally, a slight regression (fall in sea level and progradation) down to the present level (Figure 2.3D) created the barrier spit sector which prograded to the north but was eroded simultaneously in the south. The southern sector (Mar Chiquita area) began to be eroded at the same time that the drift to the north became predominant and lead to progradation in the area between Punta Medanos and Punta Rasa. (Codignotto & Aguirre, 1993)

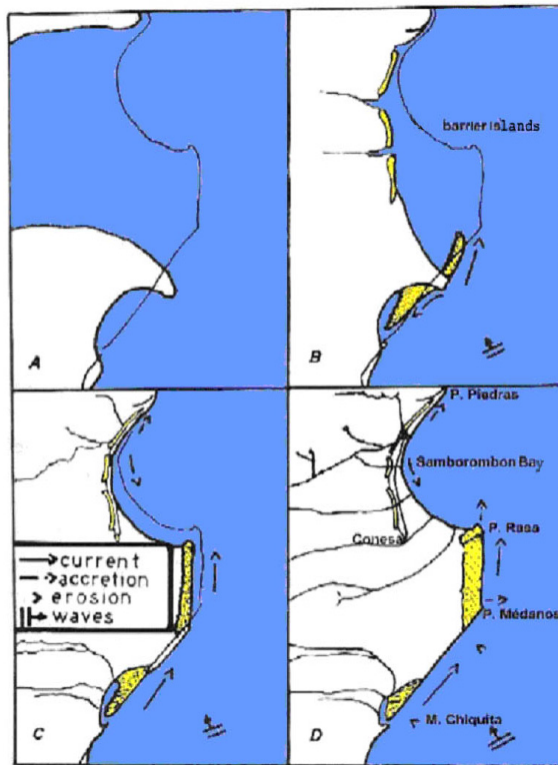


Figure 2.3 Coastal evolution north-eastern region of Buenos Aires province (Codignotto & Aguirre, 1993)

- Thin line represents the present shoreline
- A. Older than 7000 y B.P.; sea level 10 m above present MSL
 - B. 6000 y B.P.; sea level 5 m above present MSL
 - C. 3000-3500 y B.P.; sea level 5 m above the present.
 - D. Present shoreline



Photograph 2.1 Cliffs south of Mar del Plata

Mar del Plata is located on the foothills of the Tandilia Range, which continues northwest to Olavarría (Figure 2.4). Hence, the sandy has some "rocky" hardly-erodible lower Palaeozoic quartzites headlands such as at Punta Hermengo in Miramar and Punta Mogotes, and Cabo Corrientes in Mar del Plata. Near the city centre of Mar del Plata, pocket beaches are formed between these capes.

At both sides of the city, the coasts consist of Pleistocene, poorly consolidated, loess cliffs of up to 30 m high with narrow beaches of less than 40 m wide. (Crossland, Kremer, Lindeboom, Marshall Crossland, & Le Tissier, 2005)

At Lagoon Mar Chiquita and at Miramar there are large extensive dune fields. These dune fields are relatively new, since they have been formed as consequence of a Holocene sea level fluctuation (Bértola, 2006).

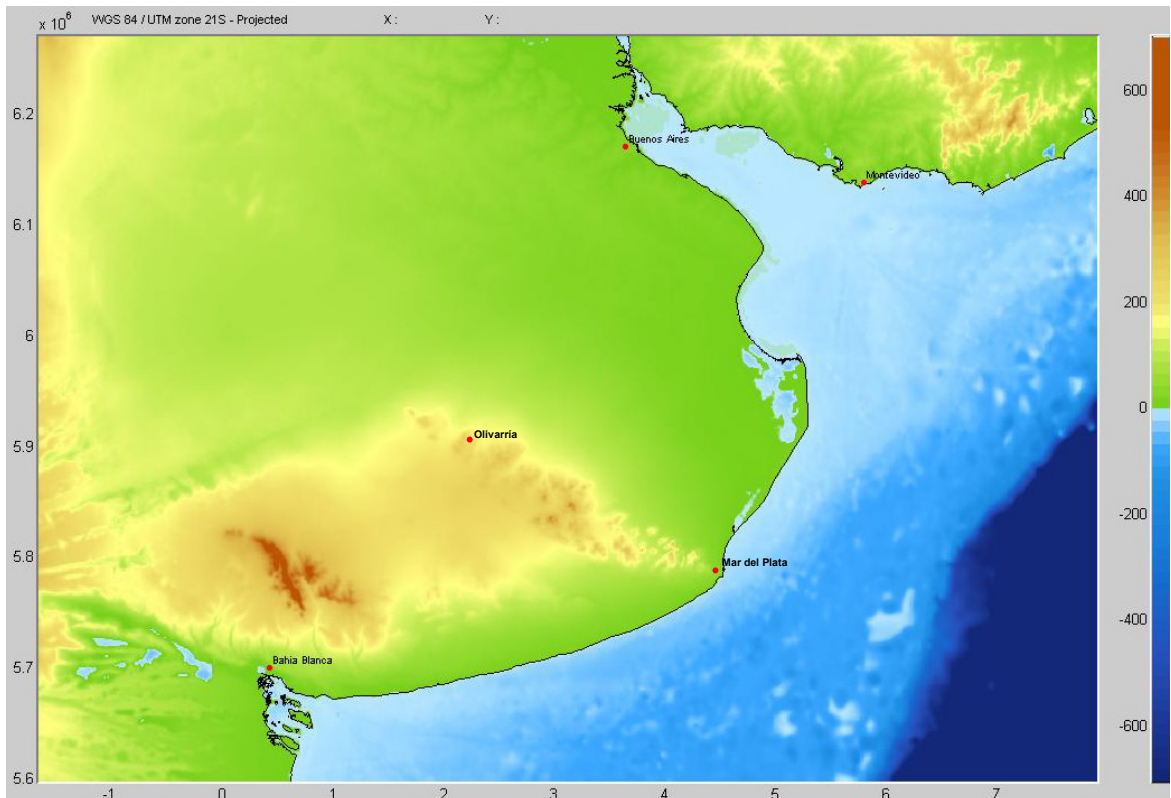


Figure 2.4 Geographic map of north of Buenos Aires province (GEBCO, 2011)

2.1.2 Morphologic developments in recent centuries

At the end of the 19th century, people started to use the beaches and dunes. As a consequence of construction of buildings and planting more vegetation, the dunes southwest of Miramar became more fixated (Isla, 2012). For the construction of large parts Mar del Plata, founded in 1874, sand was mined south of Punta Mogotes (Algera, Burger, Hartog, & De Rijke, 2004).

Shortly after the construction of the port of Mar del Plata, in 1922, a dissipative beach started to build to the south (Punta Mogotes Beach) and the large shoal formed in the port entrance. At the same time, considerable erosion occurred on most beaches north of the port.

Sand retention on the northern beaches of Mar del Plata became a priority for local and provincial authorities, with construction of a series of groins and breakwaters. As more sand was retained by the urban beaches, erosion extended to beaches further north and cliffs were exposed to wave attack, started to retreat and endangered houses, highway infrastructure and beach tourism. Finally, protective rock constructions were built from Mar del Plata to the mouth of Mar Chiquita lagoon, 40 km north (Lagrange, 1993).



Photograph 2.2 Eroded beach and dunes at Mar del Tuyu Photograph 2.3 Execution of beach and cliff protection works south of Mar del Plata

Last decades, the input of sediment in the coastal area is reduced even further by the construction of many hydropower river dams in the south of Argentina (Algera et al., 2004).

In 1998, Mar del Plata city and harbour authorities executed the first beach nourishment in this coastal area. Capital dredging of the harbour mouth produced coarse to very coarse sand that was pumped to Playa Grande, Varese, and Bristol. Unfortunately, a few months after the nourishment, a major storm produced flooding in the city and river flows from the hills that severely eroded the beaches and moved sand offshore. (Crossland et al., 2005).

2.1.3 Ecology

The continental shelf accommodates a large variety of fish species, with several species of commercial interest. The coast serves as spawning area for most of these species. Three species of large mammals inhabit the area:

- The South American Sea-Lion, *Otaria Byronia*. In spring and summer up to 500 male sea lions reside in the Reserva de Lobos Marinos, which is located inside the port area (Photograph 2.4).
- The South American Fur Seal, *Arctocephalus Australis*. Up to 50 male fur seals on Banco de Pescadores.
- The Southern Right Whale, *Eubalaena Australis*.



Photograph 2.4 Sea-Lions inside Mar del Plata port

The high natural turbidity of the seawater leaves the sandy sea bottom devoid of any seabed vegetation.

Along the rocky shores and inside the port especially the barnacle, *Balanus Glandula*, which originates from North America, is very abundant. In front of the port of Mar del Plata, (exploited) mussel banks, *Mytilus Edulis*, are located.

The lagoon of Mar Chiquita (46 km²) is the lagoon in Argentina in open connection with the Atlantic Ocean. It is an important nature reserve because of its function for migratory birds. (Boer, De Jonge, Brouwer, et al., 1997)



Photograph 2.5 Flamingos in Mar Chiquita Lagoon

2.2 Processes influencing the accessibility of the port

Sediments (mud, silt, and sand) stirred up from the bed elsewhere can be transported to the port entrance by wave induced longshore currents, tidal currents and horizontal circulation. On the leeside of the breakwaters, the wave height generally decreases rapidly resulting in a reduction of the sediment transporting capacity and hence in sedimentation in the entrance area, which may be problematic with respect to navigation.

From theory, sedimentation in the port basins, entrance and access channel can be caused by the following main processes (Van Rijn, 2005):

- Sediments supplied due to wave action from the south-western quadrant deposits at the (shadow) zone behind the tip of the breakwater due to a sudden reduction in transport capacity by reduced wave action.
- Sediments supplied from upstream (bypassing) during a northward littoral drift entering the entrance through exchange (eddies, density currents) processes in the entrance area (red in top of Figure 2.5);
- Sediments supplied from upstream (bypassing) currents during a southward littoral drift directly entering the entrance area (middle of Figure 2.5);
- Sediments supplied from downstream during a northward littoral drift by recirculation currents near the downstream shore (green in top of Figure 2.5);
- Sediments supplied by diffractive wave effects around the tip of the breakwaters (bottom of Figure 2.5);
- Bars migrating along the harbour entrance (bypassing).
- Water and sediments supplied through permeable (not sand tight) structures.
- Sediments supplied from upstream (bypassing) settle in dredged channels in the littoral zone, due to the local reduction of wave action, flow velocities, and therefore reduced transport capacity.
- Sediment supplied from rivers/drainage systems discharging into the port

Some processes can erode areas in and around and improve/maintain the accessibility of the port:

- Scour due to propeller jets and return currents of ships.
- Scour due to flow contraction of (tidal) currents, for instance between the tips of the breakwaters.
- Scour holes caused by eddies around obstacles, for instance around the tip of a breakwater.

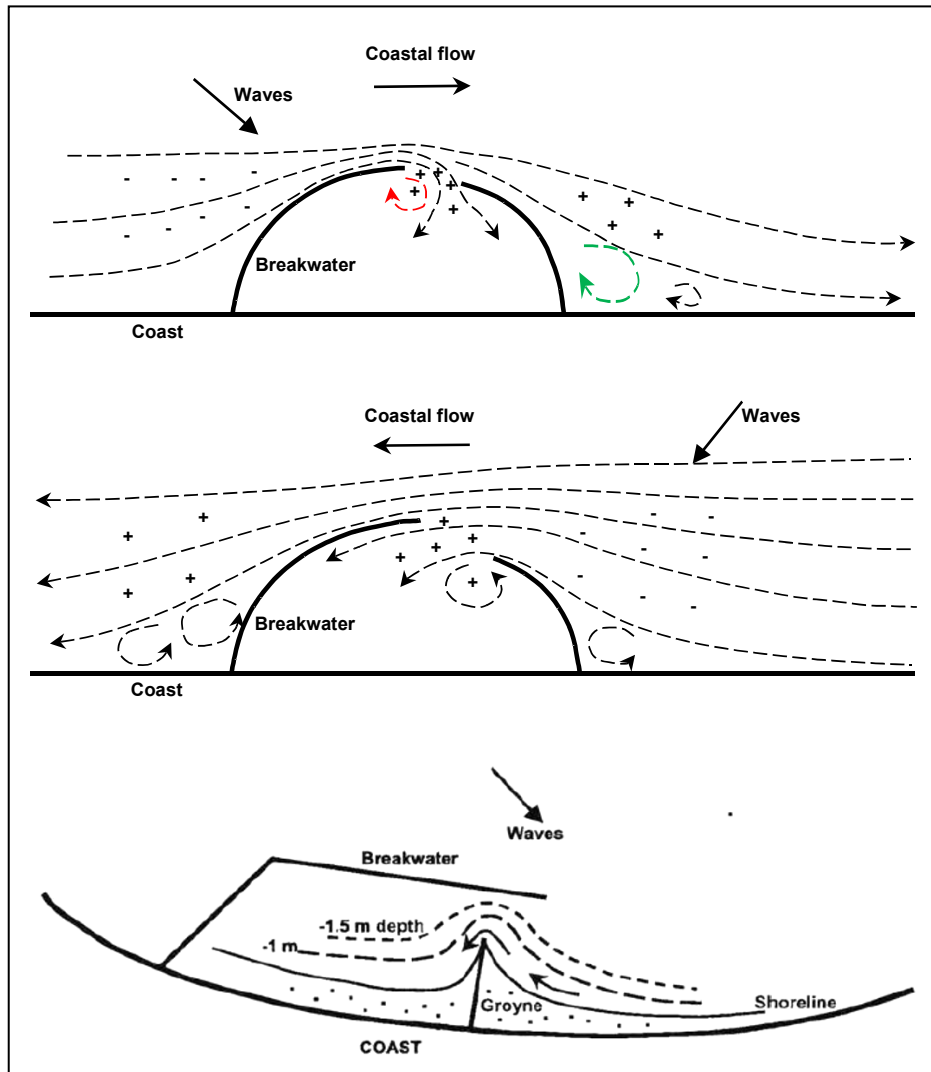


Figure 2.5 Basic sedimentation processes in port entrance (Van Rijn, 2005)

3 Data collection and review

A data assimilation and review is carried out to analyse and prioritise the quality of available data from different stakeholders, scientific papers, engineering reports, and internet sources.

During a two-week field trip in the province of Buenos Aires, different field measurements have been carried out to collect unavailable data:

- Bathymetric survey to obtain near shore depth soundings;
- Drifter tracking to estimate the magnitude and direction of tidal currents near the port entrance.
- Collection and analysis of beach and bottom sediment samples;

3.1 Wave climate

For the coast between Miramar and Mar Chiquita, little (reliable) wave data is available to determine a near shore wave climate. The available data consists of pressure sensor data near Mar del Plata, offshore visual ship observations and offshore numerical wave hindcast data.

3.1.1 Pressure sensor data

Sunrise Technical Consultants (1968) performed wave measurements for 1.5 year using a pressure sensor, moored at a depth of 11.5 m and located 500 m seaward the port entrance. The angle of approaching wave fronts was measured with respect to the north using an engineer's transit placed at the end of the southern groin. Measurements were taken four times a day and each one of them took 20 minutes, resulting in 2176 measurements (as cited in Lanfredi, Pousa, Mazio, & Dragani, 1992) (Table 3.1). From this study, no wave period information was reported or available.

| | | Mean wave direction (with respect to north) | | | | | | | | | | | | | | | | | | | | |
|--------------------------------|---------|---|---------|---------|---------|---------|---------|----------|-----------|-----------|-----------|-----------|-----------|-----------|-----------|-----------|-----------|-----------|-----------|-----------|-----------|--------|
| | | 35°-45° | 45°-55° | 55°-65° | 65°-75° | 75°-85° | 85°-95° | 95°-105° | 105°-115° | 115°-125° | 125°-135° | 135°-145° | 145°-155° | 155°-165° | 165°-175° | 175°-185° | 185°-195° | 195°-205° | 205°-215° | 215°-225° | 225°-235° | |
| Significant wave height (in m) | >2.5 | 0,00 | 0,00 | 0,00 | 0,00 | 0,00 | 0,00 | 0,23 | 0,09 | 0,00 | 0,09 | 0,14 | 0,00 | 0,09 | 0,00 | 0,00 | 0,05 | 0,00 | 0,00 | 0,00 | 0,00 | 0,69 |
| | 2.0-2.5 | 0,00 | 0,00 | 0,00 | 0,00 | 0,05 | 0,05 | 0,09 | 0,18 | 0,18 | 0,14 | 0,14 | 0,32 | 0,14 | 0,00 | 0,09 | 0,09 | 0,00 | 0,00 | 0,00 | 0,00 | 1,47 |
| | 1.5-2.0 | 0,00 | 0,00 | 0,00 | 0,14 | 0,18 | 0,14 | 0,37 | 0,51 | 0,32 | 0,97 | 0,74 | 1,38 | 0,64 | 0,69 | 0,28 | 0,28 | 0,00 | 0,00 | 0,00 | 0,00 | 6,62 |
| | 1.0-1.5 | 0,09 | 0,23 | 0,46 | 1,01 | 0,74 | 0,97 | 1,24 | 1,56 | 2,39 | 3,13 | 3,77 | 2,44 | 2,44 | 1,79 | 1,29 | 0,60 | 0,23 | 0,05 | 0,00 | 0,05 | 24,45 |
| | 0.5-1.0 | 0,46 | 1,61 | 1,42 | 4,14 | 4,55 | 3,03 | 5,10 | 5,70 | 5,47 | 6,11 | 4,09 | 2,76 | 2,34 | 2,11 | 1,15 | 0,74 | 0,46 | 0,18 | 0,05 | 0,05 | 51,52 |
| | 0-0.5 | 0,18 | 0,32 | 0,64 | 1,65 | 1,10 | 0,87 | 0,51 | 1,52 | 2,16 | 2,16 | 1,75 | 0,78 | 0,64 | 0,46 | 0,41 | 0,05 | 0,00 | 0,05 | 0,00 | 0,00 | 15,26 |
| | | 0,74 | 2,16 | 2,53 | 6,94 | 6,62 | 5,06 | 7,54 | 9,56 | 10,52 | 12,59 | 10,62 | 7,67 | 6,30 | 5,06 | 3,22 | 1,79 | 0,69 | 0,28 | 0,05 | 0,09 | 100,00 |
| | | Total | | | | | | | | | | | | | | | | | | | | |

Table 3.1 Annual directional distribution of wave heights derived from Sunrise Technical Consultants (1968) (as cited by Boer, De Jonge, Brouwer, et al., 1997)

3.1.2 Visual ship observations

Waterman (1994) published a directional distribution wave heights in which wave periods were split into two classes, i.e. wind waves and swell (Figure 3.1), based on an unreported number of ship observations between lat. 36°S to 42°S and long. 53°W to 58°W from The Met Office (1994).

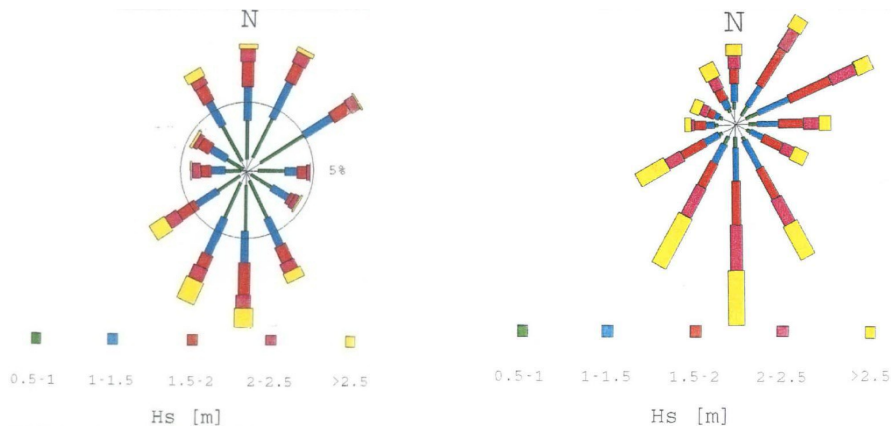


Figure 3.1 Directional distribution of wind waves (left) and swell waves (right) (The Met Office, 1994; as cited by Waterman, 1994)

In the left figure, for wind waves, two major wave directions can be observed: from the south and the north-northeast. In the directional distribution of the swell waves, also two major wave directions can be observed of which the south direction is clearly dominant. Swell waves coming from these southern directions are significantly higher than the swell waves coming from the north-eastern directions.

The observation area spans 300 km to both the north and south of Mar del Plata and 400 km offshore and therefore it only gives an indication of the local conditions closer to Mar del Plata.

Algera et al. (2004) published more quantified wave statistics for a smaller area around Mar del Plata, based on the data of 3522 ship observations between lat. 37°S to 38.5°S and long. 54.8°W to 58°W (Figure 3.2). Table 3.2 and Table 3.3 are similar to the data of Waterman (1994), but (in this area) waves from north occur more often.

Mean wave direction (with respect to north)

| Significant wave height (in m) | Mean wave direction (with respect to north) | | | | | | | | Total |
|--------------------------------|---|----------------|----------------|------------------|-----------------|------------------|-----------------|------------------|--------|
| | N 337.5°-22.5° | NE 22.5°-67.5° | E 67.5°-112.5° | SE 112.5°-157.5° | S 157.5°-202.5° | SW 202.5°-247.5° | W 247.5°-292.5° | NW 292.5°-337.5° | |
| >6.25 | 0,00 | 0,00 | 0,03 | 0,00 | 0,00 | 0,00 | 0,00 | 0,00 | 0,03 |
| 5.25-6.25 | 0,00 | 0,00 | 0,00 | 0,00 | 0,03 | 0,00 | 0,06 | 0,00 | 0,09 |
| 4.25-5.25 | 0,06 | 0,03 | 0,11 | 0,00 | 0,26 | 0,06 | 0,11 | 0,03 | 0,65 |
| 3.25-4.25 | 0,06 | 0,23 | 0,11 | 0,20 | 0,60 | 0,45 | 0,14 | 0,06 | 1,85 |
| 2.75-3.25 | 0,26 | 0,40 | 0,31 | 0,54 | 1,39 | 0,60 | 0,23 | 0,20 | 3,92 |
| 2.25-2.75 | 0,60 | 0,48 | 0,26 | 0,57 | 2,10 | 0,94 | 0,45 | 0,31 | 5,71 |
| 1.75-2.25 | 1,28 | 1,68 | 1,56 | 1,11 | 4,29 | 1,50 | 0,85 | 0,37 | 12,63 |
| 1.25-1.75 | 2,61 | 2,56 | 2,04 | 2,04 | 5,08 | 2,30 | 1,19 | 1,02 | 18,85 |
| 0.75-1.25 | 4,17 | 4,71 | 2,92 | 2,81 | 6,08 | 3,09 | 1,79 | 1,82 | 27,40 |
| 0.25-0.75 | 4,49 | 4,12 | 2,27 | 1,90 | 3,01 | 2,16 | 2,39 | 2,30 | 22,63 |
| 0-0.25 | 2,19 | 0,80 | 0,48 | 0,34 | 0,74 | 0,60 | 0,60 | 0,51 | 6,25 |
| Total | | | | | | | | | 100,00 |

Table 3.2 Directional distribution of wave heights derived from Algera et al. (2004)

Mean wave period (in s)

| Significant wave height (in m) | Mean wave period (in s) | | | | | | | | | | Total |
|--------------------------------|-------------------------|---------|---------|----------|-----------|-----------|-----------|-----------|-----------|-------|--------|
| | 3.5-5.5 | 5.5-7.5 | 7.5-9.5 | 9.5-11.5 | 11.5-13.5 | 13.5-17.5 | 15.5-17.5 | 17.5-19.5 | 19.5-21.5 | >21.5 | |
| >6.25 | 0,03 | 0,00 | 0,00 | 0,00 | 0,00 | 0,00 | 0,00 | 0,00 | 0,00 | 0,00 | 0,03 |
| 5.25-6.25 | 0,00 | 0,03 | 0,06 | 0,00 | 0,00 | 0,00 | 0,00 | 0,00 | 0,00 | 0,00 | 0,09 |
| 4.25-5.25 | 0,03 | 0,11 | 0,20 | 0,20 | 0,09 | 0,03 | 0,00 | 0,00 | 0,00 | 0,00 | 0,65 |
| 3.25-4.25 | 0,11 | 0,91 | 0,34 | 0,20 | 0,17 | 0,11 | 0,00 | 0,00 | 0,00 | 0,00 | 1,85 |
| 2.75-3.25 | 0,57 | 1,96 | 0,80 | 0,28 | 0,17 | 0,14 | 0,00 | 0,00 | 0,00 | 0,00 | 3,92 |
| 2.25-2.75 | 1,62 | 2,24 | 1,02 | 0,51 | 0,14 | 0,14 | 0,00 | 0,00 | 0,03 | 0,00 | 5,71 |
| 1.75-2.25 | 4,32 | 4,49 | 2,21 | 0,99 | 0,40 | 0,14 | 0,03 | 0,00 | 0,06 | 0,00 | 12,63 |
| 1.25-1.75 | 8,26 | 5,99 | 2,41 | 0,85 | 0,60 | 0,51 | 0,06 | 0,14 | 0,03 | 0,00 | 18,85 |
| 0.75-1.25 | 18,09 | 4,83 | 1,85 | 1,14 | 0,74 | 0,54 | 0,06 | 0,17 | 0,00 | 0,00 | 27,40 |
| 0.25-0.75 | 18,23 | 2,13 | 0,82 | 0,82 | 0,31 | 0,17 | 0,00 | 0,09 | 0,06 | 0,00 | 22,63 |
| 0-0.25 | 5,59 | 0,20 | 0,09 | 0,28 | 0,00 | 0,03 | 0,00 | 0,00 | 0,06 | 0,00 | 6,25 |
| Total | | | | | | | | | | | 100,00 |

Table 3.3 Joint probability of occurrence of wave heights vs. wave periods derived from Algera et al. (2004)

From the original data, provided by Algera et al. (2004), the seasonal variation of dominant mean wave directions is derived (Table 3.4). It can be seen that in summer, waves from northeast occur as frequent as waves from the south, but in winter, the north-eastern waves are much less dominant. According to Fiore, D’Onofrio, Pousa, Schnack, and Bértola (2009), also the largest number of storm events occur in these winter months.

Mean wave direction

| | N | NNE | NE | ENE | E | ESE | SE | SSE | S | SSW | SE | WSW | W | WNW | NW | NNW |
|--------------------|-----|------|------|-----|-----|-----|-----|-----|------|-----|-----|-----|-----|-----|-----|-----|
| Winter (Jun.-Aug.) | 9,0 | 5,3 | 6,1 | 3,1 | 4,4 | 2,9 | 4,9 | 6,9 | 12,4 | 7,2 | 8,8 | 6,7 | 7,1 | 4,4 | 6,3 | 4,6 |
| Spring (Sep.-Nov.) | 7,8 | 7,9 | 10,3 | 5,7 | 6,7 | 4,2 | 8,7 | 6,0 | 13,9 | 8,3 | 5,9 | 3,7 | 2,4 | 2,5 | 3,0 | 2,9 |
| Summer (Dec.-Feb.) | 9,5 | 10,4 | 14,9 | 6,8 | 6,1 | 2,8 | 5,9 | 5,6 | 14,9 | 7,2 | 5,8 | 2,7 | 1,2 | 1,1 | 2,5 | 2,5 |
| Autumn (Mar.-May) | 9,0 | 5,6 | 8,3 | 3,5 | 3,6 | 3,3 | 6,2 | 7,0 | 13,3 | 8,0 | 8,0 | 5,0 | 5,0 | 3,7 | 5,6 | 4,8 |

Table 3.4 Seasonal variation in distribution of mean wave directions

3.1.3 Numerical wave hindcast data

More detailed offshore wave hindcast data over a longer period was available from archived wave hindcasts reanalysis using the NOAA WAVEWATCH III (NWW3) global wave model (NOAA/NWS/NCEP, 2011). NWW3, a third generation wind wave spectral model, is the operational wave-forecasting model of the U.S. National Oceanic and Atmospheric Administration (NOAA). The global wave model covers the 'wet' areas around the globe from 77°S to 77°N with a 1° resolution in latitude and 1.25° resolution in longitude. To hindcast historical wave fields at 3-hour intervals, the global model is forced using archived reanalysed 10 m winds from the Global Forecast System (GFS) from February 1997 to September 2010 (EMC/MMAB, 2009).

For every model grid point, the available parameters are:

H_s : Significant heights of wind waves and swell (in m)

T_p : Peak wave period (in s)

D_p : Average wave direction at the peak period (oceanographic convention: towards, in degrees clockwise from geographic north)

$U_{10}(u,v)$: Easterly and northerly component of 10 m wind velocity from GFS (in m/s)

The global NWW3 model cannot be realistically applied to coastal regions with horizontal scales less than 20-30 km and water depth less than 20-30 m, because not all shallow water effects are included and because the computation would be prohibitive intensive when applied to such small-scale (Booij, Ris, & Holthuijsen, 1999). Therefore, the wave data at grid points on < 25 m water depth (white in Figure 3.2) must be ignored (EMC/MMAB, 2009).

On deeper water the difference between wave data from NWW3 and wave buoy observations seem to be relatively small; in the order of 1% (Spindler & Tolman, 2008, 2010). In combination with corresponding wind data and bathymetric, the offshore wave data can serve as input for computation of near shore wave climates (described in chapter 5).

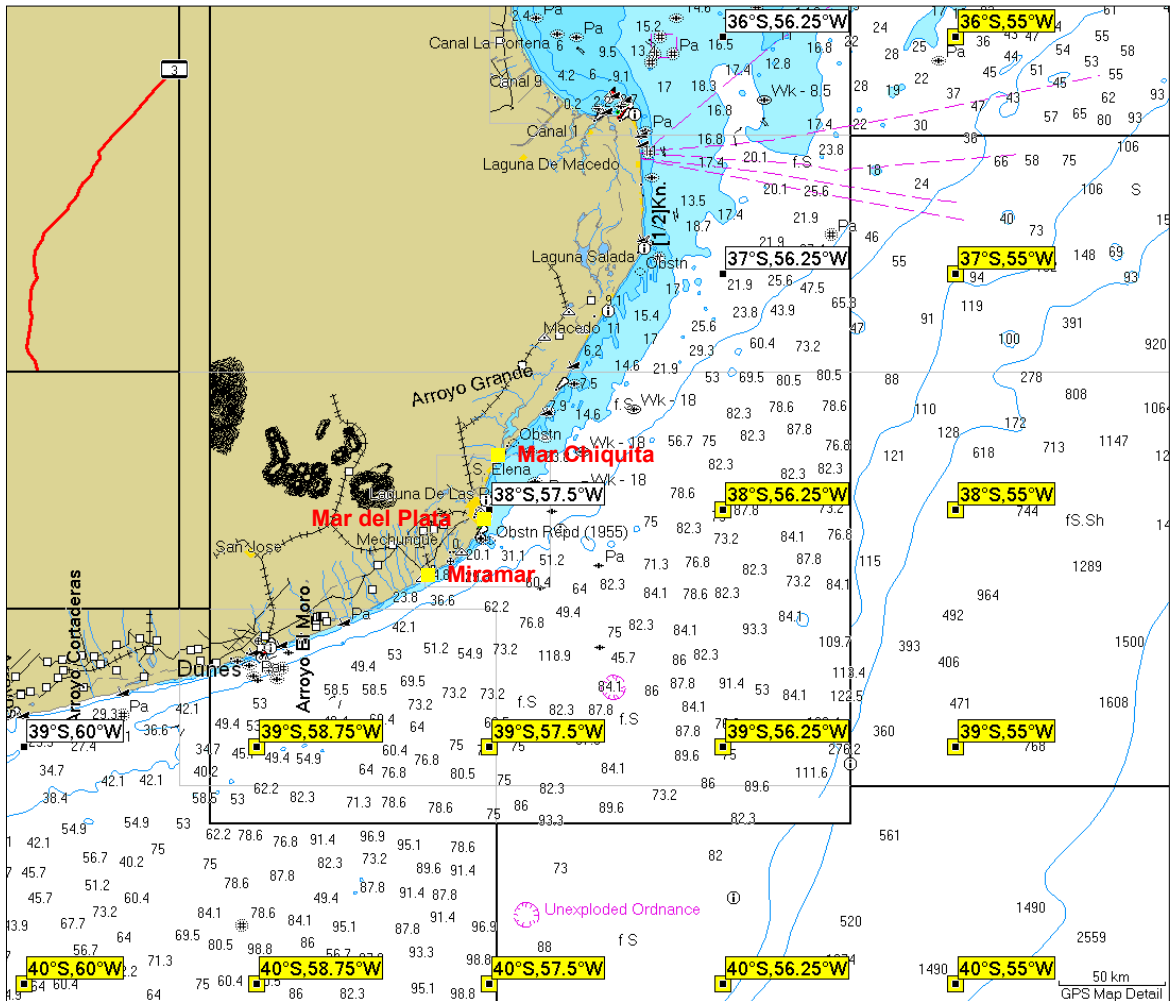


Figure 3.2 NWW3 model grid points on nautical chart (UKHO, 2006b, 2006c, 2006d, 2006e).
 Yellow points on > 25 m water depth, white points on < 25 m water depths (ignored)

For the deeper water model grid points around Mar del Plata (yellow in Figure 3.2), the 3-hourly time series of all available parameters from February 1997 to September 2010 (39,921 time steps) is extracted from the archived NWW3 data. The determination and visualisation of the mean climates, are carried out using a MATLAB tool called ORCA, for analysis, classification and transformation of metocean data (Deltares Systems, 2011) and the corresponding guidelines (Caires & Van Os, 2011).

It can be seen in Figure 3.3 that offshore waves from the south-southwest and northeast are dominant and usually have heights between 1 and 2 metres. The highest waves (exceeding 4 meters) most often come from southern directions. Waves propagating from deep to shallower waters start refracting and due to this, further nearshore south(west) and east-northeast incoming wave directions have a larger frequency of occurrence.

Figure 3.4 shows that waves from southern directions often have larger wave periods (8-10 s) than waves from east-northeast (5-9 seconds). Waves coming from the south-easterly quadrant are a combination of longer swell waves and wind generated waves. Waves from the other three quadrants are wind-generated waves.

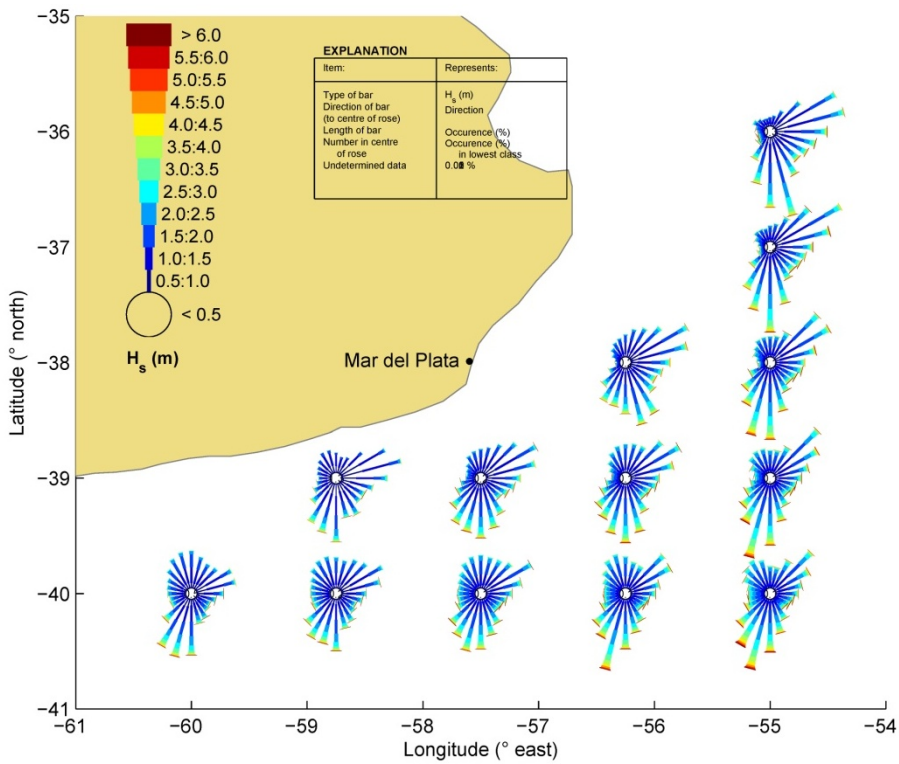


Figure 3.3 Directional distribution of wave heights from NWW3 hindcast (1997-2010)

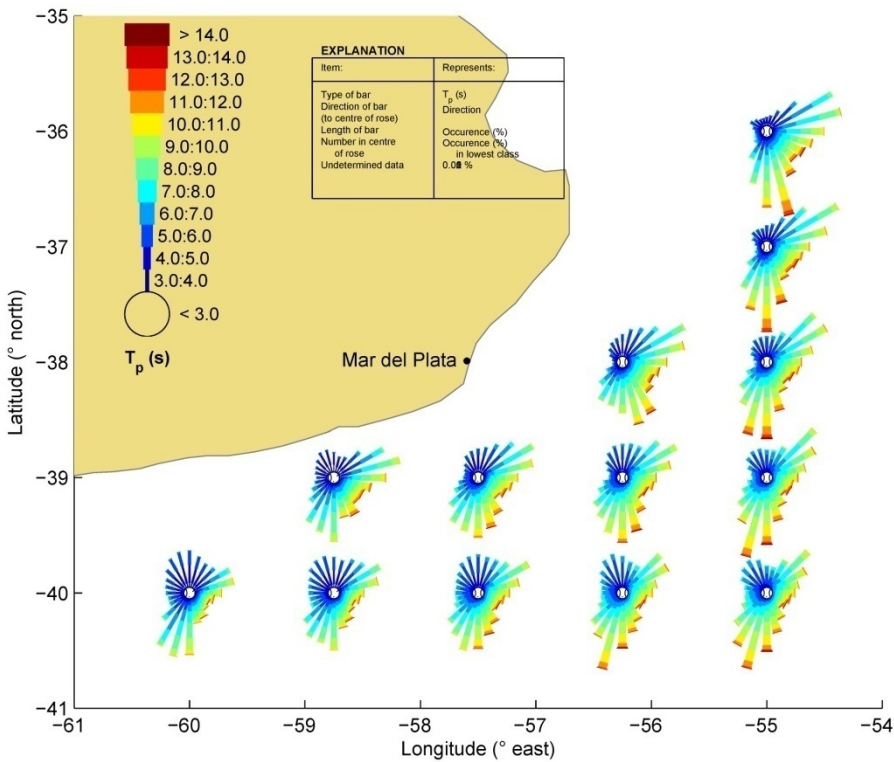


Figure 3.4 Directional distribution of peak wave periods from NWW3 hindcast (1997-2010)

3.2 Wind climate

Reanalysed 10 m winds from the Global Forecast System (GFS), are extracted from the NOAA WAVEWATCH III (NWW3) data and visualised using the ORCA tool (as described in section 3.1.3).

As showed in Figure 3.5 and Table 3.5, occurring winds are from all directions, having mean velocities within the range 4-9 m/s. Winds from the north quadrant are dominant, but the highest wind velocities are from the southwest quadrant.

Universidad Nacional de Córdoba (2007) analysed wind records between 1981 and 1990 at the airport of Mar del Plata and concluded that:

- During the summer months, winds reaches the highest average speeds (between 20 and 25 km/h) with predominant directions north, east and south, decreasing in order.
- During fall and winter, average speeds are 10 to 15% lower than in the summer, having west and north as dominant directions.
- In spring, the average speed increases again ranked among 18 and 24 km/h, having north as most dominant component.

A wind characteristic of Mar del Plata that deserves attention is the "Sea Breeze". Its main occurrence is in summer and the predominant direction is northeast. Usually it follows the following scheme: In the morning light winds from the continent. From noon, winds from the northeast sector, with peak frequencies and intensities at the end of the afternoon (sometimes reaching over 30 km/h). From sunset, winds finally decrease in intensity and turn to from continental sector again. (Universidad Nacional de Córdoba, 2007)

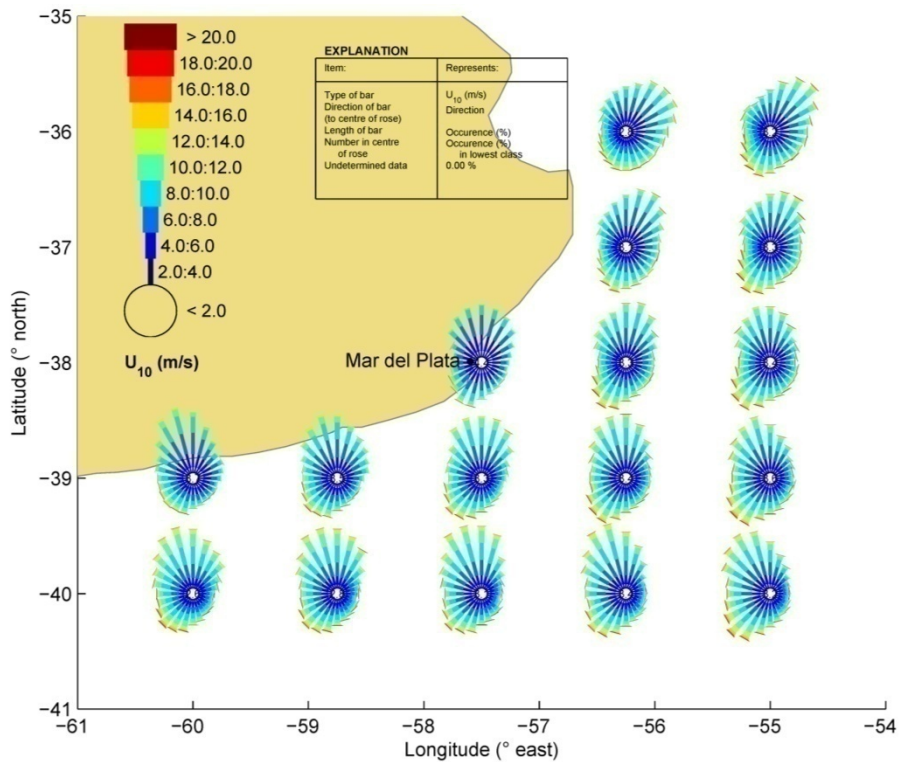


Figure 3.5 Directional distribution of winds from NWW3 model 1997-2010

| Wind magnitude | Wind direction | | | | | | | | | | | | | | | | | | | | Total | | | | | | | | | | | | | | | | | | | | | | | | | | | |
|----------------|----------------|----------|-----------|-----------|-----------|-----------|-----------|------------|-------------|-------------|-------------|-------------|-------------|-------------|-------------|-------------|-------------|-------------|-------------|-------------|-------|-------------|-------------|-------------|-------------|------|------|------|------|------|------|------|------|------|------|------|------|------|------|------|------|------|------|------|------|------|------|--------|
| | 352.5-7.5 | 7.5-22.5 | 22.5-37.5 | 37.5-52.5 | 52.5-67.5 | 67.5-82.5 | 82.5-97.5 | 97.5-112.5 | 112.5-127.5 | 127.5-142.5 | 142.5-157.5 | 157.5-172.5 | 172.5-187.5 | 187.5-202.5 | 202.5-217.5 | 217.5-232.5 | 232.5-247.5 | 247.5-262.5 | 262.5-277.5 | 277.5-292.5 | | 292.5-307.5 | 307.5-322.5 | 322.5-337.5 | 337.5-352.5 | | | | | | | | | | | | | | | | | | | | | | | |
| >20 | | | | | | | | | | | | | | 0.01 | | | | | | | | | | | | 0.01 | | | | | | | | | | | | | | | | | | | | | | |
| 19-20 | | | | | | | | | | | | | | 0.00 | | 0.00 | 0.00 | | | | | | | | | 0.01 | | | | | | | | | | | | | | | | | | | | | | |
| 18-19 | | | | | | | | | | | | | | 0.00 | 0.01 | 0.01 | | | | | 0.00 | | | | | 0.02 | | | | | | | | | | | | | | | | | | | | | | |
| 17-18 | | | | | | | | | 0.01 | | | | | 0.01 | | 0.01 | | | 0.00 | | | | | | | 0.02 | | | | | | | | | | | | | | | | | | | | | | |
| 16-17 | | | | | | | | 0.01 | 0.01 | 0.00 | 0.00 | 0.01 | 0.00 | 0.01 | 0.00 | 0.01 | 0.00 | 0.00 | | | 0.00 | | | | 0.04 | | | | | | | | | | | | | | | | | | | | | | | |
| 15-16 | | | | 0.01 | | | 0.00 | 0.00 | 0.01 | 0.01 | 0.01 | 0.00 | 0.00 | 0.02 | 0.02 | 0.01 | 0.01 | 0.00 | | | 0.00 | | | | 0.09 | | | | | | | | | | | | | | | | | | | | | | | |
| 14-15 | | | 0.00 | | | | 0.00 | 0.01 | 0.01 | | 0.01 | 0.02 | 0.02 | 0.03 | 0.04 | 0.02 | 0.02 | 0.01 | | | | | | | 0.19 | | | | | | | | | | | | | | | | | | | | | | | |
| 13-14 | | 0.01 | 0.00 | 0.01 | 0.01 | | 0.01 | 0.01 | 0.02 | 0.02 | 0.02 | 0.03 | 0.03 | 0.04 | 0.08 | 0.05 | 0.04 | 0.04 | 0.01 | | 0.00 | | | 0.01 | 0.40 | | | | | | | | | | | | | | | | | | | | | | | |
| 12-13 | | 0.02 | 0.03 | 0.01 | 0.02 | 0.01 | 0.01 | 0.02 | 0.03 | 0.05 | 0.04 | 0.03 | 0.04 | 0.10 | 0.14 | 0.08 | 0.09 | 0.04 | 0.03 | 0.00 | 0.00 | 0.02 | 0.01 | 0.02 | 0.81 | | | | | | | | | | | | | | | | | | | | | | | |
| 11-12 | 0.03 | 0.04 | 0.07 | 0.06 | 0.04 | 0.04 | 0.03 | 0.03 | 0.04 | 0.08 | 0.06 | 0.08 | 0.12 | 0.15 | 0.18 | 0.15 | 0.14 | 0.10 | 0.04 | 0.02 | 0.04 | 0.07 | 0.05 | 0.04 | 1.67 | | | | | | | | | | | | | | | | | | | | | | | |
| 10-11 | 0.10 | 0.14 | 0.15 | 0.10 | 0.09 | 0.08 | 0.05 | 0.05 | 0.06 | 0.08 | 0.11 | 0.12 | 0.15 | 0.29 | 0.32 | 0.28 | 0.17 | 0.13 | 0.07 | 0.05 | 0.07 | 0.15 | 0.18 | 0.15 | 3.09 | | | | | | | | | | | | | | | | | | | | | | | |
| 9-10 | 0.34 | 0.35 | 0.30 | 0.29 | 0.15 | 0.10 | 0.08 | 0.10 | 0.12 | 0.13 | 0.13 | 0.16 | 0.26 | 0.45 | 0.39 | 0.36 | 0.26 | 0.19 | 0.10 | 0.11 | 0.17 | 0.36 | 0.38 | 0.41 | 5.68 | | | | | | | | | | | | | | | | | | | | | | | |
| 8-9 | 0.79 | 0.69 | 0.65 | 0.44 | 0.33 | 0.20 | 0.15 | 0.12 | 0.17 | 0.20 | 0.19 | 0.30 | 0.44 | 0.53 | 0.58 | 0.40 | 0.38 | 0.30 | 0.22 | 0.19 | 0.28 | 0.49 | 0.65 | 0.64 | 9.33 | | | | | | | | | | | | | | | | | | | | | | | |
| 7-8 | 1.15 | 1.00 | 0.94 | 0.67 | 0.52 | 0.29 | 0.25 | 0.21 | 0.29 | 0.24 | 0.27 | 0.41 | 0.51 | 0.66 | 0.65 | 0.59 | 0.45 | 0.42 | 0.32 | 0.34 | 0.53 | 0.72 | 1.00 | 1.10 | 13.55 | | | | | | | | | | | | | | | | | | | | | | | |
| 6-7 | 1.56 | 1.29 | 1.02 | 0.80 | 0.58 | 0.49 | 0.42 | 0.40 | 0.34 | 0.40 | 0.40 | 0.51 | 0.61 | 0.62 | 0.60 | 0.58 | 0.49 | 0.41 | 0.37 | 0.46 | 0.55 | 0.86 | 1.05 | 1.22 | 15.69 | | | | | | | | | | | | | | | | | | | | | | | |
| 5-6 | 1.13 | 1.06 | 0.82 | 0.67 | 0.68 | 0.57 | 0.53 | 0.37 | 0.48 | 0.44 | 0.55 | 0.57 | 0.54 | 0.66 | 0.62 | 0.48 | 0.51 | 0.45 | 0.47 | 0.50 | 0.60 | 0.72 | 0.90 | 1.08 | 15.60 | | | | | | | | | | | | | | | | | | | | | | | |
| 4-5 | 0.85 | 0.76 | 0.78 | 0.76 | 0.63 | 0.56 | 0.50 | 0.52 | 0.50 | 0.45 | 0.50 | 0.48 | 0.45 | 0.55 | 0.57 | 0.44 | 0.52 | 0.43 | 0.50 | 0.53 | 0.53 | 0.67 | 0.68 | 0.78 | 13.94 | | | | | | | | | | | | | | | | | | | | | | | |
| 3-4 | 0.48 | 0.44 | 0.52 | 0.52 | 0.43 | 0.40 | 0.40 | 0.44 | 0.38 | 0.36 | 0.39 | 0.35 | 0.38 | 0.36 | 0.35 | 0.30 | 0.34 | 0.36 | 0.36 | 0.39 | 0.41 | 0.41 | 0.41 | 0.45 | 9.61 | | | | | | | | | | | | | | | | | | | | | | | |
| 2-3 | 0.24 | 0.30 | 0.26 | 0.25 | 0.24 | 0.28 | 0.22 | 0.22 | 0.23 | 0.25 | 0.24 | 0.21 | 0.23 | 0.31 | 0.23 | 0.25 | 0.17 | 0.22 | 0.24 | 0.24 | 0.24 | 0.26 | 0.31 | 0.26 | 5.89 | | | | | | | | | | | | | | | | | | | | | | | |
| 1-2 | 0.17 | 0.16 | 0.12 | 0.11 | 0.14 | 0.15 | 0.14 | 0.14 | 0.12 | 0.11 | 0.14 | 0.16 | 0.11 | 0.16 | 0.14 | 0.12 | 0.13 | 0.17 | 0.10 | 0.17 | 0.18 | 0.13 | 0.13 | 0.17 | 3.36 | | | | | | | | | | | | | | | | | | | | | | | |
| 0-1 | 0.04 | 0.02 | 0.05 | 0.06 | 0.06 | 0.04 | 0.05 | 0.05 | 0.03 | 0.05 | 0.03 | 0.05 | 0.03 | 0.03 | 0.03 | 0.05 | 0.06 | 0.05 | 0.04 | 0.05 | 0.05 | 0.04 | 0.03 | 0.04 | 1.02 | | | | | | | | | | | | | | | | | | | | | | | |
| Entire dataset | | | | | | | | | | | | | | | | | | | | | | | | 6.57 | 6.22 | 5.72 | 4.94 | 3.90 | 3.20 | 2.85 | 2.70 | 2.81 | 2.86 | 3.06 | 3.45 | 3.92 | 4.96 | 4.94 | 4.19 | 3.76 | 3.31 | 2.86 | 3.05 | 3.63 | 4.93 | 5.81 | 6.37 | 100.00 |

Table 3.5 Directional distribution of wind speeds at Mar del Plata (38°S 37.5°W) from NWW3 model 1997-2010. Wind direction towards, in degrees clockwise from geographic North

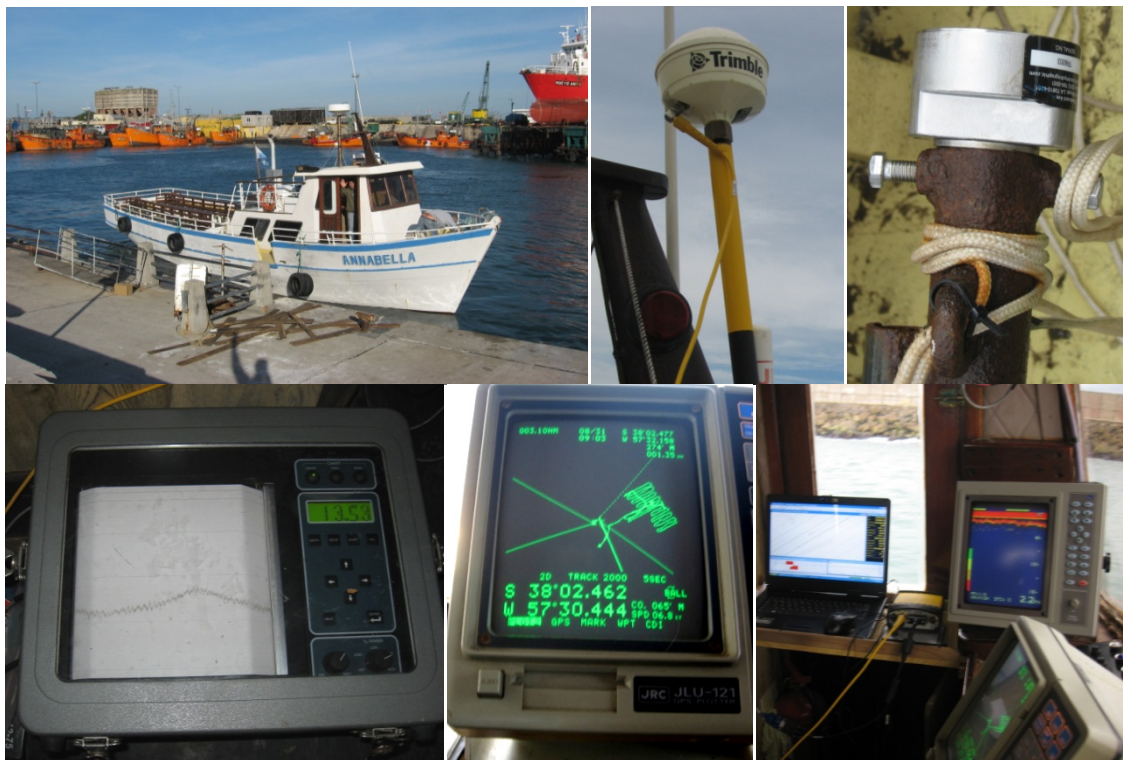
3.3 Bathymetry

The availability of good bathymetry is essential to ensure the correct modelling of wave propagation from deep water to the area of study taking into account all processes that can transform the waves (shoaling, refraction, diffraction, reflection, breaking).

Inside the port of Mar del Plata and its access channel, there are sounding charts available from March 1999 to April 2012 (DNVN, 2012a) with a grid size of 25 m (see section 3.8.2). The port authority (Dirección Nacional de Navegables) performed these soundings for navigation purposes, depths are only surveyed inside the navigation area. These measurements were performed using the following equipment:

| | |
|---------------------|--|
| Survey vessel | “Annabella”, length 18 m, width 4,0 m, draft 1,80 m, survey speed 2 knots |
| Positioning | Trimble DGPS Pathfinder PRO XRS, sub-meter precision, 7 records/s, OmniSTAR satellite differential service |
| Echosounder | Odom Hydrotrac ht97001, 210 kHz, resolution 0.01 m, 25 records/s |
| Surveying software | Trimble HydroPRO v 2.3 |
| Processing software | Trimble Terramodel v 10.40 |
| Reference level | LAT at Mar del Plata (MSL -0.91 m) |
| Methodology | Waves filtered from measurements. Depths corrected to interpolated tide, measured every 15 min inside port of Mar del Plata. Minimal squad due to relatively low survey speed. Bar check on shoal during sediment sampling using the rope of the sediment sample grab. |

Table 3.6 Equipment used for depth surveys near port of Mar del Plata



Photograph 3.1 Depth survey equipment used
 Survey vessel; DGPS receiver; Echo transducer,
 Echosounder; Navigation log; Processing hardware

To obtain depth information in littoral zone outside the navigation area, depth measurements were planned on the seaward side of both breakwaters extending 750 m off shore to depths of 10 m. During the preparation of the site visit trip in April 2012, there was no information about the availability of local depth survey equipment. Therefore, a mobile depth sounding system was composed (and tested in practice) that is relatively cheap, rigid, relatively accurate, light and compact and could be mounted on every type of boat or ship (described in appendix B.1). During the site visit trip although, for safety reasons, the port authority of Mar del Plata did not permit surveying close to the breakwater with any kind of vessel, but arranged a depth survey in the remaining part of the proposed survey area with professional equipment (Table 3.6).

In 1996, the provincial Hydraulic Department of the Ministry of Transport and Public Services measured depth profiles of the shore face, every 300 m, to depths of 10 m along the entire coast of the city Mar del Plata (MOSP, 1996). This data can be of use in areas where no recent soundings are performed.

Along the coast between Miramar and Mar Chiquita and further offshore, there is little detailed and recent bathymetric data available. The only available data for this area can be obtained from nautical charts of Servicio de Hidrografía Naval:

H-251: 1:5,000, measured 1994-2007 (SHN, 2010)

H-250: 1:50,000, measured 1970 (SHN, 2012c)

H-114: 1:250,000, measured 1968-1972 (SHN, 2012a)

H-210: 1:250,000, measured 1969-1981 (SHN, 2012b)

Depths in these maps are referred to Lowest Astronomical Tide (LAT). The main sea level in this area is 0.91 m above LAT.

Although the data on these charts is very old and the resolution of them is relatively coarse, for this coast it is still the most detailed available bathymetry.

Other available maps of the United Kingdom Hydrographic Office and National Geospatial Intelligence Agency are based on the maps of Servicio de Hidrografía Naval and therefore give no other data (NGA, 1998; UKHO, 2006b, 2006c, 2006d, 2006e).

Where nautical charts give no recent or detailed depth information, the GEBCO_08 grid can be used. A global 30 arc-second grid bathymetry chart that covers the whole world with depths related to MSL. It is largely generated by combining quality-controlled ship depth soundings with interpolation between sounding points guided by satellite-derived gravity data (GEBCO, 2010).

3.4 Tidal levels

The Atlantic coast of Buenos Aires has a mixed semidiurnal microtidal regime. According to the Naval Hydrographic Service of Argentina, at the tidal levels in port of Mar del Plata are:

| | | |
|------|--------------------------|---------|
| HHWS | Higher high water spring | +0.98 m |
| MHW | Mean high water | +0.42 m |
| MLW | Mean low water | -0.39 m |
| LLWS | Lower low water spring | -0.71 m |
| LAT | Lowest astronomical tide | -0.91 m |

Table 3.7 Tidal levels at Mar del Plata (in m to MSL) (SHN, 2012d)

The cotidal chart in Figure 3.6 displays the distribution of tidal phases over the Atlantic Ocean (in steps of $30^\circ \approx$ one hour). The Buenos Aires coast (outside the Rio del Plata estuary) is situated on a large stretch of coast with almost equal tidal phase, so spatial tidal differences are very small in this area.

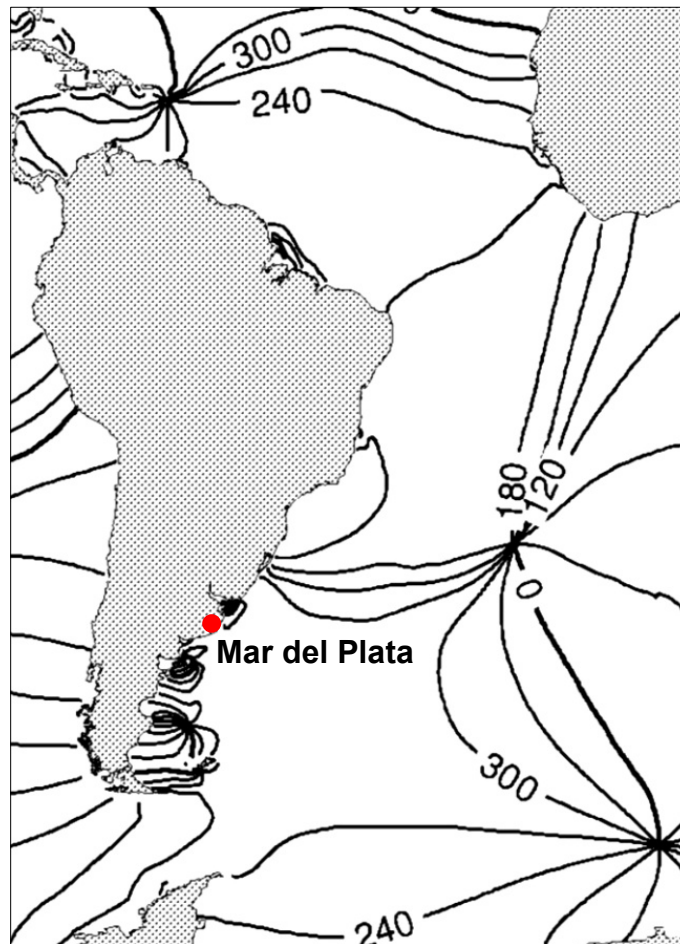


Figure 3.6 Cotidal chart of the Atlantic Ocean (Talley, Pickard, William J. Emery, & Swift, 2011)

3.5 Tidal currents

Along the almost unbroken coast of Buenos Aires, the tidal currents are very weak. Within 10 miles (18.5 km) of Mar del Plata, the tidal currents run north and south, changing direction 3 hours after low and high water by the shore. Their velocities are about 0.25 m/s (NGA, 2011; SHN, 2012a, 2012b, 2012c).

Inside the access channel of Mar del Plata maximum flow velocities of 0.4 m/s in southwest and east-southeast direction are reported (SHN, 2010).

Between Punta Rasa and Punta San Andres, 20 km southwest of Mar del Plata, there is a strong north going current during south-western winds. Its rate varies from 0.5 to 1.5 m/s. During northerly winds, there is a weaker current to the south (NGA, 2011).

During the site visit trip, the order of magnitude and directions of the local currents at different places around the port entrance are measured using a GPS-drifter (described in appendix B.3).

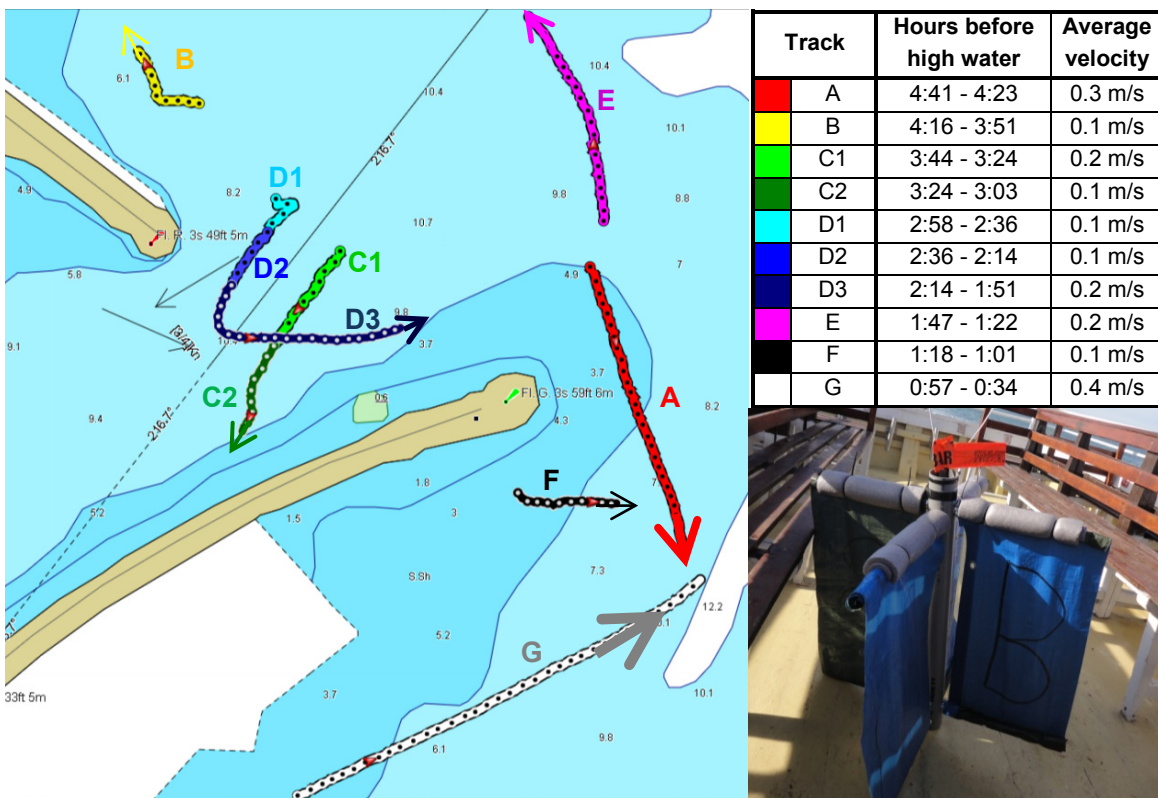


Figure 3.7 Results drifter tracking.
 Left: Drifter tracks on nautical chart (UKHO, 2006a),
 Top right: Legend and data summary
 Bottom right: Used GPS-drifter

From these measurements can be concluded that:

- The flow velocities inside the port entrance are weak (0.1 - 0.2 m/s) and have an order of magnitude of 50% of the flow velocities inside the port.
- The current parallel to the southern breakwater drives a circulating flow in the entrance.

- Track C has same direction as the flow vectors on the nautical chart, but a smaller magnitude than the maximum of 0.75 knot (0.4 m/s) denoted on the nautical chart (Figure 3.7) in the harbour mouth. This result seems to be obvious, due to the calm weather and sea state and because the measurements took place at a moment just between neap and spring tide.

3.6 Sediment characteristics

For sediment transport calculations, it is important to have insight in the grain size distribution on different locations around the port. During the site visit trip in April 2012, various sediment samples are taken at the bottom and on the beaches around the port of Mar del Plata. Sampling locations and methods are described in appendix B.2. Further analysis of these samples gives sediment characteristics sediment transport computations.

The particle size distribution of the samples in numbered plastic bags was determined by sieve analysis at the Laboratory of the faculty of Geo-Engineering of Delft University of Technology according to standard EN 933-1 (European Committee for Standardization, 2012).

Wet or humid sediment grains tend to stick to each other or to the sieves. Therefore, all samples are placed in a separate open aluminium box and dried in an oven at 110° for 38 hours before they are analysed.

The set of sieves consisted of the following mesh sizes: 500 µ, 425 µ, 250 µ, 150 µ, 125 µ, 105 µ, 75 µ, and 63 µ. Each sieve was weighted empty, then in the order from largest spacing (top) to smallest spacing (bottom), also including a closed plate at the lower end to capture all the fine sediment that was not hold by the 63-µ mesh. Each fully dried sample was placed on the top sieve of the tower. Each sieving tower was placed on the vibration machine for at least 5 minutes. Finally, each mesh was weighted with the corresponding amount of sediment. With this weight, the sieve rest on each sieve was calculated by subtracting the loaded and empty weight of each mesh. Table 3.8 shows the main properties of each sample. In Figure 3.8 it can be seen that most samples have a D₅₀ between 125 µ and 225 µ.

| Sample | <63 µ | <75 µ | <105 µ | <125 µ | <150 µ | <250 µ | <425 µ | <500 µ | D ₁₀ | D ₅₀ | D ₉₀ | Remark |
|----------|-------|-------|--------|--------|--------|--------|--------|--------|-----------------|-----------------|-----------------|----------------------------------|
| 16-04-1 | 20% | 25% | 39% | 64% | 76% | 95% | 98% | 98% | 37 µ | 114 µ | 223 µ | Very fine, some shells |
| 16-04-2 | 0% | 1% | 3% | 16% | 39% | 94% | 98% | 99% | 116 µ | 171 µ | 243 µ | |
| 16-04-3 | 1% | 2% | 11% | 34% | 56% | 94% | 98% | 98% | 101 µ | 143 µ | 239 µ | |
| 16-04-4 | 4% | 7% | 32% | 59% | 80% | 98% | 99% | 99% | 79 µ | 118 µ | 206 µ | |
| 16-04-5 | 0% | 1% | 6% | 21% | 38% | 92% | 98% | 99% | 110 µ | 172 µ | 246 µ | |
| 16-04-8 | 0% | 0% | 5% | 21% | 38% | 93% | 98% | 99% | 111 µ | 172 µ | 244 µ | Some sticky grains |
| 16-04-9 | 2% | 4% | 14% | 44% | 62% | 97% | 99% | 99% | 92 µ | 133 µ | 231 µ | Very small sample |
| 16-04-10 | 0% | 1% | 2% | 6% | 11% | 84% | 96% | 97% | 146 µ | 204 µ | 339 µ | Some sticky grains, large sample |
| 16-04-11 | 0% | 0% | 0% | 5% | 13% | 78% | 93% | 96% | 141 µ | 207 µ | 393 µ | Shells on top |
| 16-04-12 | 5% | 6% | 13% | 25% | 44% | 96% | 98% | 99% | 91 µ | 162 µ | 238 µ | Some sticky grains |
| 18-04-1 | 0% | 0% | 0% | 3% | 7% | 77% | 97% | 99% | 155 µ | 212 µ | 365 µ | |
| 18-04-3 | 0% | 0% | 1% | 7% | 17% | 93% | 98% | 99% | 132 µ | 193 µ | 246 µ | |
| 18-04-5 | 0% | 0% | 1% | 7% | 17% | 89% | 99% | 100% | 132 µ | 196 µ | 264 µ | |

Table 3.8 Cumulative grain size distribution from sieve analysis EN 933-1 (sampling locations and methods see appendix B.2)

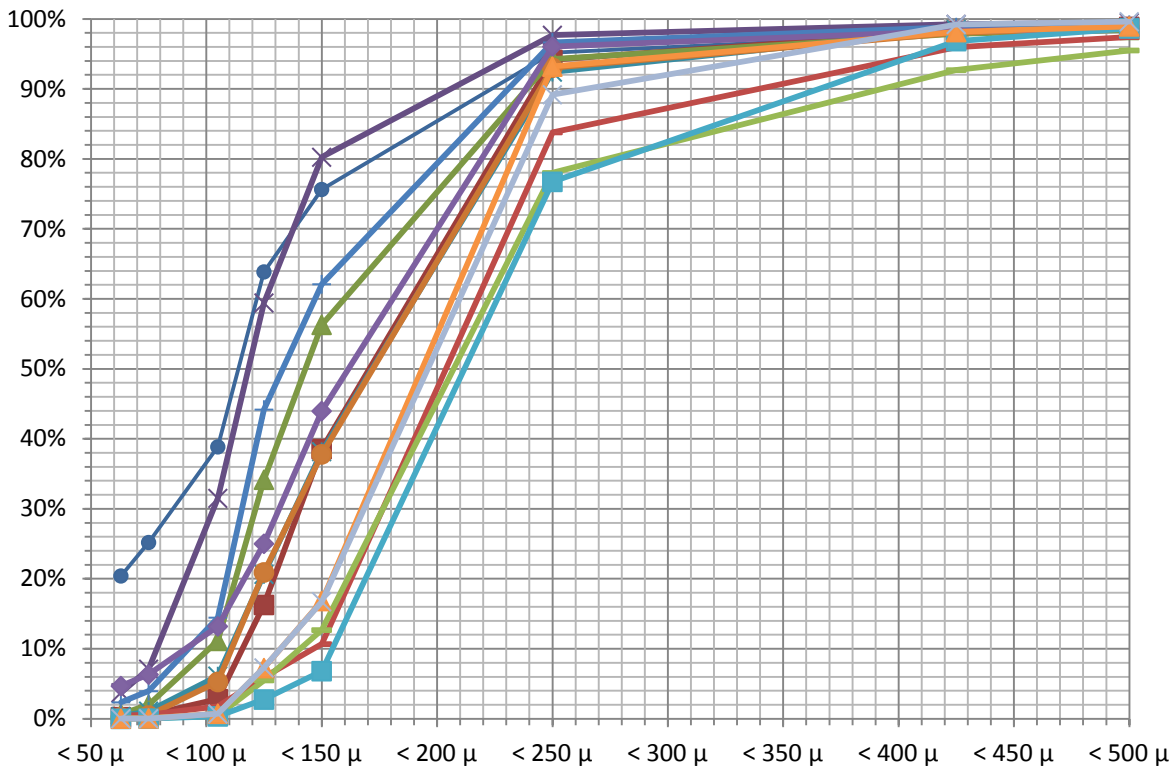


Figure 3.8 Cumulative grain size distribution obtained using EN 933-1 sieve analysis

Boer, De Jonge, Brouwer, et al. (1997) analysed the contamination of sediment inside the port and in the port entrance. They concluded that the docks in the southern part of the port contain heavily polluted sediment whereas the contamination decreases towards the entrance channel. The material on the shoal is originating from the southern part of Argentina and contains some heavy minerals.

3.7 Longshore sediment transport

There is a resulting littoral transport capacity along the coastal area between Miramar and Mar Chiquita in a northerly direction. A large part of the sediment transport that passes along Punta Mogotes is blocked by the southern breakwater of the port. What remains is the finer sediment that is mainly deposited in the large shoal in front of the harbour entrance or moved to deeper water. It is believed that only a very limited amount of these sediments are able to return to the coast at some distance downcoast of the port of Mar del Plata (Boer, De Jonge, Brouwer, et al., 1997).

Dredging activities at the port entrance for the first time were performed in 1950 using a self-propelled trailing suction hopper dredger in the area within the 11 m contour. By 1956, it appeared as if an equilibrium condition had been reached, because hydrographic surveys showed that changes in the 11 m contour were already very small. A transport rate was calculated through (unpublished) monthly dredge records (over an unknown year) giving 390,000 m³/year (Caviglia, Pousa, & Lanfredi, 1991).

Van Rijn (2008) calculated the net longshore transport capacity updrift of the port entrance based on Method Van Rijn in the range of 300,000 m³/year to 500,000 m³/year for sediments of 0.2 to 0.5 mm. Given the short length (2 to 3 km) of the littoral zone updrift of the harbour entrance and the presence of the rocky Cape Punta Mogotes blocking the supply of sediments, the actual net longshore transport is smaller than the transport capacity. Therefore, Van Rijn estimated a transport capacity in the range of 200,000 to 300,000 m³/year.

Indicative UNIBEST computations of Boer, De Jonge, Brouwer, et al. (1997) show that the net potential longshore transport of sand under average wave conditions along the coast at Mar del Plata is in northward direction at a rate between 150,000 to 200,000 m³/yr. The gross transport rates in southward and northward direction are respectively about a factor 1.25 and 0.25, indicating the relative importance of waves from south-eastern directions for the longshore transport process. It is emphasized that these values refer to potential transport rates in which limitations of the available sand and the interruption of the longshore transport by man-made structures and natural headlands are not considered. Therefore, the actual longshore transport in the existing situation may even be smaller.

Extra LT calculations have been made to estimate the by-pass of sediment along the southern breakwater of the port. At the end of the southern breakwater, a rate of roughly 50,000 m³/year is found.

Camarena Calderon (2012) performed UNIBEST LT computations along the Buenos Aires coast using wave conditions computed in a joint study to obtain near shore wave conditions. Near the port entrance of Mar del Plata, sediment transport rates were calculated of around 300,000 m³/year.

3.8 Dredging and sedimentation rates

To be able to validate model predictions of sediment rates in the port access, it is necessary to gain insight in the order of magnitude of sedimentation rates in recent history. All available dredging and depth survey data is collected from different port authorities and stakeholders. To quantify the total sedimentation volume and sedimentation rates in the port entrance over time, this data is analysed using curve-fitting technique. For a period where the data density was too low to use curve-fitting, a model to determine the trapping efficiency of a channel is used.

3.8.1 Dredge records

From meetings with different stakeholders it could be concluded that there have been different authorities responsible for the nautical accessibility of the port. The contracting and registration of dredging works have been executed in different ways by the parties involved and nowadays there are no official records available of dredging locations and volumes over time.

The available records of dredging volumes and locations over time could only be found in news articles:

- In 1998, the Dutch dredger “Amazon” executed the most recent capital dredging by removing three-million m³ solid material in both access channels and the port basins. With the dredged sand, it recovered 300% of the area of the central city beaches. It was expected that the shoal in the port access would become problematic again from 2006 on (La Capital, 2009).
- From April 2004 during a few months, the Ukrainian dredger “Perekopskiy” dredged 120,000 m³ in the port access and basin (La Capital, 2004).
- In November 2006, the “James Ensor” removed 165,400 m³ solid material from the secondary access channel and dumped it six miles offshore, but after some storms the effect in the secondary access channel was eliminated by nature (Ahorainfo, 2007).
- In November 2007, the Portuguese dredger “Acróbata” was assigned to dredge 160,000 m³ of sand in the secondary channel to retrieve a depth of 9.75 meters and an width of 100 m. Various technical problems of the dredger lead to a low progress of the work and the littoral transport of sediment made the work undone (Autoridad del Agua, 2008).
- In August 2009, the dredger “Mendoza 259-C” of the National Directorate of Waterways of Argentina started to enable the access of container vessels of 150 m trough the secondary channel (Murias, 2009a, 2009b). Since the start, the dredging activities have frequently been interrupted and delayed due to technical failures of the dredger and corresponding repair periods. Currently, this dredger has been out of order for more than one year and there is not enough money available to repair it. No record of the dredging volumes and locations are available for this dredger.

| Year(s) | Dredged volume and determination method | Location | Effect |
|-------------|--|-----------------------------|--------------------------------|
| 1998 - 1999 | 3,000,000 m ³ depth survey | Port access and basin | 7 years undisturbed navigation |
| 2004 | 120,000 m ³ reported by contractor | Port access and basin | Unreported |
| 2006 | 165,400 m ³ reported by contractor | Secondary channel | Rapidly eliminated by nature |
| 2007 | 160,000 m ³ reported by contractor | Secondary channel | Work made undone during repair |
| 2009 - 2011 | Unavailable some depth surveys | Secondary channel and basin | Short |

Table 3.9 Dredging activities during the last decades

From this information can be concluded that since the last capital dredging in 1998, three different dredgers, encountering various technical problems, dredged relatively small amounts in the secondary access channel with only a short lasting effect. The dredged volume from 2004 to the end of 2007 is less than 450.000 m³ and is based on unsurveyed reports of the different contractors (so it can be even less). From the end of 2009 till the begin of 2011 a dredger dedicated to the port tried to regularly maintain the secondary access channel but after technical problems the effect was rapidly cancelled out

3.8.2 Analysis of depth survey data

To be able to quantify the sedimentation rates around the port entrance during the recent history, all authorities and stakeholders around the ports are requested to provide all archived depth survey data.

Dirección Provincial de Saneamiento y Obra Hidráulica (Provincial Hydraulics Department) provided depth survey charts of the port entrance channel in pdf-format of the following dates:

| | | | |
|------------------|------------------|-------------------|------------------|
| 26 October 2007 | 05 December 2008 | 24 September 2009 | 23 August 2010 |
| 14 February 2008 | 12 January 2009 | 28 October 2009 | 04 October 2010 |
| 18 March 2008 | 23 February 2009 | 23 November 2009 | 20 December 2010 |
| 02 May 2008 | 13 April 2009 | 21 December 2009 | 17 January 2011 |
| 03 June 2008 | 26 May 2009 | 28 January 2010 | 14 February 2011 |
| 29 June 2008 | 14 July 2009 | 26 February 2010 | |
| 25 August 2008 | 05 August 2009 | 10 May 2010 | |
| 29 October 2008 | 31 August 2009 | 23 June 2010 | |

Dirección Nacional de Vías Navegables provided depth survey charts of the port entrance channel in pdf-format of the following dates:

11 March 1999
 20 March 2012
 16 April 2012

The depth survey data spans the period from just after completion of the last capital dredging (started in 1998) and is measured within the blue outlined area shown in Figure 3.9.

To collect depth information on different locations equally distributed over the surveyed area, a grid is generated with a grid size of 100 x 100 m creating 53 grid points (Figure 3.9). The surveyed area is subdivided in five different cells representing specific areas (Figure 3.9 and Table 3.10) to be able to analyse the sedimentation in areas with different characteristics, each depth survey chart is scaled and geo-referenced and for each grid point, the surveyed depth is registered (if depths were surveyed near that grid point). This resulted in 1281 records of xyz-location's with corresponding survey dates.

The depth survey data is converted to sand layer thickness over time ($\Delta d_{grid\ point}(j, i, t)$).

$$\Delta d_{grid\ point}(j, i, t) = d_{grid\ point}(j, i, t) - d_{grid\ point}(j, i, 0) \quad (3.1)$$

In which, j is the cell number, i the n^{th} grid point number per cell and t is the number of days after the first depth survey.

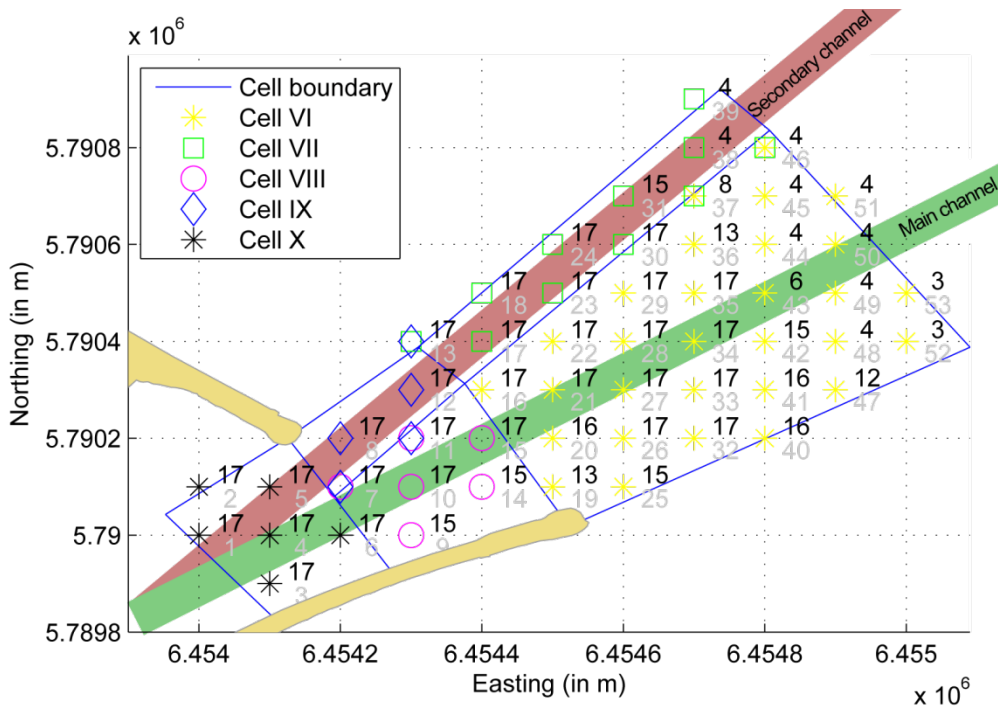


Figure 3.9 Analysed depth sounding grid points subdivided in cells (POSGAR94-6 coordinate system)
 Black: Number of observations per grid point over time, Grey: Grid point number

| Cell nr. (j) | Characterization | Nr. of grid points | Surface area |
|--------------|---------------------------|--------------------|------------------------|
| VI | Sand spit | 30 | 280,879 m ² |
| VII | Present/secondary channel | 11 | 70,156 m ² |
| VIII | Shoal between breakwaters | 6 | 65,424 m ² |
| IX | Present port entrance | 5 | 31,902 m ² |
| X | Port basin | 6 | 61,308 m ² |

Table 3.10 Cell properties

From this data, the time series of sand layer thickness per grid point ($\Delta d_{grid\ point}(j, i, t)$) is plotted and visually analysed for outliers (Figure 3.10). The time series on the sloping edge of the secondary (present) navigation channel show abrupt changes in bed level (right panel of Figure 3.10) in the period from August 2009 to January 2011 ($t \approx 3800$ to $t \approx 4300$ days). This period coincides with the period the dredger “Mendoza 259-C” was maintaining the secondary access channel. The volumes this dredger extracted are unknown and morphological processes can have caused (extra) sedimentation during and after the dredging activities. Therefore, the period from August 2009 to present has not been used to estimate the sedimentation volumes and rates over time, resulting in 710 observations shown in Figure 3.9.

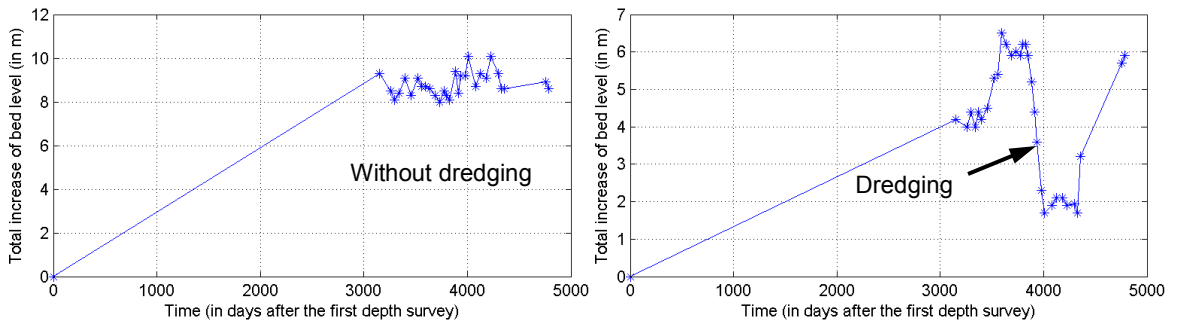


Figure 3.10 Time series of sand layer thickness on two different locations (1999 to 2012)

Left: Area without signs of dredging, in the middle of the shoal (in cell VI);

Right: Area with dredging, on the side slope of the navigation channel (on the border of cell VI).

From the time series of sand layer thickness, the sedimentation volume per grid point over time, $V_{grid\ point}(j, i, t)$, can be derived by multiplying the local sand layer thickness over time, $(\Delta d_{grid\ point}(j, i, t))$ with the area of each grid point ($A_{grid\ point} = 100\ m^2$).

$$V_{grid\ point}(j, i, t) = \Delta d_{grid\ point}(j, i, t) A_{grid\ point} \quad (3.2)$$

The total sedimentation volume per cell area over time, $V_{cell}(j, t)$, can be derived using the average sedimentation volume per grid point.

$$V_{cell}(j, t) = A_{cell}(j) \frac{\sum_{i=1}^n (V_{grid\ point}(j, i, t))}{n(j) A_{grid\ point}} \quad (3.3)$$

Figure 3.9 shows that the number of observations per grid point is not equal for all grid point and the time series per grid point show some scatter (Figure 3.10). Therefore, non-linear curve fitting techniques have been used to obtain a regular and continuous mathematical function that represents the sand layer thickness per grid point over time.

Three different non-linear curve-fitting algorithms of the MATLAB 2012b “Curve Fitting Tool” are used to obtain parameters for a mathematical function with a best fit to the series of the data points:

- Non-Robust algorithm
 - Ordinary Least Squares (OLS) fitting
- Robust algorithms
 - Least Absolute Residuals (LAR) fitting
 - Bisquare fitting

The ordinary least squares fitting method minimizes the sum of squared vertical distances between the curve and data points. With robust curve fitting the, outliers will have less influence on the outcome of the fitting process. When applying the Least Absolute Residuals (LAR) robust algorithm, the least absolute residuals are minimized. With Bisquare robust fitting the best-fit is obtained by minimizing the summed square of the residuals, and down weight outliers.

The sand layer thickness is expected to slow down in time and finally reaches an equilibrium bed level. V thus will evolve in the same way. Therefore, the following function is chosen for curve fitting:

$$V_{grid\ point}(j, i, t) = \alpha(j, i) (1 - e^{-\beta(j, i) t}) \quad (3.4)$$

In this function $\alpha(j, i)$ defines the equilibrium value of $V_{grid\ point}(j, i, t)$ and the time scale this equilibrium is reached will be depending on $\frac{1}{\beta(j, i)}$ (Figure 3.11)

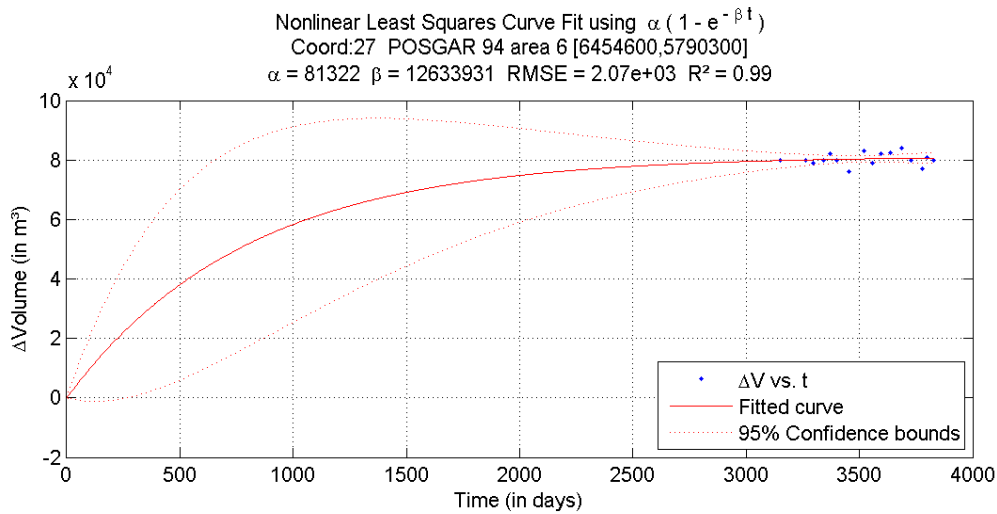


Figure 3.11 Example of Ordinary Least Squares curve fitting for volumetric change over time for one grid point

When the parameters $\alpha(j, i)$ and $\beta(j, i)$ are obtained using curve-fitting, equation 3.3 can be evaluated to estimate the sedimentation volumes per cell over time. The estimated sedimentation volumes from 1999 to 2012 in each cell are also shown in Table 3.11.

Subsequently, the sedimentation rate per grid point $S_{grid\ point}(j, i, t)$ can be estimated by taking the time derivative of equation 3.3:

$$S_{grid\ point}(j, i, t) = \frac{dV_{grid\ point}(j, i, t)}{dt} = \alpha(j, i) \beta(j, i) e^{-\beta(j, i) t} \quad (3.5)$$

The sedimentation rate of each cell can be obtained by taking the average sedimentation rate per m^2 of all grid points in a cell and multiply this with the surface area of the cell.

$$S_{cell}(j, t) = A_{cell}(j) \frac{\sum_{i=1}^n (S_{grid\ point}(j, i, t))}{n(j) A_{grid\ point}} \quad (3.6)$$

3.8.3 Sedimentation volumes and rates

| Cell | Measured total sedimentation volume 1999 - 2012 | Average measured sedimentation rate over 13 years | Estimated sedimentation in 1999 (first year after last capital dredging) 1,5 - 2,5 x average | Sedimentation in 2012 derived from two-monthly depth soundings |
|-------|--|---|--|---|
| VI | 1,400,000 m ³ | 100,000 m ³ /year 300 m ³ /day | 160,000 - 260,000 m ³ 210,000 ± 50,000 m ³ /year 575 ± 150 m ³ /day | 50,000 - 57,000 m ³ 53,500 ± 3,500 m ³ /year 150 ± 10 m ³ /day |
| VII | 230,000 m ³ + dredged 300,000 m ³ 530,000 m³ | 40,000 m ³ /year 100 m ³ /day | 60,000 - 100,000 m ³ 80,000 ± 20,000 m ³ /year 225 ± 60 m ³ /day | > 13,500 - 15,000 m ³ > 14,250 ± 750 m ³ /year > 40 ± 3 m ³ /day |
| VIII | 510,000 m ³ | 40,000 m ³ /year 100 m ³ /day | 60,000 - 100,000 m ³ 80,000 ± 20,000 m ³ /year 210 ± 50 m ³ /day | 17,000 - 27,000 m ³ 22,000 ± 5,000 m ³ /year 60 ± 15 m ³ /day |
| IX | 115,000 m ³ + dredged 145,000 m ³ 260,000 m³ | 20,000 m ³ /year 50 m ³ /day | 30,000 - 50,000 m ³ 40,000 ± 10,000 m ³ /year 110 ± 30 m ³ /day | > 7,000 ± 8,500 m ³ > 7,750 ± 750 m ³ /year > 20 ± 3 m ³ /day |
| X | 160,000 m ³ | 13,000 m ³ /year 30 m ³ /day | 20,000 - 30,000 m ³ 25,000 ± 5,000 m ³ /year 70 ± 20 m ³ /day | 10,000 - 12,000 m ³ 11,000 ± 1,000 m ³ /year 30 ± 3 m ³ /day |
| Total | 2,800,000 m ³ | 220,000 m ³ /year 600 m ³ /day | 325,000 - 540,000 m ³ 440,000 ± 100 m ³ /year 1,200 ± 300 m ³ /day | > 100,000 - 120,000 m ³ > 110,000 ± 10,000 m ³ /year > 300 ± 30 m ³ /day |

Table 3.11 Measured and estimated sedimentation volumes and rates in different cell's (plotted in Figure 3.9)

The sedimentation rate in 2012 is derived from the frequent (two monthly) depth survey data since 2007 using curve-fitting techniques. Due to the unavailability of depth survey data between March 1999 and October 2007, theoretical curve-fitting will not result in reliable estimates of (initial) sedimentation rates for the period after the completion of capital dredging in 1999. On the other hand, the total sedimentation between 1999 and 2012 and the average sedimentation rate between in over these 13 years could be accurately derived.

Based on the average sedimentation between 1999 and 2012 the sedimentation rate in 1999 is estimated using the SED-PIT model of Van Rijn (2005). This model can be used to determine the sedimentation in channels/pits/traps etc. using a relatively simple sedimentation formula to determine the trapping efficiency of a channel. The input parameters used for this model are displayed in Table 3.12.

| Input parameter SED-PIT model | Value |
|--|-------------------|
| Length of channel section (parallel to channel axis) | 1000 m |
| Width of channel section (normal to channel axis) | 300 m |
| Initial depth in channel/pit to MSL | 12 m |
| Depth outside channel/pit to MSL | 6 m |
| d ₅₀ of sand fraction | 0,2 mm |
| d ₉₀ of sand fraction | 0,3 mm |
| Significant wave height | 1,3 m |
| Peak wave period | 9 s |
| Flow approach angle | 50° |
| Depth averaged flow velocity | 0,1 - 0,2 m/s |
| Diurnal tide with water levels to MSL | + 0,5 m to -0,5 m |

Table 3.12 Input parameters SED-PIT model for estimation sedimentation rates in the navigation channel

| Year | Computed sand layer thickness in channel | Computed growth of sand layer thickness in channel |
|--|--|--|
| 1999 | 0 m | 0.50 m/year |
| 2000 | 0.50 m | 0.47 m/year |
| 2001 | 0.97 m | 0.48 m/year |
| 2002 | 1.45 m | 0.45 m/year |
| 2003 | 1.90 m | 0.44 m/year |
| 2004 | 2.34 m | 0.42 m/year |
| 2005 | 2.76 m | 0.40 m/year |
| 2006 | 3.16 m | 0.37 m/year |
| 2007 | 3.53 m | 0.35 m/year |
| 2009 | 4.23 m | 0.29 m/year |
| 2011 | 4.80 m | 0.21 m/year |
| 2014 | 5.44 m | |
| Average growth = 5.44/15 = 0.34 m/year | | |

Table 3.13 Sand layer thickness in the navigation channel estimated by SED-PIT model

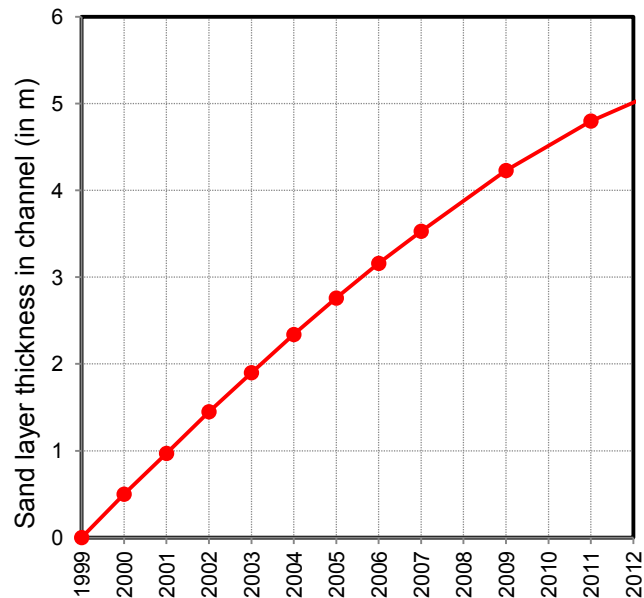


Figure 3.12 Sand layer thickness in the navigation channel estimated by SED-PIT model

The sand layer thickness in the navigation channel as function of time estimated by the SED-PIT model is shown in Table 3.13 and Figure 3.12.

The behaviour is fairly linear. With a flow velocity (20 cm/s), all suspended sand (with a settling velocity of 2 cm/s) will settle 1 m over a horizontal distance of 10 m. The maximum channel depth is 12 m, so after 120 m, all suspended sand grains are settled on the bottom of the channel (of 300 m wide). Therefore, sediment transport behaves as bottom transport in this situation and all sand will settle on the bottom.

In Table 3.13, the estimated yearly and average growth of sand layer thickness in the channel is shown. From this can be seen that:

- The estimated sedimentation rate in 1999 is a factor 1.5 larger than the average value;
 - The estimated sedimentation rate in 2012 is a factor 1.5 smaller than the average value.
- Because of modelling uncertainties, a factor 1.5 to 2.5 is applied to estimate the sedimentation in 1999 in Table 3.11.

Generally, the width and height of a shoal increases in time, so areas around the initial shoal will experience accretion in a later stage. Therefore, the assumption that for all grid point the initial increase of sand layer thickness starts just after completion of the capital dredging (in 1999) is not completely realistic.

Due to activities of the dredger “Mendoza 259-C” from August 2009 to January 2011, the sedimentation rate in the secondary access channel (cell VII and IX) is probably a bit higher than estimated using the data set from March 1999 to August 2009.

4 Potential measures to reduce sedimentation in port entrance

4.1 Inventarisation of possible measures

Historic studies to the sedimentation problems in the port entrance of Mar del Plata proposed different possible countermeasures to be studied further.

In 1959 La Comisión Mixta proposed the installation of fixed dredger at the bottom some 200 m south of the tip of the southern breakwater to extract sediment from the littoral zone and to pump the extracted sediment to the outside of the northern breakwater. Another similar facility is considered to be operated at the beginning of the southern breakwater and eventual commercialization of the sand mining to reduce costs (as cited in Lagrange, 1993).

Sunrise Technical Consultants (1968) proposed different possible solutions (as cited in Lagrange, 1993):

- To build a 500 m long offshore breakwater near the tip of the southern breakwater
- To extend the southern breakwater with 500 meters length and to build a groin perpendicular to the present tip of the southern breakwater.
- To build a 200 m long groin perpendicular to the end of the southern breakwater with a dredge pump on the south side of it to bypass sediment to the northern breakwater.

Waterman (1994) and Boer, De Jonge, Brouwer, et al. (1997) advised to regularly bypass sand over the years using a trailing suction hopper dredger by removing sand from the shoal and along the southern breakwater and nourish the beaches north of the port with this sand.

Van Rijn (2008) mentioned various methods to reduce the sedimentation processes and associated dredging from Van Rijn (2005):

- Improvement of entrance geometry; streamlining of the entrance so that the generation of eddies and dead water zones is suppressed;
- Design of a sand trap updrift of the port entrance;
- Design of a sand trap downdrift the tip of the southern breakwater;
- Design of bypassing barriers (blocking of longshore transport; elimination of recirculating flows; elimination of diffractive wave effects; no asymmetric jetties);
- Design of bypassing pump system;
- Extension of breakwaters to deeper water;
- Reduce the width and depth of the entrance as much as possible, considering the nautical requirements, to reduce horizontal circulation in the entrance area of the basin.

All possible solutions can be categorised to three main principles (visualised in section 4.2):

1. Trap sediment in an area where it does not affect the navigability:

- a. In a sand trap (overdepth) at the tip of the southern breakwater
- b. In a sand trap (overdepth) updrift along the southern breakwater
- c. Behind an offshore breakwater along the southern breakwater
- d. On the updrift side of a (T-head) groin perpendicular to the southern breakwater
- e. On the lee side of a groin obliquely to the east from the tip of the southern breakwater
- f. By moving the port entrance in westward direction by removing a part of the north breakwater and rebuilt it in the same line perpendicular to the west of the southern breakwater

2. Deflect sediment to deeper water:

- a. By extending the southern breakwater to deeper water

3. Continuous bypassing of sediment to a downdrift location:

- a. By using a crane with a pump system on a jetty or groin
- b. By constructing a pier on piles with different jets and a pump system

4.2 Discussion of measures

During this study, various discussions took place with experts and stakeholders to inventarise their policy and opinion about different measures to reduce sedimentation in the port entrance. In the following pages, all measures are discussed.

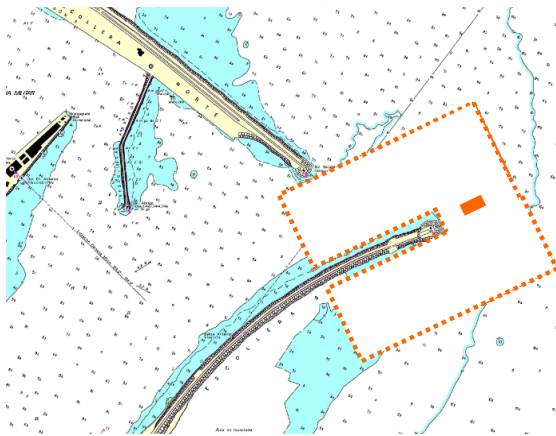


Figure 4.1 Solution 1a: Sand trap at tip breakwater

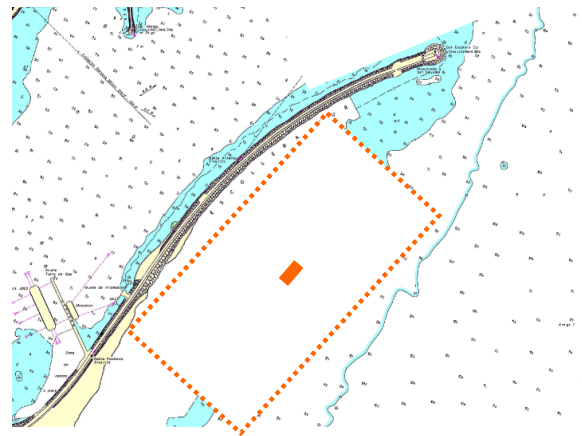


Figure 4.2 Solution 1b: Sand trap updrift

Solution 1a: Sand trap at tip southern breakwater

In a sand trap solely in inside the navigation channel (overdepth of the channel), sand will accrete on the updrift side. The downdrift side will possibly erode (Figure 4.3)

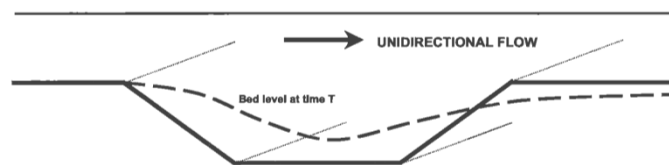


Figure 4.3 Morphological development of channel with flow perpendicular to main axis (Van Rijn, 2005)

Therefore, a wider trap is needed to ensure the alignment and width of the navigation channel during the life span of the sand trap.

Near the toe of the breakwater, dredging can affect the geotechnical its stability. If deeper or closer dredging is needed, additional toe and bed protection works are essential. Dredging close to the breakwater is assessed to be precarious and therefore the safety of the dredger must be taken into account in the design of the sand trap. Dredging inside the channel is not preferable because dredgers dredging the channel and ship traffic in this channel will disturb each other.

The construction of a sand trap in the entrance and updrift will not reduce the overall sedimentation rate but merely act as a buffer zone. The trap must provide a buffer volume that is sufficient to cover a period of several years. The dredged sediment volume can be used for local beach nourishment purposes (Van Rijn, 2008).

It must be studied if a north-eastern storm will transport sediment to the navigation channel.

Solution 1b: Sand trap updrift

This sand trap might trap large amounts of sediment and will reduce the sedimentation rate in the port entrance, but still some sediment will pass this trap. An advantage of a sand trap in this area is that ship traffic is not disturbed during maintenance. Additional toe and bed protection works might be necessary to ensure the geotechnical stability of the breakwater.

It must be studied if a north-eastern storm will transport sediment to the navigation channel.

Dredging in this area is only possible when wave conditions are calm (what is not often the case in this area). In shallow areas, small(er) or a different type of dredging equipment might be needed. The dredged sediment volume can be used for local beach nourishments.

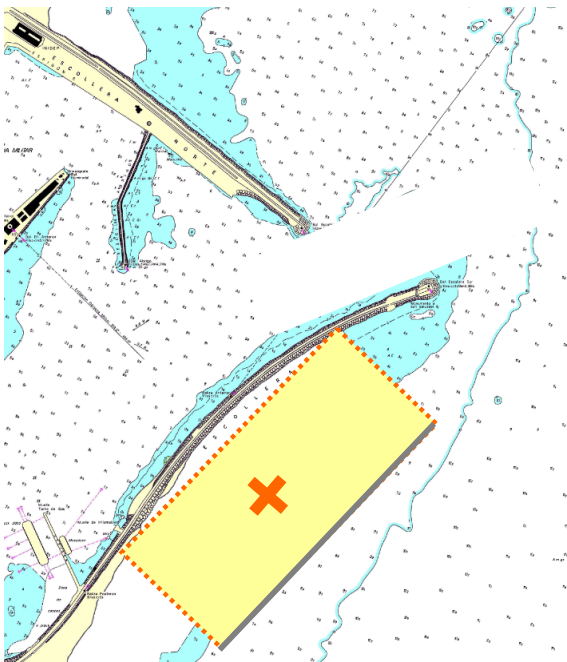


Figure 4.4 Solution 1c: Offshore breakwater

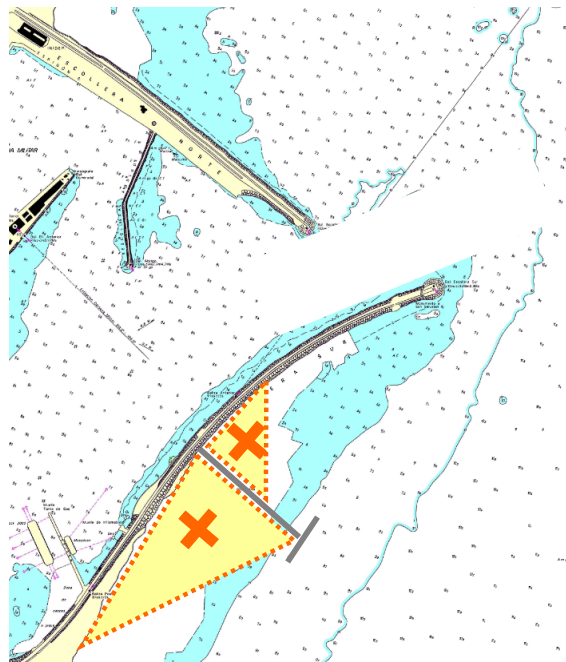


Figure 4.5 Solution 1d: (T-head) groin

Solution 1c: Offshore breakwater

For this option, a large breakwater has to be constructed in water depths of around 12 m. Behind this structure, sedimentation will occur due to a reduction of wave action and therefore reduction in transport capacity. It is questionable how the shoal behind this structure will behave during severe southern storms, because then a part of it might end up in the port entrance. In this shallow area, dredging for bypassing must be done using a cutter suction dredger with side anchors on both breakwaters.

Solution 1d: (T-head) groin

The groin should be sealed to prevent the sediments from passing through the breakwater structure (Van Rijn, 2008). If this groin is extending through the littoral zone, sediment transport will be blocked and settles updrift and/or (when deflected to deep water) settles in deep water. If this groin does not extend through the littoral zone, sediment will still pass this structure and can settle in the port entrance.

When beaches grow on the sides of the groin, it might be possible to remove it using land-based equipment on the beach or a large crane from the groin (according to coastal protection engineer S. Lochacoff, collaborator of Mar del Plata Chamber of Commerce foundation)

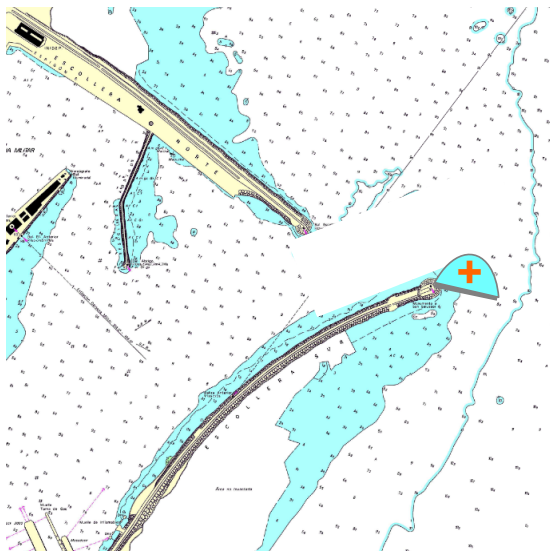


Figure 4.6 Solution 1e: Groin to the east

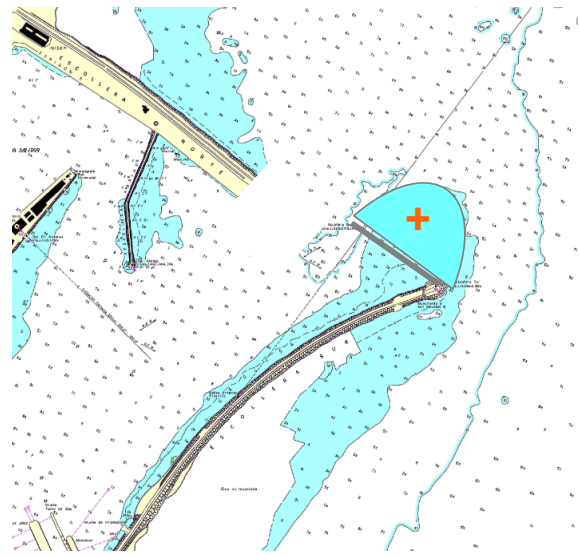


Figure 4.7 Solution 1f: Move entrance

Solution 1e: Eastward groin

For this option, a breakwater of around 150 meters has to be constructed. This will deflect the longshore current from the navigation channel and to the deeper water.

It must be studied what can the effect of a north-eastern storm, because that might transport sediment to the navigation channel.

With this measure, engineer J.C. Pérez de la Sierra of the Port authority of Mar del Plata, expects less dredging work and outside the navigation channel, so ship traffic and dredgers will experience fewer disturbances of each other.

Additional toe and bed protection works might be necessary to ensure the geotechnical stability of the southern breakwater.

The breakwater should be sealed to prevent the sediments from passing through the breakwater structure (Van Rijn, 2008).

Solution 1f: Move entrance westward

Engineer M.L. Bonavera, collaborator of Mar del Plata Chamber of Commerce foundation, proposed this solution in which material of the northern breakwater will be re-used to construct a groin west of the tip of the southern breakwater. In this option, the sailing distance to water depths of more than 10 m will be a little bit longer, but there is more space for the expected shoal. Also for this study, it must be studied if waves from the northeast can move the shoal into the navigation channel.

In addition, a navigation study is needed to determine if this option is possible in the present port layout. The new cruise terminal constructed at the end of the northern breakwater must have acceptable wave conditions and the breakwater connected to the northern breakwater may not be too close to axis of the new access channel.

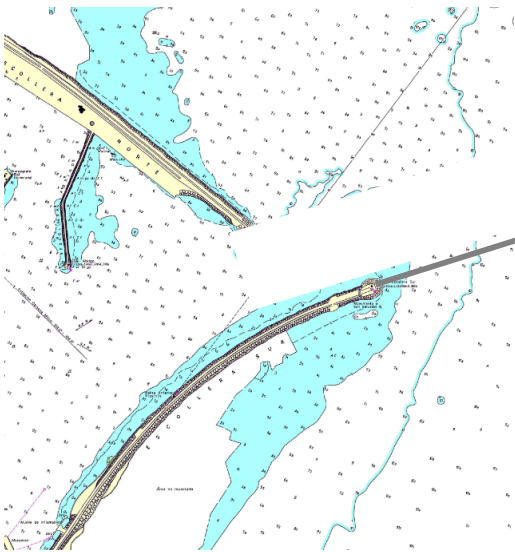


Figure 4.8 Solution 2a: Extension to deep water

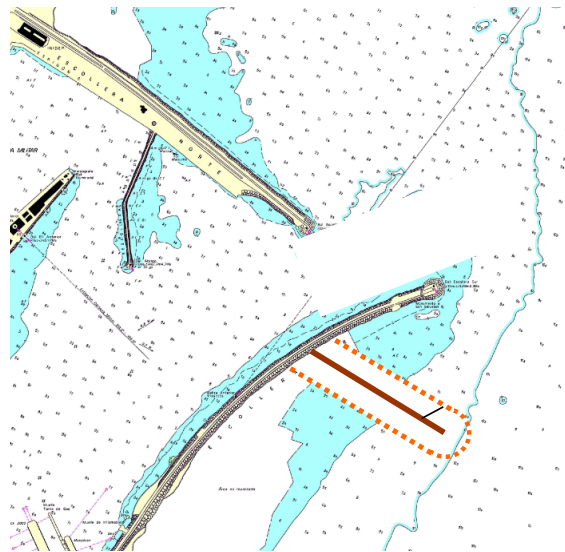


Figure 4.9 Solution 3a: Crane pier/jetty bypass

Solution 2a: Extension to deep water

For this option, a breakwater of around 600 meters has to be constructed in deep water, and must withstand strong wave attack. Therefore, execution of this work will be expensive. The breakwater should be sealed to prevent the sediments from passing through the breakwater structure (Van Rijn, 2008).

Because this breakwater extends to deep water, sediment will settle in this deep part. This will (temporally) not affect the navigability, but can increase beach erosion downdrift. Ships sailing along the tip of such a breakwater will experience an abrupt change in cross current at that point.

Solution 3a: Crane pier/jetty bypass

Artificial bypassing of sediment will lead to more sediment supply for the downdrift coast. For the deposition of the extracted sediment, an efficient and safe site must be found.

The construction costs of a pier are expected to be lower than for a groin, but the need of maintenance and its costs are higher. According to Engineer J.C. Pérez de la Sierra, a pier is exposed to severe winter storm and relatively rough wave climate compared to other locations where piers have been built in the province of Buenos Aires.

Using this solution only some part (estimated to about 30% to 50%; about 100,000 m³/year) of the total longshore drift can be removed from the littoral system (Van Rijn, 2008). Therefore, with this option, dredging will still be needed in the port entrance.

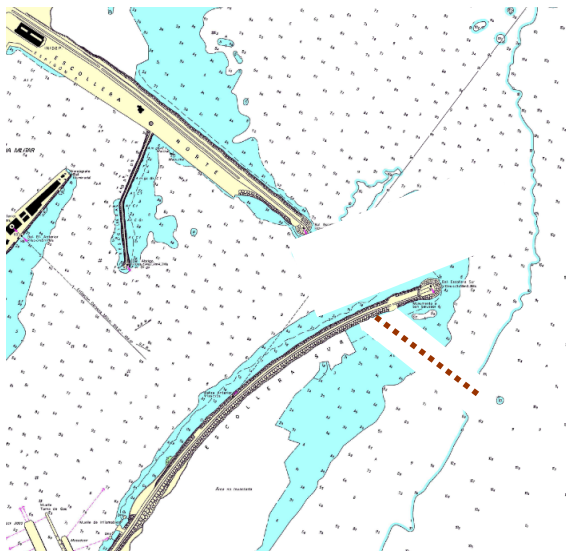


Figure 4.10 Solution 3b: Jet pier bypass

Solution 3b: Jet pier bypass

This type of solution requires a pier with a smaller width and a somewhat lighter construction, because it does not need to support an operating crane. Good maintenance of the submerged jets and pumps is needed, because malfunctions lead to direct failure of this costly solution. In addition, the construction of the pier will be exposed to severe winter storm and relatively rough wave climate.

Some part of the total longshore drift will pass this structure and dredging in the port entrance will still be needed.

4.3 Selection of most promising measures

Based on the discussion in the previous section, following solutions marked with an ✓ are judged to be feasible, durable, and efficient and are selected for further study.

1. Trap sediment where it does not affect the navigability:

- ✓ **Dredging a sand trap along the southern breakwater** will trap all sediment transport along the southern breakwater, which strongly reduces the supply of sand to the port access. The maintenance of the sand trap can be done on a regular base and the dredged sediment volume can be used for local beach nourishment purposes. The trapping efficiency and dredging frequency and volume (and corresponding costs), depend on the dimensions and location of the sand trap. The initial sedimentation rate in the sand trap and surrounding areas can be estimated using a sediment transport model.
- ✓ **Construction of an eastward groin at the tip of the southern breakwater** seems to be an effective, economical, and long-lasting measure, because it deflects sediment to deeper water and prevents the navigation channel from shoaling while the material need and cost for the construction of it are expected to be smaller than for other measures.
- ✗ **Moving the port entrance westward** is less effective than construction of an eastward groin, because it will not deflect the sediment transport, so still a shoal will develop next to the navigation channel. This shoal will increase in width and height over time and finally expands into the navigation channel. Besides that, the new cruise terminal will be exposed to higher waves and the chance for the occurrence unacceptable wave heights will increase.
- ✗ **Construction of a T-head groin** might only be effective in the long term, if it is extending through the littoral zone (to deep water), which makes the construction extremely expensive due to the large need for construction material.
An offshore breakwater needs to be long too, is built in deep water only, and therefore is even more expensive.
- ✗ **Trapping sand near the navigation channel** will definitely lead to significant sedimentation in the channel too and will therefore be not very (cost) effective.
Neither **a sand trap in the port entrance** will be an economic solution, because it increases the initial sedimentation rate inside the entrance and will move.

2. Deflect sediment to deep water using

- ✗ **An extension of the southern breakwater to deeper water** does not seem to be a durable measure because this is a relatively expensive measure at which the sediment will still settle in the navigation channel, so finally shoaling will still become a problem.

3. Continuous bypassing of sediment to a downdrift location

- ✗ Is assessed not to be feasible in the present economic and political climate in Argentina because for this type of solution, continuous maintenance is needed and some malfunctions can lead to direct (long-term) inactivity of such a costly measure.

5 Near shore wave modelling Buenos Aires

5.1 Model description

To simulate the evolution of random, short-crested wind-generated waves in (shallow) coastal areas, the SWAN model can be used. The SWAN model is a fully spectral (in all directions and frequencies) third-generation numerical model developed at Delft University of Technology. Deltares integrated the SWAN model in the Delft3D model suite (Deltares, 2011c).

The Delft3D-WAVE model accounts for the following physics:

- Wave refraction over a bottom of variable depth and/or a spatially varying ambient current
- Depth and current-induced shoaling
- Wave generation by wind
- Dissipation by whitecapping
- Dissipation by depth-induced breaking
- Dissipation due to bottom friction
- Nonlinear wave-wave interactions
- Wave blocking by flow
- Transmission through, blockage by or reflection against obstacles
- Diffraction

5.2 Model set-up

In a joint study with Camarena Calderon (2012), the Delft3D-WAVE (version 3.28.04) model is used to compute nearshore wave conditions between Bay of Samborombón to Miramar, based on the available bathymetry, offshore wave climate data and wind fields (described in chapter 3).

Bathymetry data was obtained from the Argentine nautical charts H-210 and H-114 (SHN, 2012a, 2012b), and from the General Bathymetric Chart of the Oceans (GEBCO, 2011). Depths are converted to MSL and charts are combined to generate the model bathymetry. The methods used to interpolate the depth points to the model grid were triangular interpolation and grid cell averaging.

Using a MATLAB tool called ORCA (Deltares Systems, 2011) the wind and wave climate in the computation area is derived from the NWW3 data and schematized in 125 different scenarios of wave conditions (Table 5.2) and spatial varying wind fields. These scenarios are used as conditions forcing for the Delft3D-WAVE model.

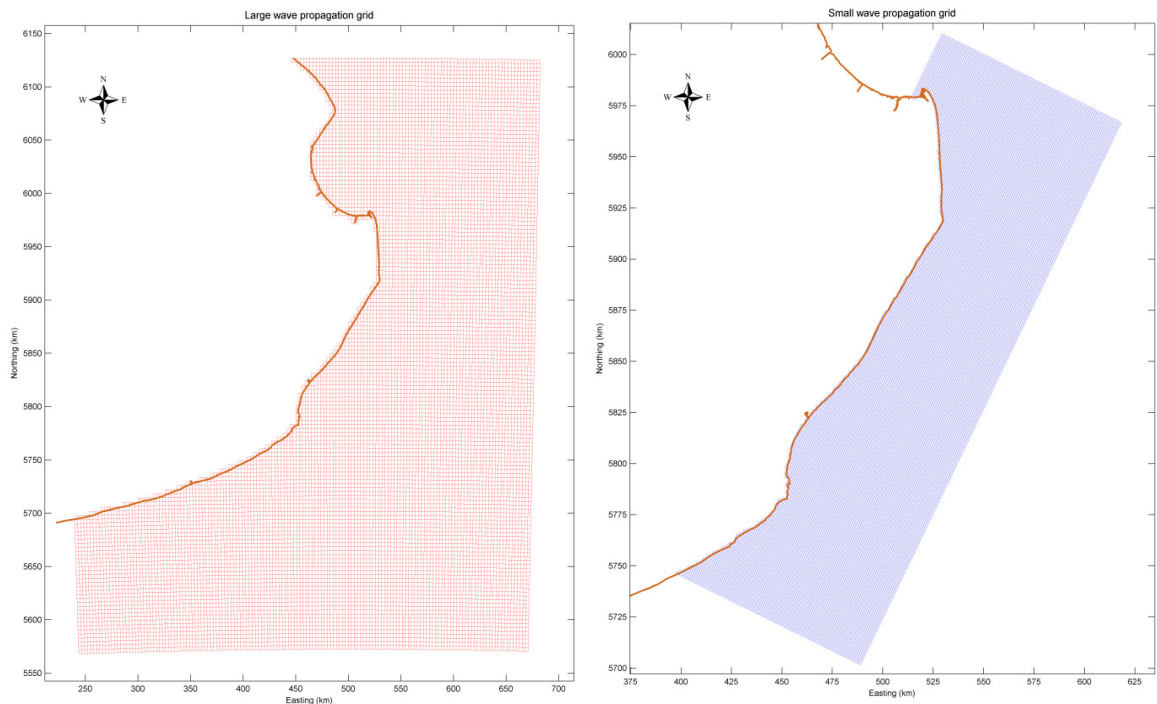


Figure 5.1 Nested grids for Delft3D-WAVE computation Left: 3,000x3,700 m grid, Right: 1,000x1,000 m grid

For a coastline of more than 500 km, the wave and wind conditions can vary significantly from one location to another as shown in section 3.1.3 and 3.2. Therefore, 12 different grid points of the NWW3 model are defined as boundary data points to generate spatial varying wave conditions.

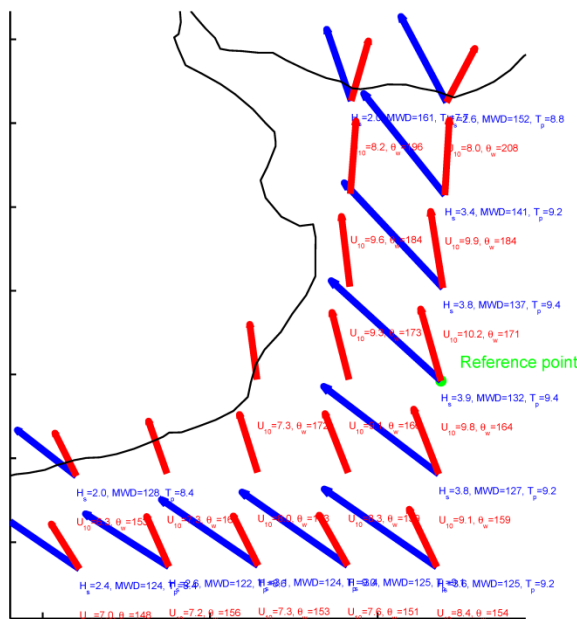


Figure 5.2 Example a scenario of simultaneous occurring wind- (in red) and wave conditions (in blue)

Using the ORCA tool, for the grid point in the middle of the east border (38°S 55°W) of the computational grid, the local wave and corresponding wind climate is schematized in 125 different scenarios. Subsequently, for every different scenario, the simultaneous occurring wind and wave conditions were looked up in every other NWW3 grid point and averaged (as visualised in Figure 5.2).

Because no wind data is available on land, it was necessary to extrapolate the wind conditions to the adjacent area in land using the MATLAB function *inpaint_nans* using method 4. This method uses a spring metaphor, assuming springs (with a nominal length of zero) connect each node with every neighbour (horizontally, vertically, and diagonally). Since each node tends to get the same value as its neighbours, extrapolation is as a constant function where this is consistent with the neighbouring nodes (D'Errico, 2006).

The final model runs are performed using the following model parameters:

| | | | |
|--------------------------------|---|--------------|----------|
| Depth-induced breaking: | Alpha: 0.1 Gamma: 0.73 | Diffraction: | Inactive |
| Non-linear triad interactions: | Alpha: 0.1 Beta: 2.2 | Wind growth: | Active |
| Bottom friction Coefficient: | JONSWAP 0.067 m ² /s ³ | Whitcapping: | Active |
| Forces: | Radiation stress | Quadruplets: | Active |
| | | Refraction: | Active |
| | | Wave set-up: | Active |

Table 5.2 Model parameters used in Delft3D-WAVE

5.3 Model results

Figure 5.3 presents the directional distribution of wave heights and periods around the port of Mar del Plata in the MSL -7 m depth contour. The east to southeast dominance of nearshore waves can be observed and shows similarities with the wave pressure sensor measurements of Sunrise Technical Consultants (1968) in Table 3.1. It can also be seen that the incoming wave angle is linked to the shape and orientation of the coast. In the south section, the occurrence of larger waves is higher.

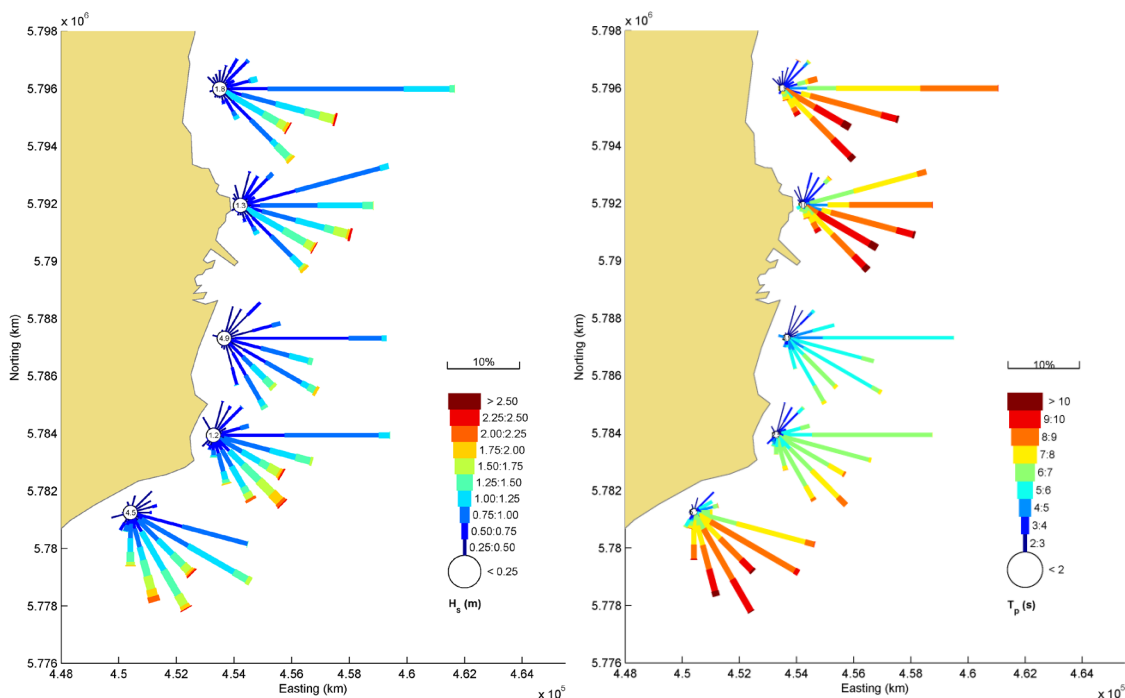


Figure 5.3 Directional distribution of nearshore significant wave heights (left) and peak wave periods (right) at MSL -7 m depth contour

6 Setup hydrodynamics & sediment transports model

6.1 Model description

To be able to identify and quantify the physical processes influencing the accessibility of the port of Mar del Plata, a model is set up in Delft3D-FLOW.

Delft3D-FLOW is a multi-dimensional (2D or 3D) hydrodynamic and transport simulation program which calculates non-steady flow and transport phenomena that result from tidal and meteorological forcing on a rectilinear or a curvilinear, boundary fitted grid. It can carry out simulations of flows, sediment transports, waves, water quality, morphological developments and ecology for coastal, river and estuarine areas (Deltares, 2011a).

6.2 Modelling approach

This model is set up and subsequently developed and analysed in the following stages:

| Stage | Model run(s) with: | Research questions to gain insight in: |
|-------|--|--|
| 1. | Tidal forcing only, with 2012 bathymetry | <ol style="list-style-type: none"> 1. What are the estimated flow directions and magnitudes around the port entrance due to tide only? 2. Are the estimated flows comparable to the field measurements of flow in the port entrance? 3. What is the direction and magnitudes of initial sediment transports due to tidal flow? |
| 2. | Wind and incoming waves only with 2012 bathymetry | <ol style="list-style-type: none"> 1. What is the effect of different angles of incoming wind and wave directions on hydrodynamics and initial sediment transports around the port? |
| 3. | Tidal forcing and representative wind and wave climate with 2012 bathymetry | <ol style="list-style-type: none"> 1. What is the effect of each scenario on hydrodynamics and initial sediment transports? 2. What are the resulting yearly weighted average initial sediment transport rates per transect over the littoral zone? 3. What is the total initial accretion or erosion rate per cell? 4. Are the outcomes of the model comparable to present sedimentation rates? |
| 4. | Different horizontal eddy coefficients with 2012 bathymetry | <ol style="list-style-type: none"> 1. What is the effect of the use of different horizontal eddy diffusivity parameters on the sediment transports 2. Which parameter is most suitable to use in this case. |
| 5. | Bathymetry with preferred navigation channel as described in (DNVN, 2011) | <ol style="list-style-type: none"> 1. What is the effect of this bathymetry on initial sediment transports? 2. What is the total initial accretion or erosion rate per area? 3. Are the outcomes of the model comparable to historic initial sedimentation rates? |
| 6. | Measures to reduce channel deposition with preferred navigation channel bathymetry | <ol style="list-style-type: none"> 1. What is the effect of each individual measure on initial sediment transports? 2. What is the total initial accretion or erosion rate per area directly after execution of each individual measure? |

Table 6.1 Overview modelling steps

6.3 Model set-up Delft3D-FLOW

For this study a Delft3D-FLOW model is set up with the aim to compute flows, waves, and sediment transports near Mar del Plata in the horizontal plane (so in 2-dimensions) with special interest near the port entrance of Mar del Plata.

The following sections describe the development and modelling considerations.

6.3.1 Domain

6.3.1.1 Land boundary

The used land boundary is based on Google Earth satellite images taken between 6 October 2011, and 29 January 2012 (Google, 2012). This boundary is constructed by linear interpolation between points picked on the high water line with average interval of 50 m and in more detail over the border of coastal structures. This data is stored to the Cartesian coordinate system UTM21S.

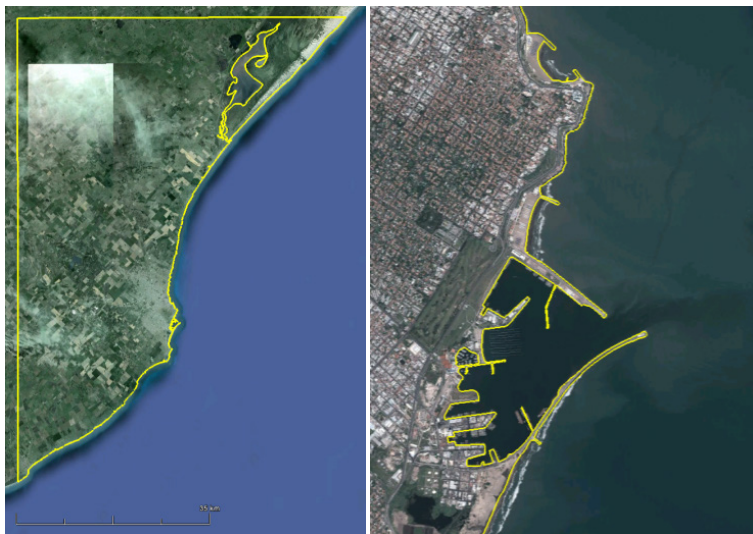


Figure 6.1 Land boundary (yellow) obtained using satellite images (Google, 2012)

6.3.1.2 Computational grid

To reduce computation time and to have detailed results in the area of interest, a curvilinear grid is constructed over the study area with a grid cell size of 250 x 500 m at the offshore boundary, smoothly decreasing to a cell size of 25 x 50 m near the port entrance (Figure 6.2). To obtain suitable flow and transport data at the grid cell borders, the grid is constructed in a way that its lines smoothly follow the northern and southern breakwater with perpendicular crossing at the port entrance and the landward boundary smoothly follows the shoreline. To reduce boundary effects and to enable correct wave refraction this grid reaches 20 km alongshore and offshore Mar del Plata (to depths of ca. 25 m).

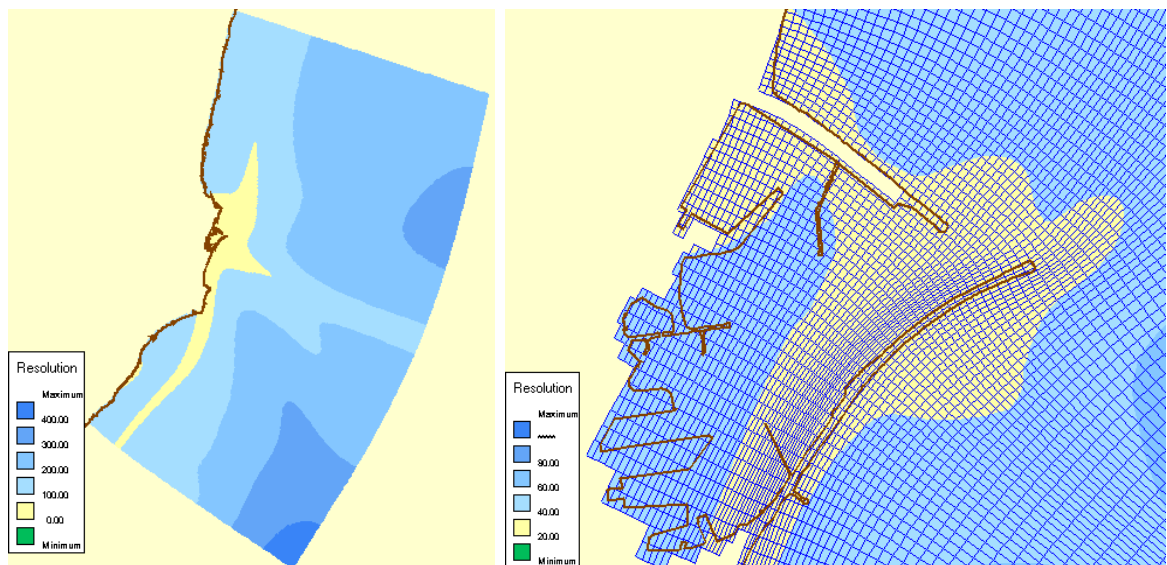


Figure 6.2 Distribution of grid size resolution (square root of grid cell area)
 Left: Full grid, Right: Detail of grid and resolution at port entrance

This grid meets the following requirements of Deltares (2011b):

- The error in the direction of the pressure gradient in Delft3D-FLOW is proportional to the deviation of the cosine value from zero. Therefore, the cell centred cosine value, called orthogonality, should be close to zero. In offshore areas, the orthogonality should be less than 0.02. Near closed boundaries, larger values can be tolerated than in the inner model area.
 - ✓ In offshore areas, this grid has a maximum orthogonality of 0.01. At the port entrance, the maximum orthogonality is 0.02.
- The grid should be smooth to minimise truncation errors in the finite difference scheme. Adjacent grid cell sizes should vary less than 20% in the area of interest, although locally exceptions may be acceptable.
 - ✓ This grid has a maximum variation of 14%
- The ratio of grid cell dimensions, value ≥ 1 , must be in the range [1,20]
 - ✓ The grid cells in this grid have an aspect ratio between 1 and 14

6.3.1.3 Bathymetry

For every corner point of the grid cells of both grids, the most recent water depth (referred to mean sea level) is obtained from the different available sources with the following order of priority:

1. Depth sounding of 16-04-2012 (DNVN, 2012a)
2. Depth sounding of 20-03-2012 (DNVN, 2012b)
3. Nautical chart of port of Mar del Plata (SHN, 2010)
4. Nautical chart of roadstead of Mar del Plata (SHN, 2012c)
5. Depth profiles of shoreface (MOSP, 1996)
6. Nautical charts of northern and southern coastal areas (SHN, 2012a, 2012b)
7. General Bathymetric Chart of the Oceans (GEBCO, 2011)

In areas where depth information has a low spatial resolution, triangular interpolation is used to derive the depths of intermediate grid cell corner points.

At the sea side of the southern breakwater there is no available depth data between the tip and the middle. Therefore two different water depths are assumed (and simulated) at the edge of the breakwater linearly increasing to the surveyed depths at around 5 m water depths (see section 0).

6.3.1.4 Thin dams and dry points

Where the land boundary crosses grid cells, the height of the land is adjusted to get a 0 m depth contour that is close to the land boundary. In situations where depths in wet areas would be affected too much by these adjustments, thin dams and dry points are introduced (as shown red in Figure 6.2).

Thin dams prohibit flow exchange between the two adjacent computational cells without reducing the total wet surface and the volume of the model. Dry points are grid cells centred around a water level point that are permanently dry during a computation, irrespective of the local water depth and without changing the water depth as seen from the wet points (Deltares, 2011a).

6.3.2 Time step

The stability of the computation, and as a consequence its accuracy, is dependent on the Courant-(Friedrichs-Lewy) number (CFL), defined by:

$$CFL = \frac{\Delta t \sqrt{gH}}{\{\Delta x, \Delta y\}} \quad (6.1)$$

Where Δt is the time step (in seconds), g is the local acceleration of gravity (9.80 m/s^2), H is the (maximum) water depth (25 m), and $\{\Delta x, \Delta y\}$ is a characteristic (minimum) value of the grid spacing in either direction (20 m). Generally, the Courant number should not exceed a value of ten (Deltares, 2011a).

For this case, a time step of 0.2 min is chosen, which meets the requirements:

$$CFL < 10 = \frac{0.2 \sqrt{9.79 \cdot 25}}{20} = 9.4 < 10 \quad (6.2)$$

6.3.3 Sediment parameters

From nine samples taken on different places near the port between the shoreline and the 7 m depth contour (Table 3.8 and Table 10.1) a mean d_{50} of 181μ is measured with a standard deviation in d_{50} of 23μ . Due to this relatively small standard deviation, one uniform sediment sort is used for this model with a d_{50} of 181μ .

6.3.4 Initial conditions

To reduce the spin-up time of the model, an initial water level of 0.4 m is used which is equal to the tidal amplitude.

6.3.5 Boundaries

At the north and south boundary of the flow grid a Neumann type of boundary is used to impose the alongshore water level gradient.

Neumann boundaries can only be applied on cross-shore boundaries in combination with a water level boundary at the seaward boundary, which is needed to make the solution of the mathematical boundary value problem well-posed (Deltares, 2011a).

At the east border a harmonic forcing is used with an amplitude of 0.4 m, equal to the average tidal amplitude (SHN, 2012d) with a vertical tide period of 12 hours (for modelling convenience). This open boundary is not reflective for short wave disturbances that propagate towards the boundary from inside the model. Over the border, a uniform (time varying) water level is used. Vertical tide is warranted due to the small spatial phase difference in this coastal area (described in section 0).

6.3.6 Physical parameters

In this model, the default physical parameters of Delft3D are preserved except for the following parameters:

Gravity: 9.80 m/s^2 (Wolfram Alpha, 2012)

Water density: 1025 kg/m^3 (average density of salt water)

Horizontal eddy diffusivity:

In Delft3D, the horizontal turbulent transport of sediment is parameterized as horizontal eddy diffusivity. By default, this user-defined parameter is assumed to be uniform in space and time.

For detailed models where much of the details of the flow are resolved by the grid, grid sizes typically tens of metres or less, the values for the eddy diffusivity are typically in the range of 1 to $10 \text{ m}^2/\text{s}$. For small-scale applications, the default value of $10 \text{ m}^2/\text{s}$ is too large (Deltares, 2011a).

The Horizontal Large Eddy Simulation (HLES) model of shallow water flows subjected to bed friction can be used to formulate spatially and temporarily varying fluctuations of the sub-grid eddy diffusivity. The resulting diffusivity is the maximum of the user-defined value and the calculated value from the HLES-model (Deltares, 2011a).

In the HLES-model a relaxation time scale of the eddies, τ , must be defined. According to Deltares (2011a), for practical applications a positive value for τ should be used; its value may be determined as 2 to 6 times the (largest) time scale of the eddies.

In this model, wind and incoming wave conditions are constant over time, so flow changes only due to tidal forcing. Because tidal conditions change in the order of 5 to 15 minutes, a relaxation time of 30 minutes is chosen.

In total three different model runs were performed using the parameters in the table below.

| Run | User-defined hor. eddy diffusivity | HLES-model |
|-----|------------------------------------|-----------------------------------|
| A | 1 m ² /s | Disabled |
| B | 10 m ² /s | Disabled |
| C | 0 m ² /s | Enabled (relaxation time 30 min.) |

Table 6.2 Model runs using different parameters for horizontal eddy diffusivity

6.3.7 Numerical parameters

In combination with the initial water level of section 6.3.4, a smoothing time of 10 min. is chosen to reduce the spin-up time of the model (to 12 hours).

6.4 Model set-up Delft3D-WAVE

6.4.1 Computational grids

The Delft3D-FLOW grid (and bathymetry) is also used as fine wave grid nested in a larger and coarser grid. This so called “wave grid” is used for the computation of wave propagation from offshore and alongshore to the boundaries of the finer computational grid (here called “flow grid”). To enable refraction of waves from south and north to and to prevent boundary effect in area of interest, the wave grid reaches 200 km to both north and south and 45 km to the east (to water depths between 40 and 80 m). The wave grid has a cell size of 2 x 1 km and consists of 7200 grid cells (Figure 6.3).

Depths of this grid are obtained from the corner points of the Delft3D-FLOW grid and from General Bathymetric Chart of the Oceans (GEBCO, 2011).

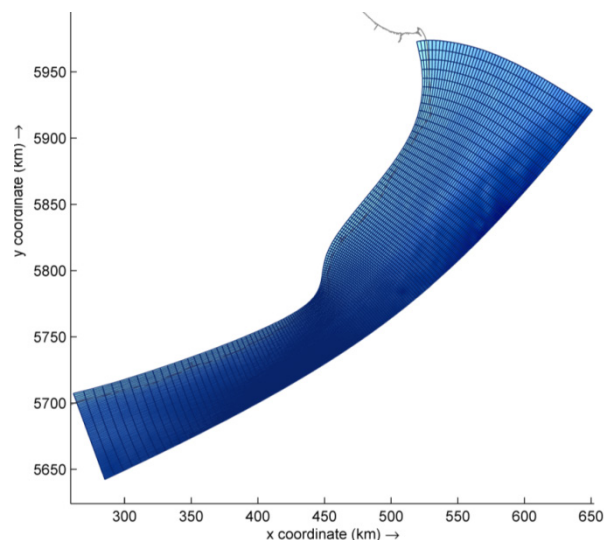


Figure 6.3 Wave grid

6.4.2 Boundaries and physical parameters

The wind and wave conditions are derived from the near shore wave model in a joint study with Camarena Calderon (2012) (described in section 5). The input is extracted at one point in the middle of the south-east boundary of the “wave grid”, at UTM21s 491126 m east, 5756185 m north on 69 m water depth. This resulted in an annual climate with 125 scenarios of simultaneous occurring wind and wave conditions is visualised in Table 6.3. The entire dataset can be found in appendix C.

| Significant wave height (in m) | Mean wave direction (with respect to north) | | | | | | | | | | | | | | | | | | | | | | | | | Total |
|--------------------------------|---|----------|-----------|-----------|-----------|-----------|-----------|------------|-------------|-------------|-------------|-------------|-------------|-------------|-------------|-------------|-------------|-------------|-------------|-------------|-------------|-------------|-------------|-------------|--------|-------|
| | 352.5-7.5 | 7.5-22.5 | 22.5-37.5 | 37.5-52.5 | 52.5-67.5 | 67.5-82.5 | 82.5-97.5 | 97.5-112.5 | 112.5-127.5 | 127.5-142.5 | 142.5-157.5 | 157.5-172.5 | 172.5-187.5 | 187.5-202.5 | 202.5-217.5 | 217.5-232.5 | 232.5-247.5 | 247.5-262.5 | 262.5-277.5 | 277.5-292.5 | 292.5-307.5 | 307.5-322.5 | 322.5-337.5 | 337.5-352.5 | | |
| >4.00 | | | | | | | | | | | | | | | | | | | | | | | | | | 0,00 |
| 3.75-4.00 | | | | | | | | | 0,10 | 0,10 | | | | | 0,01 | 0,01 | | | | | | | | | | 0,22 |
| 3.50-3.75 | | | | | | | | 0,15 | 0,04 | | | 0,46 | 0,36 | | 0,10 | 0,02 | 0,01 | | | | | | | | | 1,14 |
| 3.25-3.50 | | | | | | | | | | | | | | | | | | | | | | | | | | 0,00 |
| 3.00-3.25 | | | | | | | | | | | | | | | | | | | | | | | | | | 0,00 |
| 2.75-3.00 | | | | | | | | 0,20 | 0,15 | 0,21 | 0,35 | 1,09 | 0,95 | | 0,46 | 0,08 | 0,00 | | | | | | | | | 3,49 |
| 2.50-2.75 | | | | | 0,03 | | 0,31 | 0,29 | | 0,30 | 0,52 | | | | | | | | | | | | | | | 1,44 |
| 2.25-2.50 | | | | | | | 0,33 | 0,45 | 0,25 | 0,42 | | 1,24 | 1,00 | | 0,48 | 0,17 | 0,06 | | | | | | | | | 4,39 |
| 2.00-2.25 | | | | 0,11 | | 0,01 | | 1,06 | | | 0,92 | 1,88 | 1,46 | | 0,76 | 0,26 | | 0,05 | | | | | | | | 6,52 |
| 1.75-2.00 | 0,01 | 0,06 | | 0,33 | | 1,58 | 1,53 | | 0,71 | 1,44 | | 2,88 | 2,01 | | | | 0,07 | 0,00 | | | | | | | | 10,62 |
| 1.50-1.75 | | 0,08 | 0,25 | | 0,95 | | 1,76 | 1,28 | 1,26 | 1,81 | 3,77 | | | | 1,04 | 0,43 | 0,21 | | 0,19 | 0,06 | | | 0,01 | | | 13,09 |
| 1.25-1.50 | | | 0,70 | | 1,82 | 6,52 | 3,53 | 1,33 | | | | | | 2,81 | | 1,72 | 0,62 | | | 0,51 | | | 0,16 | | 0,22 | 19,94 |
| 1.00-1.25 | | 0,48 | 1,58 | | | 8,32 | | | 4,16 | | | | | 2,21 | 1,45 | 0,60 | | 0,38 | | 0,72 | | | 0,68 | | 0,48 | 21,05 |
| 0.75-1.00 | | 3,41 | 1,83 | | | 2,74 | 1,08 | | | | | 0,52 | | | | | 0,80 | | | | | | 1,17 | | 1,55 | 13,09 |
| 0.50-0.75 | 1,55 | | 0,37 | 0,29 | 1,02 | | | | | | | | | | | | 0,13 | | | | | | 0,98 | 0,10 | | 4,44 |
| 0.25-0.50 | 0,35 | | | | | | | | | | | | | | | | | | | | | | | | 0,24 | 0,59 |
| 0.00-0.25 | | | | | | | | | | | | | | | | | | | | | | | | | | 0,00 |
| | 1,91 | 4,03 | 4,71 | 0,73 | 6,56 | 17,52 | 7,46 | 4,75 | 6,66 | 4,27 | 6,08 | 7,55 | 10,80 | 1,45 | 5,16 | 1,71 | 1,53 | 0,06 | 1,43 | 0,06 | 0,98 | 2,10 | 0,25 | 2,24 | 100,00 | |
| | | | | | | | | | | | | | | | | | | | | | | | | Total | | |

Table 6.3 Directional distribution of wave heights (in %) derived from near shore wave model Buenos Aires at UTM21s 491126 m east, 5756185 m north on 69 m water depth

If all these conditions would directly be imposed on Delft3D, with a run-time of 200 minutes per wave condition, the computational effort would be more than 17 days. To estimate the net and gross sediment transports around Mar del Plata, the wind and wave climate therefore had to be reduced to a smaller number of scenarios of simultaneously occurring wind- and wave conditions that represent the natural variability but strongly reduce the computation time.

Input reduction always introduces errors, but the most accurate representation of full set can be found by selecting blocks based on equal weighted contribution to the sediment transport (Walstra, 2011). With this method, wave conditions with approximately equal relative weighted contribution to the sediment transport (W_i) are grouped to bins.

According to the CERC formula, the longshore transport S_{long} can be calculated as follows:

$$S_{long} = AH_{m0}^{2.5} \sin(2(\varphi_w - \varphi_c)) \tag{6.3}$$

Simplified applies:

$$S \sim H_s^{2.5} \tag{6.4}$$

Therefore, the relative contribution to the sediment transport (W_i) is:

$$W_i = \frac{P(H_{s,i}, Dir_i) H_{s,i}^{2.5}}{\sum_{i=1}^n [p_i H_{s,i}^{2.5}]} \tag{6.5}$$

Then wave conditions with approximately equal relative weighted contribution to the sediment transport (W_i) are grouped to bins in Table 6.4.

| | | Mean wave direction (with respect to north) | | | | | | | | | | | | | | | | | | | | | | | | | |
|--------------------------------|-----------|---|----------|-----------|-----------|-----------|-----------|-----------|------------|-------------|-------------|-------------|-------------|-------------|-------------|-------------|-------------|-------------|-------------|-------------|-------------|-------------|-------------|-------------|-------------|--------|-------|
| | | 362.5-7.5 | 7.5-22.5 | 22.5-37.5 | 37.5-52.5 | 52.5-67.5 | 67.5-82.5 | 82.5-97.5 | 97.5-112.5 | 112.5-127.5 | 127.5-142.5 | 142.5-157.5 | 157.5-172.5 | 172.5-187.5 | 187.5-202.5 | 202.5-217.5 | 217.5-232.5 | 232.5-247.5 | 247.5-262.5 | 262.5-277.5 | 277.5-292.5 | 292.5-307.5 | 307.5-322.5 | 322.5-337.5 | 337.5-352.5 | | |
| Significant wave height (in m) | >4.00 | | | | | | | | | | | | | | | | | | | | | | | | | 0,00 | |
| | 3.75-4.00 | | | | | | | | | 0,82 | 0,80 | | | | | | 0,06 | 0,08 | | | | | | | | 1,77 | |
| | 3.50-3.75 | | | | | | | | | 1,05 | 0,30 | | | 3,23 | 2,48 | | 0,66 | 0,12 | 0,09 | | | | | | | 7,92 | |
| | 3.25-3.50 | | | | | | | | | | | | | | | | | | | | | | | | | | 0,00 |
| | 3.00-3.25 | | | | | | | | | | | | | | | | | | | | | | | | | | 0,00 |
| | 2.75-3.00 | | | | | | | | | 0,77 | 0,58 | 0,81 | 1,38 | 4,24 | 3,70 | | 1,80 | 0,32 | 0,01 | | | | | | | | 13,61 |
| | 2.50-2.75 | | | | | 0,08 | | | 0,96 | 0,90 | | 0,92 | 1,61 | | | | | | | | | | | | | | 4,47 |
| | 2.25-2.50 | | | | | | | | 0,81 | 1,08 | 0,60 | 1,02 | | 3,01 | 2,42 | | 1,16 | 0,41 | 0,13 | | | | | | | | 10,63 |
| | 2.00-2.25 | | | | 0,21 | | | | 0,01 | 1,95 | | 1,69 | 3,44 | 2,68 | | 1,39 | 0,48 | | | | | | | | | | 11,94 |
| | 1.75-2.00 | 0,02 | 0,07 | | 0,44 | | | | 2,12 | 2,05 | | 0,95 | 1,93 | | 3,86 | 2,70 | | | | | | | 0,09 | 0,00 | | | 14,22 |
| | 1.50-1.75 | | 0,08 | 0,23 | | 0,89 | | | 1,65 | 1,19 | 1,18 | 1,69 | 3,53 | | | | 0,97 | 0,40 | 0,20 | | 0,18 | 0,05 | | | 0,01 | | 12,26 |
| | 1.25-1.50 | | | 0,43 | | 1,13 | 4,02 | 2,18 | 0,82 | | | | | | 1,74 | | 1,06 | 0,38 | | | 0,32 | | | 0,10 | 0,13 | | 12,31 |
| | 1.00-1.25 | | 0,18 | 0,59 | | | 3,11 | | | 1,55 | | | | | 0,83 | 0,54 | 0,22 | | 0,14 | | 0,27 | | | 0,25 | 0,18 | | 7,86 |
| | 0.75-1.00 | | 0,68 | 0,36 | | 0,55 | 0,22 | | | | | | | 0,10 | | | | | 0,16 | | | | | 0,23 | 0,31 | | 2,61 |
| | 0.50-0.75 | 0,13 | | 0,03 | 0,02 | 0,09 | | | | | | | | | | | | | 0,01 | | | | 0,08 | 0,01 | | | 0,38 |
| | 0.25-0.50 | 0,01 | | | | | | | | | | | | | | | | | | | | | | | 0,01 | | 0,01 |
| 0.00-0.25 | | | | | | | | | | | | | | | | | | | | | | | | | | 0,00 | |
| | | 0,16 | 1,01 | 1,65 | 0,67 | 2,73 | 9,48 | 7,64 | 7,76 | 5,98 | 7,17 | 8,31 | 17,78 | 16,53 | 0,54 | 7,33 | 2,20 | 0,82 | 0,10 | 0,76 | 0,05 | 0,08 | 0,59 | 0,02 | 0,62 | 100,00 | |
| | | | | | | | | | | | | | | | | | | | | | | | | | | | Total |

Table 6.4 Relative weighted contribution to the sediment transport (W_i)

| | | Mean wave direction (with respect to north) | | | | | | | | | | | | | | | | | | | | | | | |
|--------------------------------|-----------|---|----------|-----------|-----------|-----------|-----------|-----------|------------|-------------|-------------|-------------|-------------|-------------|-------------|-------------|-------------|-------------|-------------|-------------|-------------|-------------|-------------|-------------|-------------|
| | | 362.5-7.5 | 7.5-22.5 | 22.5-37.5 | 37.5-52.5 | 52.5-67.5 | 67.5-82.5 | 82.5-97.5 | 97.5-112.5 | 112.5-127.5 | 127.5-142.5 | 142.5-157.5 | 157.5-172.5 | 172.5-187.5 | 187.5-202.5 | 202.5-217.5 | 217.5-232.5 | 232.5-247.5 | 247.5-262.5 | 262.5-277.5 | 277.5-292.5 | 292.5-307.5 | 307.5-322.5 | 322.5-337.5 | 337.5-352.5 |
| Significant wave height (in m) | >4.00 | | | | | | | | | | | | | | | | | | | | | | | | |
| | 3.75-4.00 | | | | | | | | | | | | | | | | | | | | | | | | |
| | 3.50-3.75 | | | | | | | | | | | | | | | | | | | | | | | | |
| | 3.25-3.50 | | | | | | | | | | | | | | | | | | | | | | | | |
| | 3.00-3.25 | | | | | | | | | | | | | | | | | | | | | | | | |
| | 2.75-3.00 | | | | | | | | | | | | | | | | | | | | | | | | |
| | 2.50-2.75 | | | | | | | | | | | | | | | | | | | | | | | | |
| | 2.25-2.50 | | | | | | | | | | | | | | | | | | | | | | | | |
| | 2.00-2.25 | | | | | | | | | | | | | | | | | | | | | | | | |
| | 1.75-2.00 | | | | | | | | | | | | | | | | | | | | | | | | |
| | 1.50-1.75 | | | | | | | | | | | | | | | | | | | | | | | | |
| | 1.25-1.50 | | | | | | | | | | | | | | | | | | | | | | | | |
| | 1.00-1.25 | | | | | | | | | | | | | | | | | | | | | | | | |
| | 0.75-1.00 | | | | | | | | | | | | | | | | | | | | | | | | |
| | 0.50-0.75 | | | | | | | | | | | | | | | | | | | | | | | | |
| | 0.25-0.50 | | | | | | | | | | | | | | | | | | | | | | | | |

Table 6.5 Numbered bins of grouped wave conditions

Per bin, the representative wave height ($H_{s;rep}$) is calculated after Walstra (2011) and Roelvink and Reniers (2011).

$$H_{s;rep} = \left(\frac{\sum_i [P(H_{s,i}, Dir_i) H_{s,i}^{2.5}]}{\sum_i P(H_{s,i}, Dir_i)} \right)^{\frac{1}{2.5}} \quad (6.6)$$

The corresponding additional wave parameters are derived in the following way:

- Delft3D-WAVE used a JONSWAP spectrum and therefore representative peak wave direction (T_p) is calculated according Mangor (2007):

$$T_p \approx 5.3 \sqrt{H_s} \quad (\text{Mangor, 2007}) \quad (6.7)$$

This function gives a good fit to the data, as visualised in Figure 6.4.

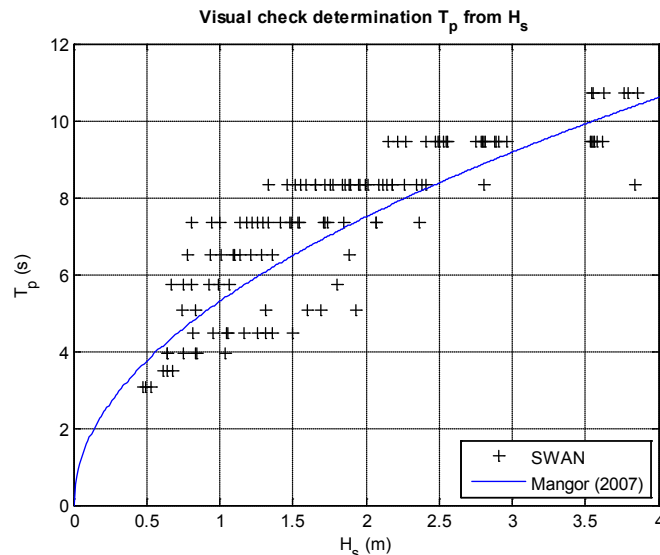


Figure 6.4 Visual check determination T_p vs. H_s according Mangor (2007) formula

- Representative mean wave direction (D_m) is calculated by taking the weighted average per bin.

$$D_m = \frac{\sum_i [p_i d_{m,i}]}{\sum_i p_i} \quad (6.8)$$

Wind parameters are correlated to wave conditions by using least squares curve fitting.

- U_{10} is defined by correlation with H_s in near shore wave model (SWAN) data.

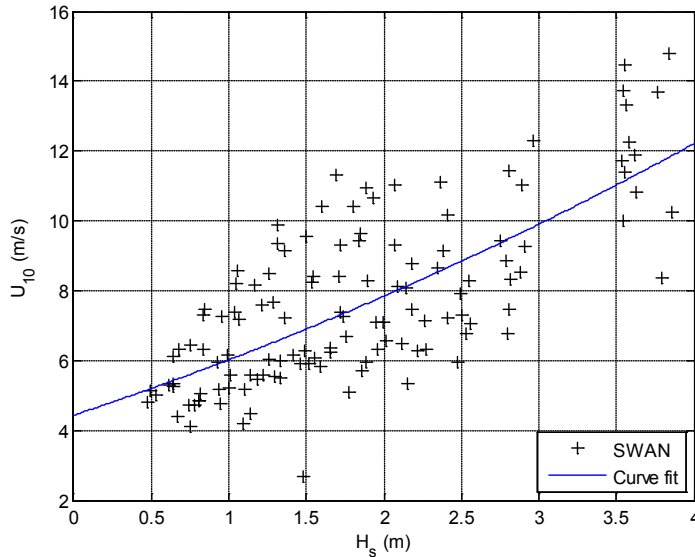


Figure 6.5 Least squares curve fitting of U_{10} against H_s

- U_{dir} is defined by correlation to D_m from SWAN data.

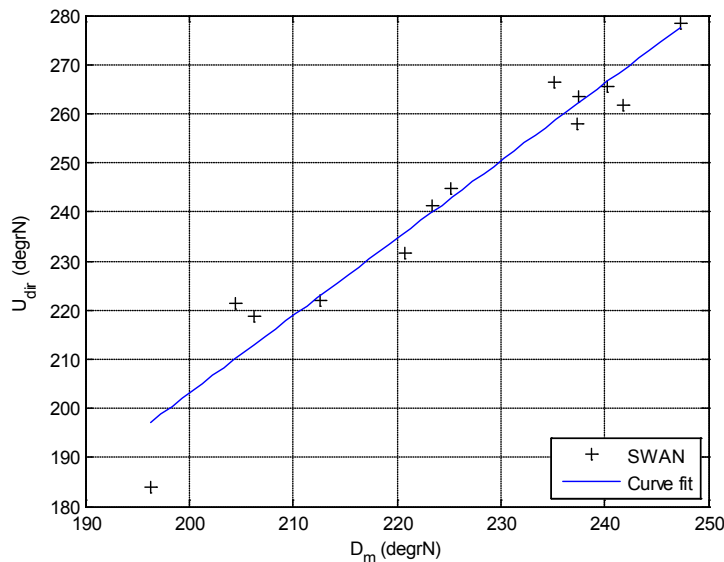


Figure 6.6 Example of least squares curve fitting between U_{dir} and D_m within bin nr. 16

- Occurrence percentage of each scenario is the sum of the occurrence percentage of all conditions within a scenario.

The derived reduced set of (16) scenarios of simultaneous occurring wind and wave conditions that represent the yearly averaged (125) conditions is displayed in Table 6.6.

| Reduced wind and wave climate | | | | | | | |
|-------------------------------|------|------|-----|------|------|-------|------|
| Scen. | Hs | Tp | Dm | U10 | Udir | P | days |
| 1 | 3,70 | 10,2 | 122 | 11,5 | 162 | 0,004 | 1,4 |
| 2 | 3,58 | 10,0 | 178 | 11,2 | 210 | 0,008 | 3,0 |
| 3 | 3,60 | 10,1 | 214 | 11,3 | 245 | 0,001 | 0,5 |
| 4 | 2,51 | 8,4 | 114 | 8,9 | 135 | 0,029 | 10,6 |
| 5 | 2,44 | 8,3 | 147 | 8,7 | 153 | 0,018 | 6,5 |
| 6 | 2,80 | 8,9 | 177 | 9,5 | 208 | 0,020 | 7,4 |
| 7 | 2,40 | 8,2 | 211 | 8,6 | 236 | 0,023 | 8,3 |
| 8 | 2,10 | 7,7 | 163 | 8,0 | 136 | 0,060 | 21,9 |
| 9 | 2,05 | 7,6 | 186 | 7,9 | 212 | 0,045 | 16,3 |
| 10 | 1,14 | 5,7 | 39 | 6,3 | 9 | 0,160 | 58,5 |
| 11 | 1,20 | 5,8 | 74 | 6,4 | 54 | 0,159 | 58,1 |
| 12 | 1,60 | 6,7 | 88 | 7,1 | 66 | 0,084 | 30,7 |
| 13 | 1,58 | 6,7 | 118 | 7,0 | 75 | 0,130 | 47,6 |
| 14 | 1,46 | 6,4 | 146 | 6,8 | 69 | 0,043 | 15,7 |
| 15 | 1,35 | 6,2 | 182 | 6,6 | 112 | 0,050 | 18,3 |
| 16 | 1,36 | 6,2 | 214 | 6,6 | 226 | 0,074 | 27,2 |

Total: 0,910 332,1

Table 6.6 Representative scenarios of wind and wave conditions at UTM21s 491126 m east, 5756185 m north on 69 m water depth.

Significant wave height (H_s), Peak wave period (T_p), Mean wave direction (D_m), Wind speed (U_{10}), Wind direction (U_{dir}), and Probability of occurrence (P)

6.4.3 Obstacles

SWAN can estimate wave transmission through a (line-)structure such as a breakwater (dam). Such an obstacle will affect the wave field in two ways, first it will reduce the wave height locally all along its length, and second it will cause diffraction around its end(s). The model is not able to account for diffraction. In irregular, short-crested wave fields, however, it seems that the effect of diffraction is small, except in a region less than one or two wavelengths away from the tip of the obstacle (Booij et al., 1992). Therefore, the model can reasonably account for waves around an obstacle if the directional spectrum of incoming waves is not too narrow. Since obstacles usually have a transversal area that is too small to be resolved by the bathymetry grid in SWAN, an obstacle is modelled as a line (Deltares, 2011c).

Therefore locations of obstacles are copied from the land boundary with heights corresponding to construction drawing of port structures (DNVN, 1968).

7 Analysis and validation of 2012 hydrodynamics & sediment transports model

The Delft3D model for the computation of hydrodynamics and sediment transports is developed and validated using consecutive model runs with:

1. Tidal forcing only
2. Wind and incoming waves only
3. Tidal forcing and representative wind and wave climate
4. Different horizontal eddy coefficients

In the following paragraphs, the results of each stage are presented and research questions of section 6.2 are answered.

7.1 Determination of effects of tide on hydrodynamics and sediment transports

To analyse and validate the computed tidal flow patterns and its contribution to sediment transports, first the Delft3D model was forced by averaged tide (described in section 6.3.5) in absence of other forcing like wind and incoming waves. The resulting hour-by-hour tide induced flow patterns over a tidal period are visualised in appendix D.

7.1.1 Estimated flow directions and magnitudes around the port entrance

Figure 7.2 to Figure 7.4 show the tidal filling of the port. These depth averaged flow velocities are ranging from 0 to 0.1 m/s. During maximum flood, ± 3 hours before high water a horizontal eddy develops at the tip of the southern breakwater, which steadily releases the tip in North-West direction (Figure 7.3) and fades away within 5 hours.

7.1.2 Validation of flow patterns and velocities

The maximum depth averaged flow velocity in the Delft3D model are in agreement with the hand calculated maximum cross section averaged flow velocity of appendix B.3.3. In addition, the computed flow directions during the 4.5 hours before high water correspond with the flow directions measured during the drift tracker measurements shown in Figure 7.2 to Figure 7.4. Because the drift trackers move with the water surface where the influence of the bottom friction to the flow is the smallest, the measured flow velocities at that level are higher than the depth averaged flow velocities. In the port entrance, the measured flow velocities at the water surface have an order of magnitude of twice the computed depth averaged flow velocities. Outside the port entrance (track E and G in Figure 7.1), the measured flow velocities are three to ten times higher than the computed tidal flow velocities. These flows are supposedly driven by the wave-induced longshore current and eddy along the Southern breakwater.

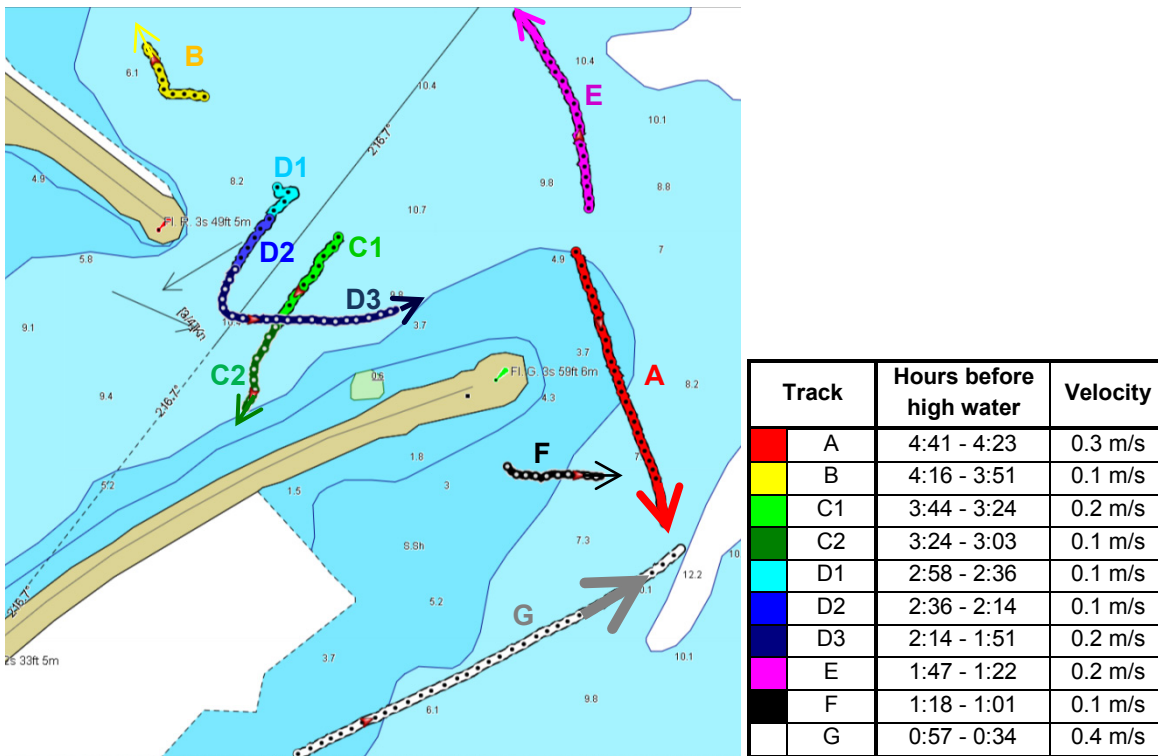


Figure 7.1 Measured magnitudes and directions of tidal currents, using GPS-drifter tracking. Left: Drifter tracks on nautical chart (UKHO, 2006a), Right: Legend and data summary

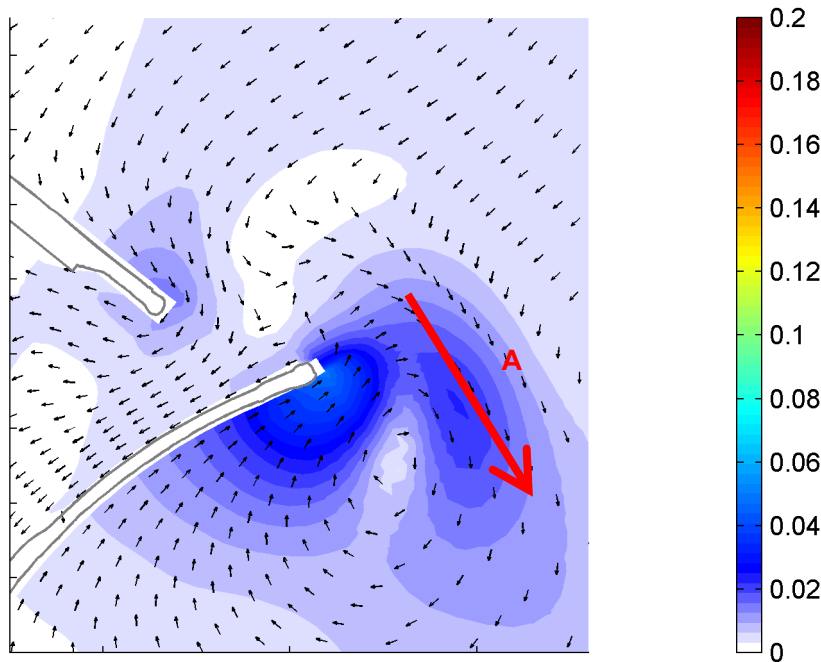


Figure 7.2 Model prediction of averaged tidal flow velocities (in m/s) and directions 5.5 hours before HW

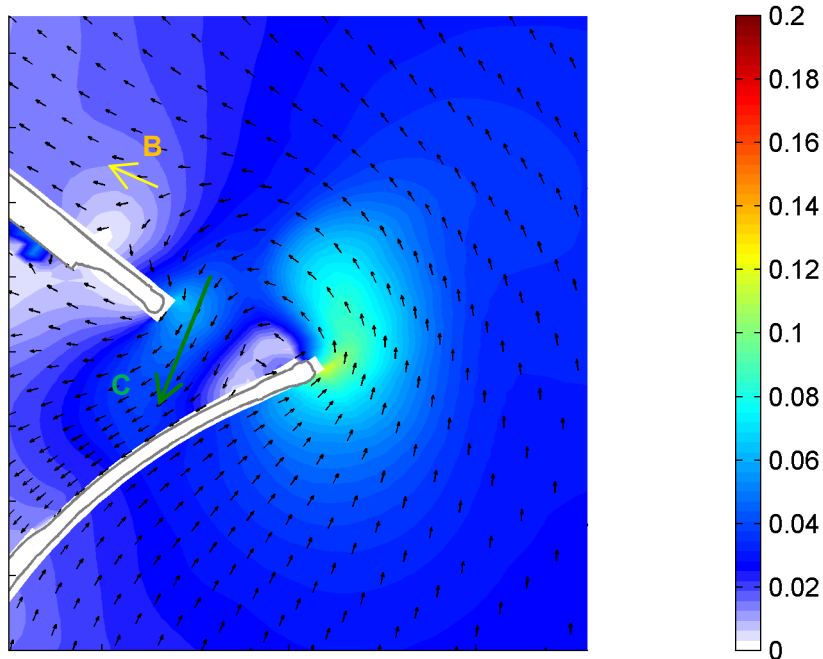


Figure 7.3 Model prediction of averaged tidal flow velocities (in m/s) and directions 2.5 hours before HW

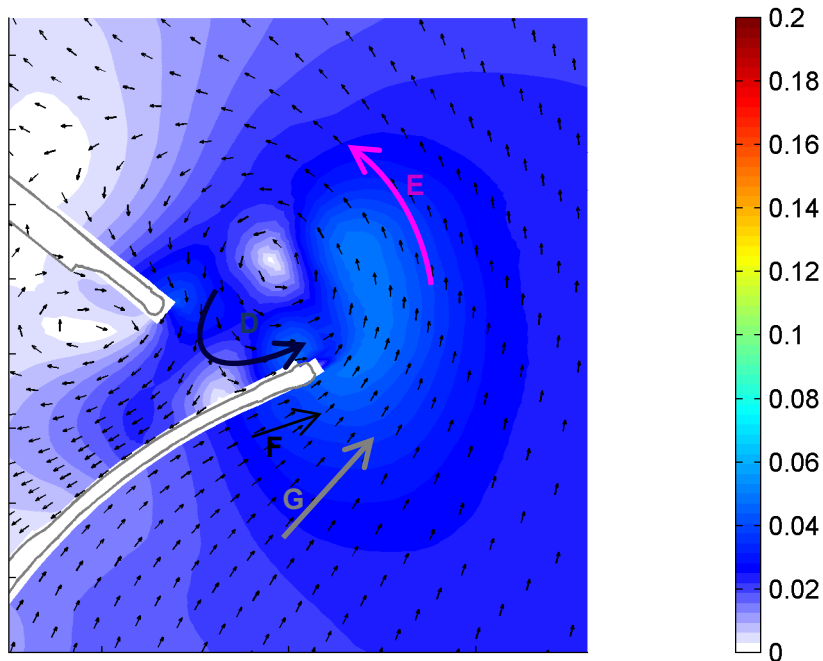


Figure 7.4 Model prediction of averaged tidal flow velocities (in m/s) and directions 0.5 hour before HW

7.1.3 Resulting initial sediment transports around the port entrance

As can be seen in Figure 7.5, tidal currents drive marginal and only local sediment transports in the order of $10^{-9} \text{ m}^3/\text{s}/\text{m}$ ($\approx 0.03 \text{ m}^3/\text{year}/\text{m}$), so tidal currents have no significant contribution to sediment transports at the port entrance of Mar del Plata.

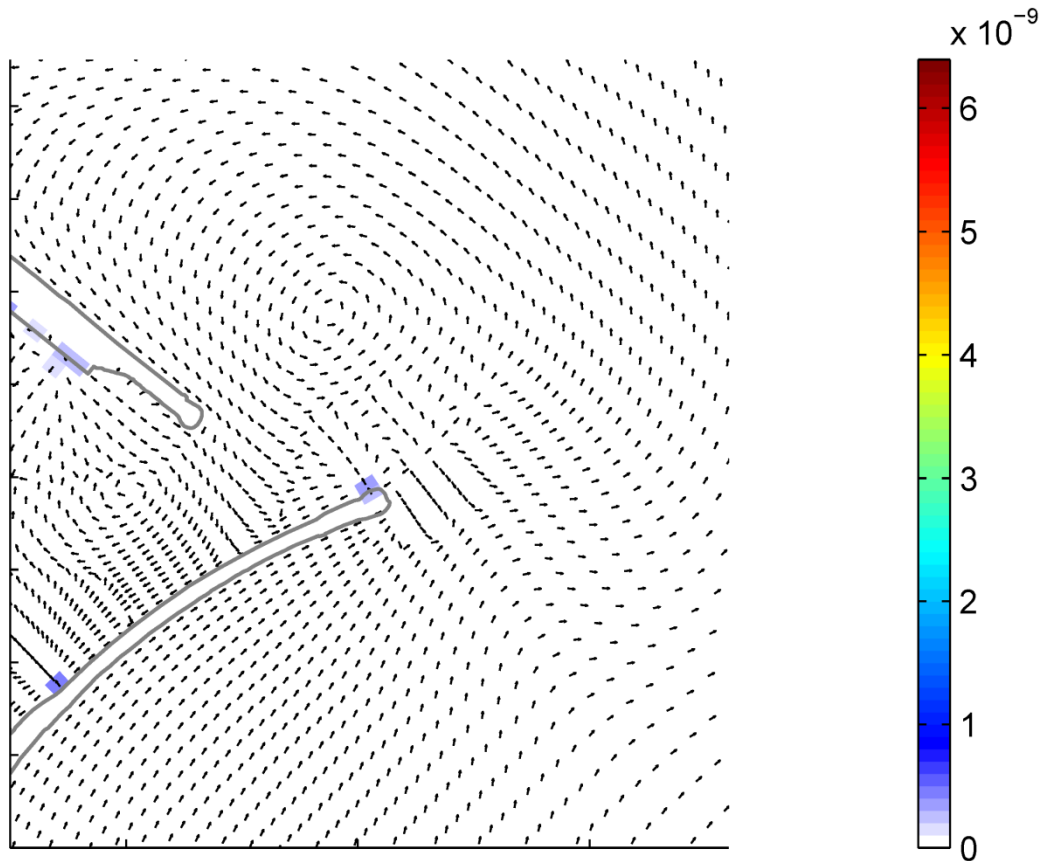


Figure 7.5 Mean total sediment transport over one tidal period
(colours indicating magnitude in $\text{m}^3/\text{s}/\text{m}$, coordinates in 10^2 m to UTM21s)

7.2 Determination effects waves on hydrodynamics and sediment transports

To systematically analyse the effect of different angles of incoming wind and wave directions on flow and sediment transport patterns and magnitudes around the port, eight different model runs were performed using the 2012 bathymetry and the wind and wave conditions in Table 7.1. The wave height at the model boundary and the wind speed over the model was kept constant at 3 m while the (equal) wave and wind direction was systematically varied (sectors of 45°).

| Run | Wave conditions at model boundaries | | | Uniform wind conditions over entire model | |
|-----|-------------------------------------|----------------|-------------------|---|-----------------|
| | H _s | T _p | Mean wave dir. | Wind direction | U ₁₀ |
| A. | 3 m | 7 s | 0° w.r.t. North | 0° w.r.t. North | 8 m/s |
| B. | 3 m | 7 s | 45° w.r.t. North | 45° w.r.t. North | 8 m/s |
| C. | 3 m | 7 s | 90° w.r.t. North | 90° w.r.t. North | 8 m/s |
| D. | 3 m | 7 s | 135° w.r.t. North | 135° w.r.t. North | 8 m/s |
| E. | 3 m | 7 s | 180° w.r.t. North | 180° w.r.t. North | 8 m/s |
| F. | 3 m | 7 s | 225° w.r.t. North | 225° w.r.t. North | 8 m/s |
| G. | 3 m | 7 s | 270° w.r.t. North | 270° w.r.t. North | 8 m/s |
| H. | 3 m | 7 s | 315° w.r.t. North | 315° w.r.t. North | 8 m/s |

Table 7.1 Wave conditions and wind conditions for model runs without tide

7.2.1 Effect on hydrodynamics and sediment transports

In appendix E, the magnitude and direction of the resulting wave fields, flow patterns, and sediment transport around the port are visualised. In Table 7.2, the most prominent resulting phenomena are described.

| Run | Wind & waves from | Resulting conditions and phenomena around the port | | |
|-----|-------------------|--|--|---|
| | | Waves | Flows | Sediment transports |
| A. | 0° w.r.t.N. | 1 m waves from NE refracting to both sides of the Southern breakwater (S. bw.) | Weak south going current | Almost no transports |
| B. | 45° w.r.t.N. | 1.5 m waves from ENE | Weak southward flows | Weak southward transports along S. bw., Shoal spread out by transports |
| C. | 90° w.r.t.N. | 2 m waves from East | Rip current north of port and strong current along S. bw to the South. | Large Southward transports along S. bw., Shoal moves west |
| D. | 135° w.r.t.N. | 2 m waves from SW breaking almost perpendicular to S. bw | Rip current in the middle of the S. bw. Other flows to the north. | Large transports from tip to middle of S. bw. From rip current, sediment is transported to the port access. |
| E. | 180° w.r.t.N. | 1,5 m waves from SSE | Strong northward flow along S. bw. | Northward sediment transport to tip of S. bw. |
| F. | 225° w.r.t.N. | 1 m waves from South | Weak current to the north | Weak Northward transport delivering sediment to tip bw. |
| G. | 270° w.r.t.N. | 0.5 m waves from South | Weak northward current | Almost no transports |
| H. | 315° w.r.t.N. | Almost no waves | Almost no flows | Marginal transport |

Table 7.2 Description of resulting conditions and phenomena around the port per wind and wave direction (visualised in appendix E)

The wave, flow, and sediment transport patterns of the scenarios driving the largest sediment transports are visualised in the figures below.

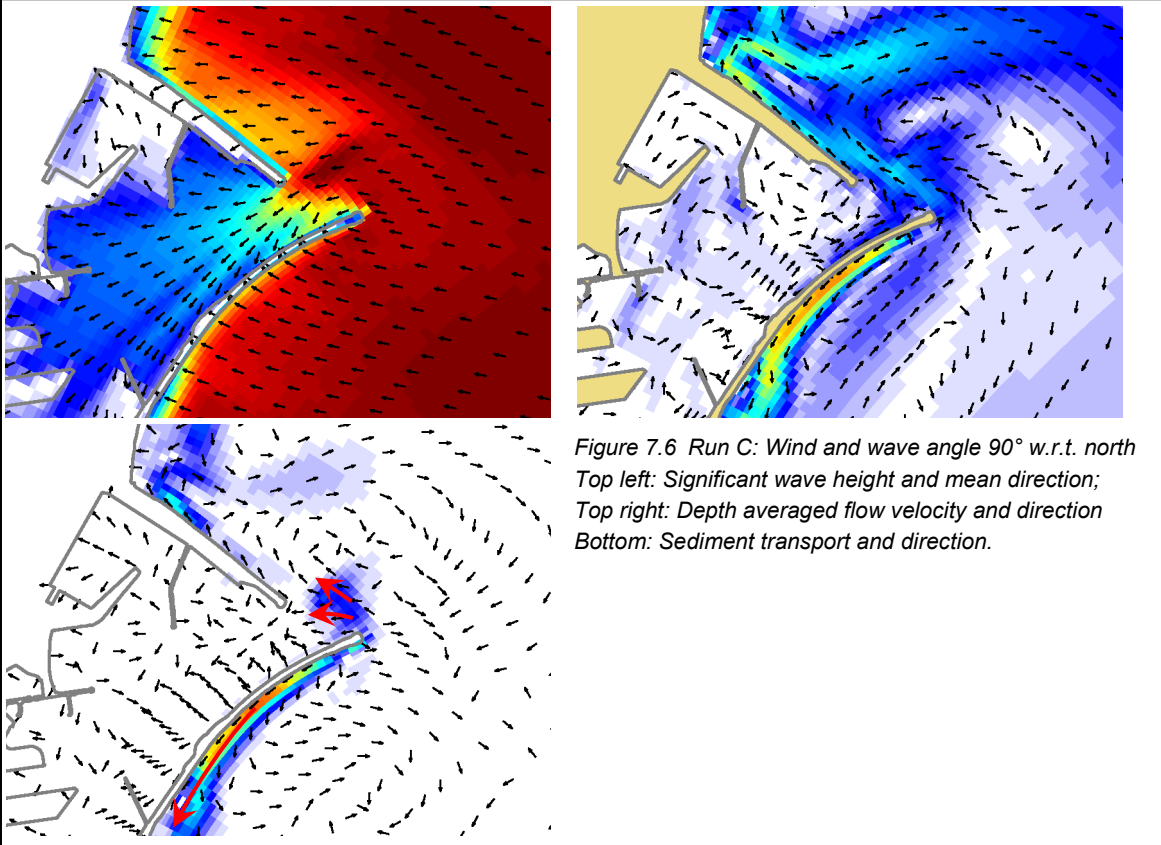


Figure 7.6 Run C: Wind and wave angle 90° w.r.t. north
 Top left: Significant wave height and mean direction;
 Top right: Depth averaged flow velocity and direction
 Bottom: Sediment transport and direction.

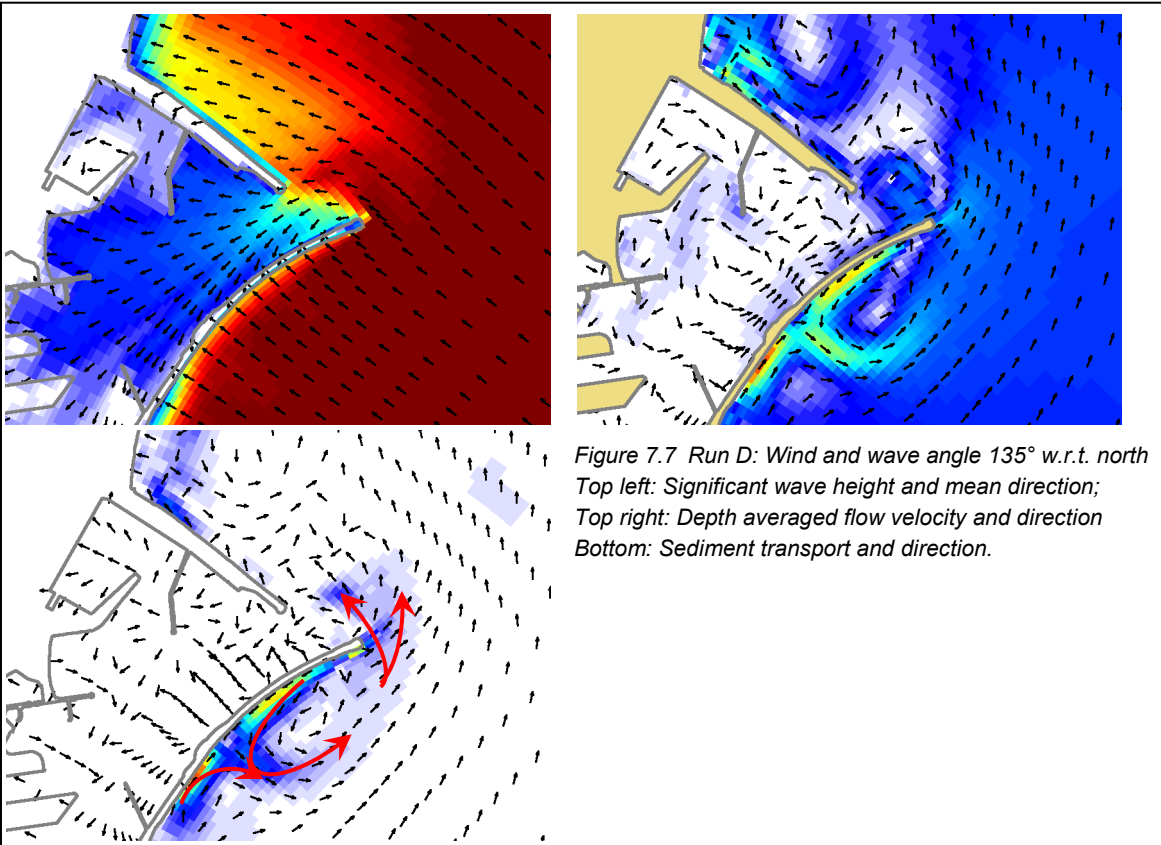


Figure 7.7 Run D: Wind and wave angle 135° w.r.t. north
 Top left: Significant wave height and mean direction;
 Top right: Depth averaged flow velocity and direction
 Bottom: Sediment transport and direction.

These results show that that significant sediment transport takes place during incoming waves from east to southwest, leading to spreading, retreat, and growth of the shoal and accretion near the tip of the southern breakwater. It can be concluded that north-eastern winds and waves do not contribute to sedimentation in the port entrance, because under these conditions there is no sediment transports to the port entrance and a southward sediment transport along the southern breakwater, which will erode sand where the transport originates and increases. Another unmistakable observation is that waves from south-eastern directions arrive almost perpendicular to middle of the curved Southern breakwater and drives a rip current at that location.

7.3 Tidal forcing and representative wind and wave climate

Model runs have been performed using:

- The 2012 bathymetry;
- Tidal forcing;
- Horizontal eddy diffusivity of 1 m²/s;
- Scenarios of simultaneous occurring wind and wave conditions that represent the yearly averaged wind and wave conditions (Table 7.3 derived in section 6.4.2).

| Reduced wind and wave climate | | | | | | | |
|-------------------------------|------|------|-----|------|------|-------|------|
| Scen. | Hs | Tp | Dm | U10 | Udir | P | days |
| 1 | 3,70 | 10,2 | 122 | 11,5 | 162 | 0,004 | 1,4 |
| 2 | 3,58 | 10,0 | 178 | 11,2 | 210 | 0,008 | 3,0 |
| 3 | 3,60 | 10,1 | 214 | 11,3 | 245 | 0,001 | 0,5 |
| 4 | 2,51 | 8,4 | 114 | 8,9 | 135 | 0,029 | 10,6 |
| 5 | 2,44 | 8,3 | 147 | 8,7 | 153 | 0,018 | 6,5 |
| 6 | 2,80 | 8,9 | 177 | 9,5 | 208 | 0,020 | 7,4 |
| 7 | 2,40 | 8,2 | 211 | 8,6 | 236 | 0,023 | 8,3 |
| 8 | 2,10 | 7,7 | 163 | 8,0 | 136 | 0,060 | 21,9 |
| 9 | 2,05 | 7,6 | 186 | 7,9 | 212 | 0,045 | 16,3 |
| 10 | 1,14 | 5,7 | 39 | 6,3 | 9 | 0,160 | 58,5 |
| 11 | 1,20 | 5,8 | 74 | 6,4 | 54 | 0,159 | 58,1 |
| 12 | 1,60 | 6,7 | 88 | 7,1 | 66 | 0,084 | 30,7 |
| 13 | 1,58 | 6,7 | 118 | 7,0 | 75 | 0,130 | 47,6 |
| 14 | 1,46 | 6,4 | 146 | 6,8 | 69 | 0,043 | 15,7 |
| 15 | 1,35 | 6,2 | 182 | 6,6 | 112 | 0,050 | 18,3 |
| 16 | 1,36 | 6,2 | 214 | 6,6 | 226 | 0,074 | 27,2 |

Total: 0,910 332,1

Table 7.3 Representative scenarios of wind and wave conditions at UTM21s 491126 m east, 5756185 m north on 69 m water depth. Significant wave height (H_s), Peak wave period (T_p), Mean wave direction (D_m), Wind speed (U_{10}), Wind direction (U_{dir}), and Probability of occurrence (P)

7.3.1 Effect of each scenario on hydrodynamics and initial sediment transport

In appendix F, identical resulting flow patterns, sediment transport patterns, and areas of erosion/accretion are grouped per scenario and visualised. In Table 7.4, the typical effects on hydrodynamics and sediment transports per group of scenarios are described. The scenarios with the largest yearly contribution to the sedimentation in the port entrance are schematically visualised in Figure 7.8 to Figure 7.10.

| Scenarios | Hydrodynamics | Sediment transports |
|-----------------|--|--|
| 1, 4, 5, 8 | North dominant flow of 0.5 to 0.8 m/s. Rip current in front of southern breakwater (S. bw.) Rip current of scenario 1 and 4 in the middle of the S. bw. At scenario 5 and 8, rip current closer to breakwater tip. | Sediment transport from east side of shoal to west side. Sand eroded in front of end of S. bw. is deposited at the start point of the rip current. |
| 2 & 6 | Northward 1 m/s current along S. bw. without rip currents. | Sediment transports to area around tip of S. bw. and to secondary access channel |
| 3, 7, 9 | Northward current along S. bw. of 0.3 to 0.6 m/s without rip currents | Sediment transports to tip of S. bw |
| 10, 11, 15 & 16 | Almost no flow along Southern breakwater. At scenario 10 and 11, there is a weak southward flow of 0.1 to 0.2 m/s north of the port. | Almost no transport along S. bw. In scenario 10 and 11, small amounts of sediment are transported from the top of the shoal to the tip of S. bw. |
| 12, 13 & 14 | South dominant flow of 0.2. Small rip current in the middle of the S. bw. | Small amounts of sediment are transported from the east side of the shoal to west side of the shoal. |

Table 7.4 Description of typical effects on hydrodynamics and sediment transports per group of scenarios (visualised in appendix F)

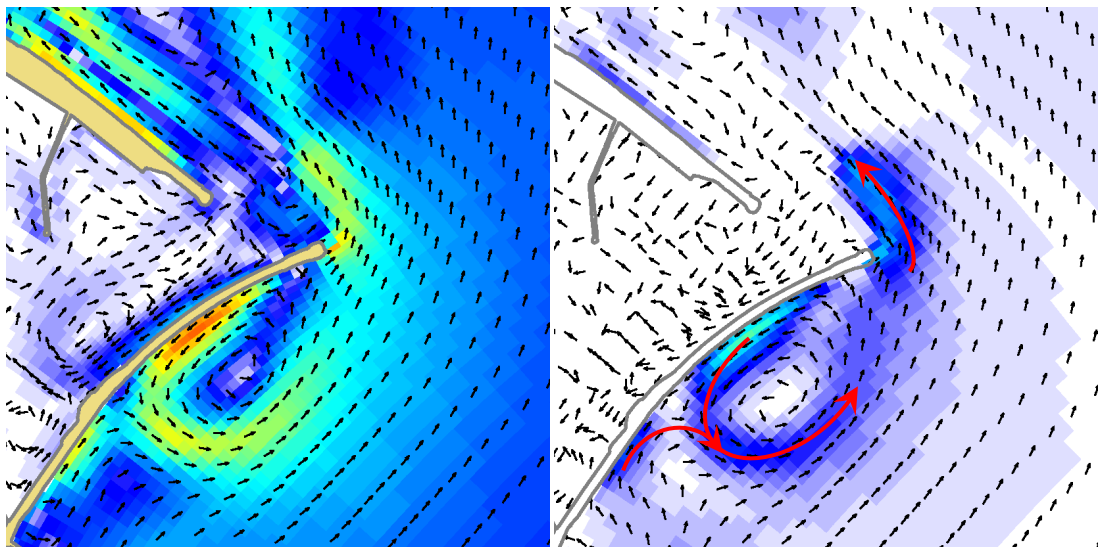


Figure 7.8 Estimated depth averaged flow velocities (left), and sediment transports (right) for scenario 1

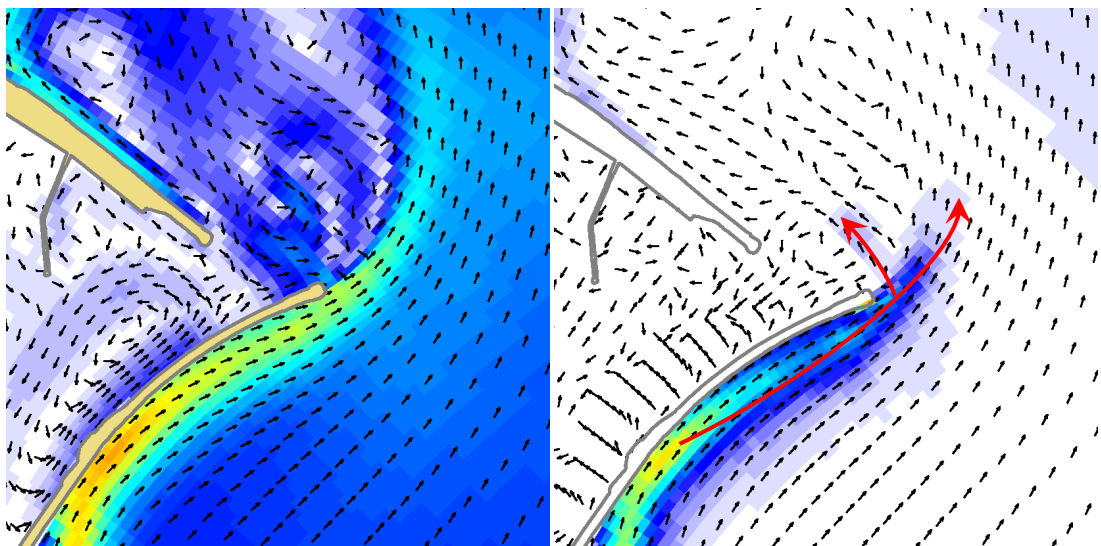


Figure 7.9 Estimated depth averaged flow velocities (left), and sediment transports (right) for scenario 2

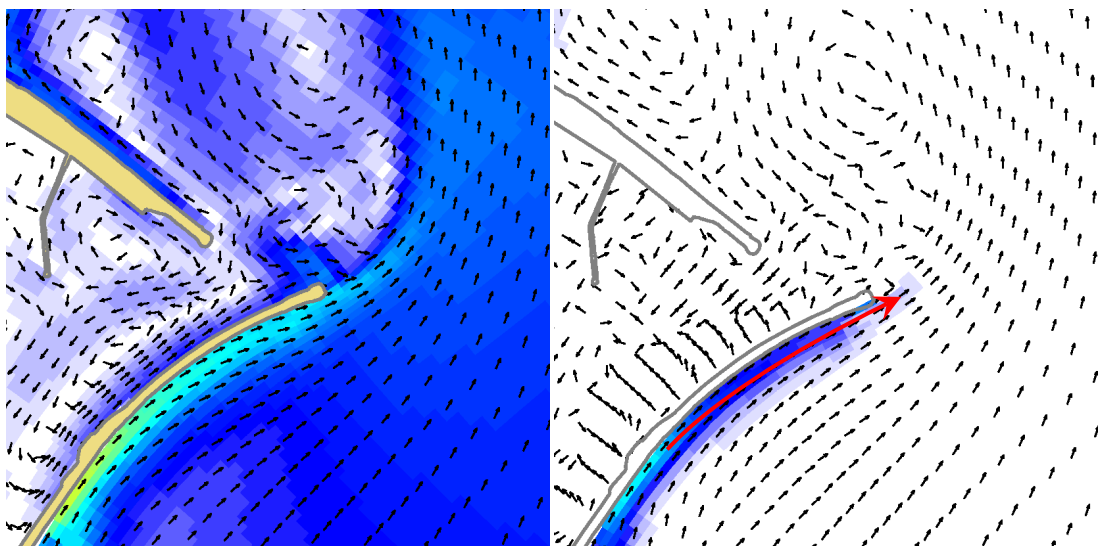


Figure 7.10 Estimated depth averaged flow velocities (left), and sediment transports (right) for scenario 3

7.3.2 Average sediment transport rates

To gain insight in the sediment fluxes in different areas around the port of Mar del Plata, different transects have been defined from the high water line to water depths of more than 10 m where sediment transports are marginal (shown in Figure 7.11).

The present net sediment fluxes are computed from the Delft3D output by taking the sum of the mean total sediment transport per run (representing one day) multiplied by the number of days each scenario occurs per year.

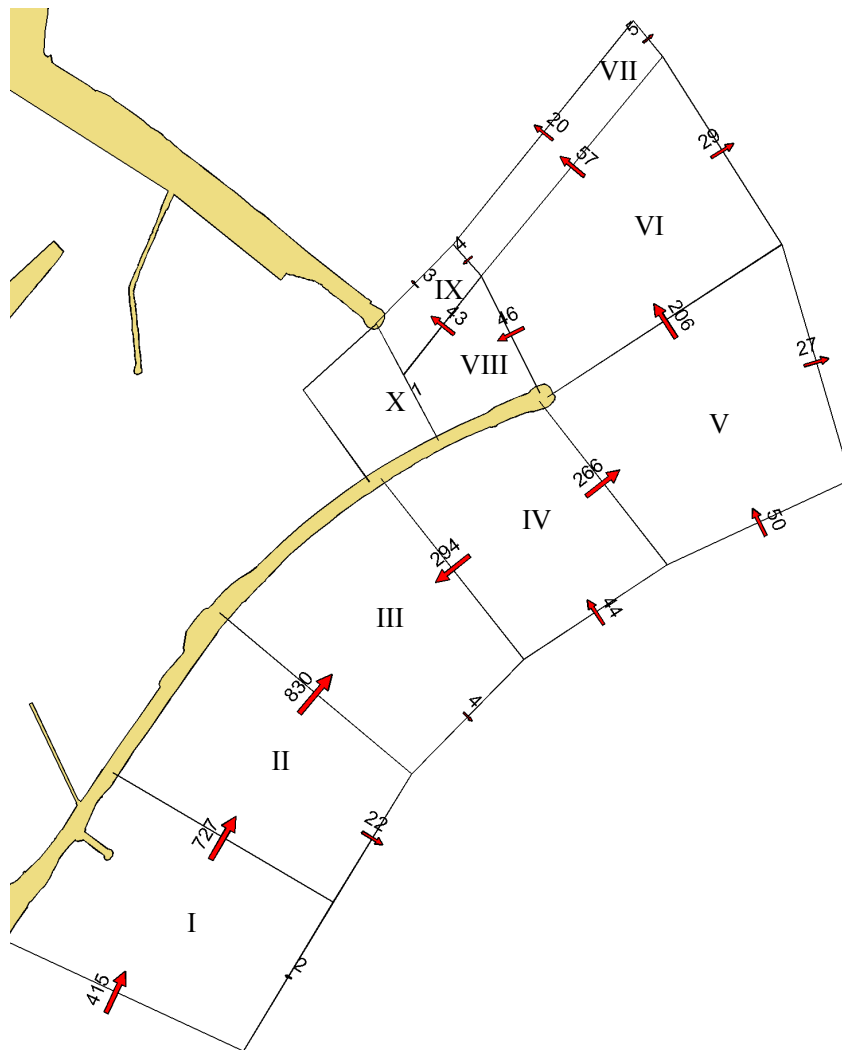


Figure 7.11 Estimated present net sediment transport per transect (in m³/day) based on all scenarios (using hor. eddy diffusivity of 1 m²/s)

Table 7.5 shows the contribution of each individual scenario to the sedimentation/accretion in different littoral cells (shown in Figure 7.11). The remarkable high initial sedimentation rate in cell III and the vast erosion in cell I, II and IV make clear that the assumed (unmeasured) bottom profile is not yet the equilibrium bottom profile. With initial transport computations, there is no intermediate update of the bottom depth. In nature, the resulting changes in bottom depth would quickly interact with the hydrodynamics and sediment transports until the natural equilibrium is reached.

| Weighted erosion or accretion in cell per scenario (in m ³ per day) | | | | | | | | | | | | | | | | | |
|--|------|-----|----|------|-----|------|----|------|-----|-----|-----|-----|------|-----|----|----|-------|
| Cell | 1 | 2 | 3 | 4 | 5 | 6 | 7 | 8 | 9 | 10 | 11 | 12 | 13 | 14 | 15 | 16 | Total |
| I | -1 | -6 | 0 | -71 | -10 | 5 | -8 | -32 | -23 | -16 | -20 | -42 | -71 | -13 | -9 | 7 | -310 |
| II | 7 | -81 | -8 | 186 | -63 | -138 | 3 | -104 | -18 | -9 | -36 | 24 | 87 | 4 | 12 | 10 | -125 |
| III | 109 | 102 | 8 | 132 | 205 | 174 | 16 | 282 | 67 | 0 | -3 | -13 | 9 | 19 | 11 | 0 | 1119 |
| IV | -124 | 57 | 6 | -331 | -76 | 75 | 14 | -9 | 39 | 0 | -3 | -47 | -109 | -11 | 1 | 2 | -515 |
| V | -61 | 43 | 2 | -54 | 9 | 31 | 4 | 38 | 11 | 1 | 5 | 14 | 30 | 8 | 2 | 0 | 83 |
| VI | 91 | 27 | 0 | 45 | 10 | -2 | -1 | -19 | -3 | 6 | 3 | -22 | -52 | -8 | -1 | 0 | 74 |
| VII | 16 | 2 | 0 | 7 | 1 | 1 | 0 | 1 | 0 | 0 | 0 | 0 | 0 | 0 | 0 | 0 | 28 |
| VIII | 3 | -3 | 0 | 8 | -1 | -2 | 0 | -4 | -1 | -7 | -8 | 7 | 13 | -2 | 0 | 0 | 2 |
| IX | 1 | 2 | 0 | 27 | 3 | 2 | 0 | 3 | 0 | 0 | 0 | 1 | 4 | 0 | 0 | 0 | 44 |
| X | 0 | 0 | 0 | 0 | 0 | 0 | 0 | 0 | 0 | 0 | 0 | 0 | 0 | 0 | 0 | 0 | 1 |

Table 7.5 Contribution of wind- and wave scenarios with tide to sedimentation. (red) and erosion (blue) per littoral cell (in m³/day)

7.3.3 Comparison with other studies to longshore transport rates

The estimated net yearly sediment fluxes at the three most southern transects are not disturbed by rip currents. The net yearly sediment transports over these transects vary between 150,000 and 300,000 m³/year. This is in the same order of magnitude as the net transports derived by Van Rijn (2008) and Camarena Calderon (2012) (described in section 3.7).

7.4 Different horizontal eddy coefficients

As explained in section 6.3.6, the horizontal turbulent transport of sediment is parameterized as horizontal eddy diffusivity. By default, this user-defined parameter is assumed to be uniform in space and time, but the HLES-model can be used to formulate spatially and temporarily varying fluctuations of the eddy diffusivity. The resulting diffusivity is the maximum of the user-defined value and the calculated value from the HLES-model.

To analyse the effect of the use of different horizontal eddy diffusivity parameters, three runs were performed using the parameters in the table below (explained in section 6.3.6).

| Run | User-defined hor. eddy diffusivity | HLES-model |
|-----|------------------------------------|-----------------------------------|
| A | 10 m ² /s | Disabled |
| B | 1 m ² /s | Disabled |
| C | 0 m ² /s | Enabled (relaxation time 30 min.) |

Table 7.6 Model runs using different parameters for horizontal eddy diffusivity

7.4.1 Effects on sediment transports

The resulting net sediment fluxes of run A (Figure 7.12) and run B (Figure 7.11) are not very similar, while run B and C (Figure 7.12) give almost equal directions and magnitudes. The effect on sedimentation or erosion per cell are displayed in Table 7.7

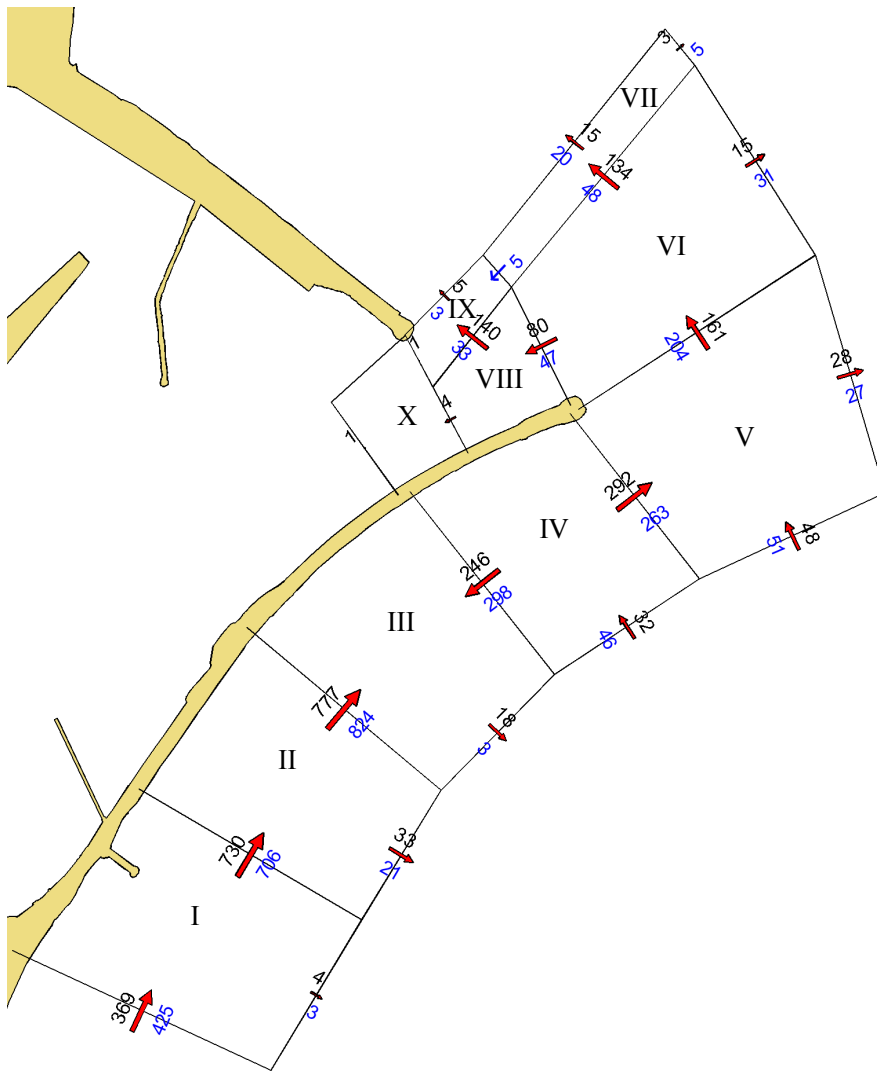


Figure 7.12 Estimated net sediment transport in 2012 per transect (in m³/day) based on all wind and wave scenarios with tide using different hor. eddy diffusivity coefficients
In black: horizontal eddy diffusivity of 10 m²/s. In blue: using HLES-model

| Cell | Horizontal eddy diffusivity coefficient | | | Estimated deposition in 2012 (from analysis of measurements) |
|------|--|---|-------------------------------------|--|
| | Uniform value | | Spatial varying | |
| | 10 m ² /s (black in Figure 7.12) | 1 m ² /s (black in Figure 7.11) | HLES-model (blue in Figure 7.12) | |
| I | -366 m ³ /day | -310 m ³ /day | -278 m ³ /day | |
| II | -79 m ³ /day | -125 m ³ /day | -140 m ³ /day | |
| III | 1005 m ³ /day | 1119 m ³ /day | 1119 m ³ /day | |
| IV | -506 m ³ /day | -515 m ³ /day | -515 m ³ /day | |
| V | 151 m ³ /day | 83 m ³ /day | 83 m ³ /day | |
| VI | -68 m ³ /day | 74 m ³ /day | 77 m ³ /day | 150 m ³ /day |
| VII | 116 m ³ /day | 28 m ³ /day | 19 m ³ /day | > 40 m ³ /day |
| VIII | -64 m ³ /day | 2 m ³ /day | 13 m ³ /day | 60 m ³ /day |
| IX | 135 m ³ /day | 44 m ³ /day | 35 m ³ /day | > 20 m ³ /day |
| X | 5 m ³ /day | 1 m ³ /day | 0 m ³ /day | 30 m ³ /day |

Table 7.7 Effect on sedimentation of different horizontal eddy coefficients.
(red) or erosion (blue) rate in different cells

7.4.2 Data comparison and evaluation

A horizontal eddy diffusivity of $10 \text{ m}^2/\text{s}$ leads to remarkable results:

- Erosion in cell VI and VIII while present depth soundings display accretion (Table 7.7);
- Severe accretion in cell VII and IX, while from data analysis the estimated sedimentation is much lower (Table 7.7);
- Strong offshore turning of net longshore sediment transport along the southern breakwater (Figure 7.13) while the beach profile is expected to be more or less stable.

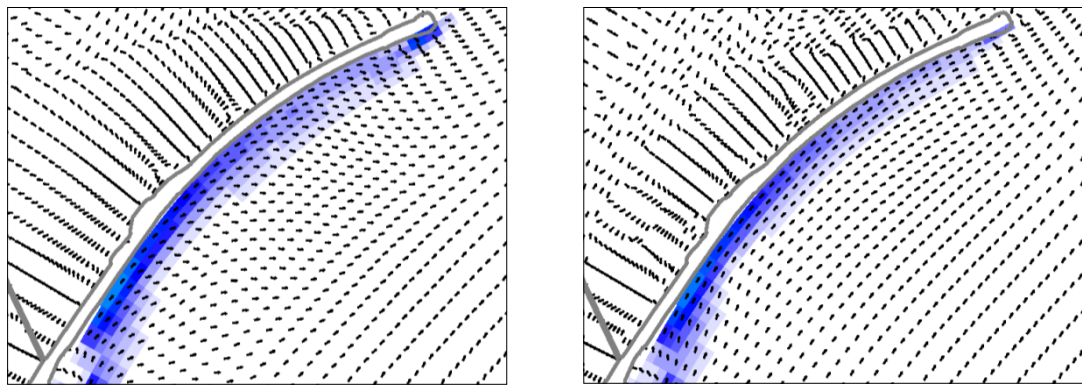


Figure 7.13 Example of sediment transport for scenario 9 using different hor. eddy diffusivity coefficients
 Left: uniform value of $10 \text{ m}^2/\text{s}$, offshore turning; Right: uniform value of $1 \text{ m}^2/\text{s}$, no turning.

Table 7.7 shows that the use of the default horizontal eddy diffusivity of $10 \text{ m}^2/\text{s}$ results in unrealistic sedimentation rates compared to the estimated deposition from measurements. Results that are more consistent are obtained using a uniform value of $1 \text{ m}^2/\text{s}$ or a combination of HLES with a user-defined uniform value of $0 \text{ m}^2/\text{s}$. The last option seems to be the most suitable parameter to use for further modelling because it results in similar patterns as using a uniform value of $1 \text{ m}^2/\text{s}$, but it has the least deviation from the results of the data analysis.

8 Evaluation effects of measures

8.1 Bathymetry with preferred navigation channel without additional measures

For a situation dredged to the preferred depth of DNVN (2011), shown in Figure 8.1, the effect on initial sediment transports of each different measure can only be estimated and compared if the sediment transport patterns and magnitudes of the so-called “zero option” (without additional measures) are studied for that bathymetry.

In this new bathymetry, the primary access channel is navigable again to depths of MSL -12.5 m the shoal is completely removed and a safety zone is dredged next to the navigation channel.

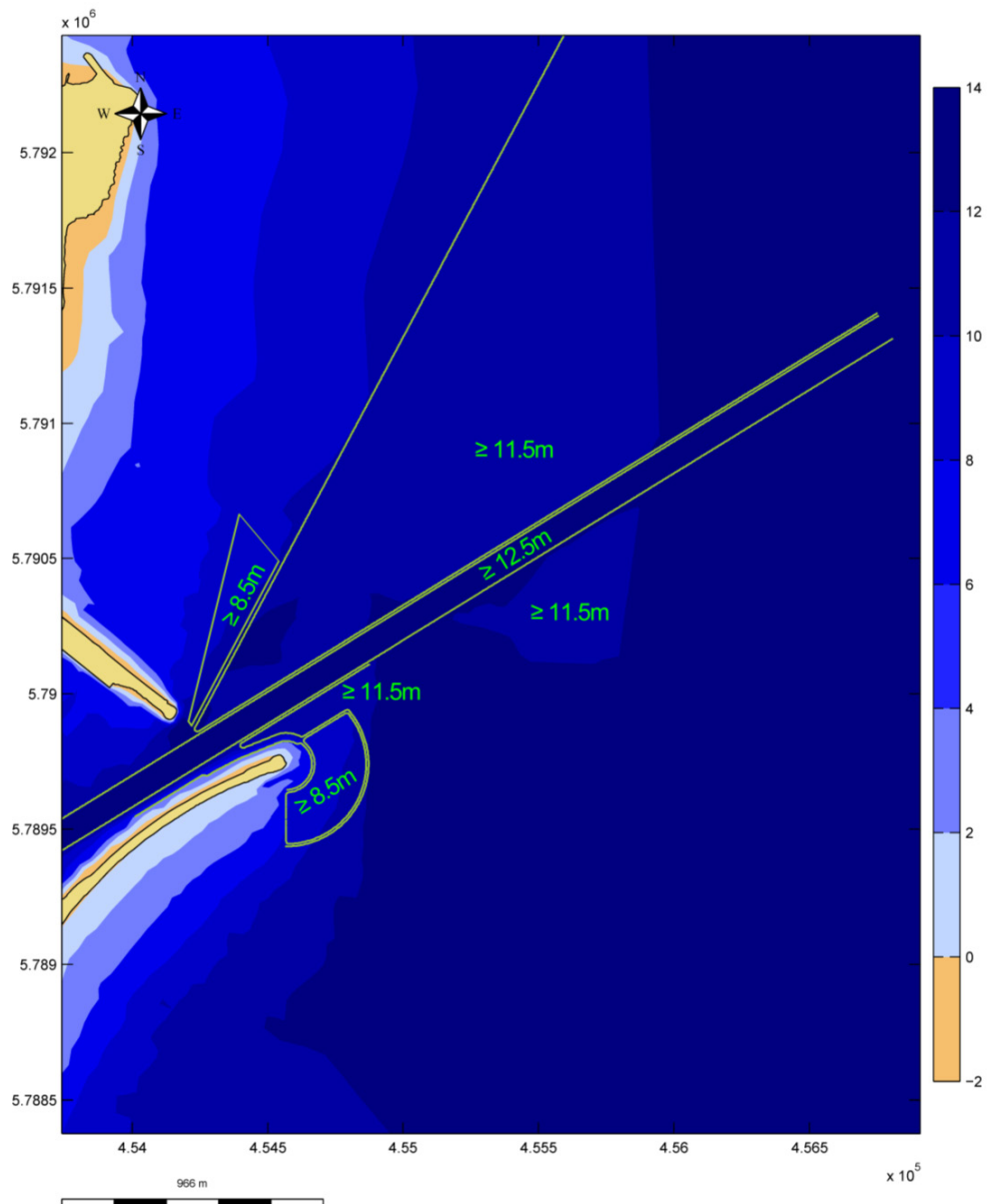


Figure 8.1 Bathymetry with preferred navigation channel according to DNVN (2011) (depths in m below MSL)

8.1.1 Effects on sediment transports

It is expected that the dredged parts of the ports will experience sedimentation due to the local decrease of transport capacity. In Figure 8.2 the net sediment transport per transect just after completion of the dredging works is plotted. This figure indeed shows a much larger sediment flux around the head of the southern breakwater towards the primary access channel (compared to Figure 7.11). Table 8.1 shows that this new bathymetry also leads to erosion in cell V.

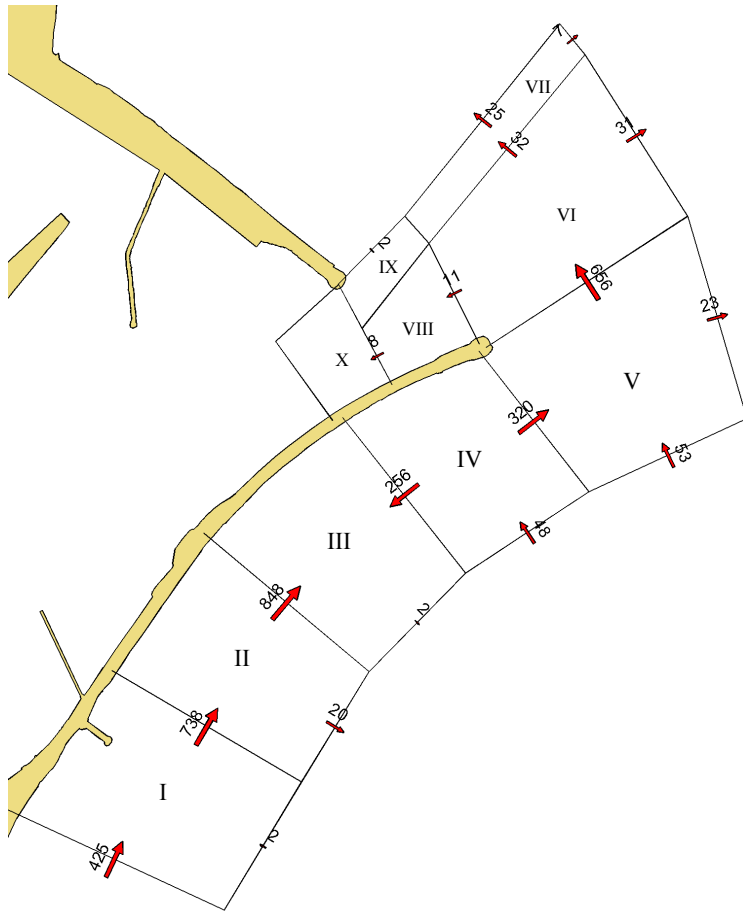


Figure 8.2 Estimated net sediment transport per transect (in m³/day) just after completion of the dredging works

| Cell | 2012 bathymetry | | Bathymetry with preferred navigation channel | |
|------|------------------|--|--|---|
| | Model estimation | Estimated deposition in 2012 from analysis of measurements | Model estimation | Estimated deposition after capital dredging in 1999 from analysis of measurements |
| I | 137 | | -311 | |
| II | 198 | | -129 | |
| III | -70 | | 1101 | |
| IV | -441 | | -528 | |
| V | 82 | | -306 | |
| VI | 371 | 150 | 583 | 575 |
| VII | 0 | > 40 | 0 | 225 |
| VIII | -1 | 60 | 2 | 214 |
| IX | -1 | > 20 | -1 | 110 |
| X | 8 | 30 | 8 | 69 |

Table 8.1 Initial sedimentation rate (in m³/day) per cell for different bathymetries

8.1.2 Data comparison and evaluation

The model results for the bathymetry with preferred navigation channel in Table 8.1 are not in agreement with historic initial sedimentation rates. This is due to the following reasons:

- The initial sedimentation rates in cell VII to X are marginal because the shoal will start growing in cell VI, slowly expanding in width towards other cells.
- The initial sedimentation rates are estimated using simple sedimentation formulas due to a lack of depth surveyed after the last capital dredging (section 3.8).

Because this model is verified for the present situation, the model results for the bathymetry with preferred navigation channel are estimated to be realistic too.

8.2 Bathymetry with preferred navigation channel and sand trap

Two different sand traps have been designed and tested to trap sand before it can enter the navigation channel. The areas and depths of the sand traps are visualised in Figure 8.3.

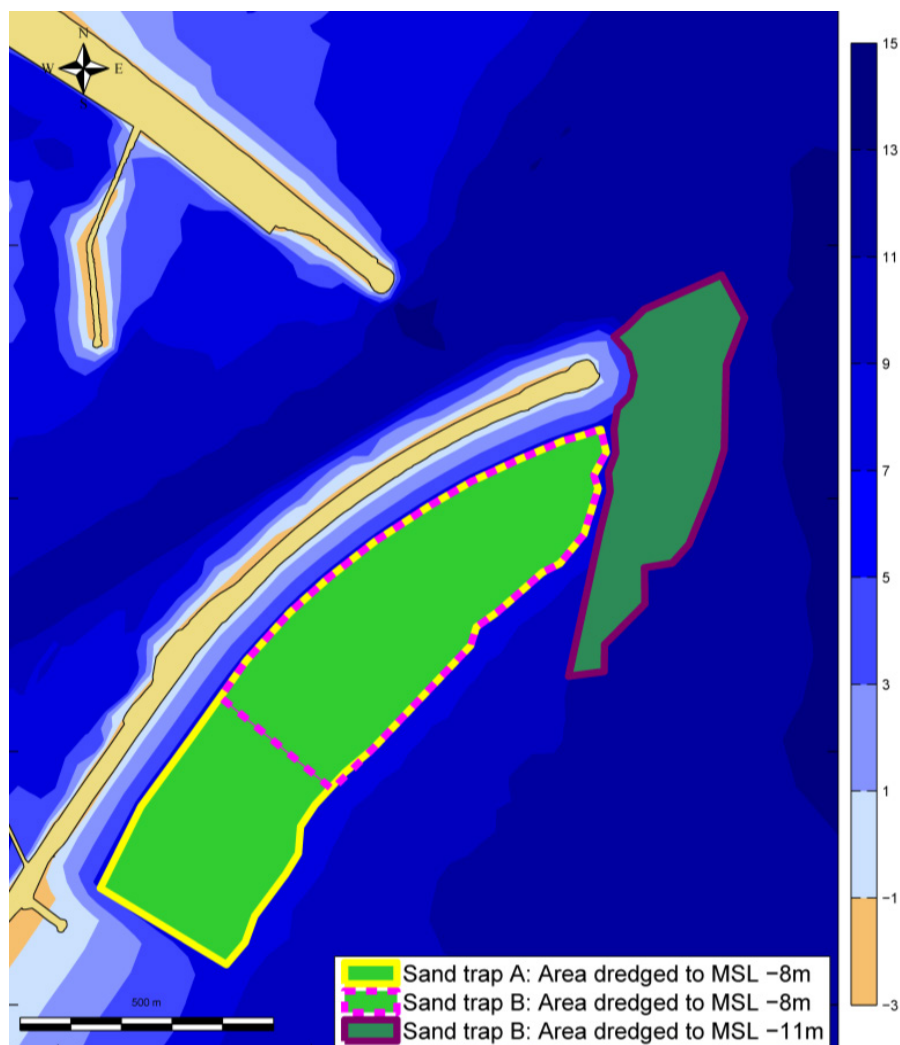


Figure 8.3 Locations and depths of the modelled sand traps

| Sand trap | Volume | Longshore width | Cross-shore length | Depth (to MSL) |
|-----------|--------------------------|-----------------|--------------------|----------------|
| A | 1,000,000 m ³ | 1400 m | 400 m | -8 m |
| B | 1,000,000 m ³ | 1000 m | 400 m | -8 m to -11 m |

Table 8.2 Specifications of modelled sand traps

The volume of the sand trap has been chosen for an estimated lifetime of at least 3 years. Because the net longshore transport of sediment is in the order of 150,000 to 300,000 m³/year (section 7.3.3), the estimated life span of this sand trap is three to six years. The depth of the sand trap is more than the estimated critical depth below which significant littoral transport takes place. With the computed nearshore wave climate, almost all sediment transport takes place between the 0 and 8 m depth contours. In water deeper than 8 m the Delft3D-model predicted marginal sediment transports.

The cross-shore length of the sand trap is defined by the position of the depth contour.

8.2.1 Effects on sediment transports

In Figure 8.4, the resulting net transports for both sand traps are shown. In sand trap A, the initial sediment transports are relatively small and have opposing directions, while in sand trap B; the net transports are relatively high but all north going. The initial sediment flux around the tip of the breakwater to the location of the present shoal (from cell V to cell VI) is with sand trap A 3.5 times higher than for sand trap B. After passing the tip of the breakwater, the sediment flux continues to the north with sand trap A, and north-north-east with sand trap B. This can be explained due to the larger depth near the tip of the breakwater and hence a higher flow velocity due to the lower influence of bottom friction.

Table 8.3 shows that, with sand trap A, the sedimentation rate in cell VI is also relatively high compared to sand trap B, but it still reduces the estimated sedimentation with almost 40% compared to a situation without a sand trap.

It must be stated, that the relatively large initial sediment transport gradients lead to relatively fast bed level changes and therefore changing hydrodynamic conditions and changing sediment transport capacities. Due to that, the sediment transports with sand trap A are expected to become more uniform in space and time, but these type processes can only be predicted using morphodynamic modelling.

Sand trap B appears to be more efficient than sand trap A with a reduction of almost 90% compared to when no additional measures are taken after dredging of the preferred navigation channel profile.

The marginal sedimentation rates in cell VII to X are expected to increase when the shoal grows towards these areas.

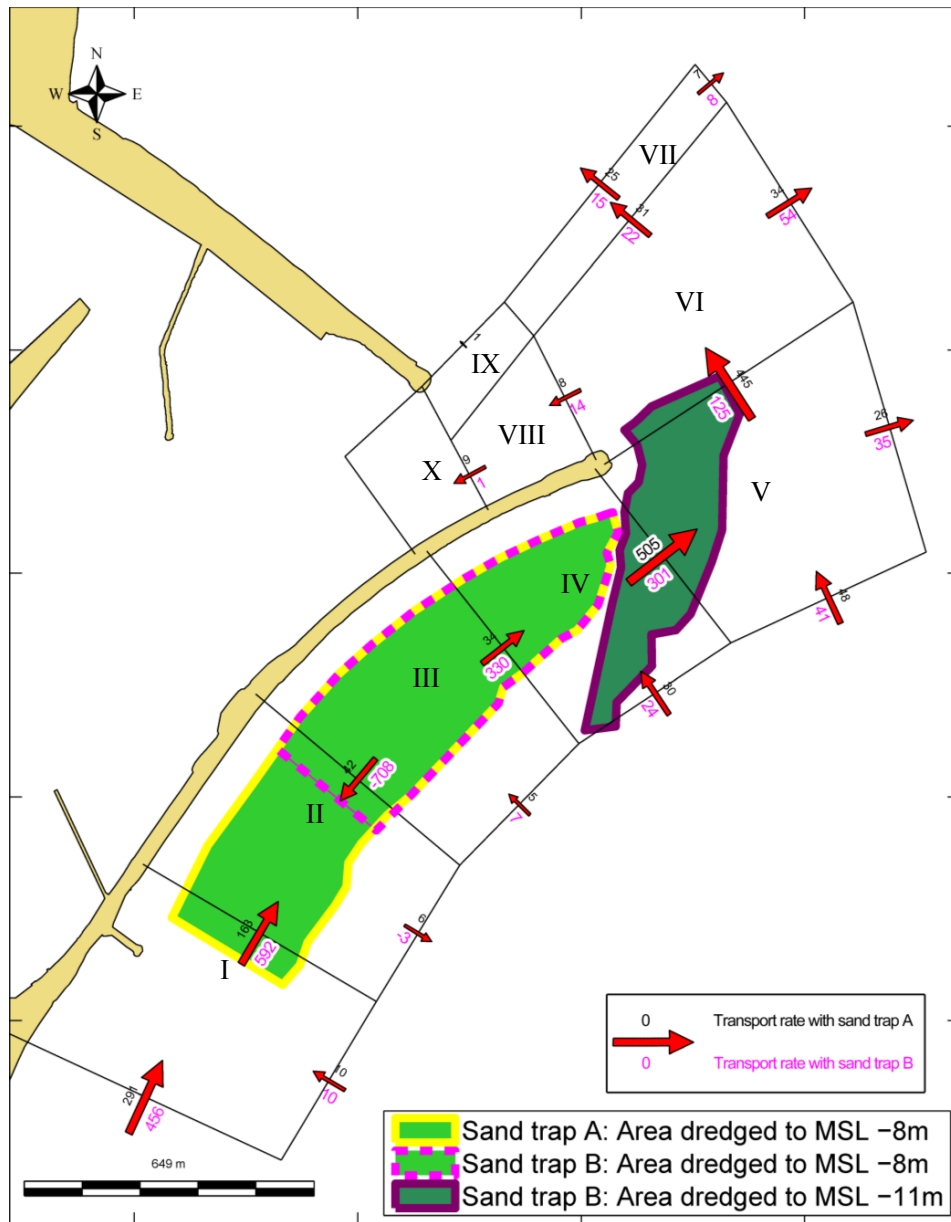


Figure 8.4 Estimated initial net sediment transports per transect (in m³/day) for different sand trap designs

| Cell | Bathymetry with preferred navigation channel | | | |
|------|--|---|------------------|------------------|
| | Model estimation without additional measures | Estimated deposition after capital dredging in 1999 from analysis of measurements | Model estimation | |
| | | | With sand trap A | With sand trap B |
| I | -311 | | 137 | -126 |
| II | -129 | | 198 | -112 |
| III | 1101 | | -70 | 384 |
| IV | -528 | | -441 | 53 |
| V | -306 | | 82 | 182 |
| VI | 583 | 575 | 371 | 63 |
| VII | 0 | 225 | 0 | -1 |
| VIII | 2 | 210 | -1 | -15 |
| IX | -1 | 110 | -1 | 0 |
| X | 8 | 70 | 8 | 1 |

Table 8.3 Initial sedimentation rate (in m³/day) per cell for different sand traps

8.3 Bathymetry with preferred navigation channel with eastward groin

To deflect the littoral transport from the port access to deeper water, three groins of different lengths orientated with an angle of 45° w.r.t. the axis of the southern breakwater (Figure 8.5) have been tested using the Delft3D model. These groins are attached to the head of the southern breakwater and reach to water depths between 8 and 11 m. The water depths around the groins are interpolated from 2 m water depth just in front of the groin to the surrounding water depths. Because change in water depth resulted in a permeable structure a so-called “thin dam” have been placed in the flow-grid to prevent flow through the grid cell borders close to the structure. For correct computation of wave propagation, these groins have also been inserted in the wave obstacle files.

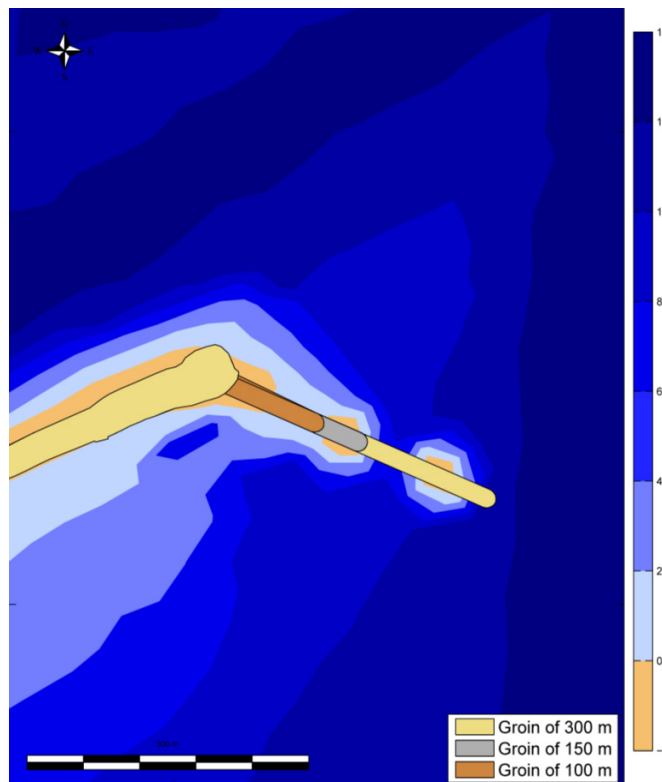


Figure 8.5 Location and lengths of the modelled groins

8.3.1 Effects on sediment transports

The resulting net sediment transports for all groins are plotted in Figure 8.6. This figure shows that the sediment flux around the tip of the southern breakwater is reversely proportional to the length of the groin. There are no signs that higher waves from the northeast will cause extra sedimentation in the port entrance due to the presence of these groins.

Table 8.4 shows that these groins reduce the initial sedimentation in cell VI for respectively 80%, 90% and 95%. The influence of the groins in updrift littoral cells appears to be relatively small.

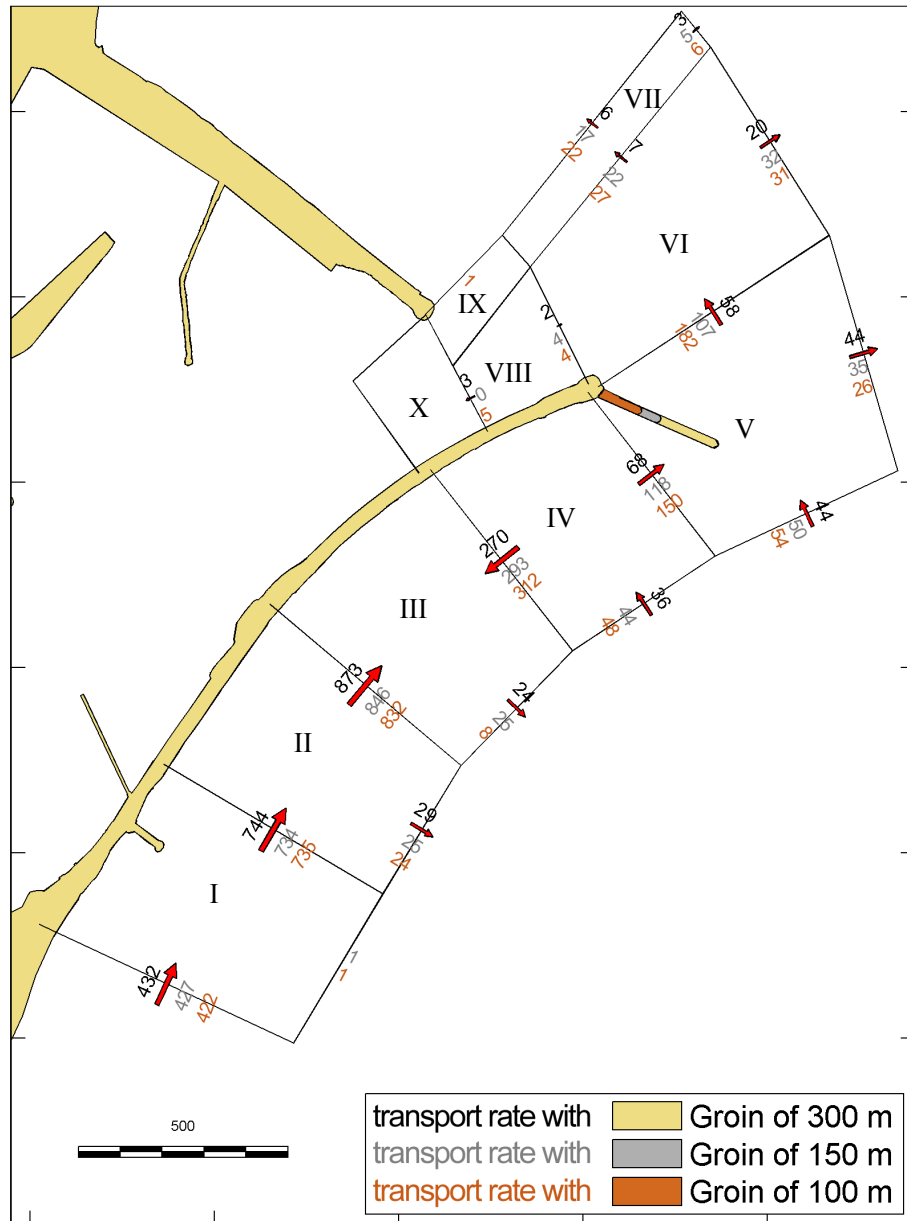


Figure 8.6 Estimated initial net sediment transport per transect (in m³/day) for different groin designs

| Cell | Bathymetry with preferred navigation channel | | | | |
|------|--|---|--------------------|--------------------|--------------------|
| | Model estimation without additional measures | Estimated deposition after capital dredging in 1999 from analysis of measurements | Model estimation | | |
| | | | With groin of 100m | With groin of 150m | With groin of 300m |
| I | -311 | | -311 | -305 | -311 |
| II | -129 | | -121 | -137 | -158 |
| III | 1101 | | 1137 | 1127 | 1119 |
| IV | -528 | | -418 | -368 | -302 |
| V | -306 | | -1 | 27 | 10 |
| VI | 583 | 575 | 119 | 54 | 32 |
| VII | 0 | 225 | -1 | 0 | -1 |
| VIII | 2 | 210 | -1 | -4 | -5 |
| IX | -1 | 110 | -1 | 0 | 0 |
| X | 8 | 70 | 5 | 4 | 3 |

Table 8.4 Initial sedimentation rate (in m³/day) per cell for different groins

Table 8.5 shows a comparison of the resulting initial sedimentation rate per measure.

| Cell | Bathymetry with preferred navigation channel | | | | | |
|------|--|------------------|------------------|--------------------|--------------------|--------------------|
| | Without additional measures | With sand trap A | With sand trap B | With groin of 100m | With groin of 150m | With groin of 300m |
| I | -311 | 137 | -126 | -311 | -305 | -311 |
| II | -129 | 198 | -112 | -121 | -137 | -158 |
| III | 1101 | -70 | 384 | 1137 | 1127 | 1119 |
| IV | -528 | -441 | 53 | -418 | -368 | -302 |
| V | -306 | 82 | 182 | -1 | 27 | 10 |
| VI | 583 | 371 | 63 | 119 | 54 | 32 |
| VII | 0 | 0 | -1 | -1 | 0 | -1 |
| VIII | 2 | -1 | -15 | -1 | -4 | -5 |
| IX | -1 | -1 | 0 | -1 | 0 | 0 |
| X | 8 | 8 | 1 | 5 | 4 | 3 |

Table 8.5 Initial sedimentation rate (in m³/day) per cell for different measures

8.4 Estimation costs of initial work and maintenance over 50 years

During the last capital maintenance dredging (completed in 1999), the total dredged volume was 3,000,000 m³. 7 years later (in 2006), the same volume needed to be dredged again (section 3.8.1). Dredging cost in Argentina range between 5 and 11 US\$/m³. Prices for breakwater construction range from 15,000 €/m¹ to 30,000 €/m¹. The lifetime a groin is estimated to be 50 year. The Future Value Concept, the benefits of accessibility for large vessels, the benefits of possible regular beach nourishments, and the possible share in the costs of tourism sector, are not taken into account in this cost estimation.

The initial investment needed for execution of capital dredging and the construction of individual measures are calculated in Table 8.6.

Table 8.7 shows the expected maintenance cost over 50 years in which the relative reduction in sedimentation rate per measure is estimated by dividing the resulting sedimentation rate in cell VI for each measure by the sedimentation rate in cell VI when no measures are taken.

| Measure | Initial capital dredging (5-11 €/m ³) | Initial sand trap dredging (5-11 €/m ³) | Groin construction (15,000-30,000 €/m ¹) | Initial construction costs |
|--|---|---|--|----------------------------|
| Preferred navigation channel bathymetry only | 3.000.000 m ³ | | | € 15 - 33 million |
| Preferred navigation channel bathymetry + groin 100 m | 3.000.000 m ³ | | 100 m ¹ | € 17 - 36 million |
| Preferred navigation channel bathymetry + groin 150 m | 3.000.000 m ³ | | 150 m ¹ | € 17 - 38 million |
| Preferred navigation channel bathymetry + groin 300 m | 3.000.000 m ³ | | 300 m ¹ | € 20 - 42 million |
| Preferred navigation channel bathymetry + long sand trap | 3.000.000 m ³ | 1.000.000 m ³ | | € 20 - 44 million |
| Preferred navigation channel bathymetry + deep sand trap | 3.000.000 m ³ | 1.000.000 m ³ | | € 20 - 44 million |

Table 8.6 Initial costs per measure

| Measure | Sand trap maintenance dredging (every 3 years) | Sedimentation reduction in entrance | Entrance maintenance dredging frequency (3,000,000 m ³) | Maintenance costs in 50 years |
|--|--|-------------------------------------|---|-------------------------------|
| Preferred navigation channel bathymetry only | | 0% | 1/7 years | € 107 - 236 million |
| Preferred navigation channel bathymetry + groin 100 m | | 80% | 1/34 years | € 22 - 48 million |
| Preferred navigation channel bathymetry + groin 150 m | | 90% | 1/76 years | € 10 - 22 million |
| Preferred navigation channel bathymetry + groin 300 m | | 95% | 1/127 years | € 6 - 13 million |
| Preferred navigation channel bathymetry + long sand trap | 1.000.000 m ³ | 35% | 1/11 years | € 152 - 333 million |
| Preferred navigation channel bathymetry + deep sand trap | 1.000.000 m ³ | 90% | 1/65 years | € 95 - 209 million |

Table 8.7 Maintenance costs per measure over 50 years

| Measure | Initial construction costs | Maintenance costs in 50 years | Total costs in 50 years |
|--|----------------------------|-------------------------------|-------------------------|
| Preferred navigation channel bathymetry only | € 15 - 33 million | € 107 - 236 million | € 122 - 269 million |
| Preferred navigation channel bathymetry + groin 100 m | € 17 - 36 million | € 22 - 48 million | € 38 - 84 million |
| Preferred navigation channel bathymetry + groin 150 m | € 17 - 38 million | € 10 - 22 million | € 27 - 59 million |
| Preferred navigation channel bathymetry + groin 300 m | € 20 - 42 million | € 6 - 13 million | € 25 - 55 million |
| Preferred navigation channel bathymetry + long sand trap | € 20 - 44 million | € 152 - 333 million | € 172 - 377 million |
| Preferred navigation channel bathymetry + deep sand trap | € 20 - 44 million | € 95 - 209 million | € 115 - 253 million |

Table 8.8 Total costs per measure over 50 years

9 Conclusions, discussion and recommendations

9.1 Conclusions

Most promising feasible measures

Based on the identified processes influencing the accessibility of the port and discussions with experts and stakeholders, various measures are evaluated. The most feasible, durable, and efficient measures, which were analysed using a hydrodynamics and sediment transport model, are:

- Construction and maintenance of a sand trap (deepened area) along the southern breakwater is selected as promising measure because sediment transported along the southern breakwater will be trapped, which strongly reduces the supply of sediment to the port access. The maintenance of the sand trap can be executed on a regular base (without disturbance for other ship traffic) and the dredged material can be used to nourish the eroding northern beaches.
- Construction of an eastward groin at the tip of the southern breakwater is selected as promising measure. It seems to be an effective, economical, and long-lasting measure, because it deflects sediment to deeper water and prevents the navigation channel from shoaling while the material need and cost for the construction of it are expected to be smaller than for other measures.

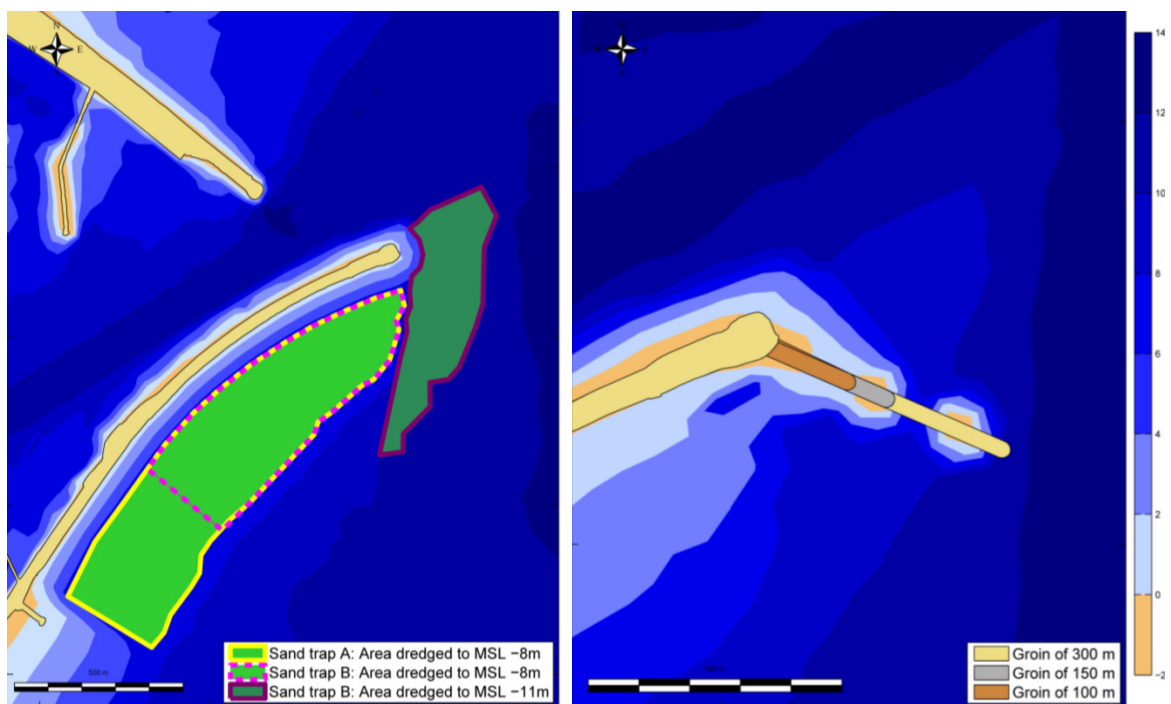


Figure 9.1 Selected and simulated most promising measures to reduce sedimentation in the port entrance: Left: two sand trap designs (of equal volume); Right: three groins of different lengths.

Estimated costs

The initial investments needed for execution of capital dredging with(out) additional measures and the resulting costs of needed maintenance dredging are estimated (based on the results of simulations in the hydrodynamics and sediment transport model) and summed in the table below.

| Measure | Initial construction costs | Maintenance costs in 50 years | Total costs in 50 years |
|--|----------------------------|-------------------------------|-------------------------|
| Preferred navigation channel bathymetry only | € 15 - 33 million | € 107 - 236 million | € 122 - 269 million |
| Preferred navigation channel bathymetry + groin 100 m | € 17 - 36 million | € 22 - 48 million | € 38 - 84 million |
| Preferred navigation channel bathymetry + groin 150 m | € 17 - 38 million | € 10 - 22 million | € 27 - 59 million |
| Preferred navigation channel bathymetry + groin 300 m | € 20 - 42 million | € 6 - 13 million | € 25 - 55 million |
| Preferred navigation channel bathymetry + long sand trap | € 20 - 44 million | € 152 - 333 million | € 172 - 377 million |
| Preferred navigation channel bathymetry + deep sand trap | € 20 - 44 million | € 95 - 209 million | € 115 - 253 million |

Table 9.1 Total costs per measure over 50 years

9.2 Discussion

Preferred navigation channel bathymetry without additional measures

- The cost estimation makes clear that, due to the high maintenance costs, it is not economic to execute maintenance dredging without taking additional measures that prevent/reduce the shoaling of the port access. Maintaining this situation also leads to frequent disturbance of the ship traffic and result in irregular nourishments of beaches. These irregular and uncertain circumstances are not attractive for possible investors in the port and tourism and lead to higher costs for shipping companies and smaller beaches for tourist.

Construction and maintenance of a sand trap along the southern breakwater

- Cost estimations show that a long sand trap seems to be less cost efficient than a shorter and deeper sand trap. Although the total cost in 50 year of a deeper sand trap are only a few percent less than taking no measures, it strongly reduces the maintenance need inside the navigation channel for 90%. Therefore, the estimated disturbance for the ship traffic is the much smaller, which is attractive for possible investors in the port. In addition, the regular (3 yearly) maintenance of the sand trap, gives the opportunity for more frequent beach nourishments and a more constant width of the beaches for tourism.

Construction of an eastward groin at the tip of the southern breakwater

- The construction of an eastward groin at the tip of the southern breakwater appears to be the most economical solution to reduce sedimentation because it is a relatively small one-time investment with a long-term effect.
- A groin perpendicular to the southern breakwater should be designed as impermeable structure to prevent the sediments from passing through the breakwater structure (Van Rijn, 2008).
- A possibility is to construct a groin in stages. E.g., initially construct a groin of 100 m and lengthen it in a later stage with 50 m (or more).
- The disadvantage of a large groin can be that the sediment will be deflected to deep water, and less sediment will flow to the downdrift (northern) beaches leading to more beach erosion.
- If the groin is accessible for a crawler crane, the groin can be used to extract sand on the updrift (south) side of the groin. This sand can be transported by trucks or a pipeline to regularly nourish the eroding downdrift (northern) beaches. Excavation of accumulating sand on the updrift side of the groin also reduces the chance that, in a later stage, a beach can arise on the updrift side of the groin that can reduce the effect of the groin. It can also reduce the need for a longer groin. Small outcrops along south side of the groin of e.g. 20 m with an intermediate distance of e.g. 50 m can enlarge the area reached by a crane.

9.3 Recommendations

General recommendations

- The costs of dredging works in the port of Mar del Plata can be reduced when (regular) dredging works are combined in one joined tender with other Argentinian ports. The contractor then can optimally plan the different works to minimise the travel and waiting costs.
- The dredging for navigation purposes can be combined with other activities, e.g. beach nourishments for tourism, ecology and coastal defence and other works. With this Integrated Coastal Zone Management approach, also different stakeholders (authorities, companies, and regional and national government) can invest and benefit in this project.
- To be able to perform more accurate model simulations, the model input must be accurate and reliable too. Therefore, it is advisable to place and maintain wave buoys along the coast to obtain a more accurate local wave climate. Also regular surveys of the foreshore of the entire coastal area are needed to be able to set-up and validate models to forecast hydrodynamic and morphodynamic processes. This can be performed by simple equipment like a jet ski with GPS and echosounder.
- The availability of reliable recent and historic data for future studies and projects can improve the quality and lower the uncertainties, risks and costs and prevents that valuable data will be lost. A (maintained) digital data system with up to date and historic data for and from different authorities and stakeholders can be very useful.

Recommendations for further research

- In this study, the initial effects on hydrodynamics and sediment transports of different measures are studied. To better estimate the morphological and hydrodynamic effects of each measure in time, morphodynamic modelling is needed. With this kind of model, the development of sedimentation and erosion in and around the port access and in the surrounding coastal area can be forecasted and quantified, to better estimate the need for maintenance in the port access and to assess the consequences for the surrounding coastal area as part of the required Environmental Impact Assessment.
- This report gives some insight in the varying effects of different designs of groins and sand traps. Therefore, it is recommendable to do a study to design optimisations.
- In shallow areas, only small(er) or a different type of dredging equipment can be used, which often have a lower production and therefore higher costs than a large dredger. A possible cost reduction is to adapt the initial design bathymetry for larger equipment. This can be done by planning pits close to shallow areas and so that natural processes (geotechnical and morphodynamic processes) will result in the preferred bottom profile.
- Furthermore, the effect on the (geotechnical and hydrodynamic) risks of instability of the present port breakwaters must be assessed before an additional measure will be executed. Additional toe and bed protection works can be considered to ensure the geotechnical stability of the southern breakwater.
- For a better evaluation of different measures, an extensive cost estimation is advised based on: accurate present market prices, taking into account the Future Value Concept, the benefits of accessibility of the for large vessels, the benefits of possible regular beach nourishments, and the possible share in the costs of tourism sector.

References

- 'd Angremond, K., & Pluim-Van der Velden, E.T.J.M. (2001). *Introduction coastal engineering*. Delft: VSSD.
- Ahorainfo. (2007, November 22). Puerto Mar del Plata: La draga "Acróbata" llegó al puerto de la vecina ciudad. *ahorainfo.com.ar - Provinciales*, from <http://ahorainfo.com.ar/2007/11/puerto-mar-del-plata-la-draga-acrobata-llego-al-puerto-de-la-vecina-ciudad/>
- Ahorainfo. (2009, April 23). Mar del Plata: La draga "Mendoza" 259-C llegó al puerto local. *ahorainfo.com.ar - Regionales*, from <http://ahorainfo.com.ar/2009/04/mar-del-plata-la-draga-mendoza-259-c-llego-al-puerto-local/>
- Algera, A., Burger, B., Hartog, W.M., & De Rijke, Q.C. (2004) *A Study on the Reconstruction of Los Acanilados Beach*. Delft: Delft University of Technology - Section Hydraulic Engineering.
- Autoridad del Agua. (2008, August 19). Buenos Aires: ¿Draga la Draga?: La Acróbata bajo la lupa. *Programa InfoAGUA - Informacion General*, from <http://intra.ada.gba.gov.ar/intra/infoagua/200808/noticias/112458.html>
- Bértola, G.R. (2006). Morfodinamica de playas del sudeste de la provincia de buenos aires (1983 a 2004). *Latin American Journal of Sedimentology and Basin analysis*, 13(1), 31-57.
- Boer, S., De Jonge, A.M., Brouwer, H., Eversdijk, P.J., Evertse, M., & Van der Sluijs, W.J.H. (1997). *Port and Coastal Study Mar del Plata*. (WB1062-4-96045). Unpublished Report. Directorate-General for Public Works and Water Management (Rijkswaterstaat). Utrecht.
- Boer, S., De Jonge, A.M., Uit het Broek, H.G.M., & Meesen, P.J. (1997). *Port and Coastal Study Mar del Plata*. (WB1062-4-97053). Unpublished Report. Directorate-General for Public Works and Water Management (Rijkswaterstaat). Utrecht.
- Booij, N., Ris, R.C., & Holthuijsen, L.H. (1999). A third-generation wave model for coastal regions 1. Model description and validation. *Journal of Geophysical Research*, 104(C4), 7649-7666. doi: 10.1029/98jc02622
- Caires, S., & Van Os, J. (2011). *ORCA Guidelines*. (1201959-000). Deltares. Delft.
- Camarena Calderon, R.A. (2012). *Feasibility of a marina port along the Buenos Aires coast, Argentina*. (M.Sc. Thesis), Delft University of Technology.
- Caviglia, F.J., Pousa, J.L., & Lanfredi, N.W. (1991). A determination of the energy flux constant from dredge records. *Journal of Coastal Research*, 7(2), 543-549.
- Codignotto, J.O., & Aguirre, M.L. (1993). Coastal evolution, changes in sea level and molluscan fauna in northeastern Argentina during the Late Quaternary. *Marine Geology*, 110(1-2), 163-175. doi: 10.1016/0025-3227(93)90112-9
- Crossland, C.J., Kremer, H.H., Lindeboom, H.J., Marshall Crossland, J.I., & Le Tissier, M.D.A. (2005). *Coastal Fluxes in the Anthropocene*: Springer.
- D'Errico, J. (2006). `inpaint_nans`. *MATLAB Central - File Exchange* Retrieved 26 June, 2012, from http://www.mathworks.com/matlabcentral/fileexchange/4551-inpaintnans/content/Inpaint_nans/inpaint_nans.m

- Deltares. (2011a). *Delft3D-FLOW User Manual - Simulation of multi-dimensional hydrodynamic flows and transport phenomena, including sediments*. Delft: Deltares.
- Deltares. (2011b). *Delft3D-RGFGRID User Manual - Generation and manipulation of curvilinear grids for Delft3D-FLOW and Delft3D-WAVE*. Delft: Deltares.
- Deltares. (2011c). *Delft3D-WAVE User Manual - Simulation of short-crested waves with SWAN*. Delft: Deltares.
- Deltares Systems. (2011). ORCA. *Design and analysis tools - Hydro*, from <http://www.deltaresystems.com/hydro/product/1023790/orca>
- DNVN. (1968). Puerto Mar del Plata *Detalle Muros y Espigones*. Mar del Plata: Direccion Nacional de Construcciones Portuarias y Vías Navegables,.
- DNVN. (2011). Canal de acceso Puerto Mar del Plata *Espicificaciones técnicas* Mar del Plata: Direccion Nacional de Vías Navegables.
- DNVN. (2012a). Puerto Mar del Plata Canal de Acceso Exterior (16-04-2012) [Depth Sounding]: Direccion Nacional de Vías Navegables.
- DNVN. (2012b). Puerto Mar del Plata Canal de Acceso Exterior (20-03-2012) [Depth Sounding]: Direccion Nacional de Vías Navegables.
- Eikelkamp. (2006). P1.41 Cable Operated Sediment Samplers *Product Knowledge Database*. Giesbeek: Eikelkamp Agrisearch Equipment.
- Elgue, A.E. (2009). Escolleras Norte y Sur: Entrada Puerto MdP [Aerial photograph].
- EMC/MMAB. (2009). *NWW3 implementations* Retrieved 17 November, 2011, from <http://polar.ncep.noaa.gov/waves/implementations.shtml>
- European Committee for Standardization. (2012). NEN-EN 933-1:2012 *Tests for geometrical properties of aggregates - Part 1: Determination of particle size distribution - Sieving method*. Delft: Nederlands Normalisatie-instituut.
- Fiore, M.M.E., D'Onofrio, E.E., Pousa, J.L., Schnack, E.J., & Bértola, G.R. (2009). Storm surges and coastal impacts at Mar del Plata, Argentina. *Continental Shelf Research*, 29(14), 1643-1649. doi: 10.1016/j.csr.2009.05.004
- Garmin. (2007a). *eTrex H Owner's Manual*: GARMIN Ltd.
- Garmin. (2007b). *GPSMAP 60CSx Owner's Manual*: GARMIN Ltd.
- GEBCO. (2010). *User Guide to the GEBCO_08 Grid*. Liverpool: British Oceanographic Data Centre.
- GEBCO. (2011). General Bathymetric Chart of the Oceans *GEBCO_08 grid* (20100927 ed.). Liverpool: British Oceanographic Data Centre.
- Google. (2012). GeoEye Images *Google Earth*: Google Inc.
- Inman, D.L., & Nordstrom, C.E. (1971). The tectonic and morphologic classification of coasts. *The Journal of Geology*, 79(1), 1-21.

- Isla, F.I. (2012). From touristic villages to coastal cities: The costs of the big step in Buenos Aires. *Ocean & Coastal Management*, (In Press, Corrected Proof). doi: 10.1016/j.ocecoaman.2012.02.005
- Koorevaar, C., Van den Akker, A., & Tilman, J.G. (1994). Inspection Fleet of Dirección Nacional de Vías Navegables *Trailing suction hopper dredger Mendoza 259-C*: Ballast Nedam, Boskalis & Van Oord ACZ.
- La Capital. (2004, April 27). La draga comenzó a operar en el Puerto. *La Capital - Mar del Plata*, from http://www.mdp.com.ar/noticias/la_draga_comenzo_a_operar_en_el_puerto/
- La Capital. (2009, July 4). Prometen que la draga estaría operativa dentro de 15 ó 20 días. *La Capital - Mar del Plata*, from <http://www.lacapitalmdp.com/noticias/La-Ciudad/2009/07/04/114269.htm>
- La Capital. (2012, September 27). El puerto perdió de exportar unas 30 mil toneladas por falta de portacontenedores. *La Capital - Mar del Plata*, from http://www.mdp.com.ar/noticias/la_draga_comenzo_a_operar_en_el_puerto/
- Lagrange, A.A. (1993). *Mar, Playas y Puerto*. Mar del Plata: Fundación Bolsa de Comercio de Mar del Plata.
- Lanfredi, N.W., Pousa, J.L., Mazio, C.A., & Dragani, W.C. (1992). Wave-power potential along the coast of the province of Buenos Aires, Argentina. *Energy*, 17(11), 997-1006. doi: 10.1016/0360-5442(92)90016-s
- Lowrance. (2003). *M52 S/GPS Installation and Operation Instructions*. Tulsa: Lowrance Electronics, Inc.
- Mangor, K. (2007). Coastal Wiki. *Statistical description of wave parameters* Retrieved 31 October, 2012, from http://www.coastalwiki.org/coastalwiki/Statistical_description_of_wave_parameters#Peak_wave_period
- MOSP. (1996) *Relevamiento Planialtimétrico de la Costa de la Ciudad de Mar del Plata*. Mar del Plata: Ministerio de Obras y Servicios Públicos de la Provincia de Buenos Aires, Dirección Provincial de Hidráulica, Departamento Obras Marítimas.
- Murias, A. (2009a, August 5). Dredging starts in Mar del Plata. *Fish Information & Services Worldnews*, from <http://fis.com/fis/worldnews>
- Murias, A. (2009b, July 20). Dredging urgently needed for port of Mar del Plata: Prefecture. *Fish Information & Services Worldnews*, from <http://fis.com/fis/worldnews>
- Murias, A. (2009c, July 8). Halt in dredging activity imperils Mar del Plata port. *Fish Information & Services Worldnews*, from <http://fis.com/fis/worldnews>
- Murias, A. (2010a, February 10). Attempts made to reverse shipping firms' call. *Fish Information & Services Worldnews*, from <http://fis.com/fis/worldnews>
- Murias, A. (2010b, February 12). Local shipping firm picks up Mar del Plata route. *Fish Information & Services Worldnews*, from <http://fis.com/fis/worldnews>
- Murias, A. (2010c, February 8). Two shipping firms suspend Mar del Plata route. *Fish Information & Services Worldnews*, from <http://fis.com/fis/worldnews>

- Murias, A. (2012, April 20). Fisheries sector concerned at temporary cancellation of exports. *Fish Information & Services Worldnews*, from <http://fis.com/fis/worldnews>
- NGA. (1998). 23142: Mar del Plata and Ensenada Mogotes (10th Edition, 22 August 1998, Corrected to NTM 1998/48) [Nautical Chart]. Bethesda: National Imagery and Mapping Agency.
- NGA. (2011). *Pub. 124 - Sailing Directions (Enroute): East Coast of South America* (11th ed.): Springfield.
- NOAA/NWS/NCEP. (2011). WAVEWATCH III Ocean Wave Model version 2.22 Hindcast Reanalysis (GRIB-files). Retrieved 2011, November 17, from National Oceanic and Atmospheric Administration <ftp://polar.ncep.noaa.gov/pub/history/waves/>
- Roelvink, J.A., & Reniers, A.J.H.M. (2011). *A Guide to Modelling Coastal Morphology*. Singapore: World Scientific Publishing Company Incorporated.
- SHN. (2010). H-251: Puerto Mar del Plata (6a. Edición 2006, Última corrección 2010 - 49) [Nautical Chart]. Buenos Aires: Servicio de Hidrografía Naval de la Armada Argentina.
- SHN. (2012a). H-114: De Faro San Antonio a Faro Miramar (6a. Edición 2004, Última corrección 2012 - 43) [Nautical Chart]. Buenos Aires: Servicio de Hidrografía Naval de la Armada Argentina.
- SHN. (2012b). H-210: De Punta Mogote a Faro Claromecó (3a. Edición 2008, Última corrección 2012 - 43) [Nautical Chart]. Buenos Aires: Servicio de Hidrografía Naval de la Armada Argentina.
- SHN. (2012c). H-250: Rada Mar del Plata (2a. Edición 2003, Última corrección 2012 - 43) [Nautical Chart]. Buenos Aires: Servicio de Hidrografía Naval de la Armada Argentina.
- SHN. (2012d). Puerto Mar del Plata. *Tablas de Marea* Retrieved 13 February, 2012, from http://www.hidro.gov.ar/Oceanografia/Tmareas/Form_Tmareas.asp
- Spindler, D.M., & Tolman, H.L. (2008). Technical Note 259 - *Example of WAVEWATCH III for the NE Pacific*: NOAA/NWS/NCEP/MMAB.
- Spindler, D.M., & Tolman, H.L. (2010). Technical Note 266 - *Example of WAVEWATCH III for the Alaska area*: NOAA/NWS/NCEP/MMAB.
- Sunrise Technical Consultants. (1968) *Estudio mediante ensayo hidráulico sobre modelo del puerto de Mar del Plata y sus alrededores* (Vol. I to III). Tokio.
- Talley, L.D., Pickard, G.L., William J. Emery, & Swift, J.H. (2011). *Descriptive Physical Oceanography*. Boston: Elsevier.
- Tarback, E.J., Lutgens, F.K., & Tasa, D. (2011). *Earth Science* (13th ed.): Pearson Education.
- The Met Office. (1994). Frequency analysis, wave height versus wave direction for area lat. 36°S to 42°S long. 53°W to 58°W.
- UKHO. (2006a). Gb531: Puerto Mar del Plata (Edition 27-04-2006, Correction 25-10-2006) [Nautical Chart]. In GARMIN BlueChart Americas 9.5 (Ed.), *GARMIN MapSource 6.12.4*. London: United Kingdom Hydrographic Office.

- UKHO. (2006b). Gb556: Tramandai to Mar del Plata (Edition 03-04-2003, Correction 29-11-2006) [Nautical Chart]. In GARMIN BlueChart Americas 9.5 (Ed.), *GARMIN MapSource 6.12.4*. London: United Kingdom Hydrographic Office.
- UKHO. (2006c). Gb557: Mar del Plata Comodoro Rivadavia (Edition 10-04-2003, Correction 29-11-2006) [Nautical Chart]. In GARMIN BlueChart Americas 9.5 (Ed.), *GARMIN MapSource 6.12.4*. London: United Kingdom Hydrographic Office.
- UKHO. (2006d). Gb3065: Punta Piedras to Quequén (Edition 16-07-1976, Correction 29-11-2006) [Nautical Chart]. In GARMIN BlueChart Americas 9.5 (Ed.), *GARMIN MapSource 6.12.4*. London: United Kingdom Hydrographic Office.
- UKHO. (2006e). Gb3066: Quequén to Río Negro (Edition 04-12-1987, Correction 09-08-2006) [Nautical Chart]. In GARMIN BlueChart Americas 9.5 (Ed.), *GARMIN MapSource 6.12.4*. London: United Kingdom Hydrographic Office.
- Universidad Nacional de Córdoba. (2007). *Asesoramiento vinculado al proyecto de Sistemas de Rompeolas Aislados al Sur de Punta Mogotes en la ciudad de Mar del Plata*. Informe Final. Unpublished Report.
- Van Rijn, L.C. (2005). *Principles of Sedimentation and Erosion Engineering in Rivers, Estuaries and Coastal Seas*. Amsterdam: Aqua Publications.
- Van Rijn, L.C. (2008). *Coastal Erosion Problems Mar del Plata, Argentina*. (H5236 No. 2). Unpublished Report. Deltares. Delft.
- Walstra, D.J.R. (2011). Webinar. *How to perform realistic morphodynamic simulations with acceptable run-times*, from <http://oss.deltares.nl/web/morphology/inputreduction>
- Waterman, R.E. (1994). *Sand Bypassing at Mar Del Plata - A Solution to Coastal and Port Problems*. Unpublished Report. Delft.
- WindGURU. (2012). Mar del Plata. *GFS 50 km / NWW3 daily archive* Retrieved 17 April, 2012, from <http://www.windguru.cz/int/historie.php>
- Wolfram Alpha. (2012). EGM2008. *Gravitational acceleration, Mar del Plata, Buenos Aires, Argentina*, from <http://www.wolframalpha.com/input/?i=gravitational+acceleration%2C+Mar+del+Plata%2C+Buenos+Aires%2C+Argentina>

A Site visit trip Buenos Aires coast, Argentina

A.1 Objectives

The site visit trip of 2 weeks was planned to:

- A. Set up discussions with client.
- B. Collect local data and knowledge.
- C. Present the aim and the expected results of the study, and work completed to date.
- D. Site recognition at Mar del Plata and the coastal area around it.
- E. Perform depth soundings.
- F. Collect beach and bottom sediment samples in and around the port.
- G. Perform measurements on direction and magnitude of tidal currents at the port entrance.

A.2 Itinerary

Day: 09-04-2012

Time: 10:00-22:00 (local time)

Location: Flight from Amsterdam to hotel in Buenos Aires

Day: 10-04-2012

Time: 09:00-20:00

Locations: Travel to Mar del Plata by car, visiting places along the coast of the Buenos Aires province. San Clemente (small port), Punta Rasa (sand spit), and Mar del Tuyu (severe beach and dune erosion and collapsing roads)

People: Sergio Loschacoff; P.K. Tonnon; R.A. Camarena Calderon; J.M. Luteijn;

Day: 11-04-2012

Time: 10:00-12:30

Location: Port of Mar del Plata

Meeting with:

- Alejandro Gomez (President Mar del Plata Chamber of Commerce foundation)
- Maria Luisa Loidi (Personal assistant of Alejandro Gomez)
- Eduardo Tomás Pezzati (President of the Mar del Plata Chamber of Commerce and the director of the Port of Mar del Plata)
- Sergio Loschacoff (Coastal protection engineer, collaborator of Mar del Plata Chamber of Commerce foundation)
- José Carlos Perez de la Sierra (Argentine waterways chief, Quequen and Mar del Plata)
- Other people from the Mar del Plata Port authorities
- P.K. Tonnon.
- R.A. Camarena Calderon
- J.M. Luteijn

Meeting description:

The objectives and the methodology of the study were presented to the port authorities.

The president granted their full support for this study

The field measurement campaign was explained and arranged with the people in charge of the measuring equipment and the boat. Using a smaller boat for the drifter tracking was considered very unsafe.

Many people gave their opinion and advice about the topic and contact details (for the planning of further meetings) were exchanged

Bathymetric information was provided in paper form.

The reference conditions for the next planned dredging were also provided, showing the expected depths after dredging.

Day 11-04-2012

Time: 13:00-15:45

Location: Sheraton Hotel

Meeting with:

- Alejandro Gomez (President Mar del Plata Chamber of Commerce foundation)
- Maria Luisa Loidi (Personal assistant of Alejandro Gomez)
- Eduardo Tomás Pezzati (President of the Mar del Plata Chamber of Commerce and the director of the Port of Mar del Plata)
- Sergio Loschacoff (Coastal protection engineer, collaborator of Mar del Plata Chamber of Commerce foundation)
- Other stakeholders and managers from Mar del Plata.
- P.K. Tonnon.
- R.A. Camarena Calderon
- J.M. Luteijn

Meeting description:

The main purpose of the meeting was to briefly explain the objectives of the project and to give a brief explanation about the expertise of Deltares.

Other managers gave some brief presentations.

Day: 11-04-2012

Time: 16:00-19:30

Location: CAECE University, Mar del Plata

Meeting with:

- Alejandro Gomez (President Mar del Plata Chamber of Commerce foundation)
- Geronimo Rizzo (Collaborator of Mar del Plata Chamber of Commerce foundation)
- Maria Luisa Loidi (Personal assistant of Alejandro Gomez)
- Alejandro A. Garcia (Local stakeholder from the Engineering faculty of the FASTA University)

- Eduardo Tomás Pezzati (President of the Mar del Plata Chamber of Commerce and the director of the Port of Mar del Plata)
- Sergio Loschacoff (Coastal protection engineer, collaborator of Mar del Plata Chamber of Commerce foundation)
- José Carlos Perez de la Sierra (Argentine waterways chief, Quequen and Mar del Plata)
- Walter M. Wischnivetzky (Public works from Mar Chiquita)
- Walter Sivina (Regional port consortium-Marina development)
- Maria Muller (Environmental studies from Quequen)
- Federico German Moran (Industrial plant development)
- Marcelo Requena (Public works manager from Mar del Plata)
- Marcelo Fuster (Advisor for the regional port consortium)
- Marina Iturrarte (Port consortium Mar el Plata)
- Luis del Rio (Quequen beach monitoring)
- Other authorities from the port of Mar del Plata.
- Authorities from other cities and municipalities of the Buenos Aires province.
- Other stakeholders and managers from Mar del Plata.
- P.K. Tonnon.
- R.A. Camarena Calderon
- J.M. Luteijn

Meeting description:

On this meeting, an introductory presentation about Deltares was done by P.K. Tonnon, followed by the MSc project presentations by R.A. Camarena Calderon and J.M. Luteijn.

A more detailed explanation was given compared to previous meetings.

Different possible alternative solutions were presented and discussed. (Described in chapter 4.2)

Possible useful information was mentioned:

- Wave data for 3 years near the port of Quequen.
- Profile measurements near the port of Quequen.
- Study about the coastal evolution near the port of Quequen.

Day: 12-04-2012

Time: 09:30-18:00

Locations: Visiting places along the coast of the Buenos Aires province: Mar Chiquita (lagoon area and tidal inlet), Los Acantilados (offshore breakwaters construction), Miramar (protected beaches and reconstruction of pier).

People: Sergio Loschacoff; P.K. Tonnon; R.A. Camarena Calderon; J.M. Luteijn;

Day: 13-04-2012

Time: 10:00-12:30

Location: Office of Dirección Provincial de Saneamiento y Obra Hidráulica (Provincial Hydraulics Department).

Meeting with:

- Roberto Sciarrone (Hydraulics Department of the Buenos Aires province)
- Geronimo Rizzo (Collaborator of Mar del Plata Chamber of Commerce foundation)
- Sergio Loschacoff (Coastal protection engineer, collaborator of Mar del Plata Chamber of Commerce foundation)
- P.K. Tonnon.
- R.A. Camarena Calderon
- J.M. Luteijn

Meeting description:

It was mentioned that the lack of coastal information is a big problem for the province.

A new report by RWS was found, copies of the report would be collected in the coming days.

Day: 16-04-2012

Time: 05:30-16:30

Location: Port of Mar del Plata.

People: José Perez de la Sierra; Ricardo Caminos, Boat crew (4 persons); R.A. Camarena Calderon; J.M. Luteijn;

Description: The port authorities specially arranged a ship of with specialised equipment and personnel.

While sailing over the predefined survey lines, opinions about different possible alternative solutions were exchanged and discussed. (Described in chapter 4.2)

After completing the depth sounding, the sediment samples were grabbed on the predefined locations.

After low water, the float tracking started. It was hard to visually follow (and find back) both floaters when they were placed on different locations simultaneously. The drifters drifted a complex pattern. Because the cost of the ship (and the large crew) and the experimental character of the last measurement it was considered as unprofitable to execute these measurements for another day.

Day: 17-04-2012

Time: 05:30-16:30

Location: Port of Mar del Plata.

Description: Processing the data of the field measurements.

Exploration of the port from land by bike and taking notes and photographs of different aspects of the port, which can be of importance for this study.

Day: 18-04-2012

Time: 10:00-11:00

Location: Port of Mar del Plata offices

Meeting with:

- José Carlos Perez de la Sierra (Argentine waterways chief, Quequen and Mar del Plata)
- R.A. Camarena Calderon
- J.M. Luteijn

Meeting description:

Data collection:

- Bathymetries
- Port plans
- Dredging information
- Dredging costs
- Breakwater Argentine costs

Exchange of field measurements data:

- Profiles in and out of the port, and in the access channel
- Sediment samples coordinates
- Discussion of drifter measurement results

Day: 19-04-2012

Time: 12:30-17:30

Location: Office Dirección Provincial de Saneamiento y Obra Hidráulica (Provincial Hydraulics Department).

Meeting with:

- Roberto Sciarrone (Hydraulics Department of the Buenos Aires province)
- Sergio Loschacoff (Coastal protection engineer, collaborator of Mar del Plata Chamber of Commerce foundation)
- R.A. Camarena Calderon
- J.M. Luteijn

Meeting description:

A copy of the latest RWS report was provided.

Depth soundings from October 2007 to February 2011 were provided in pdf-format.

An old hand drawn bathymetric survey around the port is photographed.

Description further activities: Site revisit at Mar Chiquita with Romina Troisi (Mar Chiquita municipality) with a lot of explanation about the history of the lagoon and the inlet, measurers against erosion and the present situation.

Day: 20-04-2012

Time: 08:30-17:30

Locations: Visiting places along the coast of the Buenos Aires province to the Hotel in Buenos Aires: Villa Gesell (large stable beach) and Lavalle (West from Punta Rhasa)

People: Sergio Loschacoff; R.A. Camarena Calderon; J.M. Luteijn;

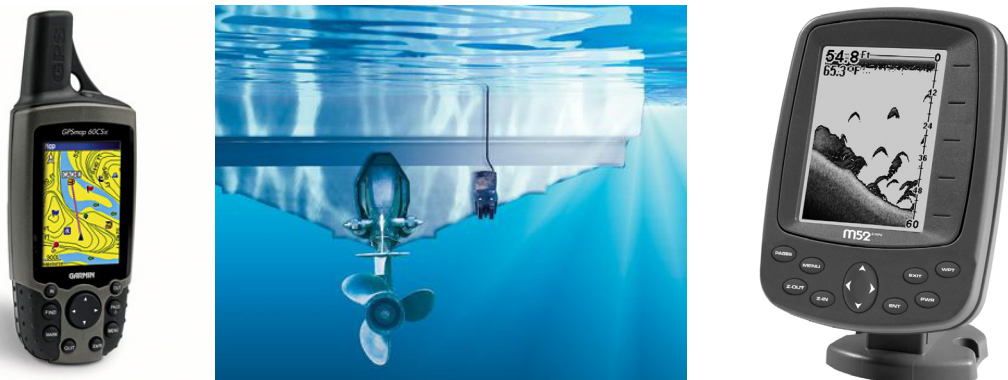
B Field measurements

B.1 Alternative depth sounding method

Initially depth soundings were planned using a self-made automatic depth survey set. This set consisted of a Garmin® GPSmap 60CSx handheld GPS receiver for horizontal positioning. This receiver is selected because of its low cost, low power requirements, compactness, naval applications, Wide Area Augmentation System (WAAS) capability, and NMEA 0183 connectivity. The horizontal accuracy is < 3 meters (with WAAS) (Garmin, 2007b).

A Lowrance® M52i Fish-finding Sonar & GPS Plotter would be used as single beam echo sounder because of its low cost, low power requirements, compactness, NMEA 0183 connectivity, and transducer that can operate with a 0.1 m vertical accuracy on 200 kHz frequencies with a 20° cone angle and temperature measuring capabilities. The footprint/depth ratio is 0.35. This translates to a footprint diameter of 3 m at a depths of 8.5 m, thus within GPS accuracy to this water depth.

The best fitting location is horizontally on the back of a boat so that its centreline is level with the boat hull. This will give the best combination of smooth water flow and protection from collisions with drifting materials or hitting the bottom (Lowrance, 2003).



Photograph 10.1 Alternative depth survey set
 Garmin GPS (l), Transom mount transducer (m), Lowrance fish finder (r)

The echo sounder continuously measures depths and transmits its data to the GPS receiver, which can be configured to store records using time or distance intervals. The GPS receiver is mounted as close as possible to the transducer and the GPS receiver and fish finder display their position, accuracy, and bed profile to the boat operator.

The optimal survey pattern will be determined considering a number of constraints, namely time available, wave, tide, and weather conditions and bottom topography and depth and is uploaded to the GPS receiver. These uploaded rays can be used to navigate the boat, where at obstructions one can briefly take another course and then return to the grid.

The stored data can finally be downloaded to a (portable) PC and must be corrected with the tide curve to main sea level.

This equipment is tested and verified in practice on the 25th of March on the Western Scheldt at Flushing. During manual measurements using a log line at different positions, the sonar displayed the same depth as manually measured. Also monitoring the display of the sonar during sailing to and off the shore, the sonar displayed and stored a comparable profile as displayed on the nautical chart.

B.2 Sediment sampling

At Mar del Plata, sediment samples are extracted at the following locations:



Figure 10.1 Sediment sampling locations

| Sample | Location | Coordinates | Elevation |
|----------|----------------------|---------------------|-----------|
| 16-04-1 | Mar del Plata Port A | 38.0344°S 57.5133°W | -13.0 m |
| 16-04-2 | Mar del Plata Port B | 38.0360°S 57.5190°W | -5,0 m |
| 16-04-3 | Mar del Plata Port C | 38.0522°S 57.5290°W | -6.0 m |
| 16-04-4 | Mar del Plata Port D | 38.0596°S 57.5314°W | -7.2 m |
| 16-04-5 | Mar del Plata Port E | 38.0601°S 57.5336°W | -4.9 m |
| 16-04-8 | Mar del Plata Port F | 38.0398°S 57.5170°W | -6.6 m |
| 16-04-9 | Mar del Plata Port G | 38.0383°S 57.5131°W | -12.7 m |
| 16-04-10 | Mar del Plata Port H | 38.0366°S 57.5220°W | -9.0 m |
| 16-04-11 | Mar del Plata Port I | 38.0376°S 57.5189°W | -3.6 m |
| 16-04-12 | Mar del Plata Port J | 38.0342°S 57.5245°W | -5.8 m |
| 18-04-1 | Mar del Plata A | 38.0513°S 57.5328°W | 0.0 m |
| 18-04-3 | Mar del Plata B | 38.0284°S 57.5306°W | 0.0 m |
| 18-04-5 | Mar del Plata C | 38.0150°S 57.5295°W | 0.0 m |

Table 10.1 Sediment sampling locations

Per location, a numbered rigid plastic bag will be filled with ca. 100 grams and the corresponding location will be registered.

On shore, a sample was taken using a sampling bucket to avoid separation of sediment fractions during excavation. Bottom samples are taken using a manually controlled stainless steel Van Veen grab (illustrated in Figure 10.2).

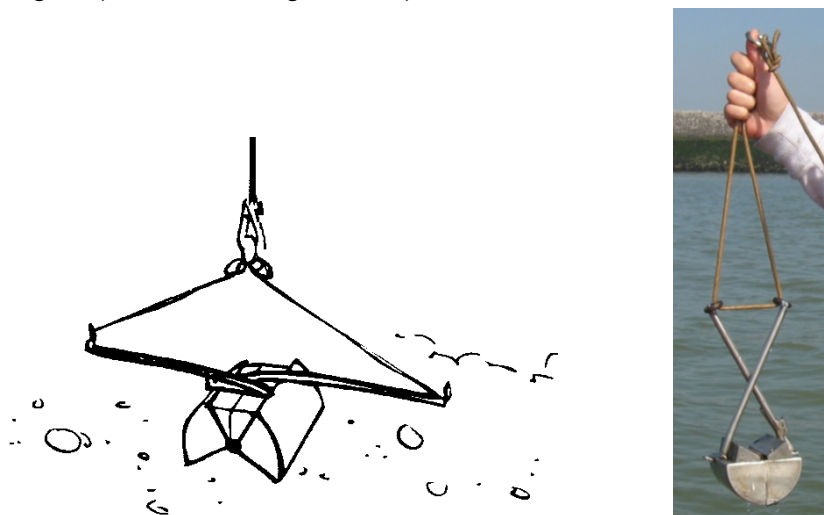


Figure 10.2 Van Veen grab in opened and closed position

At the surface, the jaws are pushed open and kept in that position by a hook. To keep the hook in the right position the Van Veen grab should be sunk at a steady, not too high, pace. As soon as the jaws touch the bottom, the hook loosens its grip, so that, when hoisting the rope again the jaws will shut tight because of the leverage by the rods. The amount of drawn sample mainly depends on the compactness of the bottom. Therefore the grab have been fitted with weighting blocks.

In spite of the heavy closing force, it can happen that a pebble sticks between the buckets. In such case the sample is not representative; the smaller parts may have escaped during hoisting (Eikelkamp, 2006).

To gain more experience using the Van Veen grab, a rehearsal is executed on 25 March on the Western Scheldt at Flushing under wave ($H_{\text{shipwaves}} \approx 1$ m) and flow conditions ($U_{\text{flood; surface}} \approx 1,5$ m/s). At some attempts, the Van Veen grab was still open, when it was raised above water after touching the bottom too soft. After some attempts, the closing of the grab could be recognised by a slight increasing tensile force while lifting the grab from the bottom. At some attempts, a shell was stuck between the buckets and the content of the bucket was very small, but the sampling could easily be repeated on the same spot, resulting in a good grab.

B.3 Drifter tracking

B.3.1 Methodology

To estimate the direction and magnitude of the local currents near the port entrance, a GPS-drifter was tracked. Due to limited budget and availability of a safe vessel, the measurements took place at one day from 1 hour after low water to 1 hour before high water. The drifter was placed on different locations +/- 400m upstream the port entrance. When the floaters moved uniformly for 20 min, it was picked up and placed upstream again.

This drifter was designed to: move with the water at the surface, avoid displacement by wind, stay above water to guarantee GPS reception, be rigid, reliable, easily transportable, and cheap. To avoid displacement by wind, this drifter had a minimum volume above water and a relative large lateral plane. Because the drifters must also be able to float over shallow areas of less than 2 meters, the depth is restricted. To reduce transport weight (in the airplane), the drifters were ballasted on site by putting a closed bag of beach sand in the shaft of the drifter or by attaching a weight using tie wraps.

On top of the drifter, a waterproof Garmin® eTrex H GPS receiver was mounted. This stores its location over time with an horizontal location accuracy of < 3 m (Garmin, 2007a). After the measurements, this data was transferred to a pc in .gpx-format for further processing.



Photograph 10.2 GPS-Drifters constructed and used for measurements

| | | |
|------------------------------------|---|--------------|
| PVC pipe Ø 60 x 1000 mm | € | 2,70 |
| 2 Broom sticks Ø 23 x 1200 mm | € | 4,58 |
| 8 Hose clamps | € | 6,36 |
| Tie wraps | € | 3,45 |
| Vinyl sail | € | 3,00 |
| Pipe isolation | € | 2,10 |
| Nails and staples | € | 0,00 |
| Garmin eTrex H GPS receiver | € | 0,00 |
| Data cable (GPS to PC) | € | 0,00 |
| 2 AA batteries | € | 1,75 |
| Plastic bag filled with beach sand | € | 0,00 |
| Boat hook | € | 0,00 |
| Measuring sheets | € | 0,00 |
| Writing-case | € | 0,00 |
| Watch with time synced to GPS time | € | 0,00 |
| Photo camera | € | 0,00 |
| | € | <u>23,94</u> |

Table 10.2 Materials used for GPS-drifter measurements

The GPS continuously measures its position after it is turned on. To be able to only record advection by natural flow:

- At the moment the drifter is dropped into the water and free from ship propeller jet, the time is recorded using a time synced watch.
- When the ship started to sail to the drifter to pick it up, again the time is registered.
- During the measurements, the drifters were continuously monitored to notice special conditions that might influence the movements of the drifters.

These drifters were tested and verified in practice on 25 March on the Western Scheldt at Flushing under wave ($H_{\text{shipwaves}} \approx 1$ m) and flow conditions ($U_{\text{flood;surface}} \approx 1.5$ m/s). Initially the upper half of the shaft was filled with pipe insulation and the lower half with a plastic bag of +/- 0.5 kg sand. Then the drifter was too high on the water, so it caught too much wind. After removing the inner pipe insulation, the drifter was more stable and only the pipe insulation was only half above water.

At the start of the measurements, the tidal data was retrieved from the website of the Naval Hydrographic Service of Argentina. Actual wind and wave data was retrieved from the GFS and NWW3 model delivered by WindGURU (2012).

Argentina - Mar del Plata, Lat: -38, Lon: -57.55

Last quarter (neap tide): 13-04-2012

New moon (spring tide): 21-04-2012

Low water: 16-04-2012, 10:54, -0.51 m to MSL

High water: 16-04-2012, 16:21, +0.22 m to MSL

| GFS (50 km) | Wind speed 10 m above surface (m/s) | | | | | | | | Wind direction | | | | | | | |
|----------------|-------------------------------------|-----|-----|-----|-----|-----|-----|-----|----------------|-----|-----|-----|-----|-----|-----|-----|
| | 00h | 03h | 06h | 09h | 12h | 15h | 18h | 21h | 00h | 03h | 06h | 09h | 12h | 15h | 18h | 21h |
| 14.04.2012 | 4.7 | 6.4 | 6.5 | 5.9 | 5.2 | 4.4 | 2.7 | 2.2 | ↗ | ↗ | ↗ | ↑ | ↑ | ↑ | | |
| 15.04.2012 | 1.4 | 2.4 | 3.2 | 3.5 | 0.9 | 1.1 | 2.7 | 3.9 | | → | → | → | → | → | | ↘ |
| 16.04.2012 | 4.6 | 4.3 | 4.4 | 5.1 | 7.8 | 7.7 | 6.6 | 6.5 | ↘ | ↘ | ↘ | ↘ | ↘ | ↘ | ↘ | ↘ |

| MWW3 | Significant wave height (m) | | | | | | | | Direction of the dominant waves | | | | | | | | Peak wave period (s) | | | | | | | | |
|------------|-----------------------------|-----|-----|-----|-----|-----|-----|-----|---------------------------------|-----|-----|-----|-----|-----|-----|-----|----------------------|-----|-----|-----|-----|-----|-----|-----|----|
| | 00h | 03h | 06h | 09h | 12h | 15h | 18h | 21h | 00h | 03h | 06h | 09h | 12h | 15h | 18h | 21h | 00h | 03h | 06h | 09h | 12h | 15h | 18h | 21h | |
| 14.04.2012 | 0.7 | 0.7 | 0.8 | 0.8 | 0.8 | 0.7 | 0.7 | 0.7 | ← | ← | ← | ← | ← | ← | ← | ← | 8 | 8 | 8 | 8 | 8 | 8 | 8 | 10 | 10 |
| 15.04.2012 | 0.7 | 0.7 | 0.7 | 0.7 | 0.7 | 0.7 | 0.7 | 0.7 | ← | ← | ← | ← | ← | ← | ← | ← | 9 | 9 | 9 | 8 | 8 | 8 | 8 | 8 | 8 |
| 16.04.2012 | 0.6 | 0.6 | 0.6 | 0.6 | 1.1 | 1.1 | 1.0 | 0.9 | ← | ← | ← | ← | ↘ | ↘ | ↘ | ↘ | 8 | 8 | 8 | 8 | 3 | 4 | 4 | 4 | 4 |

Table 10.3 Tide, wind, and wave data before and during drifter tracking (SHN, 2012d; WindGURU, 2012)

B.3.2 Results

| Colour | Track | Time | Hours before high water | Average velocity |
|------------|-------|---------------|-------------------------|------------------|
| Red | A | 11:40 - 11:58 | 4:41 - 4:23 | 0.3 m/s |
| Yellow | B | 12:05 - 12:30 | 4:16 - 3:51 | 0.1 m/s |
| Green | C1 | 12:37 - 12:57 | 3:44 - 3:24 | 0.2 m/s |
| Dark Green | C2 | 12:57 - 13:18 | 3:24 - 3:03 | 0.1 m/s |
| Cyan | D1 | 13:23 - 13:45 | 2:58 - 2:36 | 0.1 m/s |
| Blue | D2 | 13:45 - 14:07 | 2:36 - 2:14 | 0.1 m/s |
| Dark Blue | D3 | 14:07 - 14:30 | 2:14 - 1:51 | 0.2 m/s |
| Magenta | E | 14:34 - 14:59 | 1:47 - 1:22 | 0.2 m/s |
| Black | F | 15:03 - 15:20 | 1:18 - 1:01 | 0.1 m/s |
| White | G | 15:24 - 15:47 | 0:57 - 0:34 | 0.4 m/s |

Table 10.4 Data summary drifter tracks

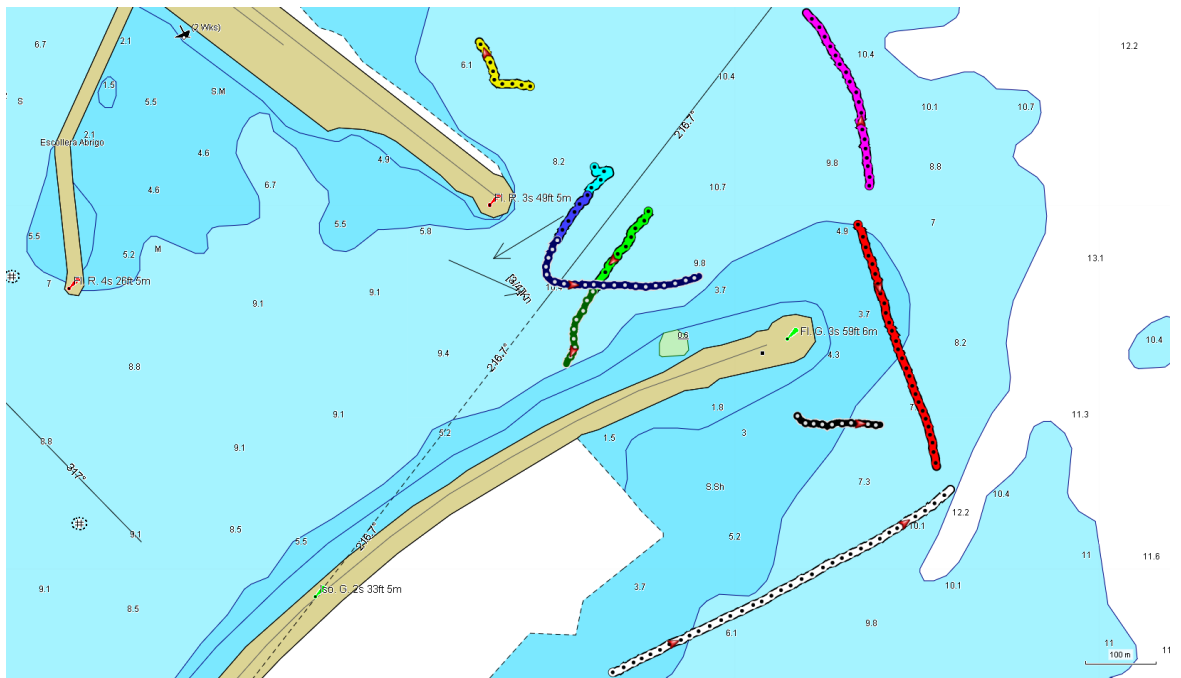


Figure 10.3 Overview drifter tracks

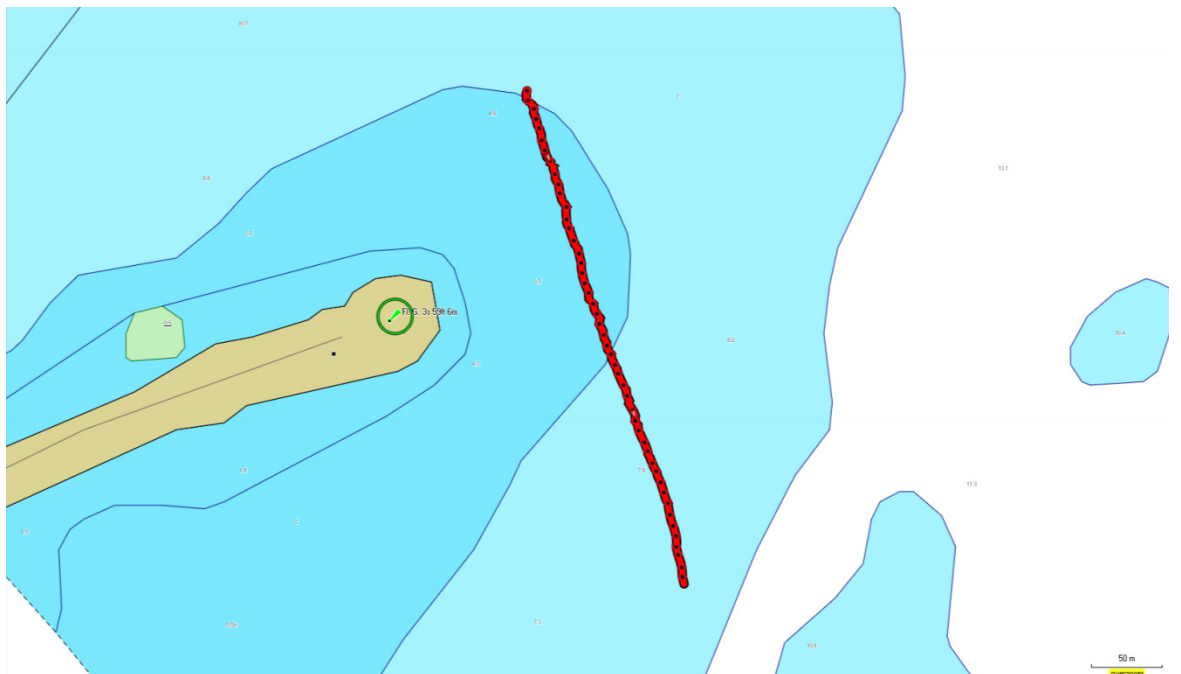


Figure 10.4 Drifter track A: ca. 4.5 hours before HW



Figure 10.5 Drifter track B: ca. 4 hours before HW

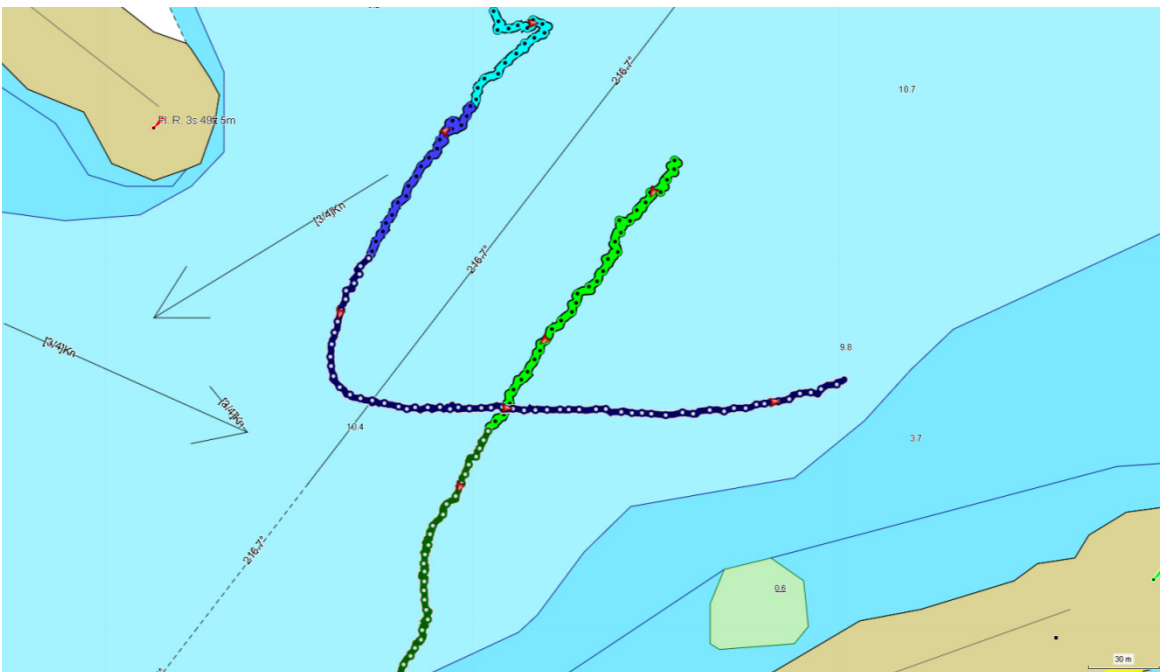


Figure 10.6 Drifter track C1-C3 (Green): ca. 3.5 hours before HW and Track D1-D3 (Blue): ca. 2.5 hours before HW



Figure 10.7 Drifter track E: ca. 1.5 hours before HW

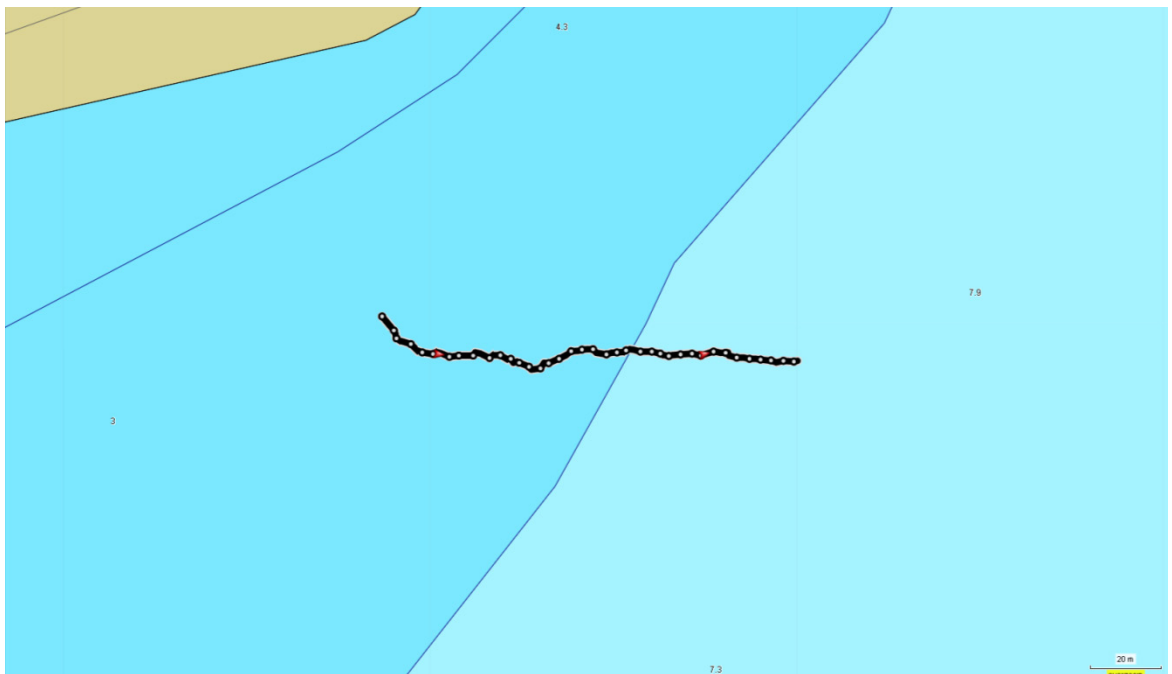


Figure 10.8 Drifter track F: ca. 1 hour before HW



Figure 10.9 Drifter track G: ca. 45m before HW.

B.3.3 Data comparison and evaluation

From continuity, the maximum cross section averaged flow velocity through the access channel can be expected.

$$\hat{v}_{channel,average\ tide} = \frac{L_{basin} \cdot W_{basin} \cdot \Delta h \cdot \text{maximum fraction in one hour}}{A_{channel} \cdot 3600\ sec.} \quad (10.1)$$

$$\hat{v}_{channel,average\ tide} = \frac{2000 \cdot 1000 \cdot 0.81 \cdot \frac{1}{4}}{(50 \cdot 90 + 250 \cdot 2) \cdot 3600} = 0.1\ m/s \quad (10.2)$$

The measurements were performed between spring and neap tide; therefore, average tidal velocities are expected. At the surface and in the deeper parts of the channel, higher flow velocities are expected. This port is relatively very short compared to the length of tidal wave, so the maximum flood velocity is expected 3.25 hours after low water. The flow velocities of track C (0.2 to 0.1 m/s) apply to this theory.

From these measurements can be concluded that:

- The flow velocities inside the port entrance are weak (0.1 - 0.2 m/s). Currents outside the port have an order of magnitude of twice the flow velocities inside the port. These currents are likely to be wave-induced longshore currents.
- The current parallel to the southern breakwater drives a circulating flow in the port entrance.
- Track C has same direction as the flow vectors on the nautical chart and a smaller magnitude than the maximum of 0.75 knot (0.4 m/s) denoted on the nautical map. This result seems to be obvious, due to the calm weather and sea state and because the measurements took place at a day between the days of neap tide and spring tide.

C Computed deep water wave climate near Mar del Plata

The wind and wave conditions are derived from the near shore wave model of Buenos Aires in a joint study with Camarena Calderon (2012) (described in section 5). The input is extracted at one point in the middle of the south-east boundary of the “wave grid” (at UTM21s 491126 m east, 5756185 m north on 69 m water depth). This resulted in an annual climate with 125 scenarios of simultaneous occurring wind and wave conditions written down in Table 10.5 to Table 10.7.

| Annual climate of 125 scenarios simultaneous occurring wind and wave conditions at UTM21s 491126 m east, 5756185 m north on 69 m water depth | | | | | | |
|---|---------------|---------------|-----------------------------|------------------|-------------------------------|---|
| Scenario | Hs (m) | Tp (s) | Dm (° w.r.t. N.) | U10 (m/s) | Udir (° w.r.t. N.) | Average duration per year (days) |
| 1 | 0,69 | 2,7 | 29 | 7,9 | 344 | 1,75 |
| 2 | 0,56 | 2,3 | 30 | 6,3 | 0 | 5,94 |
| 3 | 0,88 | 3,0 | 27 | 9,7 | 330 | 0,05 |
| 4 | 0,95 | 3,1 | 32 | 9,8 | 342 | 0,05 |
| 5 | 0,83 | 3,0 | 38 | 8,6 | 321 | 0,15 |
| 6 | 0,54 | 2,4 | 62 | 5,2 | 46 | 1,62 |
| 7 | 0,82 | 3,0 | 43 | 7,3 | 354 | 2,54 |
| 8 | 0,76 | 2,8 | 44 | 6,9 | 3 | 5,75 |
| 9 | 0,66 | 2,6 | 47 | 6,2 | 17 | 6,67 |
| 10 | 0,93 | 3,2 | 41 | 8,8 | 338 | 0,30 |
| 11 | 0,90 | 3,1 | 43 | 7,7 | 347 | 0,91 |
| 12 | 1,14 | 5,0 | 101 | 8,3 | 268 | 0,03 |
| 13 | 1,74 | 5,4 | 82 | 8,5 | 10 | 0,09 |
| 14 | 1,12 | 4,3 | 73 | 7,8 | 331 | 1,20 |
| 15 | 1,17 | 4,1 | 76 | 6,8 | 12 | 3,47 |
| 16 | 1,04 | 4,0 | 81 | 5,9 | 23 | 6,66 |
| 17 | 0,95 | 3,6 | 83 | 5,6 | 55 | 12,46 |
| 18 | 1,18 | 4,8 | 92 | 8,4 | 295 | 0,41 |
| 19 | 0,63 | 2,8 | 74 | 4,6 | 42 | 4,30 |
| 20 | 0,81 | 3,3 | 83 | 5,4 | 57 | 14,72 |
| 21 | 1,31 | 4,5 | 94 | 6,4 | 65 | 5,78 |
| 22 | 0,74 | 3,1 | 75 | 5,1 | 35 | 4,19 |
| 23 | 1,11 | 4,1 | 92 | 5,7 | 56 | 11,35 |
| 24 | 1,47 | 4,9 | 98 | 6,8 | 77 | 2,74 |
| 25 | 0,91 | 3,5 | 84 | 5,4 | 39 | 12,97 |
| 26 | 1,82 | 5,9 | 107 | 7,2 | 125 | 1,12 |
| 27 | 1,74 | 5,1 | 106 | 8,3 | 105 | 1,22 |
| 28 | 2,58 | 6,3 | 119 | 11,0 | 138 | 0,55 |
| 29 | 1,65 | 5,3 | 106 | 7,2 | 90 | 1,33 |
| 30 | 1,22 | 4,6 | 100 | 5,6 | 63 | 6,42 |

Table 10.5 Annual offshore wind and wave climate near Mar del Plata (part 1 of 3)

| Scenario | Hs (m) | Tp (s) | Dm (° w.r.t. N.) | U10 (m/s) | Udir (° w.r.t. N.) | Average duration per year (days) |
|----------|--------|--------|------------------|-----------|--------------------|----------------------------------|
| 31 | 0,81 | 3,4 | 85 | 5,2 | 40 | 2,68 |
| 32 | 2,05 | 6,2 | 117 | 8,1 | 150 | 0,72 |
| 33 | 1,48 | 4,9 | 102 | 6,9 | 73 | 2,84 |
| 34 | 1,02 | 3,9 | 92 | 5,4 | 44 | 7,28 |
| 35 | 2,65 | 6,2 | 125 | 11,3 | 148 | 0,16 |
| 36 | 1,85 | 6,0 | 110 | 7,0 | 107 | 1,06 |
| 37 | 0,77 | 3,3 | 88 | 4,7 | 37 | 2,10 |
| 38 | 1,71 | 5,9 | 115 | 6,0 | 107 | 1,63 |
| 39 | 1,54 | 5,2 | 111 | 6,3 | 83 | 2,54 |
| 40 | 2,77 | 7,8 | 121 | 8,3 | 181 | 0,37 |
| 41 | 1,04 | 4,0 | 97 | 5,4 | 40 | 5,61 |
| 42 | 1,25 | 4,7 | 104 | 6,1 | 42 | 4,65 |
| 43 | 1,85 | 5,8 | 120 | 7,6 | 132 | 0,91 |
| 44 | 2,12 | 6,0 | 126 | 9,0 | 159 | 0,54 |
| 45 | 2,05 | 6,2 | 129 | 8,1 | 175 | 0,76 |
| 46 | 1,87 | 5,7 | 127 | 7,9 | 143 | 1,08 |
| 47 | 1,67 | 5,6 | 126 | 6,8 | 137 | 1,54 |
| 48 | 1,27 | 4,7 | 112 | 6,0 | 66 | 4,60 |
| 49 | 1,47 | 5,2 | 119 | 5,9 | 95 | 2,59 |
| 50 | 1,06 | 4,1 | 106 | 5,8 | 55 | 4,86 |
| 51 | 0,70 | 2,9 | 74 | 4,8 | 31 | 1,51 |
| 52 | 2,72 | 7,3 | 132 | 9,7 | 183 | 0,36 |
| 53 | 0,69 | 2,9 | 79 | 5,0 | 46 | 1,85 |
| 54 | 0,98 | 3,8 | 105 | 5,4 | 47 | 6,14 |
| 55 | 1,59 | 5,7 | 133 | 5,8 | 139 | 3,36 |
| 56 | 1,18 | 4,5 | 118 | 5,9 | 64 | 6,60 |
| 57 | 1,37 | 5,1 | 127 | 5,6 | 83 | 5,25 |
| 58 | 2,28 | 5,9 | 146 | 11,2 | 195 | 0,36 |
| 59 | 1,77 | 6,2 | 136 | 6,3 | 155 | 1,89 |
| 60 | 1,93 | 6,5 | 136 | 7,0 | 173 | 1,29 |
| 61 | 0,88 | 3,4 | 100 | 5,4 | 50 | 9,02 |
| 62 | 0,56 | 2,5 | 65 | 5,2 | 46 | 2,12 |
| 63 | 1,09 | 4,2 | 122 | 5,6 | 63 | 13,76 |
| 64 | 1,26 | 4,9 | 132 | 5,3 | 79 | 10,51 |
| 65 | 1,58 | 6,2 | 145 | 5,6 | 200 | 4,54 |
| 66 | 1,38 | 5,8 | 143 | 4,7 | 173 | 6,86 |
| 67 | 1,77 | 6,7 | 145 | 6,5 | 202 | 3,97 |
| 68 | 2,20 | 6,7 | 147 | 9,5 | 208 | 1,33 |
| 69 | 2,10 | 6,3 | 153 | 10,5 | 218 | 1,30 |
| 70 | 1,42 | 5,5 | 153 | 7,0 | 219 | 3,65 |
| 71 | 1,04 | 4,8 | 151 | 4,8 | 220 | 7,35 |
| 72 | 1,24 | 5,1 | 154 | 6,3 | 222 | 5,33 |
| 73 | 0,86 | 4,9 | 148 | 1,0 | 185 | 10,27 |
| 74 | 0,74 | 3,5 | 123 | 4,1 | 55 | 8,07 |
| 75 | 1,63 | 5,7 | 154 | 8,6 | 218 | 3,47 |
| 76 | 0,55 | 2,7 | 95 | 4,0 | 45 | 1,89 |
| 77 | 1,84 | 5,6 | 162 | 12,1 | 236 | 0,35 |
| 78 | 1,15 | 4,3 | 162 | 7,9 | 227 | 2,77 |
| 79 | 0,63 | 3,5 | 152 | 3,8 | 205 | 5,29 |

Table 10.6 Annual offshore wind and wave climate near Mar del Plata (part 2 of 3)

| Scenario | Hs (m) | Tp (s) | Dm (° w.r.t. N.) | U10 (m/s) | Udir (° w.r.t. N.) | Average duration per year (days) |
|----------|--------|--------|---------------------|-----------|-----------------------|-------------------------------------|
| 80 | 0,95 | 3,9 | 163 | 7,1 | 225 | 3,79 |
| 81 | 0,80 | 3,3 | 167 | 6,0 | 225 | 6,29 |
| 82 | 1,24 | 4,8 | 165 | 9,0 | 238 | 1,75 |
| 83 | 0,45 | 2,3 | 64 | 4,3 | 12 | 1,05 |
| 84 | 1,50 | 4,9 | 165 | 10,9 | 236 | 1,68 |
| 85 | 1,32 | 4,4 | 173 | 11,4 | 247 | 0,30 |
| 86 | 0,83 | 3,1 | 178 | 8,3 | 247 | 1,56 |
| 87 | 0,58 | 2,8 | 168 | 5,0 | 233 | 2,19 |
| 88 | 0,66 | 2,9 | 176 | 7,2 | 243 | 2,25 |
| 89 | 1,15 | 3,9 | 173 | 10,2 | 248 | 0,61 |
| 90 | 0,99 | 3,6 | 175 | 9,3 | 249 | 0,95 |
| 91 | 0,40 | 2,2 | 183 | 4,6 | 237 | 0,47 |
| 92 | 1,61 | 5,0 | 170 | 13,2 | 254 | 0,05 |
| 93 | 1,81 | 5,0 | 171 | 14,6 | 243 | 0,04 |
| 94 | 1,01 | 3,4 | 181 | 10,9 | 259 | 0,20 |
| 95 | 0,45 | 2,1 | 195 | 6,2 | 257 | 0,95 |
| 96 | 0,54 | 2,2 | 201 | 7,6 | 261 | 1,37 |
| 97 | 0,77 | 2,9 | 189 | 9,6 | 263 | 0,24 |
| 98 | 0,39 | 2,1 | 197 | 5,0 | 275 | 0,29 |
| 99 | 0,67 | 2,6 | 188 | 8,3 | 262 | 0,78 |
| 100 | 1,24 | 3,9 | 181 | 13,0 | 270 | 0,01 |
| 101 | 1,56 | 4,7 | 171 | 13,8 | 260 | 0,05 |
| 102 | 0,79 | 2,8 | 202 | 10,6 | 279 | 0,19 |
| 103 | 0,40 | 2,0 | 213 | 6,0 | 274 | 1,68 |
| 104 | 0,56 | 2,2 | 278 | 9,3 | 288 | 0,69 |
| 105 | 0,26 | 1,5 | 342 | 5,1 | 319 | 0,37 |
| 106 | 0,41 | 1,8 | 293 | 7,4 | 291 | 2,64 |
| 107 | 0,49 | 2,0 | 284 | 8,3 | 289 | 1,87 |
| 108 | 1,62 | 5,8 | 165 | 12,0 | 265 | 0,01 |
| 109 | 0,70 | 2,4 | 227 | 10,7 | 278 | 0,01 |
| 110 | 0,58 | 2,2 | 329 | 10,0 | 300 | 0,20 |
| 111 | 0,52 | 2,0 | 342 | 9,7 | 310 | 0,57 |
| 112 | 0,42 | 1,9 | 339 | 8,4 | 310 | 2,48 |
| 113 | 0,36 | 1,7 | 341 | 7,4 | 312 | 4,26 |
| 114 | 0,27 | 1,6 | 358 | 4,8 | 332 | 0,87 |
| 115 | 0,28 | 1,5 | 330 | 6,1 | 308 | 3,58 |
| 116 | 0,73 | 2,4 | 356 | 11,2 | 321 | 0,05 |
| 117 | 1,94 | 5,6 | 163 | 13,9 | 239 | 0,03 |
| 118 | 0,54 | 2,2 | 6 | 8,1 | 329 | 1,75 |
| 119 | 0,47 | 2,1 | 4 | 7,3 | 330 | 5,65 |
| 120 | 0,63 | 2,4 | 5 | 9,0 | 327 | 0,46 |
| 121 | 0,46 | 2,1 | 12 | 6,3 | 342 | 5,65 |
| 122 | 0,35 | 1,8 | 10 | 5,2 | 343 | 1,27 |
| 123 | 0,64 | 2,5 | 11 | 8,7 | 325 | 0,33 |
| 124 | 0,49 | 2,3 | 43 | 5,2 | 18 | 1,33 |
| 125 | 0,61 | 2,4 | 23 | 7,1 | 350 | 6,50 |

Total: 365,00

Table 10.7 Annual offshore wind and wave climate near Mar del Plata (part 3 of 3)

D Computed average hour-by-hour tidal flow in port access

The computed average hour-by-hour tidal flow patterns (expressed in hours before and after high water) are visualised below. Background colours indicate the local depth averaged flow velocity (in m/s), while the vectors point in the direction of the flow.

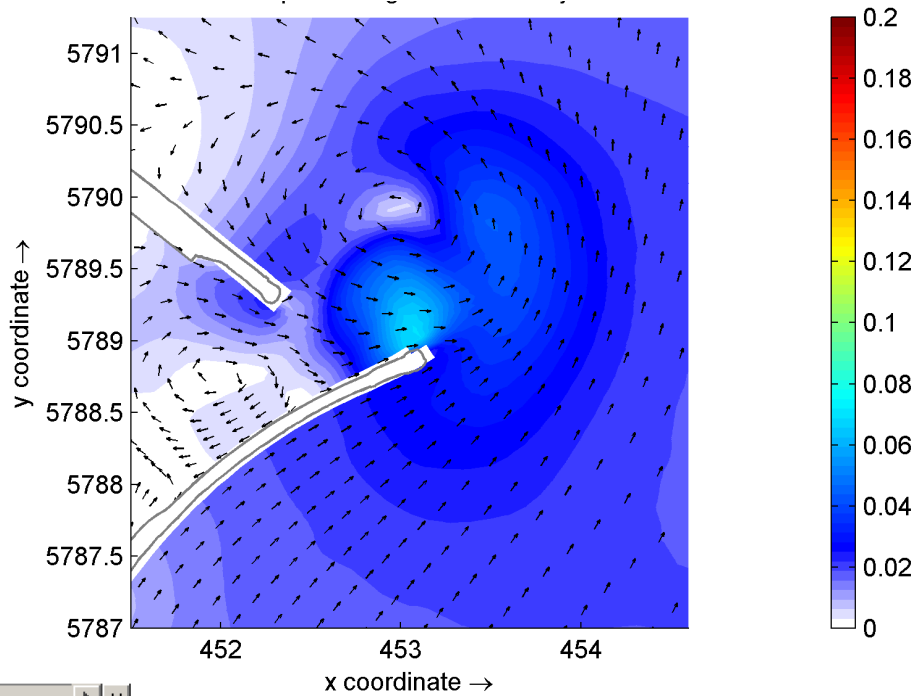


Figure 10.10 Computed depth averaged flow velocities (in m/s) and directions 0.5 hour after HW

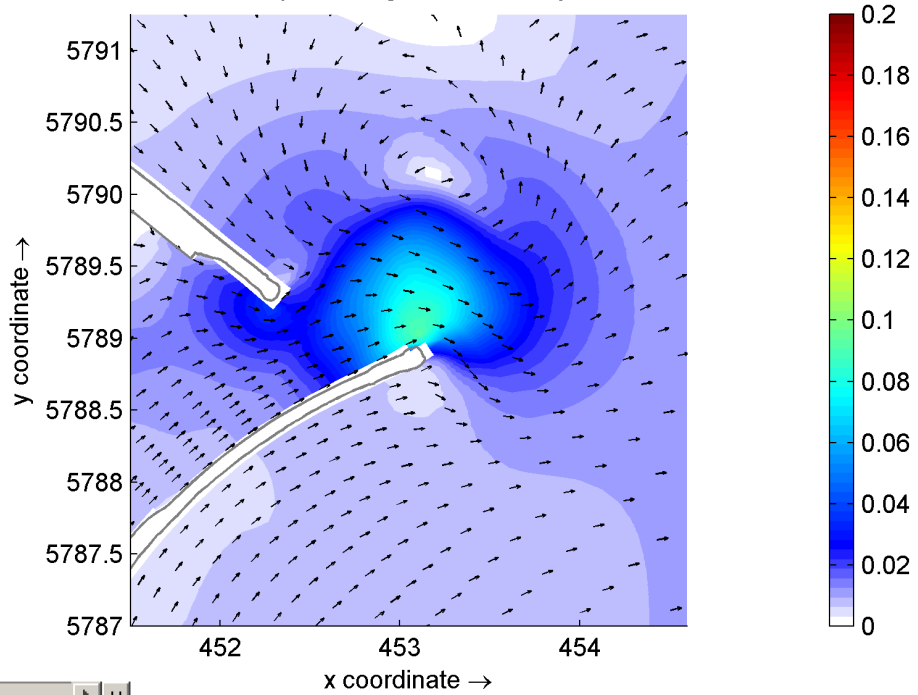


Figure 10.11 Computed depth averaged flow velocities (in m/s) and directions 1.5 hours after HW

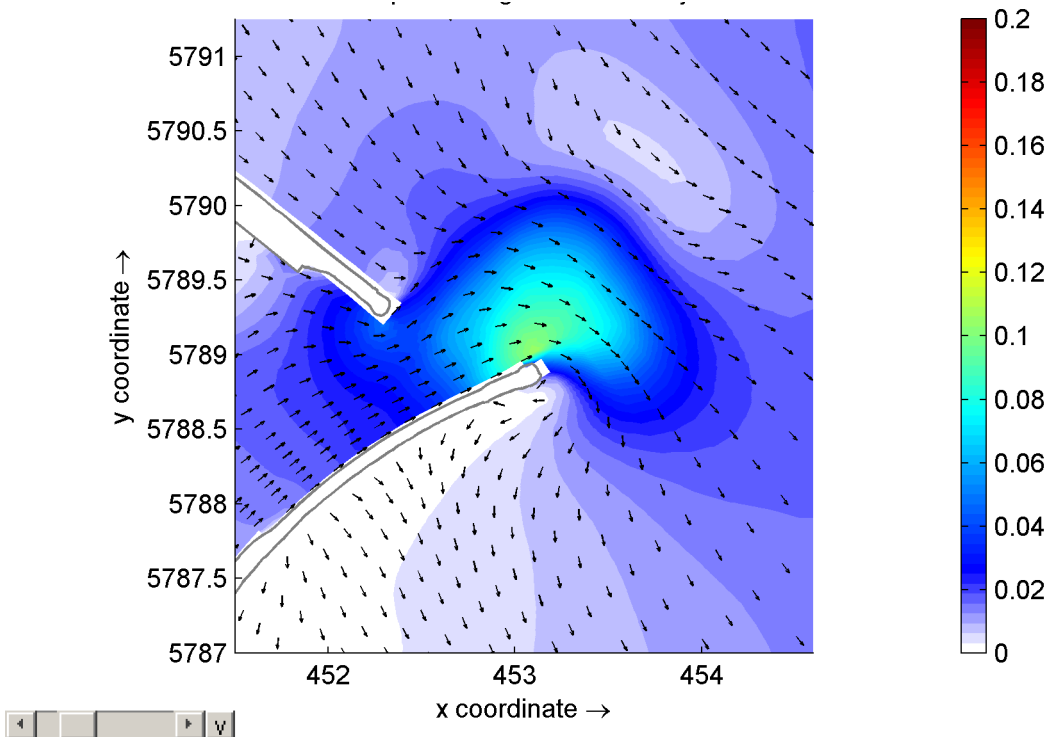


Figure 10.12 Computed depth averaged flow velocities (in m/s) and directions 2.5 hours after HW

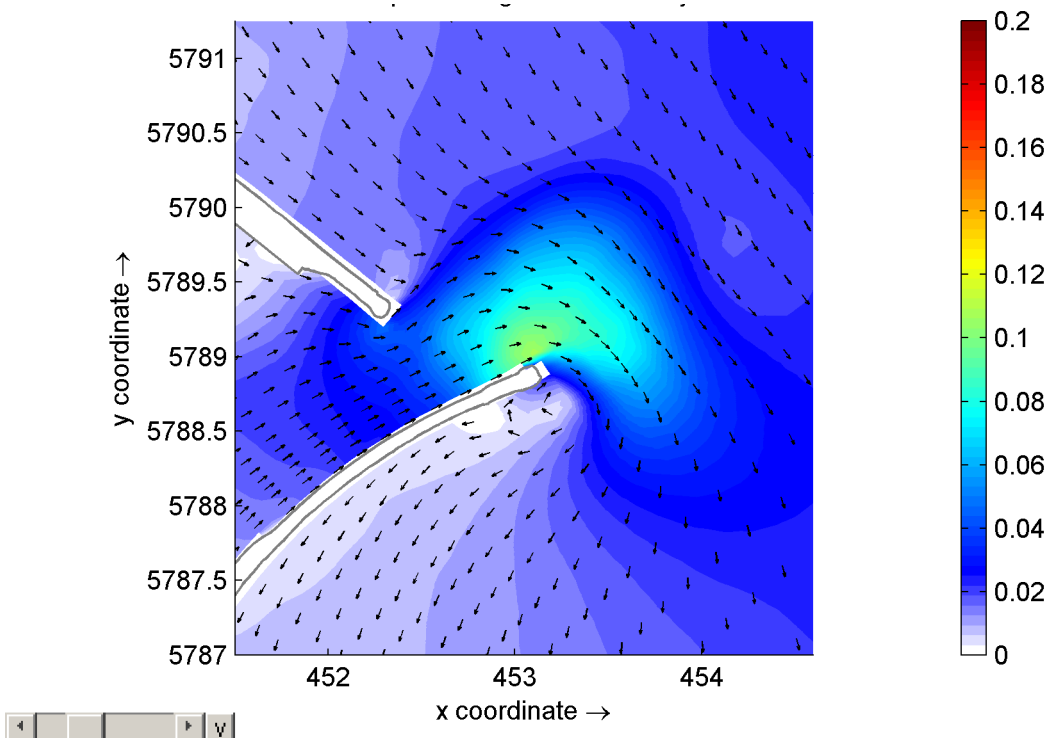


Figure 10.13 Computed depth averaged flow velocities (in m/s) and directions 3.5 hours after HW

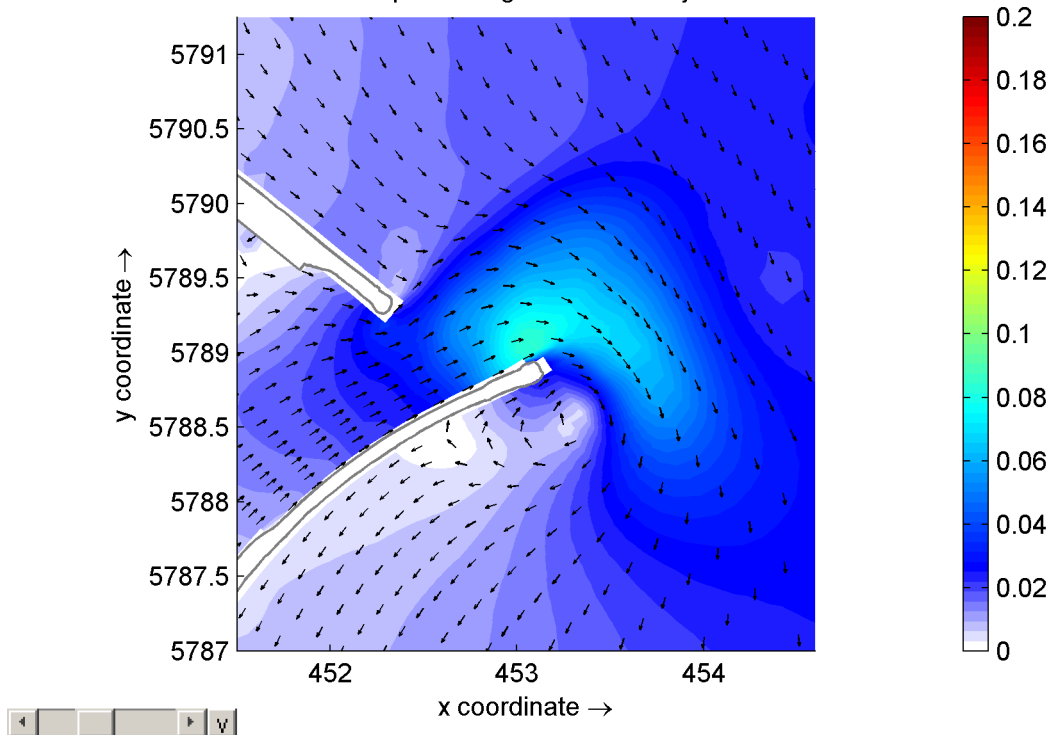


Figure 10.14 Computed depth averaged flow velocities (in m/s) and directions 4.5 hours after HW

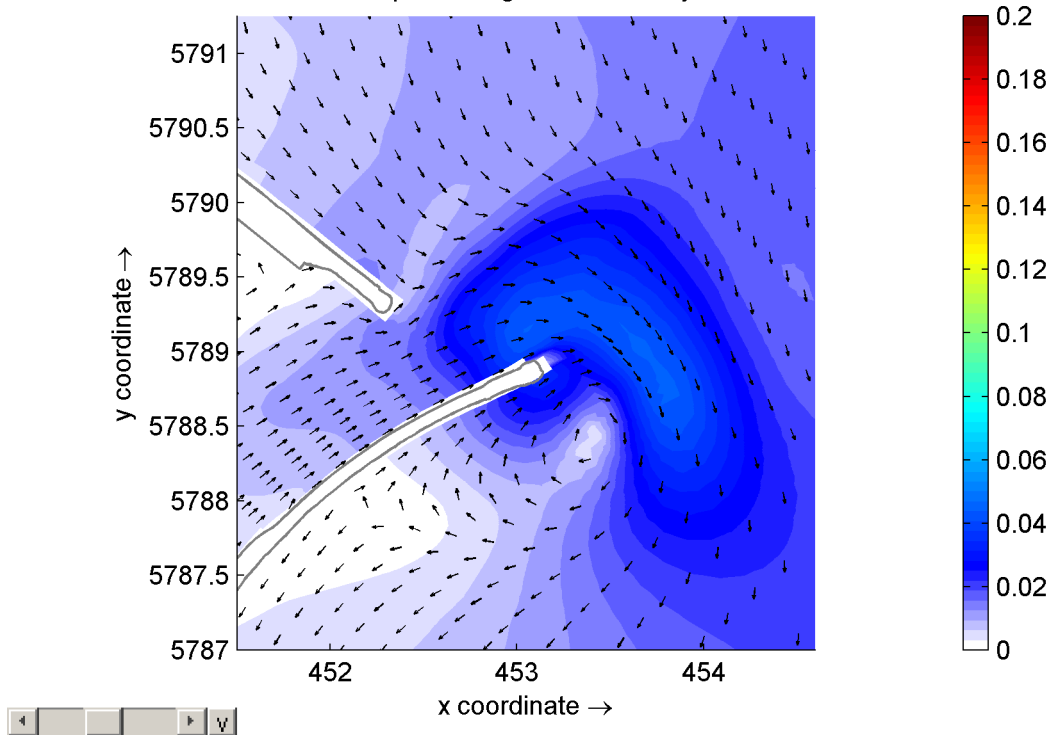


Figure 10.15 Computed depth averaged flow velocities (in m/s) and directions 5.5 hours after HW

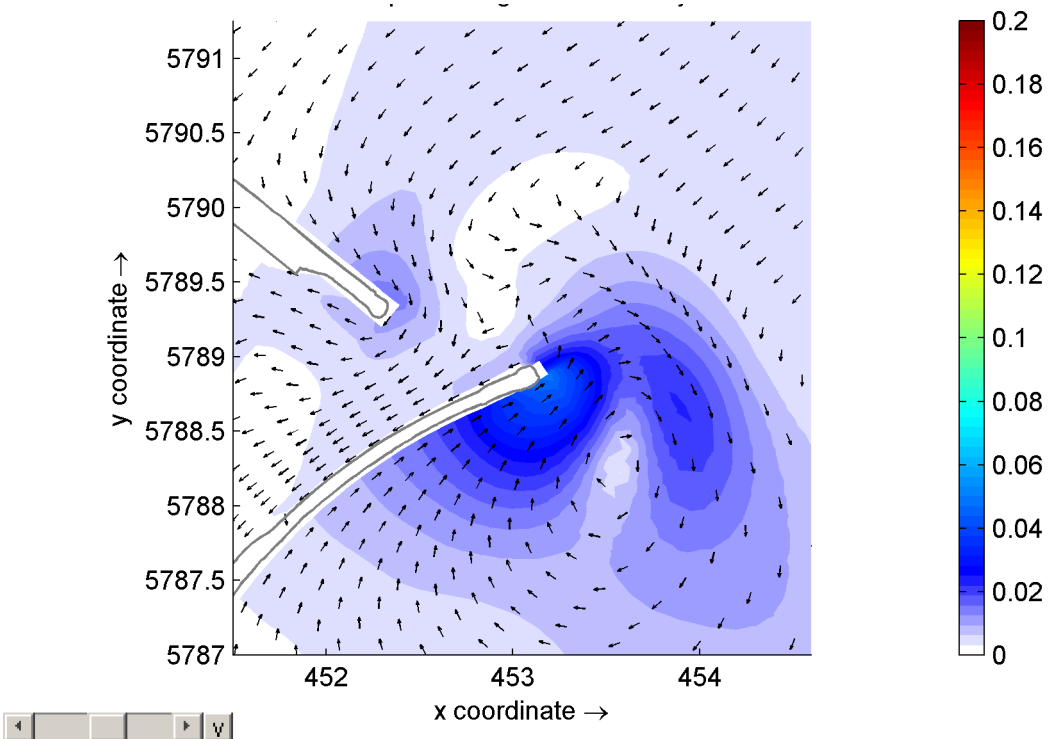


Figure 10.16 Computed depth averaged flow velocities (in m/s) and directions 5.5 hours before HW

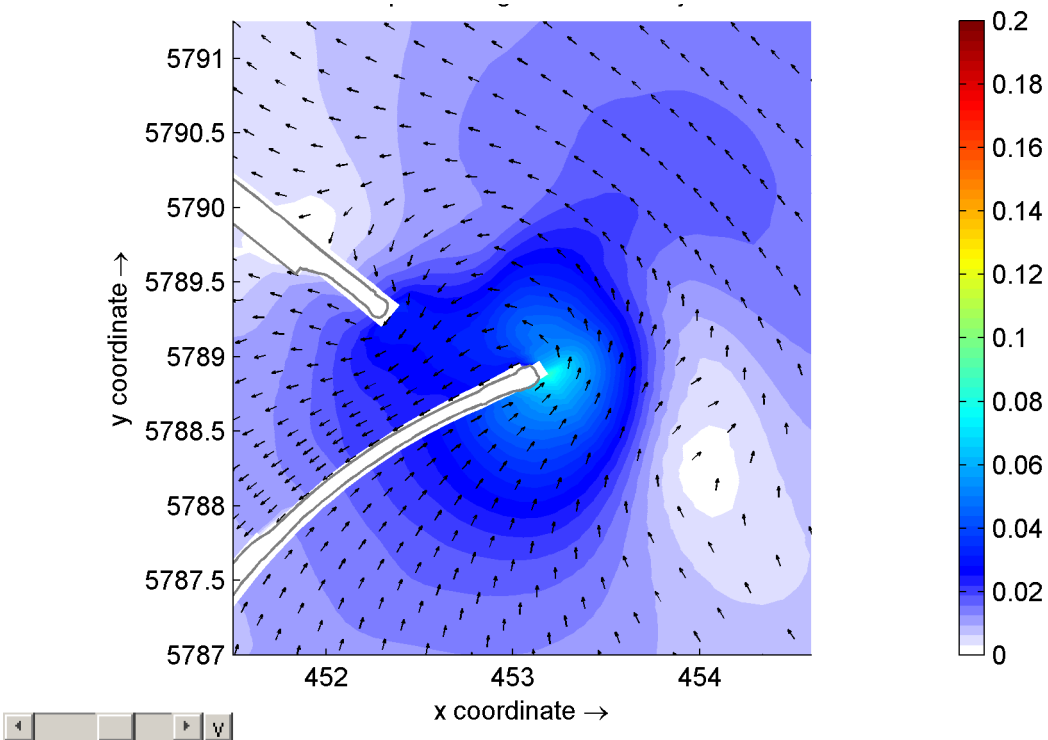


Figure 10.17 Computed depth averaged flow velocities (in m/s) and directions 4.5 hours before HW

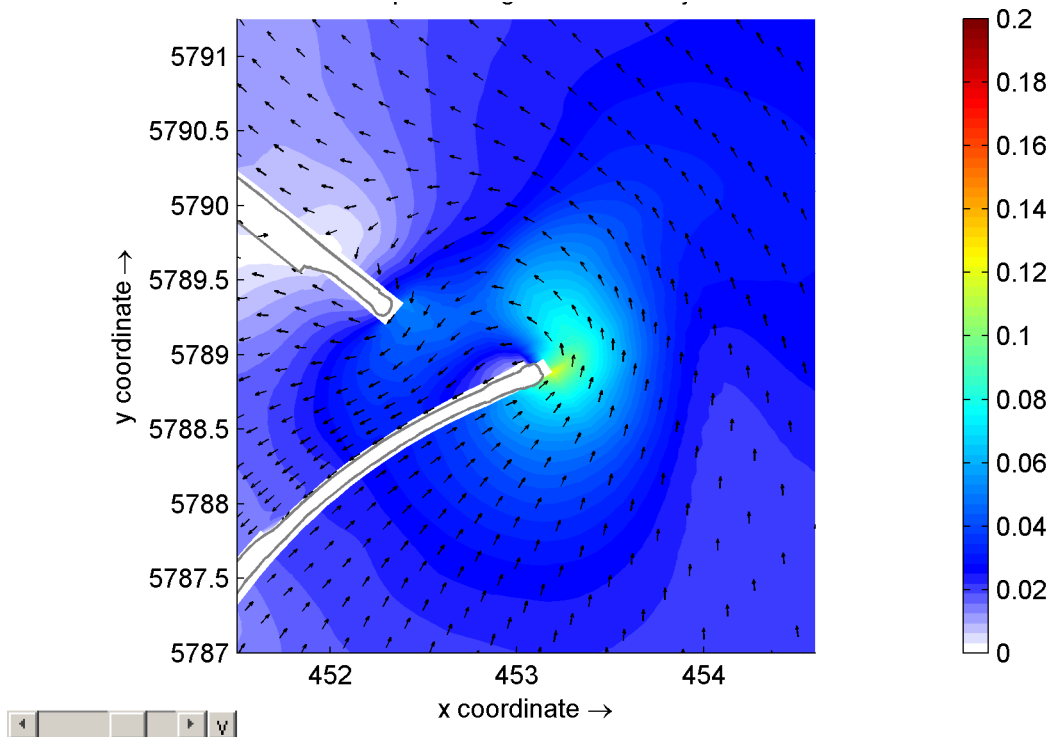


Figure 10.18 Computed depth averaged flow velocities (in m/s) and directions 3.5 hours before HW

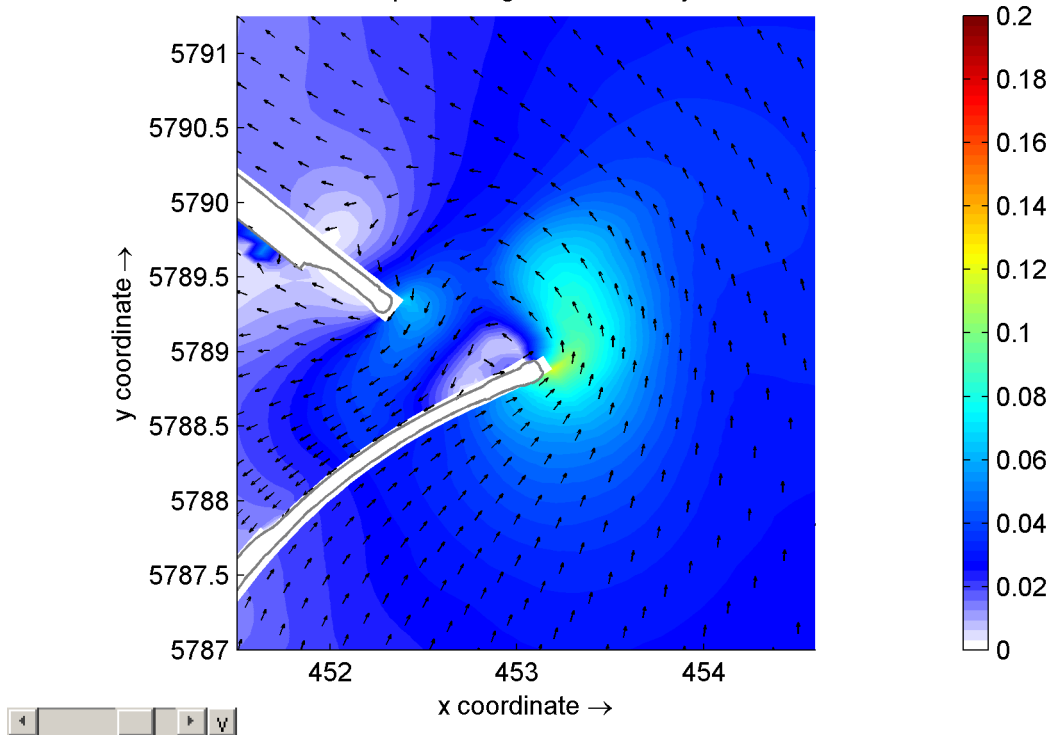


Figure 10.19 Computed depth averaged flow velocities (in m/s) and directions 2.5 hours before HW

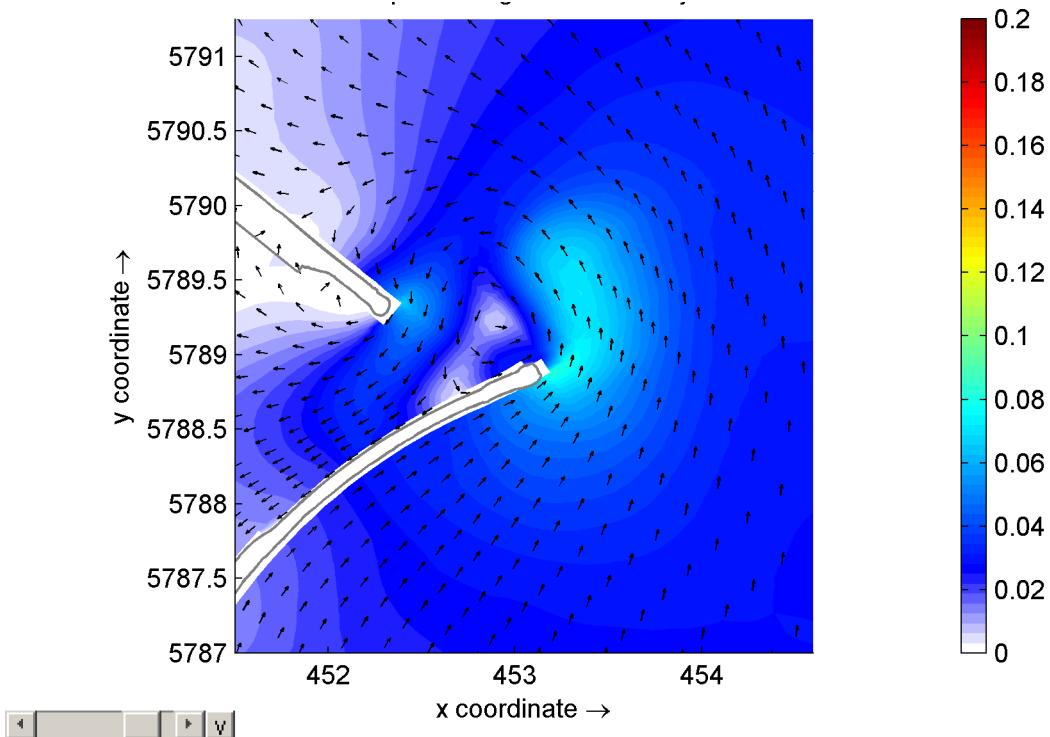


Figure 10.20 Computed depth averaged flow velocities (in m/s) and directions 1.5 hours before HW

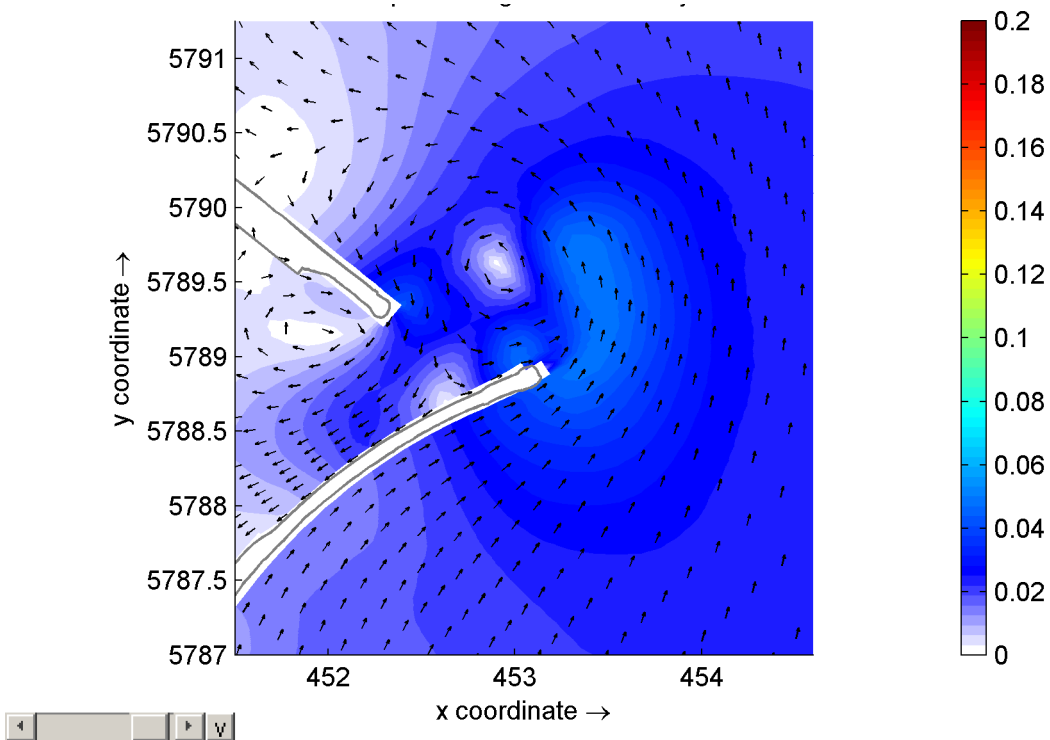


Figure 10.21 Computed depth averaged flow velocities (in m/s) and directions 0.5 hour before HW

E Computed effect waves from varying directions (without tide)

Eight different model runs were performed using the 2012 bathymetry and the following wind and wave conditions (without tidal forcing):

| Run | Wave conditions at boundary | | | Wind conditions over domain | |
|-----|-----------------------------|----------------|---------------------|-----------------------------|-----------------|
| | H _s | T _p | Mean wave direction | Wind direction | U ₁₀ |
| A | 3 m | 7 s | 0° w.r.t. North | 0° w.r.t. North | 8 m/s |
| B | 3 m | 7 s | 45° w.r.t. North | 45° w.r.t. North | 8 m/s |
| C | 3 m | 7 s | 90° w.r.t. North | 90° w.r.t. North | 8 m/s |
| D | 3 m | 7 s | 135° w.r.t. North | 135° w.r.t. North | 8 m/s |
| E | 3 m | 7 s | 180° w.r.t. North | 180° w.r.t. North | 8 m/s |
| F | 3 m | 7 s | 225° w.r.t. North | 225° w.r.t. North | 8 m/s |
| G | 3 m | 7 s | 270° w.r.t. North | 270° w.r.t. North | 8 m/s |
| H | 3 m | 7 s | 315° w.r.t. North | 315° w.r.t. North | 8 m/s |

Table 10.8 Wind and wave conditions for model runs without tide

On the following pages the resulting wave fields, flow patterns, and sediment transport are visualised per model run.

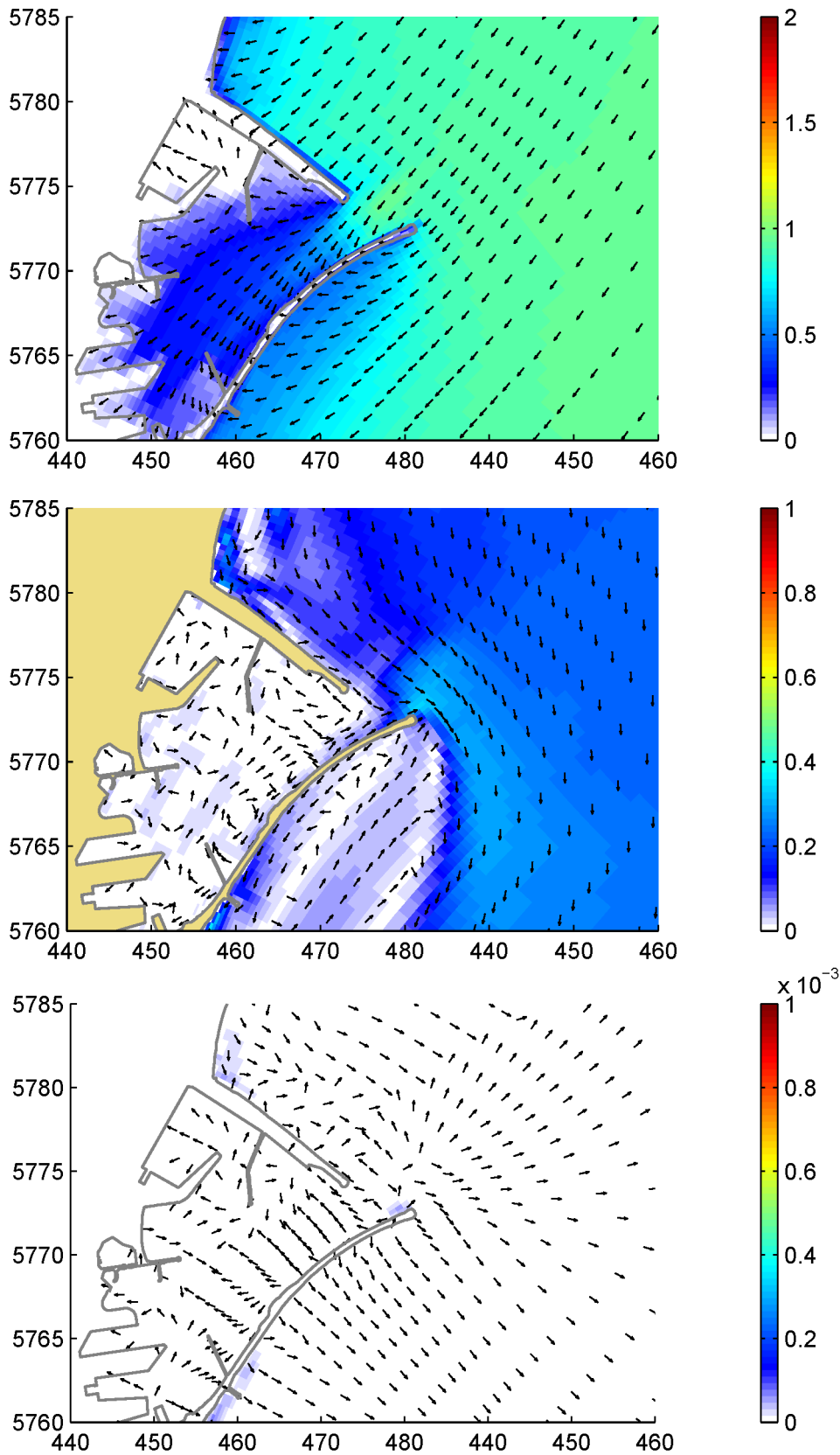


Figure 10.22 Run A: Wind and wave angle 0° w.r.t. north
 Top: Significant wave height (in m) and mean direction;
 Middle: Depth averaged flow velocity (in m/s) and direction;
 Bottom: Sediment transport rate (in $\text{m}^3/\text{s}/\text{m}$) and direction.

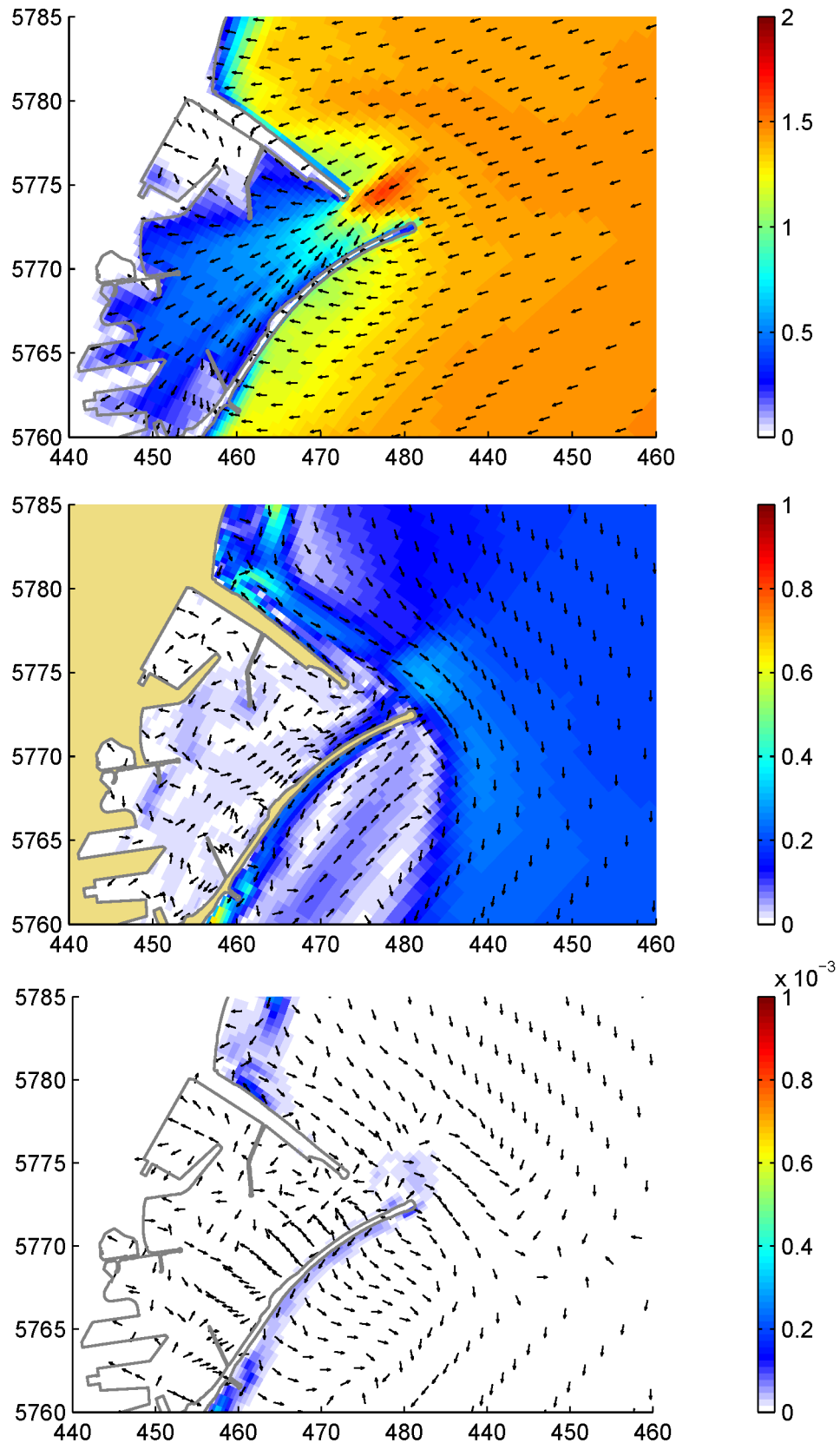


Figure 10.23 Run B: Wind and wave angle 45° w.r.t. north
 Top: Significant wave height (in m) and mean direction;
 Middle: Depth averaged flow velocity (in m/s) and direction;
 Bottom: Sediment transport rate (in $\text{m}^3/\text{s}/\text{m}$) and direction.

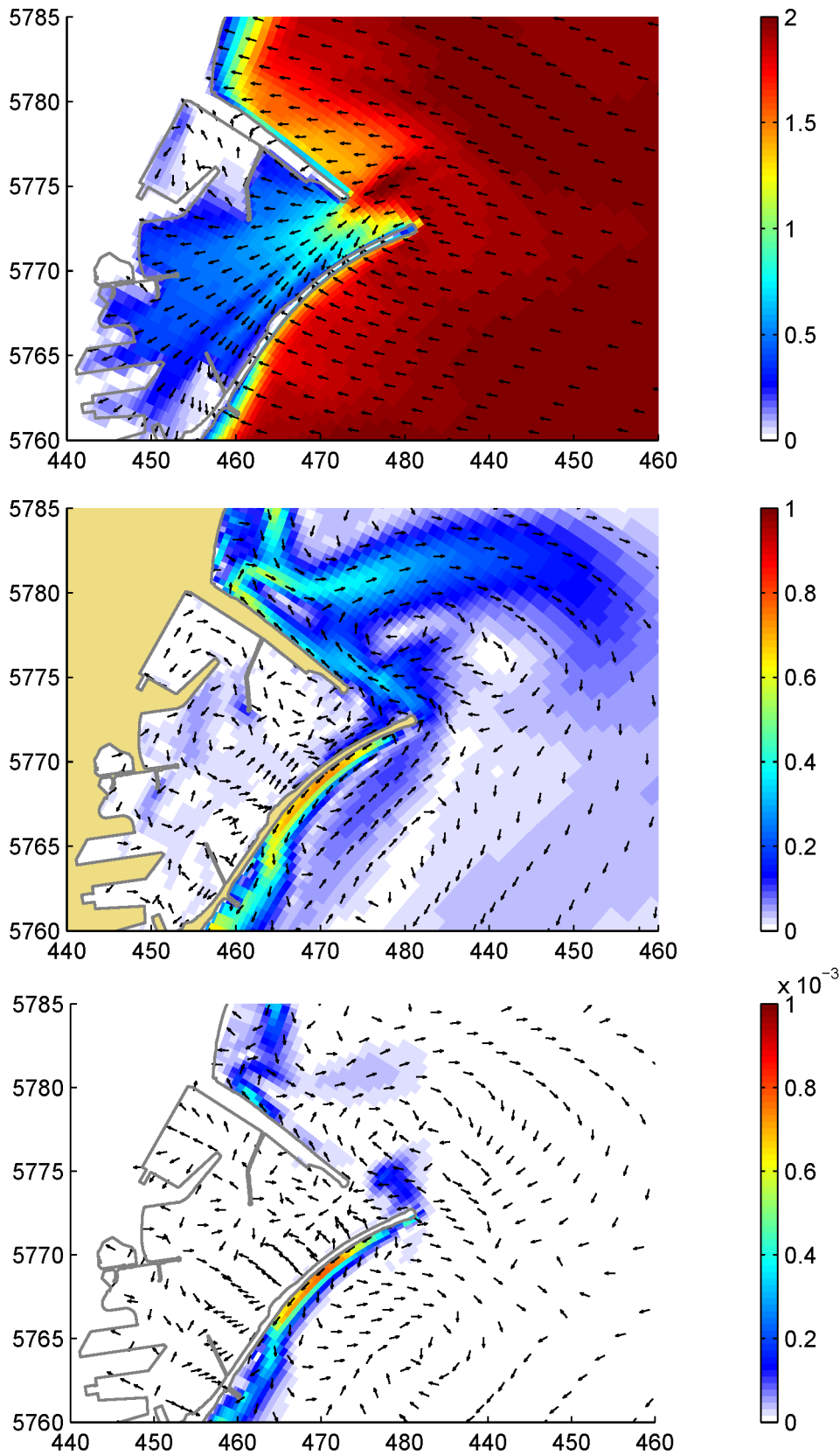


Figure 10.24 Run C: Wind and wave angle 90° w.r.t. north
 Top: Significant wave height (in m) and mean direction;
 Middle: Depth averaged flow velocity (in m/s) and direction;
 Bottom: Sediment transport rate (in $\text{m}^3/\text{s}/\text{m}$) and direction.

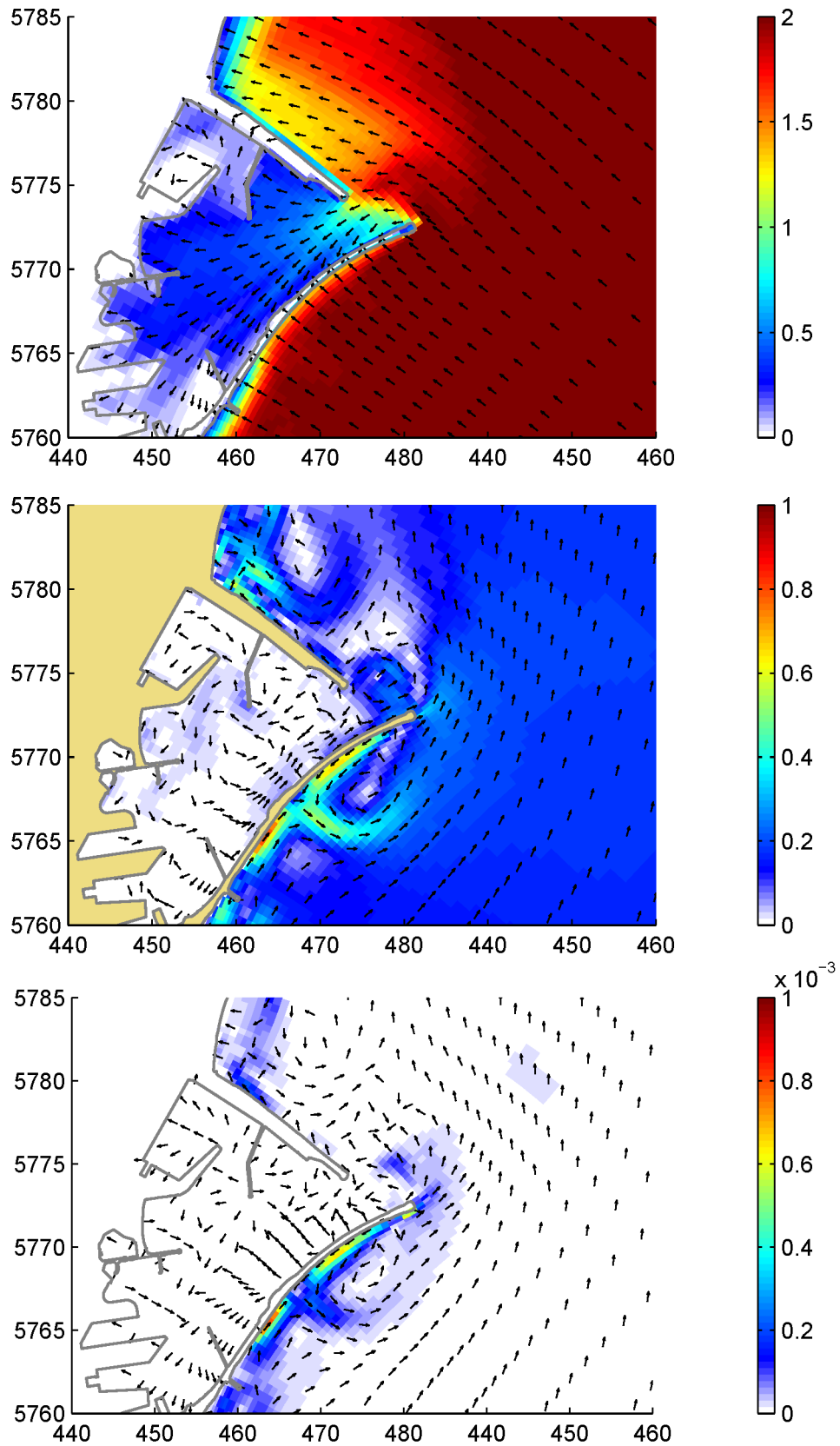


Figure 10.25 Run D: Wind and wave angle 135° w.r.t. north
 Top: Significant wave height (in m) and mean direction;
 Middle: Depth averaged flow velocity (in m/s) and direction;
 Bottom: Sediment transport rate (in $m^3/s/m$) and direction.

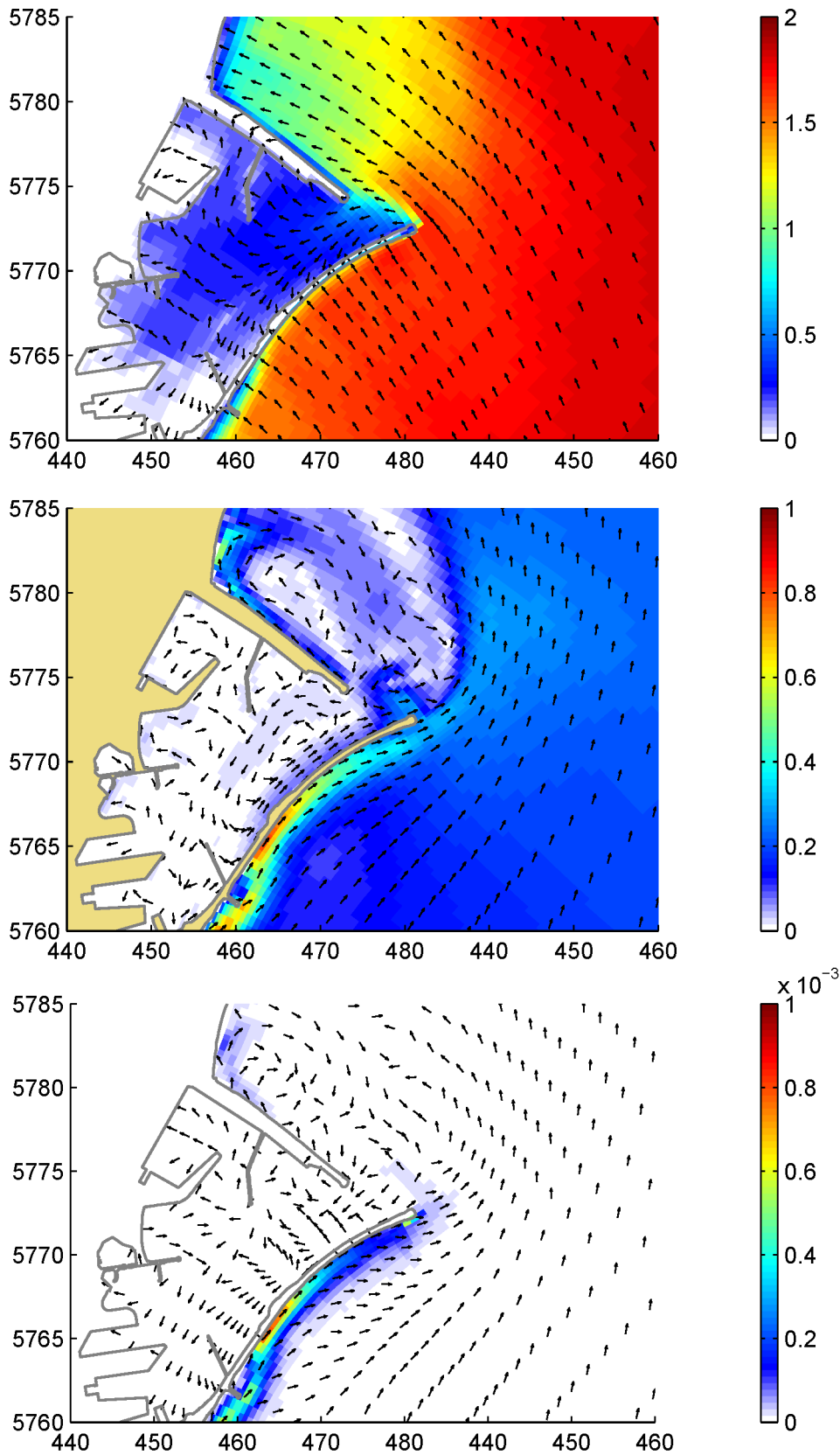


Figure 10.26 Run E: Wind and wave angle 180° w.r.t. north
 Top: Significant wave height (in m) and mean direction;
 Middle: Depth averaged flow velocity (in m/s) and direction;
 Bottom: Sediment transport rate (in $\text{m}^3/\text{s}/\text{m}$) and direction.

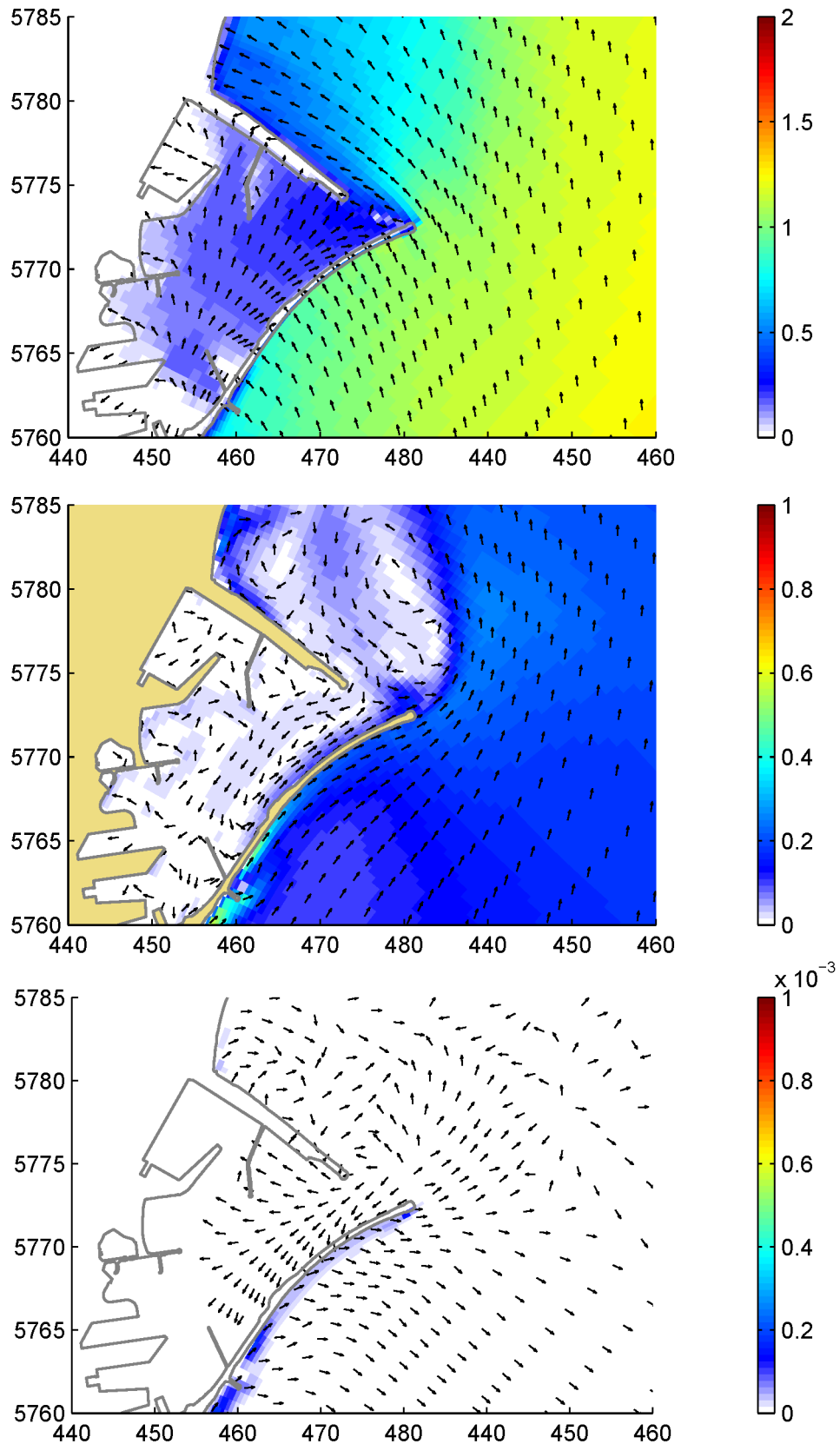


Figure 10.27 Run F: Wind and wave angle 225° w.r.t. north
 Top: Significant wave height (in m) and mean direction;
 Middle: Depth averaged flow velocity (in m/s) and direction;
 Bottom: Sediment transport rate (in $m^3/s/m$) and direction.

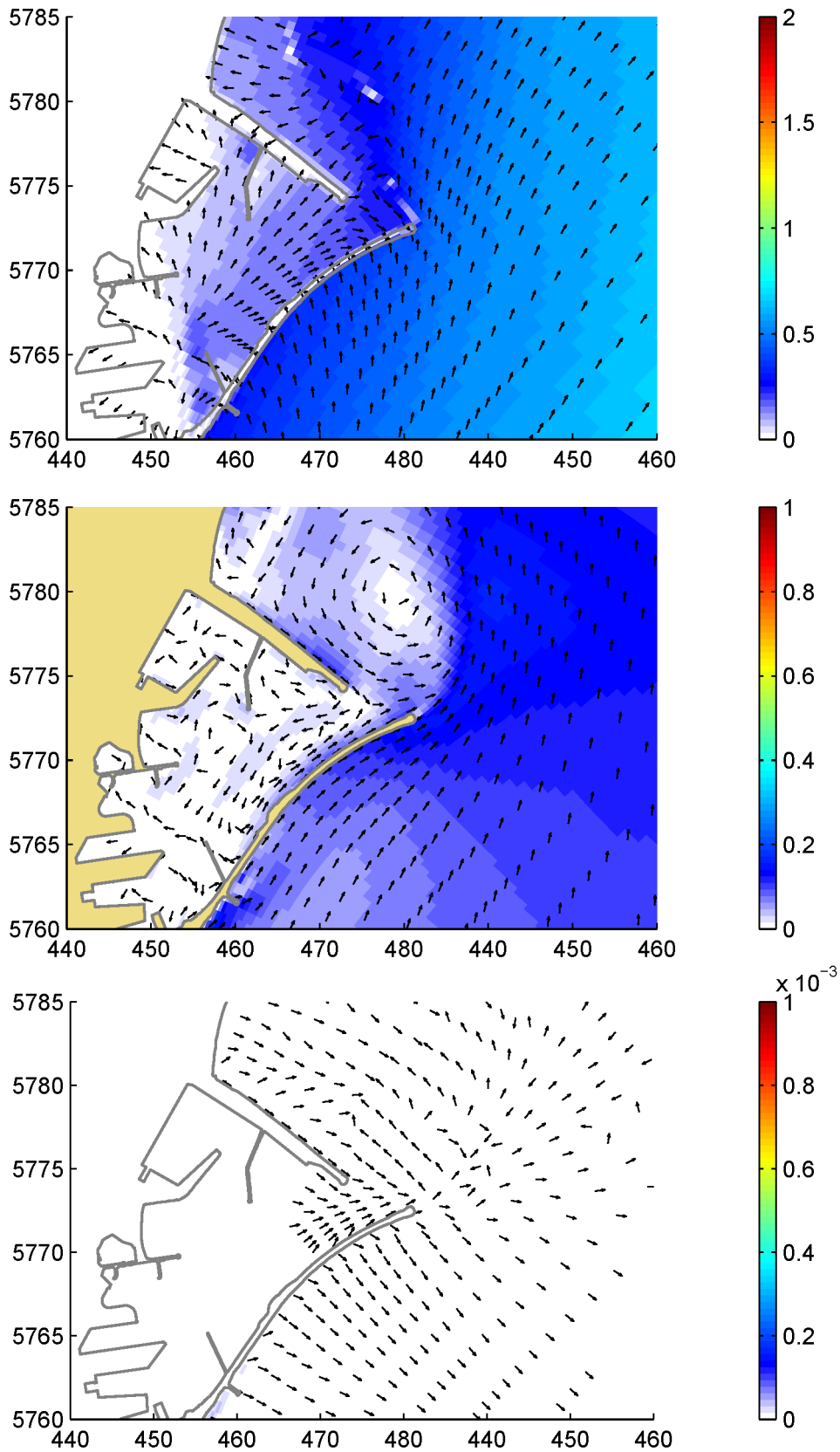


Figure 10.28 Run G: Wind and wave angle 270° w.r.t. north
 Top: Significant wave height (in m) and mean direction;
 Middle: Depth averaged flow velocity (in m/s) and direction;
 Bottom: Sediment transport rate (in $m^3/s/m$) and direction.

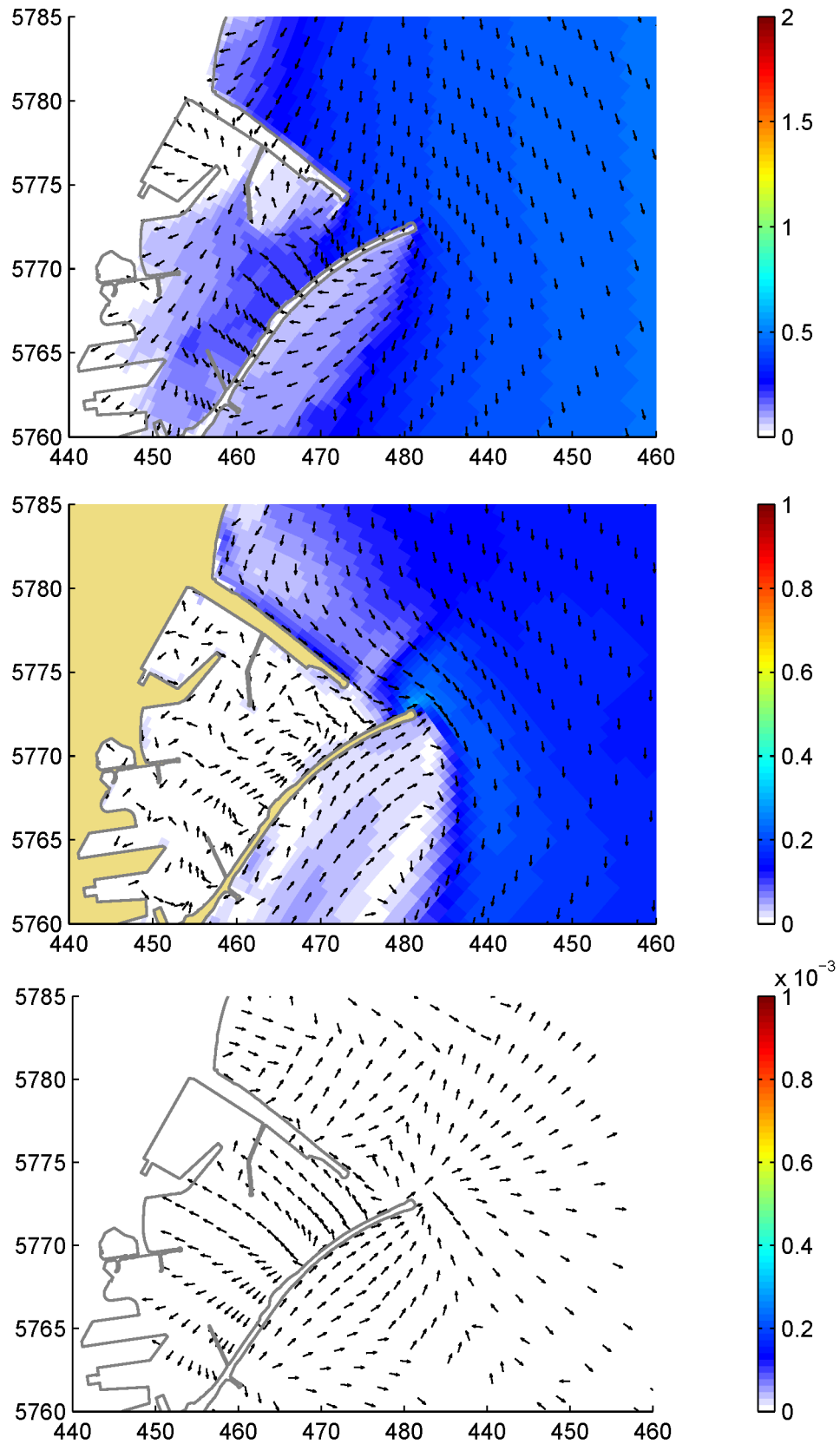


Figure 10.29 Run H: Wind and wave angle 315° w.r.t. north
 Top: Significant wave height (in m) and mean direction;
 Middle: Depth averaged flow velocity (in m/s) and direction;
 Bottom: Sediment transport rate (in $m^3/s/m$) and direction.

F Computed hydrodynamics and sediment transports per scenario

Model runs have been performed using: the 2012 bathymetry, tidal forcing, and the following scenarios of simultaneous occurring wind and wave conditions that represent the yearly averaged wind and wave conditions in the table below. The generation of the scenarios and parameters is described in section 6.4.2.

| Reduced wind and wave climate | | | | | | | |
|-------------------------------|------|------|-----|------|------|-------|------|
| Scen. | Hs | Tp | Dm | U10 | Udir | P | days |
| 1 | 3,70 | 10,2 | 122 | 11,5 | 162 | 0,004 | 1,4 |
| 2 | 3,58 | 10,0 | 178 | 11,2 | 210 | 0,008 | 3,0 |
| 3 | 3,60 | 10,1 | 214 | 11,3 | 245 | 0,001 | 0,5 |
| 4 | 2,51 | 8,4 | 114 | 8,9 | 135 | 0,029 | 10,6 |
| 5 | 2,44 | 8,3 | 147 | 8,7 | 153 | 0,018 | 6,5 |
| 6 | 2,80 | 8,9 | 177 | 9,5 | 208 | 0,020 | 7,4 |
| 7 | 2,40 | 8,2 | 211 | 8,6 | 236 | 0,023 | 8,3 |
| 8 | 2,10 | 7,7 | 163 | 8,0 | 136 | 0,060 | 21,9 |
| 9 | 2,05 | 7,6 | 186 | 7,9 | 212 | 0,045 | 16,3 |
| 10 | 1,14 | 5,7 | 39 | 6,3 | 9 | 0,160 | 58,5 |
| 11 | 1,20 | 5,8 | 74 | 6,4 | 54 | 0,159 | 58,1 |
| 12 | 1,60 | 6,7 | 88 | 7,1 | 66 | 0,084 | 30,7 |
| 13 | 1,58 | 6,7 | 118 | 7,0 | 75 | 0,130 | 47,6 |
| 14 | 1,46 | 6,4 | 146 | 6,8 | 69 | 0,043 | 15,7 |
| 15 | 1,35 | 6,2 | 182 | 6,6 | 112 | 0,050 | 18,3 |
| 16 | 1,36 | 6,2 | 214 | 6,6 | 226 | 0,074 | 27,2 |

Total: 0,910 332,1

Table 10.9 Representative scenarios of wind and wave conditions of Significant wave height (H_s), Peak wave period (T_p), Mean wave direction (D_m), Wind speed (U_{10}), Wind direction (U_{dir}), and Probability of occurrence (P)

Identical resulting flow patterns and sediment transport patterns are grouped per scenario and visualised on the following pages.

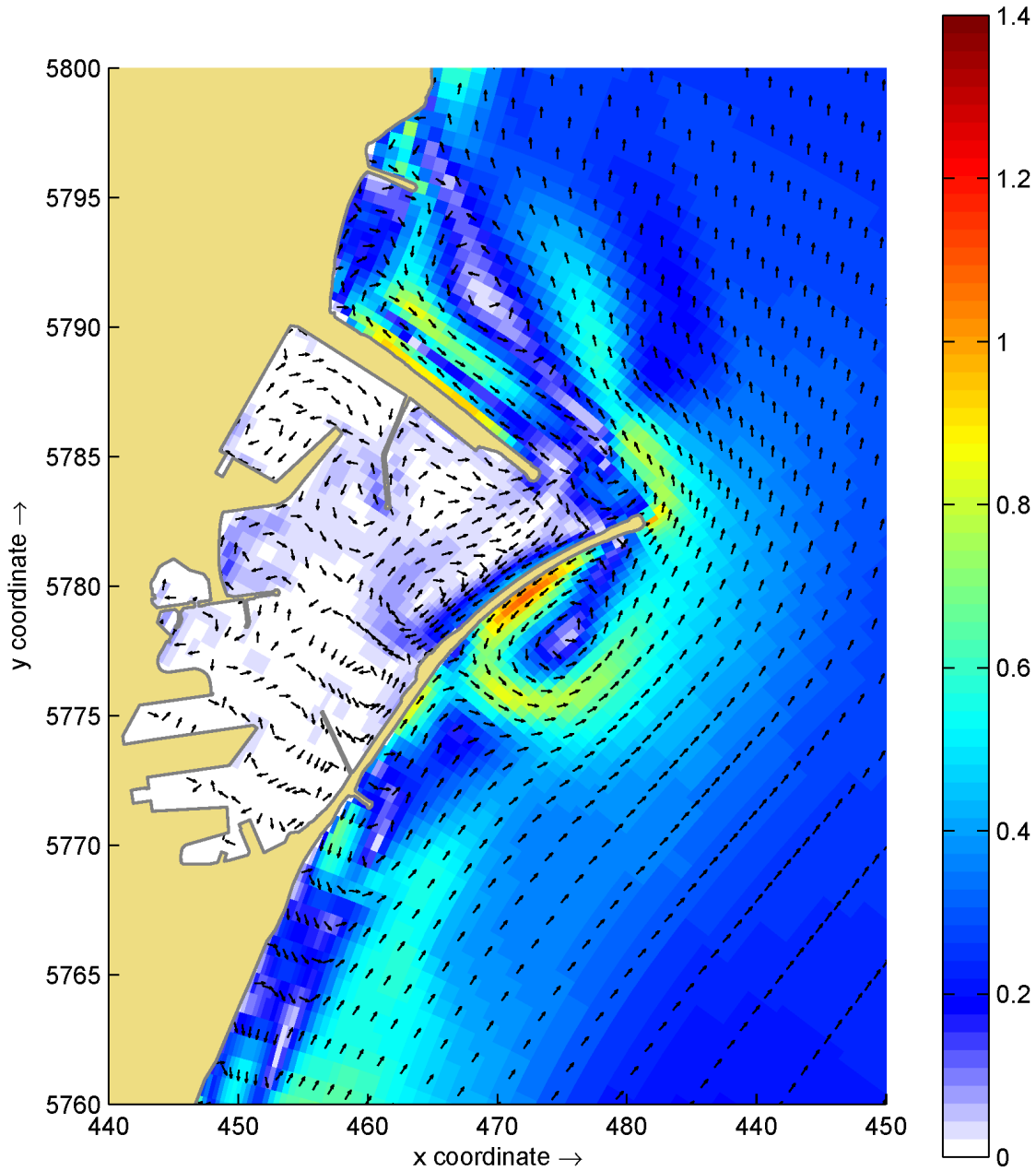


Figure 10.30 Estimated depth averaged flow velocities (in m/s) for scenario 1

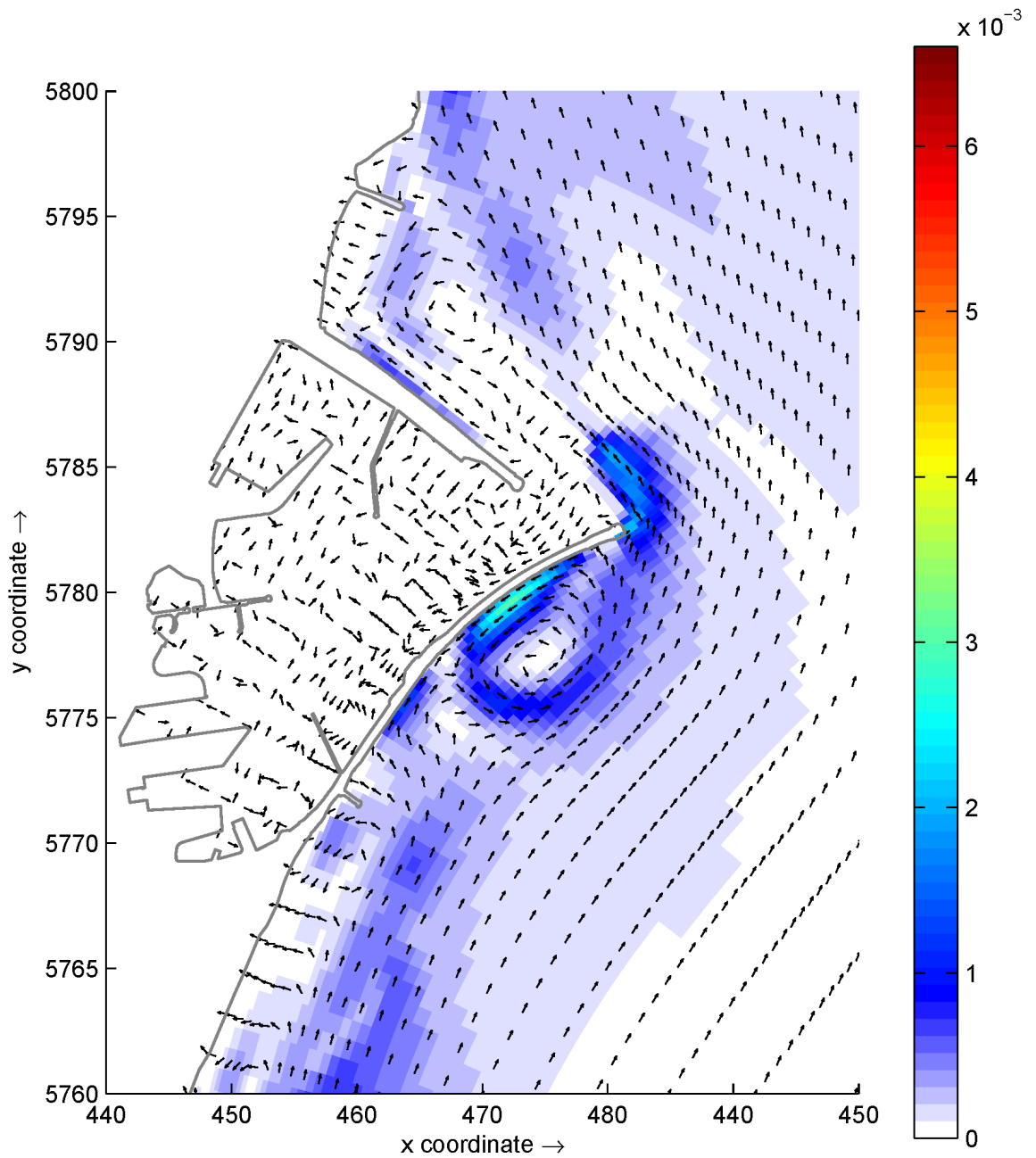


Figure 10.31 Estimated sediment transports (in $m^3/s/m$) for scenario 1

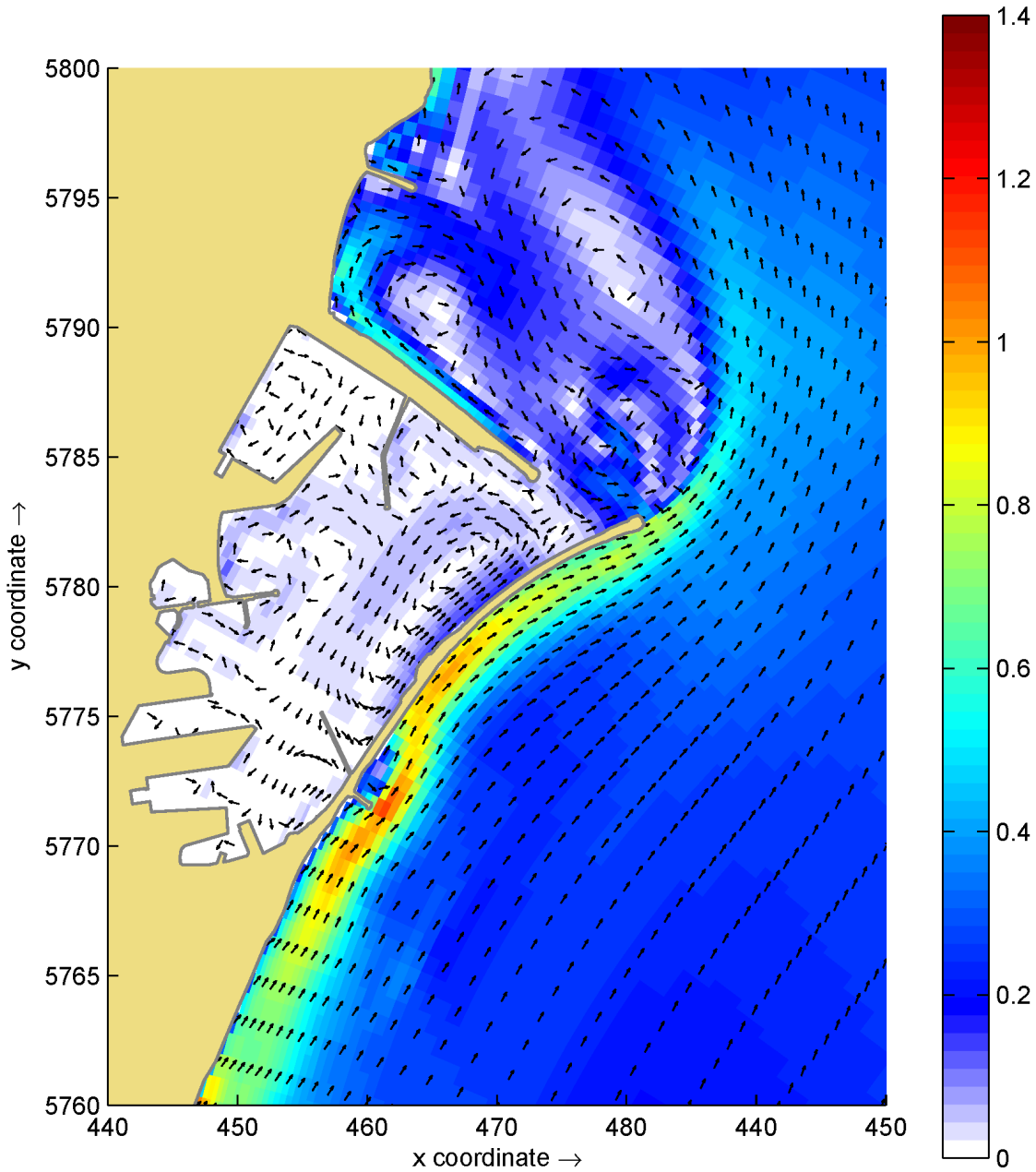


Figure 10.32 Estimated depth averaged flow velocities (in m/s) for scenario 2

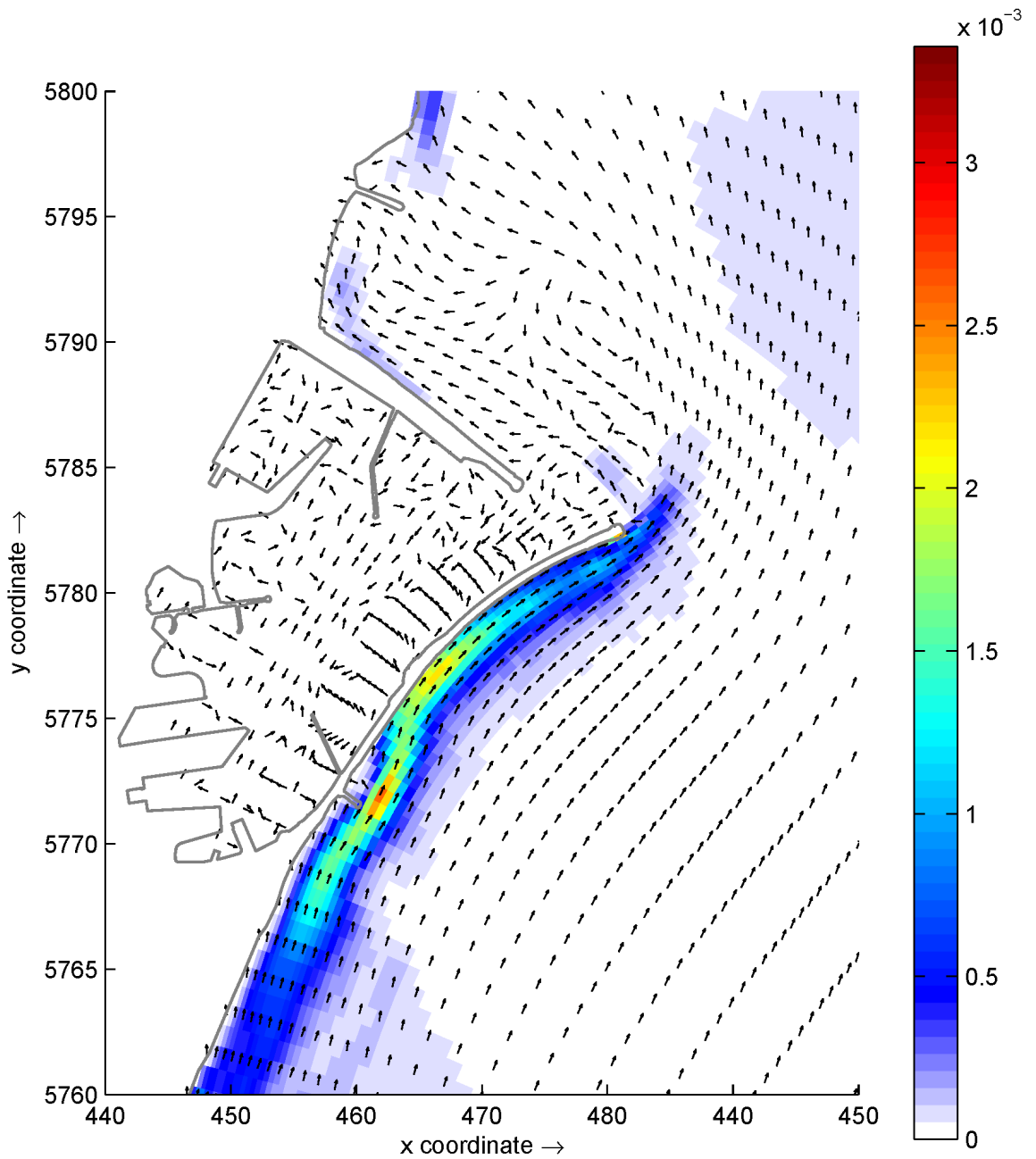


Figure 10.33 Estimated sediment transports (in $m^3/s/m$) for scenario 2

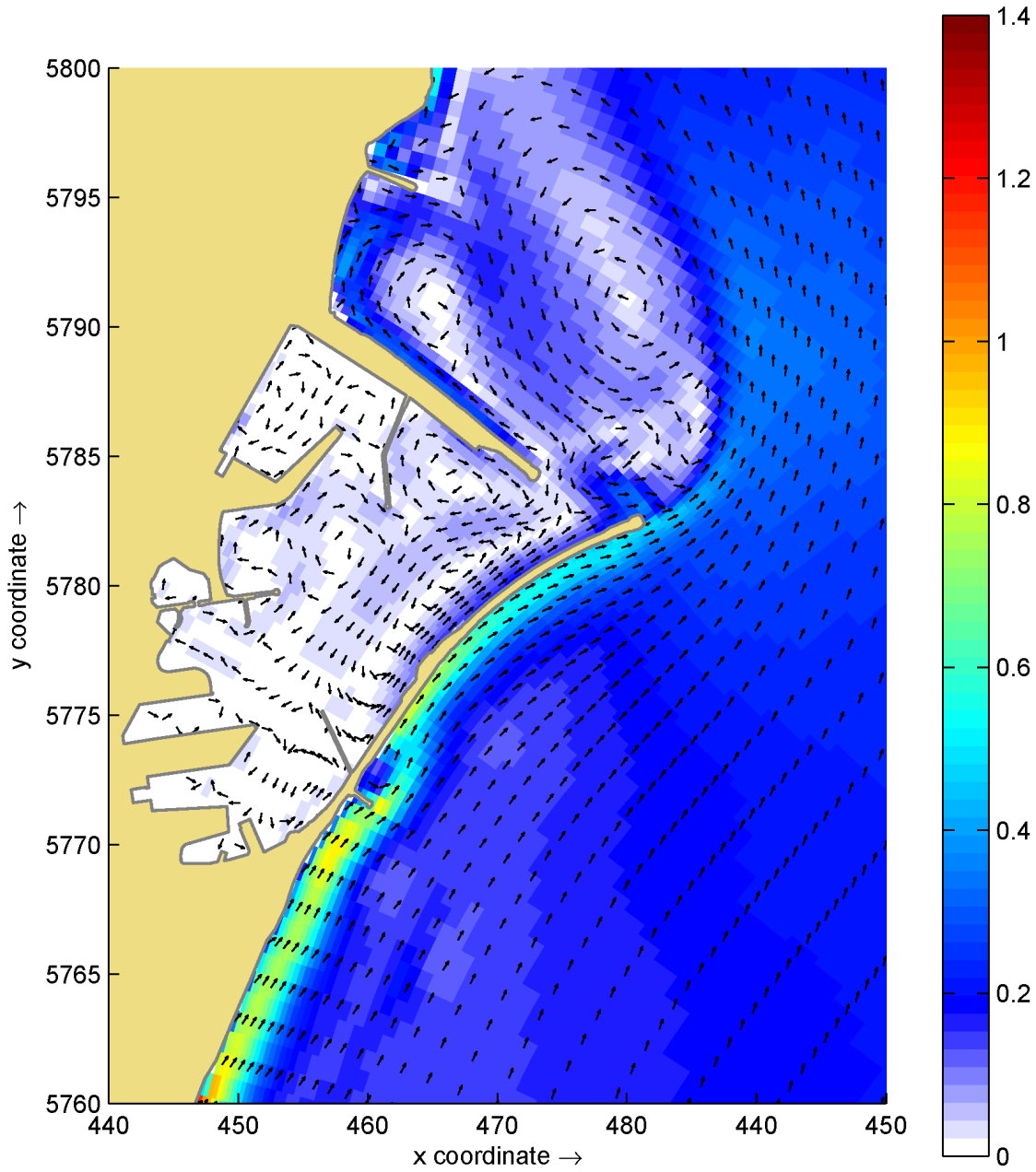


Figure 10.34 Estimated depth averaged flow velocities (in m/s) for scenario 3

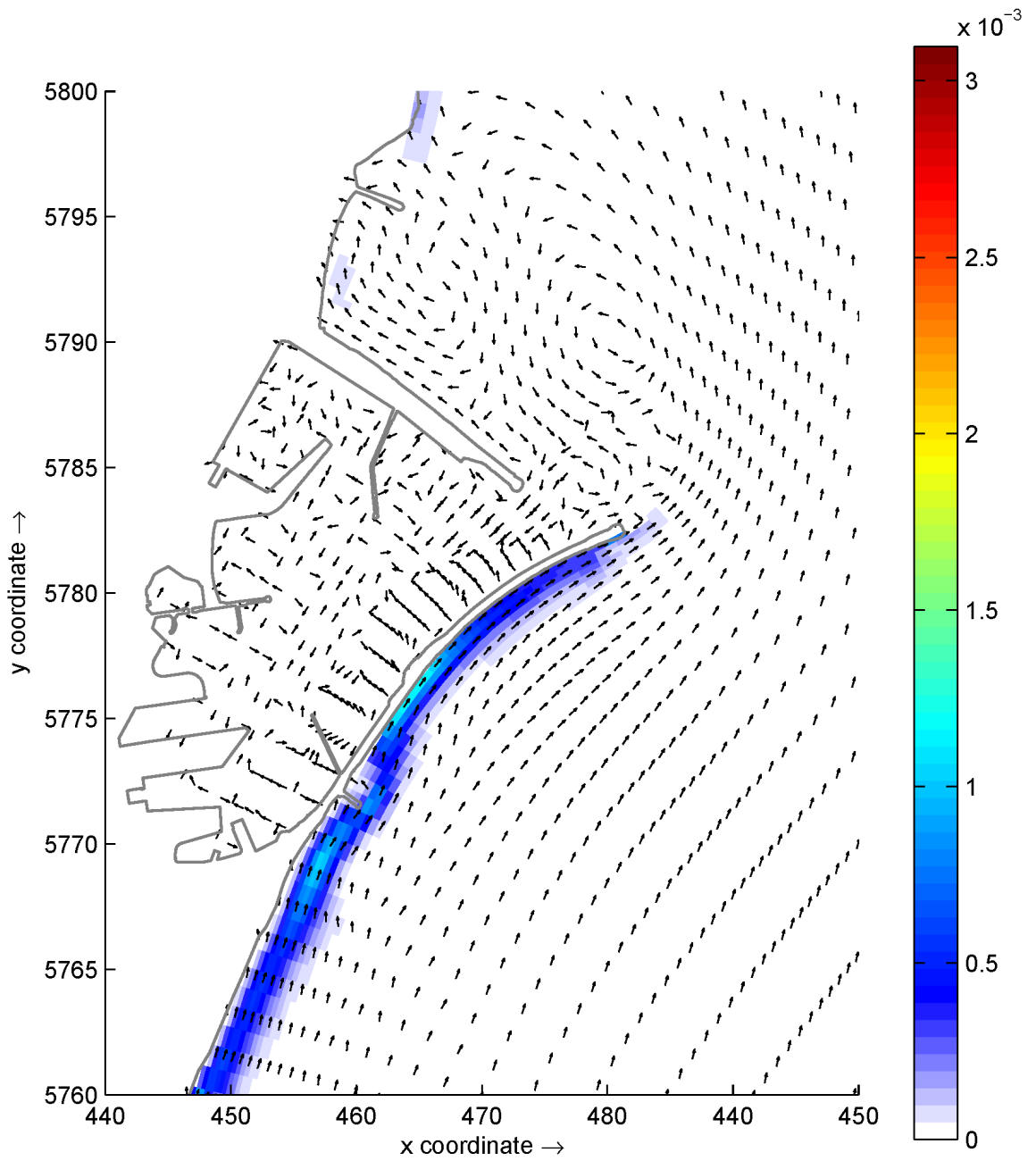


Figure 10.35 Estimated sediment transports (in $\text{m}^3/\text{s}/\text{m}$) for scenario 3

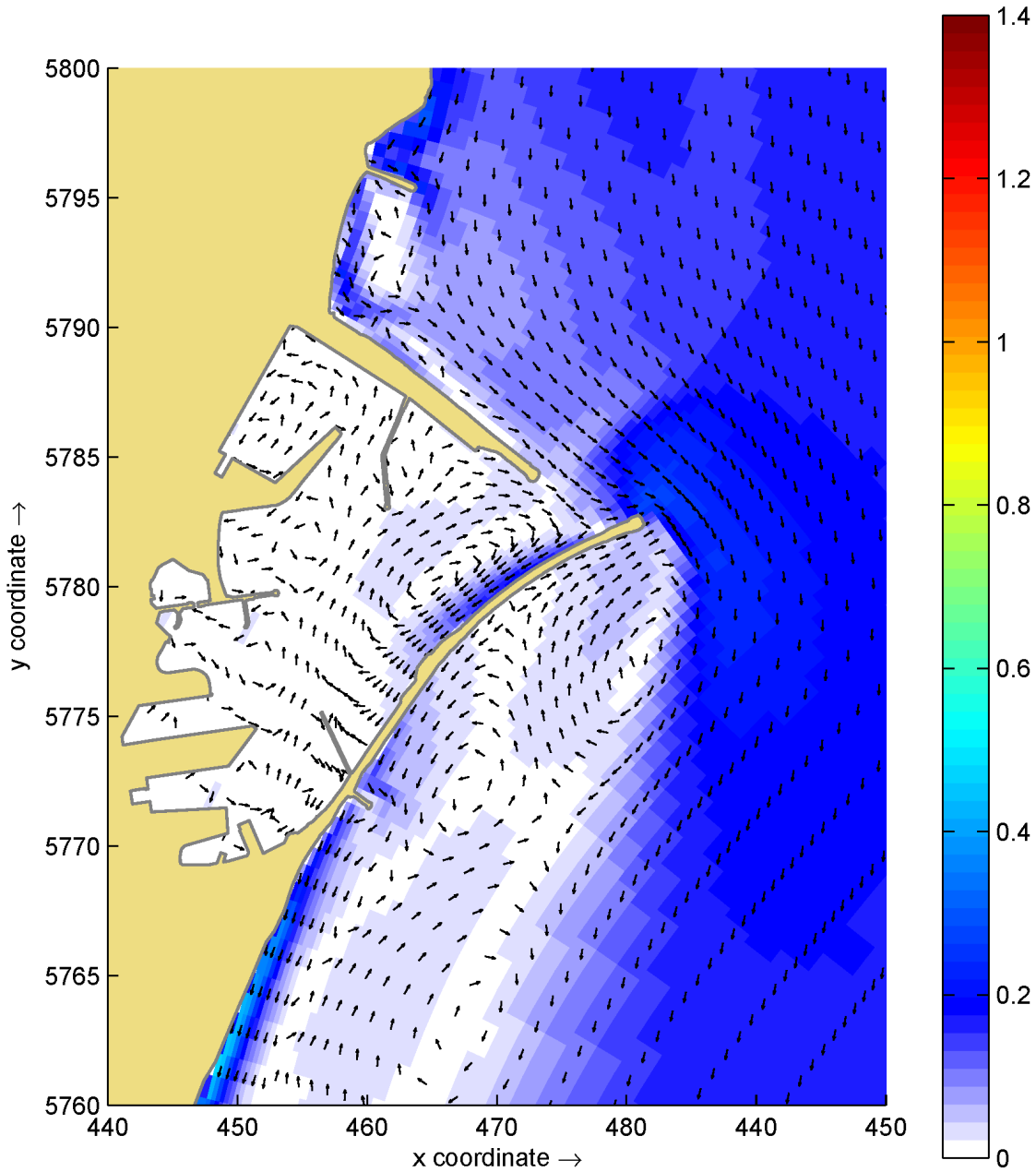


Figure 10.36 Estimated depth averaged flow velocities (in m/s) for scenario 10

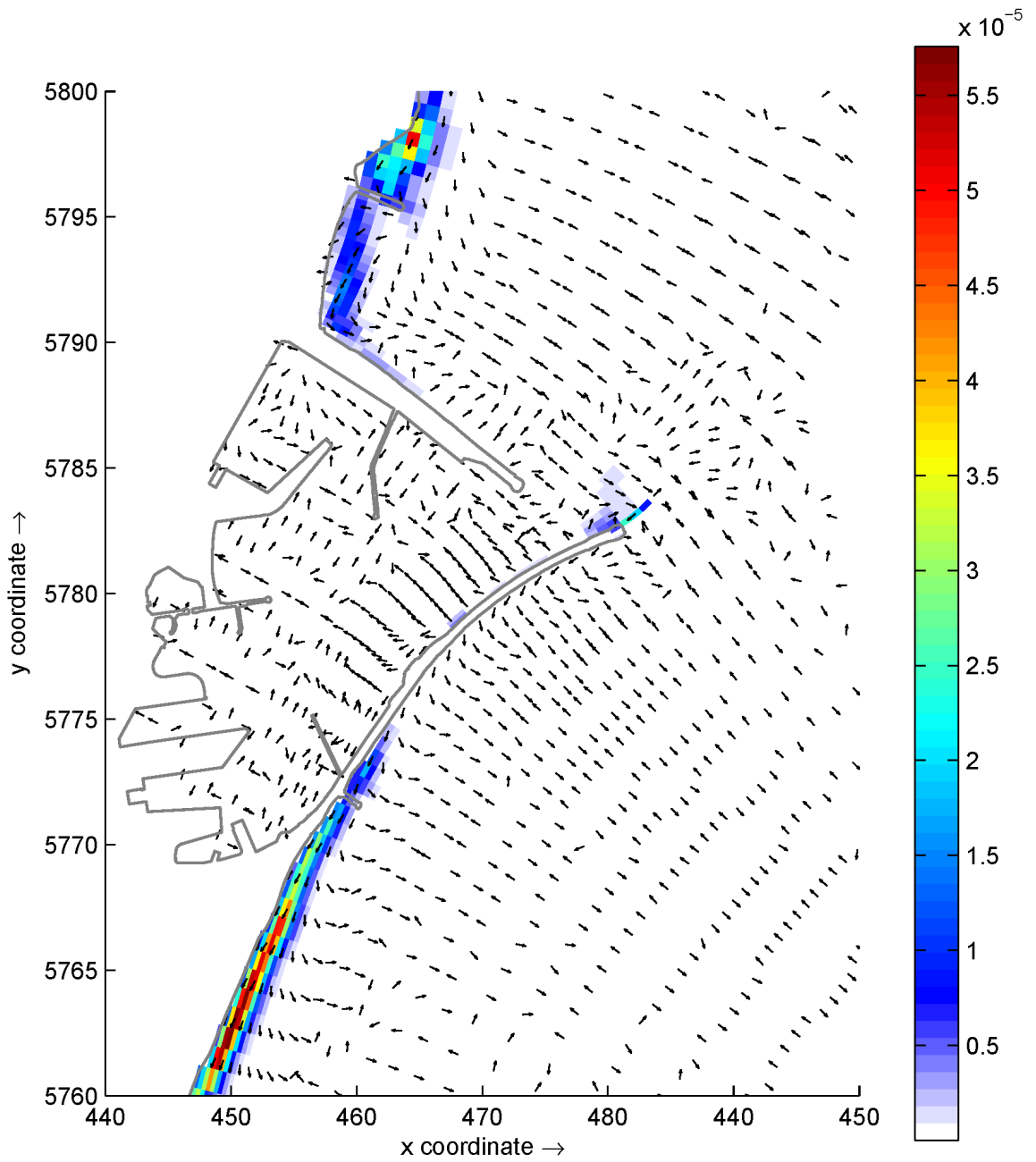


Figure 10.37 Estimated sediment transports (in $m^3/s/m$) for scenario 10

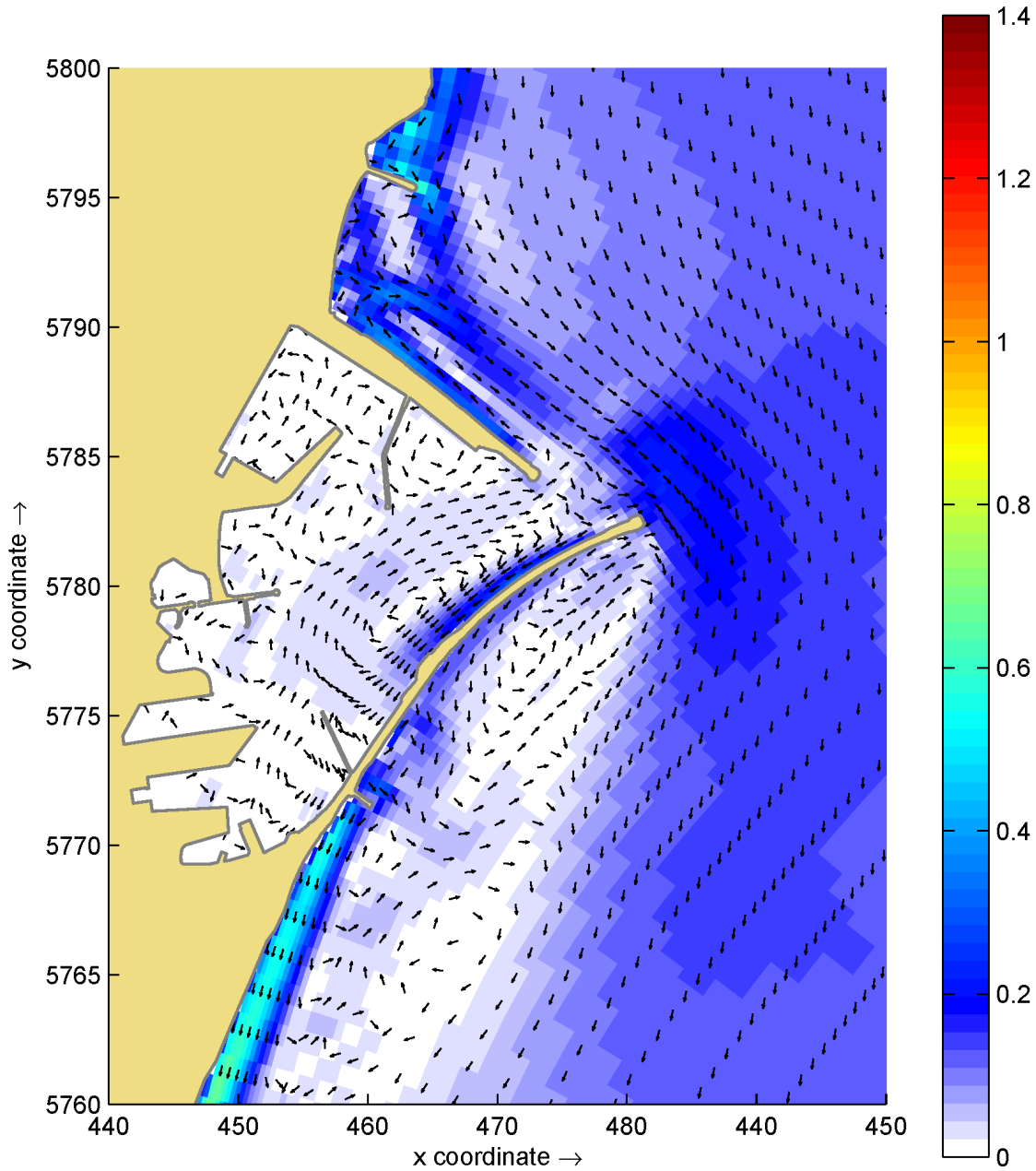


Figure 10.38 Estimated depth averaged flow velocities (in m/s) for scenario 12

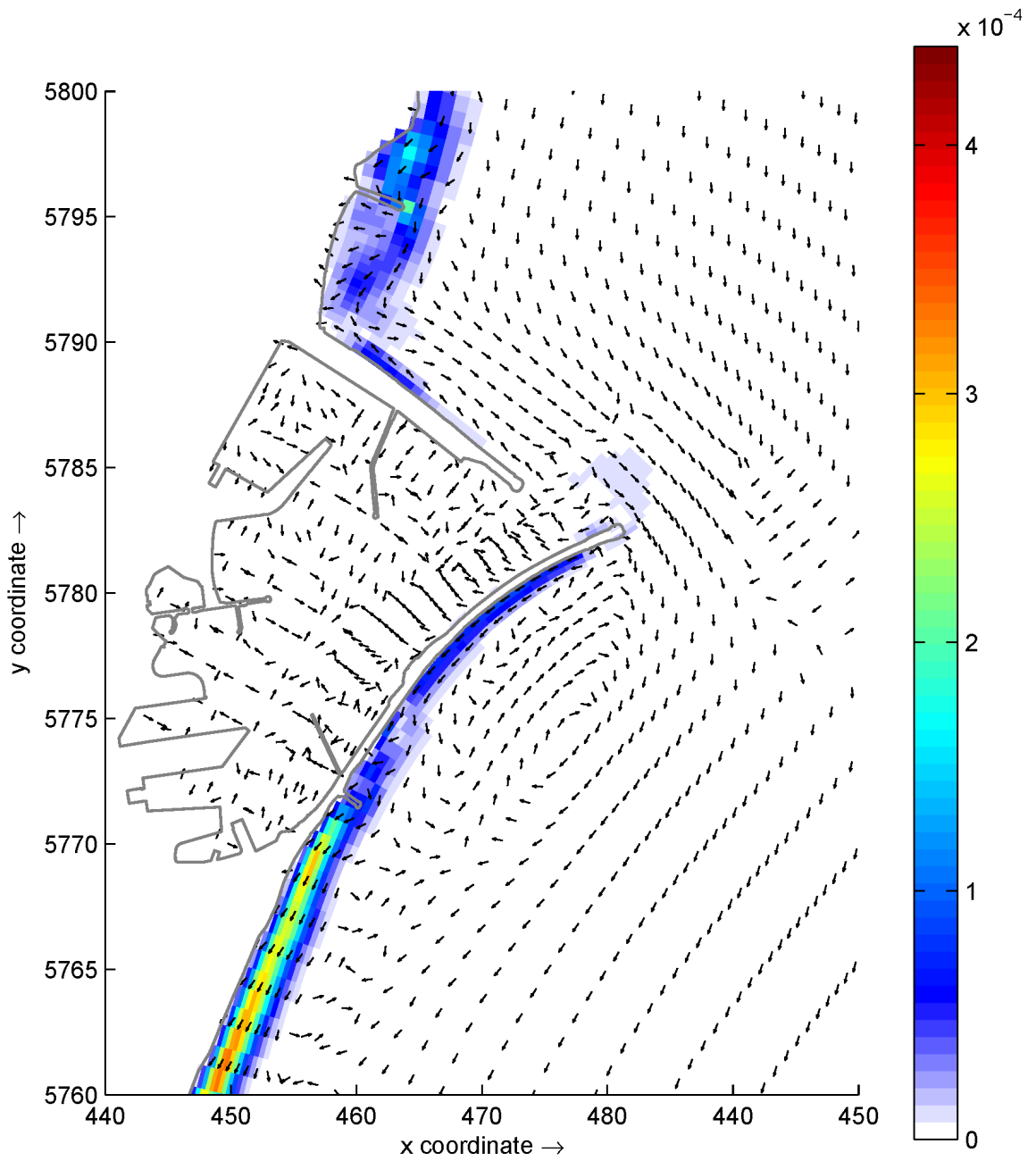


Figure 10.39 Estimated sediment transports (in $\text{m}^3/\text{s}/\text{m}$) for scenario 12